AUGER ELECTRON AND CHARACTERISTIC ENERGY LOSS SPECTROSCOPY OF SOME METALS

being

a thesis presented for the

Degree of Doctor of Philosophy

at the University of Keele.

by

M. Suleman M.Sc.

Physics Department,
University of Keele,
Staffordshire.

November, 1971

BEST COPY AVAILABLE.

VARIABLE PRINT QUALITY

CONTAINS PULLOUTS

ABSTRACT

A sensitive high resolution three grid electron energy analyser has been constructed and has been used to measure the Auger electron and characteristic energy loss spectra of clean Cu, Au, Be, Al and Fe. In addition spectra of Cu black and Au black surfaces have been obtained. The experimental resolution of the instrument has proved to be ~0.2% (which may be compared with a figure of about 2% for normal commercial analysers). All surfaces were prepared in ultra high vacuum (working pressure ~10^{-10}torr) with the exception of Cu black and Au black, which were transferred to the UHV system from high vacuum after preparation. Changes in the electron spectra of Al, Be and Fe due to slow oxidation from residual oxygen were extensively studied. For these metals (Be, Al and Fe) fine structure in the Auger spectra involving the valence band has been interpreted in terms of the density of states of the valence band. Additional fine structure in the Auger spectrum of clean Al has been attributed to plasmon gain and loss mechanisms. In addition explanations of various other changes in the electron spectra of the metals, Be, Al and Fe, as a result of oxidation have been included.

ACKNOWLEDGEMENTS

The author wishes to express his thanks and gratitude to:

Professor D.J.E. Ingram for the use of laboratory and research facilities of the Department;

Dr. E.B. Pattinson for his excellent supervision and guidance throughout this work;

Dr. S. Thomas for his helpful suggestions in the early stages of this work;

Mr. P. Harris and other colleagues in the Physics Department for useful discussions;

Mr. G. Dudley and his staff in the workshop for assistance in constructional work;

Mr. F. Rowerth, Mr. W. Brearley and the technical staff of the Department for their cooperation;

Mr. M.T. Cheney for carrying out the photographic work;

Miss K.B. Davies for much care and patience in the typing and duplication of this thesis;

The University of Keele for the provision of a research grant for the three years 1968-1971.

CONTENTS

CHAPTER I

INTRODUCTION

Secondary electron emission properties of solids have been the subject of numerous investigations for many years. For this reason the literature is vast and the subject embraces a wide range of phenomena of interest both from an academic point of view (where the aim is to understand the various interactions and excitations) to those of technical importance, where the phenomena are either utilised (e.g. electron multipliers) or suppressed (electron collectors, microwave windows etc.). However, over the past few years considerable and renewed interest has developed in aspects of the energy analysis of the secondary electrons resulting from both incident radiation and various particles. This energy analysis of the secondaries is important since it includes electrons originating from Auger transitions and thus provides the basis of a highly sensitive technique for surface analysis, namely the technique of Auger electron spectroscopy[1,2,3,4]. The main subject of this dissertation is various aspects of Auger electron spectroscopy and characteristic energy losses induced by electron bombardment. In this introductory chapter a brief survey of three main aspects of electron induced secondary electron emission will be described. These are as follows:

(i) Secondary electron yield

(ii) Characteristic energy losses

(iii) Auger electron emission.

1.1 Secondary Electron Emission

The secondary electron emission process is basically the interaction of energetic electrons with solids, in which incident electrons are scattered elastically and inelastically. In the inelastic process, for example, the energy lost in the solid is used to produce electronic excitations such as interband transitions, X-ray level excitations and plasmon excitations. These excitation processes may produce secondary electrons which are emitted from the solid provided they have sufficient energy to surmount the surface potential barrier along with the elastically backscattered electrons.

1.1.1 Secondary electron yield

The secondary electron yield, δ, or more commonly known as total yield or secondary emission co-efficient, can be defined as the ratio of the total number of emitted secondaries to the total number of primary electrons striking the solid surface. If i_s is the total secondary current and i_p is the primary current, then

$$\delta = \frac{i_s}{i_p}$$

The secondary electrons emitted from a solid may be divided for convenience into two groups of electrons, namely the backscattered electrons (elastically and inelastically) and the arbitrarily defined true secondary electrons with energies less than 50eV. The backscattering coefficient, η, is the ratio of the total number of backscattered electrons to the total number of primary electrons. Thus

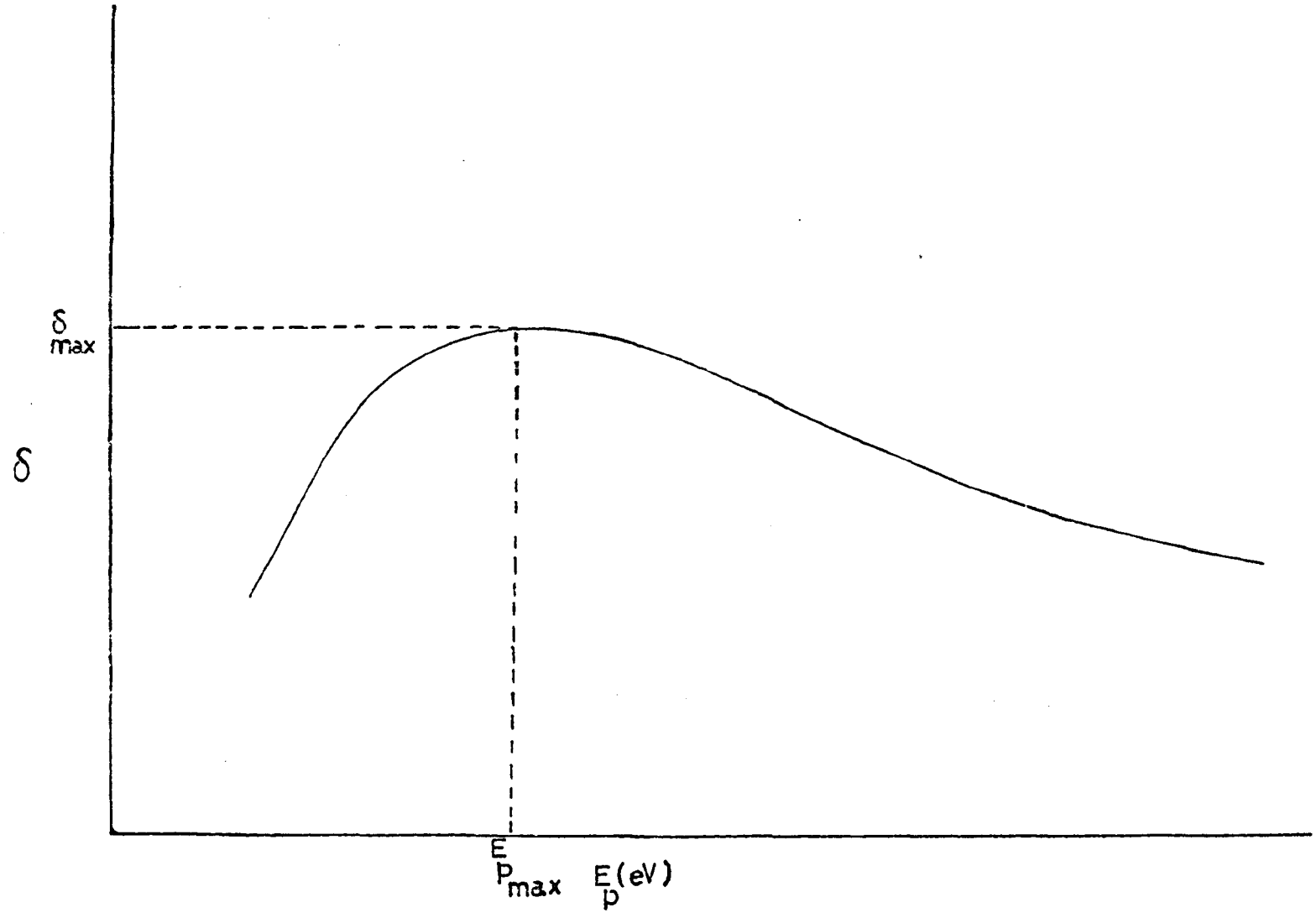

Fig. 1.1 General shape of the yield curve

$$\eta = \frac{i_{bs}}{i_p}$$

where i_{bs} is the current due to backscattered electrons. The relationship between η and δ is given by $\delta = \eta + \delta_s$, where δ_s represents the yield of true secondary electrons.

1.1.2 Yield curve

The variation of total yield δ with the primary energy E_p is an important property of secondary electron emission and has been studied most extensively. The general shape of the yield curve which is a plot of δ against E_p is shown in Fig. (1.1). It follows from the yield curve that the yield increases rapidly at low primary energies. This increase reaches a maximum as the primary energy is increased and then begins to decrease slowly with the further increase in the primary energy. The shape of the yield curve for almost all solids is very similar. A qualitative explanation of the variation of yield with the primary energy can be given as follows. At low primary energies the penetration depth of the primaries is relatively small, and thus the energy dissipated by the primaries to create secondaries is in a region close enough to the surface for a large fraction of the excited internal secondaries to escape. As the primary energy increases, the yield continues to increase until it attains its maximum value at some value of the primary energy when the penetration depth of the primaries becomes approximately equal to the escape depth of the secondaries. At high primary energies, the yield decreases because the penetration depth of the primary electrons becomes large compared to the

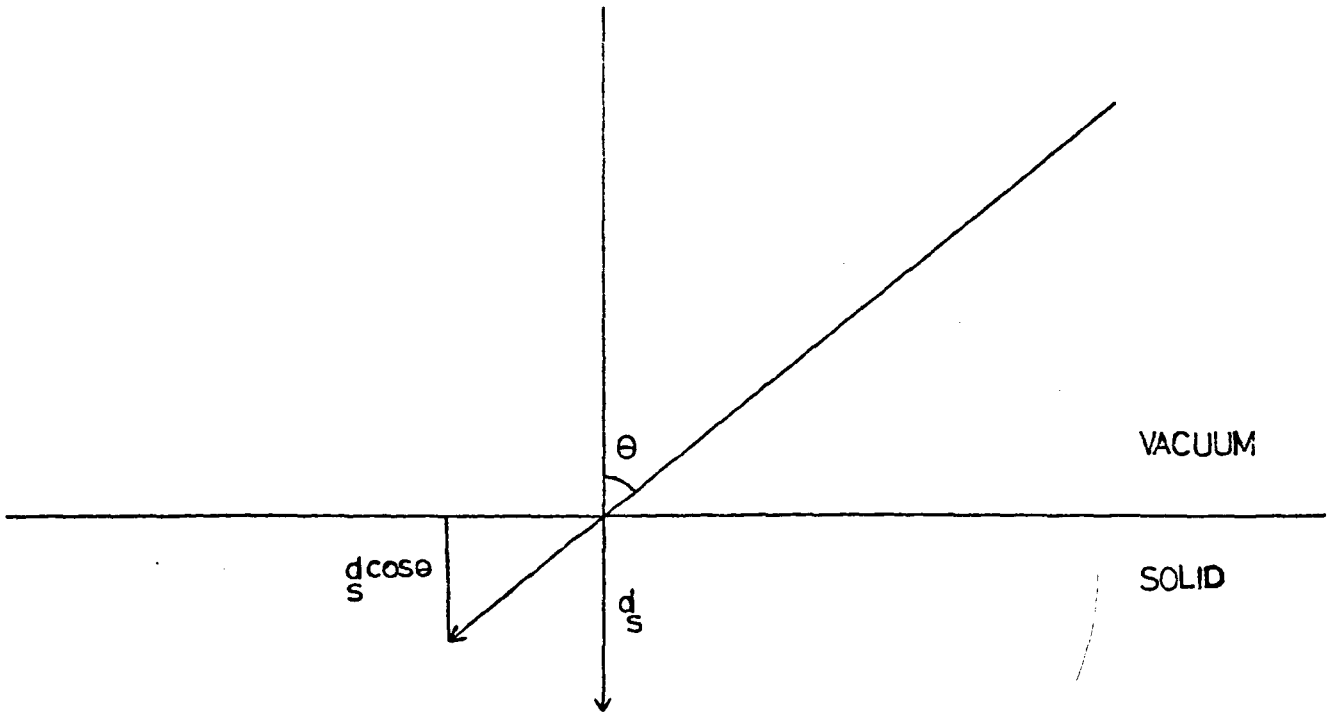

Fig. 1.2 Variation of the mean depth of origin of secondaries with angle of incidence of primaries.

escape depth for the secondary electrons. In addition the number of internal secondaries created within the escape depth of the surface decreases with increasing primary energy because the number of secondaries created per unit path length is a decreasing function of energy.

1.1.3 Angular Variation of Yield

The increase in yield with the increase in angle of incidence has been observed by several investigators. This increase is attributed to the change in the mean depth of origin of the secondary electrons. If d_s is the mean depth of origin of the secondaries (Fig.(1.2)) for normal incidence, then for an angle of incidence θ of the primary electrons, this depth would be $d_s \cos\theta$ from the surface of the solid. The variation of yield with angle of incidence is more prominent for high energy primary electrons as compared to low energy ones. This is because for low primary energies, there is little change in the mean depth of origin of the secondaries with the change in the angle of incidence, while, for high primary energies this change is greater. Also for larger angles of incidence, δ_{max} is shifted to higher values of primary energies. Bruining[5] has derived a relation for variations of yield with angle of incidence. It is assumed that the secondaries produced at a depth $d \cos\theta$ in the solid are absorbed exponentially on their way to the surface. If α be the absorption coefficient and C a constant, then for normal incidence

$$\delta_o = C \exp(-\alpha d_s) \qquad (i)$$

and for angle of incidence θ

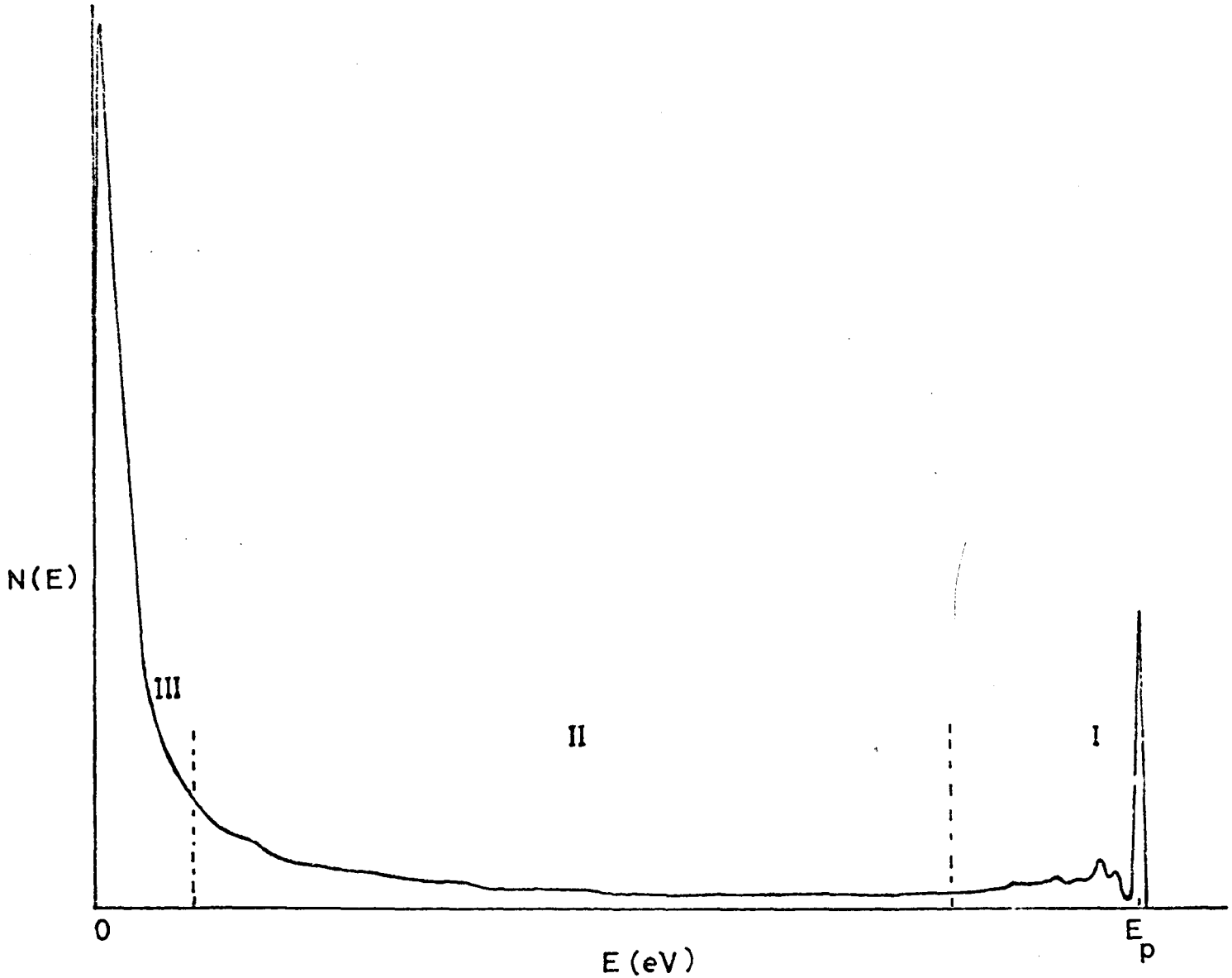

Fig. 1.3 General shape of the energy distribution curve.

$$\delta_\theta = C \exp(-\alpha d_s \cos\theta) \qquad \text{(ii)}$$

From expressions (i) and (ii)

$$\log(\delta_\theta/\delta_o) = \alpha d_s(1 - \cos\theta)$$

From this expression, an estimate of the depth of origin can be obtained if α is known. The secondary yield is considerably affected by the surface contaminations and other surface conditions such as roughness. The presence of an impurity on a surface may result in the increase or decrease of yield. It is therefore of paramount importance that clean surfaces should be maintained in order to observe the true yield characteristic of the surface.

A rough surface is known to exhibit a lower secondary yield as compared to a smooth surface of the same element. This lower yield is believed to be due to trapping of the secondary electrons within the surface region due to its unevenness.

1.2 Energy Distribution of Secondary Electrons

The energy distribution of secondary electrons emitted from various solids is similar in general outline although fine structure in the energy distribution differs appreciably from one solid to another. The general shape of an energy distribution curve is shown in Fig.(1.3). The distribution falls into three distinct regions.

(i) Region I consists of a sharp peak and some fine structure below it. The sharp peak is believed to be due to electrons which have suffered elastic collisions with the lattice and are backscattered without energy

loss. The small peaks close to this elastic peak are presumably due to the electrons which have suffered inelastic collisions. Most of these electrons have lost discrete amounts of energy in the excitation of, for example, plasmons or interband transitions. These loss peaks are characteristic of the material and are usually known as characteristic energy losses. They are always a fixed distance from the elastically reflected peak and are thus measured relative to this peak.

(ii) The second region appears to be relatively flat with a few poorly defined peaks. However under high sensitivity and resolution, a great deal of fine structure may be observed. The peaks in this region may be due to either ionisation losses or Auger emission.

(iii) The third region consists of a large peak, the maximum of which occurs at a few electron volts. This peak is believed to be due to true secondaries (with energies <50eV). Some peaks due to Auger emission may occur in this region, superimposed on the very much larger peak due to slow secondaries. It is evident from the above description of the energy distribution of the secondary electrons that, apart from the two main peaks (elastic peak and slow secondaries peak), there are distinctly two types of processes involved which result in the appearance of small peaks. The first type is due to a characteristic energy loss process and occurs at a fixed amount of energy loss from the elastic peak and is measured relative to the elastic peak. The second type is due to Auger electron emission. The energy of these electrons is independent of the primary energy of bombarding electrons, thus their energy is measured relative to zero energy.

1.2.1 Characteristic energy losses

The interactions responsible for the discrete energy losses suffered by the incident electrons are (i) single particle or electron-electron interaction and (ii) the plasmon excitation process.

In a single particle interaction an incident electron may lose energy to an electron in the solid, and this may result in the excitation of that electron to some higher empty energy level. The result may be the ionization of the particular atom of the solid if some core electron is expelled, or an intraband or an interband transition for valence electrons. The ionization losses are quite significant since these can be used for surface elemental analysis, and this technique of surface analysis has more recently become known as the ionization spectroscopy[6]. In an ionization process, if E_p be the primary energy and E_s the energy of the backscattered electrons which have suffered an energy loss E_L and if E_K be the binding energy of the K^{th} shell, where $E_p >> E_K$, then $E_L = E_p - E_s = E_K$. The ionization losses are spread over a wide range of energy and usually appear as 'steps' or very weak humps in the energy distribution curve. However, these peaks can be observed more clearly in the derivative of the energy distribution. In order to achieve maximum intensity of these peaks, it is essential to have the primary energy 3-5 times[7] the binding energy of the energy level to be ionized. The study of ionization losses is also important in Auger spectroscopy since it can aid the correct identification of the 'corresponding' Auger peak which may arise as a result of the ionization of the core electrons. Extra care must be taken in the identification of the ionization losses since these losses sometimes appear very

close to the Auger peaks in the differential distribution. This overlapping can be avoided by changing the primary energy. In such a case the ionization peak would shift in energy by an amount equal to the change in the primary energy.

1.2.2 Plasmon excitations

Incident electrons may suffer discrete energy losses in the excitation of plasmons - a collective oscillation of the valence electrons of the solid. This was first pointed out by Bohm and Pines[8] who developed the theory of plasma oscillations in solids. A simple qualitative explanation is as follows. The solid may be considered to be made up of ion cores which contain the nucleus and strongly bound electrons and loosely bound valence electrons. It is assumed that the charge of the ion core is to be smeared out over the solid so as to form a background of positive charge and this charge is neutralised by the valence electrons which are considered to be free. Thus the charge density of electrons and ions on the average is zero. However, a chance fluctuation in the thermal motion may result in the reduction of the charge density below the average in some region. The positive background in the region no longer neutralised and the excess positive charge attracts the neighbouring electrons to restore the charge neutrality. But because of their relatively high mobility, electrons gather sufficient momentum and produce excess negative charge in the region. This results in the repulsion of the electrons from the region again and thus collective oscillations are set up which are usually known as plasma oscillations. The energy levels of these oscillations are quantized in

intervals of $\hbar\omega_p$ where ω_p is the plasma frequency given by the expression

$$\omega_p = \left(\frac{4\pi ne^2}{m}\right)^{\frac{1}{2}}$$

where n = electron density

e = electronic charge

m = mass of an electron.

The plasma oscillations can be represented by a finite set of harmonic oscillators with angular frequency ω_p. Pines has given the name 'plasmon' to a quantized plasma oscillator. The energy of such an oscillator must have values given by the expression $(N + \frac{1}{2})\hbar\omega_p$, where N is a positive integer or zero. The ground state energy (for N = 0) of the plasmons is given by $\frac{1}{2}\hbar\omega_p$. The energy required to raise the plasmons from the ground state to that of next higher energy - the excitation energy - is

$$\hbar\omega_p = \hbar\left(\frac{4\pi ne^2}{m}\right)^{\frac{1}{2}}$$

The energy loss suffered by incident electrons in this mode of excitation of plasmons is known as a volume or bulk plasmon loss. If A be the atomic weight of the solid, d its density, n_v the number of valence electrons, then the value of the bulk plasmon loss is given by the expression

$$\hbar\omega_p = 28.8\left(\frac{n_v d}{A}\right)^{\frac{1}{2}} \text{ eV} .$$

Thermal excitation of the plasmons can be neglected since the excitation energy of a plasmon ($\hbar\omega_p$) is several electron volts, very much greater than the thermal energy of any electron at normal temperatures.

Thus the plasmons will remain in their ground state unless excited by some other method, such as the passage of energetic electrons. Ritchie[9], in 1957, pointed out that in addition to the excitation of the bulk plasmons in the solid, incident electrons may lose energy in the excitation of 'surface plasmons' at interface between the solid surface and the vacuum. The frequency of the surface oscillations is given by $\omega_p/\sqrt{2}$, and the excitation energy of these surface oscillations is then $\hbar\omega_p/\sqrt{2}$.

Stern and Ferrell[10] derived a more generalised expression for the surface plasmons, considering the case of a semi-infinite electron gas bounded by a semi-infinite dielectric medium. If ε be the dielectric constant of the bounding medium, then ω_s, the frequency of the surface oscillations, is given by the relation

$$\omega_s = \frac{\omega_p}{(1+\varepsilon)^{\frac{1}{2}}}$$

For a plasma bounded by vacuum, $\varepsilon = 1$, then the above expression is reduced to Ritchie's result. However, if the dielectric medium bounding the solid surface is not vacuum, as it may be in the case of a contaminated surface, then $\varepsilon \neq 1$ and consequently the frequency of the surface oscillations would also be changed. This dependence of the frequency of the surface plasma oscillations on the media surrounding the solid surface explains the extreme sensitivity of the surface plasmon loss to contamination.

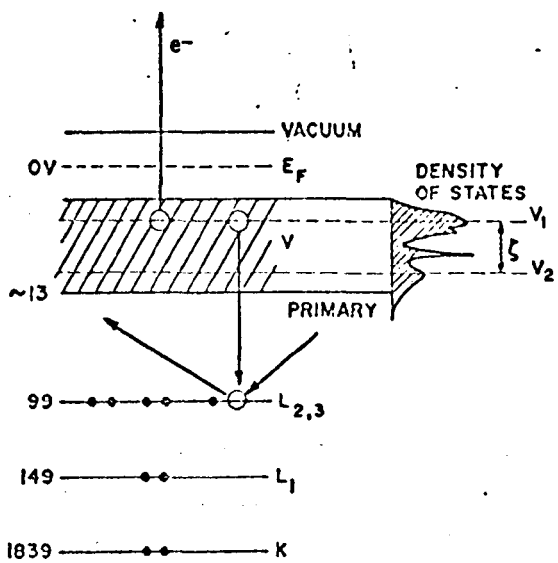

Fig. 1-4 X-ray energy level diagram of silicon with the density of states drawn into the valence band. An $L_{2,3}VV$ Auger process is depicted.

1.3 Auger Electron Emission

It has been pointed out in the previous section that the small peaks in the region (ii) and (iii) of the energy distribution curve may be due to Auger electron emission. These peaks were first reported by Lander[1], who correctly identified them as due to Auger electrons. The discovery of these electrons was first made by P. Auger[11] in 1925, from their tracks in a Wilson Cloud chamber and he correctly explained their origin.

Although Lander[1] suggested that the identification of the Auger peaks could provide an excellent means for surface analysis since these peaks are characteristic of the element from which they originate, the technique was not applied subsequently until quite recently because of poor sensitivity. However, Harris[2] demonstrated that a considerable improvement in sensitivity could be achieved by observing the derivative of the energy distribution obtained by electronic differentiation. Since then, the technique of Auger electron spectroscopy has quickly emerged as a very sensitive method for surface analysis.

1.3.1 The Auger electron emission mechanism

The Auger electron emission process is basically the result of three physical processes. These are (i) the ionization of inner shell electrons by an energetic beam of incident electrons (or other particle); (ii) de-excitation through Auger process and (iii) the escape of the Auger electrons in the vacuum without significant loss of energy. These effects are illustrated in the schematic energy band diagram of Fig.(1.4).

An incident electron ejects an electron from the $L_{2,3}$ shell and thereby the atom becomes ionized. The vacancy thus created is filled by an electron from the valence band. In the Auger process, the transition energy must be given to another electron (in this case the valence band) rather than to a photon. In such a case, if the energy is sufficient, the electron may be emitted as shown in Fig.(1.4). The energy of the emitted Auger electron will be then given approximately by

$$E = E_{L_{2,3}} - E_V - E_V$$

and would be designated the $L_{2,3}VV$ transition. It is clear that in an Auger process an atom is ionized twice. Therefore after the first ionization the binding energies of the electrons in the various bands would increase. To account for this in the calculation of the energy of Auger electrons, the binding energy of the 'third' electron (which is to be emitted as the Auger electron) is taken as $E_V(Z + \Delta)$, where Z is the atomic number of the element and the value of Δ lies between $\frac{1}{2}$ and $\frac{3}{4}$, as observed experimentally[12]. However, the Auger electron energies calculated for $\Delta = 1$, show a remarkably good agreement with the experimentally observed energies of Auger electrons.

A general formula for the calculation of Auger electron energies can thus be written in the form

$$E(Z) = E_A(Z) - E_B(Z) - E_C(Z+1) - \phi_a$$

where E(Z)= the kinetic energy of the Auger electrons, $E_A(Z)$, $E_B(Z)$ and $E_C(Z+1)$ are the binding energies of the electrons in A, B and C shells for

atomic number Z and (Z+1) respectively, ϕ_a is the effective work function of the surface of the energy analyser directly involved in the energy analysis.

1.3.2 Ionization cross-section

The initial process in the Auger electron emission is the ionization of the core electrons by the incident electrons. Bishop and Riviere[7] suggest that the modified Born approximation of Worthington and Tomlin[13] which has proved successful for X-rays, is adequate for estimating the ionization cross-section, σ. This expression is

$$\sigma = (2\pi e^2/E_p E_c)\, b\, \ell n(4E_p/B)$$

where e = electronic charge

E_p = incident electron energy

E_c = critical ionization potential of ionized shell

b = 0.35 for K shell electrons

and b = 0.25 for L shell electrons.

For $E_p >> E_c$, B takes the value of $1.65E_c$. The ionization cross-section should be zero for $E_p = E_c$. To allow this to happen and also to make the variations of σ with the incident energy, Worthington and Tomlin put

$$B = \left[1.65 + 2.35 \exp(1 - U)\right] E_c$$

where $U = E_p/E_c$. Substituting this in the above value of σ and also substituting the values of constants the expression becomes

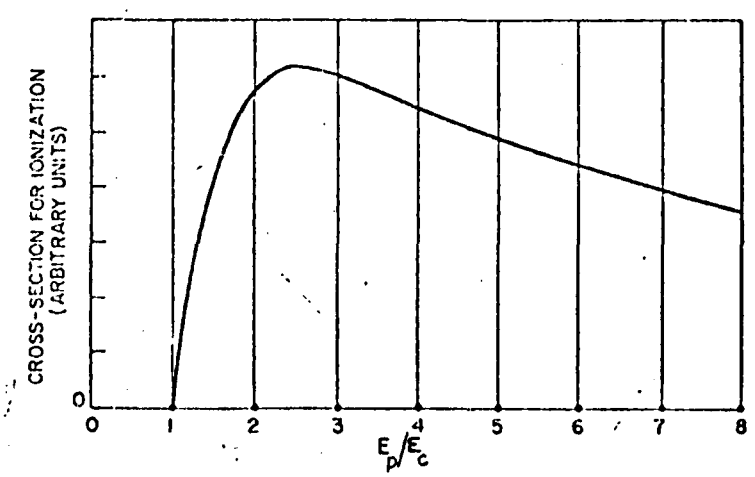

Fig. 1.5 Variation of the ionization cross-section with the ratio of primary energy E_p to the level energy E_c (from ref. 7).

$$\sigma E_c^2 = 1.3 \times 10^{-13} b \frac{1}{U} \ell n \left[4U/\{1.65 + 2.35 \exp(1 - U)\}\right] cm^2(eV)^2$$

The plot of function $\frac{1}{U} \ell n\left[4U/\{1.65 + 2.35 \exp(1 - U)\}\right]$ is shown in Fig.(1.5). It rises steeply from zero at $E_p = E_c$, to a maximum between U = 2 and U = 3 and then decreases slowly with increasing U.

It may be pointed out that in the above calculations the effect of secondary ionization has not been taken into account. Secondary electrons with energies greater than E_c may cause ionization, increasing the effective incident beam current. The effect can greatly enhance ionization[14] especially for surface atoms and for smaller values of the binding energies of the inner shells involved in the ionization, because of the rapidly increasing number of secondary electrons at lower energies. This is presumably the reason that the Auger peaks are generally larger than the 'corresponding' ionization losses.

1.3.3 Photon production and Auger efficiency

The second process in Auger electron emission involves the de-excitation through the Auger process after the initial ionization. The alternative mode of de-excitation of course is by photon (X-ray) emission. The probability of photon production[15] is given by the equation

$$\omega = (1 + \alpha Z^{-4})^{-1}$$

where $\alpha = 1.12 \times 10^6$ for K electrons

and $\alpha = 6.4 \times 10^7$ for L_{III} electrons.

Z = atomic number.

Using the above relation it can be easily shown that the probability of photon production is negligible for the energy ranges generally used in Auger spectroscopy (viz. 0 - 3000 volts). Therefore the Auger efficiency is much higher as compared to that for X-ray emission especially in the case of the lighter elements where the energy of the inner shell to be ionized is <500eV. The Auger efficiency becomes roughly comparable to X-ray production at about 2 keV. The relative efficiencies depend more on E_A and E_B (the binding energies of the inner shell to be ionized and the second electron which fills the vacancy) rather than the atomic number Z. Therefore the Auger current for higher Z elements will be relatively constant provided the lower energy transitions are investigated. Such transitions are further favoured since higher Z elements have larger numbers of outer shell electrons.

1.3.4 Escape depth of Auger electrons

The third process (iii) regarding the Auger emission is the escape of Auger electrons into the vacuum without significant loss of energy. The escape depth of Auger electrons depends on the kinetic energy of the Auger electrons and the substrate materials. Experimental results[4] indicate that this depth is only a few Angstroms for Auger electrons with energy less than 500eV. It is this particular feature of Auger electron emission that makes the technique of Auger spectroscopy an especially valuable and excellent tool for surface studies. The range of the primary electrons is, however, much larger than the escape depth of the Auger electrons. This means that the Auger electrons are ejected from a much

narrower region than that excited by the energetic primary beams, since this excited region is determined by the range of the primary electrons. It may be pointed out that the Auger emission region in a solid can be increased by using a grazing incidence for the primary electrons. The optimum angle lies between 15^0 and 20^0 from the solid surface[16].

1.3.5 Auger peak width and associated fine structure

Auger peaks are usually 2 - 10eV wide. The width is larger for the transitions involving the valence band. One such transition is depicted in Fig.(1.4). The energy of the Auger electrons for the $L_{2,3}V_1V_1$ transition is given by

$$E_1 = E_{L_{2,3}} - 2E_{V_1}$$

Since there are no known selection rules, unlike the case of X-ray emission, any other electron within the band may be emitted as the Auger electron. If E_2 be the energy of such an Auger electron for a transition $L_{2,3}V_2V_2$, then

$$E_2 = E_{L_{2,3}} - 2E_{V_2} = E_1 - 2\varepsilon$$

where $\varepsilon = V_2 - V_1$. Thus for a bandwidth of ε the width of the Auger peak will be 2ε. This, however, may not result in a single peak of width 2ε due to the variations in the density of states within the valence band. In addition Auger peaks are also affected by lifetime broadening due to the short transition times involved ($\sim 10^{-16}$sec)[17].

Almost all Auger peaks seem to have a 'tail' on the low energy side. This was first observed by Lander[1] and has been reported by several workers recently. This tailing structure (on the low energy side of the Auger peaks) is attributed to the Auger electrons which have lost a discrete amount of energy in the excitation of plasmons, on their way to the surface. In such a case, if E be the energy of the main Auger peak and E_{pl} the excitation energy of the volume plasmons, then the energy E_1 of the 'tail peak' will be given by

$$E_1 \approx E - E_{pl}$$

The effect has been experimentally observed by Mularie and Rusch[18] and others[19,20]. In the course of present work, under high sensitivity and resolution conditions, fine structure was also resolved[21] on the high energy side of the Auger peaks, similar to the structure on the low energy side of the main Auger peak. Since this work was done, a similar structure has been reported by Jenkins and Chung[22]. This structure on the high energy side of the Auger peak is considered to be due to the Auger electrons which have gained energy from the excited plasmons. In this case the energy E_2 of the peak on the high energy side of the main Auger peak is $E_2 \approx E + E_{pl}$. This work will be considered and reported in greater detail in Chapter V.

1.3.6 Chemical effects

An important aspect of Auger electron spectroscopy is that valuable information can be obtained from the changes in the Auger spectra of

elements as they form compounds. Changes in the chemical state of the surface atom may be reflected in several ways, including a shift in energy, a change in the relative size of the Auger peaks, and the appearance of 'new' Auger peaks. Small chemical shifts may take place in the case of the transitions involving inner shell electrons. This shift can be attributed to the shift in the binding energy of the core electrons due to the redistribution of valence electrons on forming a chemical bond. More drastic chemical effects may take place in the Auger spectrum as a result of chemical bonding if the Auger transitions involve a valence band. These effects again will be described in more detail with experimental data in Chapter V. It may be noted that the energy shifts observed in Auger spectra are only indirectly related to the actual shifts in the energy levels.

1.4 Conclusion

The basic processes along with the other important features of secondary electron emission have been described. There are three parameters of secondary electron emission which are highly significant. These are

1) the total secondary electron yield,
2) the characteristic energy loss phenomenon,
3) Auger electron emission.

The simple principles and the other relevant aspects of the technique of Auger electron spectroscopy - which is based on the Auger electron emission - have been described. A review of the relevant experimental work is presented in the next chapter.

CHAPTER II

REVIEW OF PREVIOUS EXPERIMENTAL WORK

2.1 Introduction

Although Auger spectroscopy is one of the more recent techniques for surface studies, a considerable amount of experimental work has already been published. The technique has perhaps drawn more attention because of the ease with which existing LEED systems can be modified to do experimental Auger analysis, and also because analysis of the data obtained is relatively simple. A review of the experimental work is presented in this chapter. The experimental work describing the characteristic Auger spectra and the various parameters involved in Auger spectroscopy are given in section 2.2.1. A comparative study of various energy analysers currently in use is presented in section 2.2.2. Recent work on the characteristic energy losses is described in section 2.2.3.

2.2.1 Previous experimental work on Auger spectroscopy

As mentioned in Chapter I, it was Lander[1] who first observed Auger emission in the study of the energy spectra of the secondary electrons from a number of elements. He suggested that the identification of the Auger peaks provided a method for surface analysis. However the sensitivity of the method was extremely low.

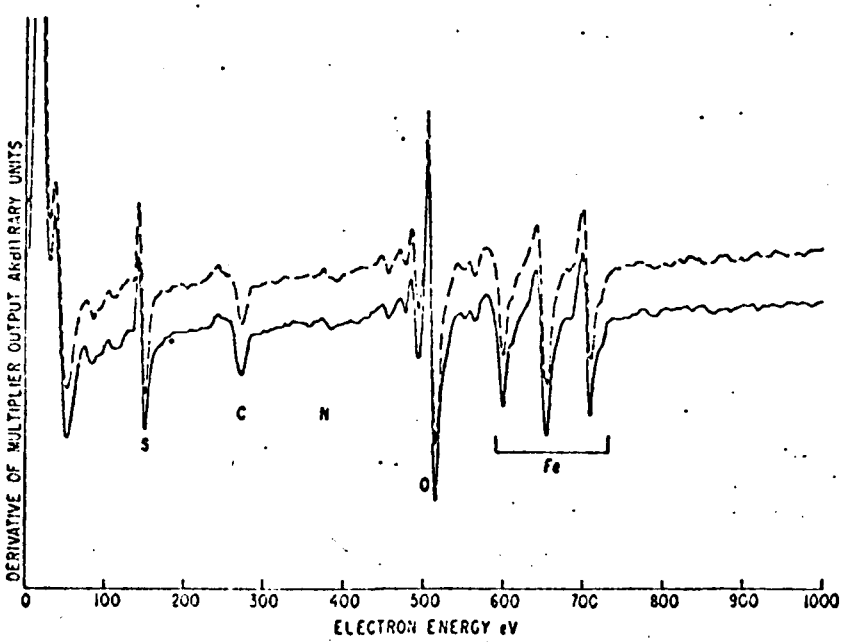

Fig. 2.1 Auger spectrum of an uncleaned alloy steel as observed by Harris[2].

A few years after Lander's[1] paper, Harrower[23] reported the Auger spectra of tungsten and molybdenum. Although he took great care to obtain clean surfaces and maintained lower base pressures during the measurements, there was no improvement in the sensitivity. A similar attempt to observe the Auger spectra of tungsten, graphite and copper was made by Scheibner and Tharp[24]. The main feature of their studies was that they, for the first time, used a LEED system for energy distribution studies. Again the limiting factor was the comparatively low sensitivity of the method. This 'sensitivity problem' was overcome by Harris[2] who demonstrated that a significant increase in sensitivity could be obtained if the first derivative of the energy distribution was observed, instead of the energy distribution itself. He used a 127^{o} velocity analyser, and a typical Auger spectrum he obtained is shown in Fig.(2.1). It is evident from the spectrum that poorly defined humps in the energy distribution curve become quite large sharp peaks in the differential distribution. Using this technique, Harris[2] was able to study the surface composition of alloys of Ni and Cu, and various types of steels. He also identified several common contaminants previously undetectable in the magnitudes involved on the 'uncleaned' surfaces. However, he was unable to evaluate the sensitivity of the method for minimum amounts of impurity, because of segregation of bulk impurities at the sample surface. A quantitative assessment of the sensitivity of the method was reported by Weber and Peria[3] who used a LEED system for their studies. They evaporated known amounts of Cs on Si and found that quantities as small as one tenth of

a monolayer could be detected. The limiting factor was the slope on which the Cs Auger peak was superimposed. Although the last limit of the sensitivity has not yet been fully established, some workers[25,26] have reported that amounts ≤1% of a monolayer are possibly detectable. In Auger spectroscopy the information about the surface composition depends on the depth from which the Auger electrons are ejected. An estimate of the escape depth of Auger electrons was obtained by Palmberg and Rhodin[4]. They evaporated silver, layer by layer onto a gold substrate and observed the decay of the 72eV Au Auger peak and, at the same time, build-up of the 362eV silver Auger peak. The escape depths for 72 and 362eV electrons were found to be only 4Å and 8Å respectively. Similar results have been reported by Charig and Skinner[26] and Jacobi and Hölzl[27]. Although no absolute calibration of the technique for general applications has yet been devised, some absolute calibrations have been obtained in several specific cases. Weber and Johnson[23] found that, by evaporating known amounts of K on Ge, the amplitude of 252eV K Auger peak increased linearly with the surface coverage up to a monolayer. Uebbing[29] applied the technique of Auger spectroscopy quantitatively to monitor the carbon contamination on the GaAs-Cs-O photocathodes. It was found that approximately one monolayer of carbon was sufficient to reduce the photo yield to zero.

Vrakking and Meyer[30] have recently reported that the Auger peak height was proportional to the surface coverage up to 1.5 monatomic layers. Their calibration involved the measurement of adsorption of Oxygen on a silicon surface using ellipsometry.

The variation of the Auger peak amplitude with the primary energy - the Auger yield - for a clean surface has been reported by Haas et al.[31] and Bishop et al.[32]. The optimum primary energy for the maximum ionization of the inner shell was found to be some 3 - 4 times the ionization potential of the inner shell involved in the Auger transition. This is in agreement with the theoretical calculation of Bishop and Riviere[7]. However, in the case of contaminated surfaces[32] the primary energy for the maximum Auger yield is somewhat higher (about 5 - 6 times the ionization potential of the inner shell). Chemical effects such as a shift in the Auger peak of one element on chemical bonding with another have been reported by several workers[33,19,21,34]. These effects will be discussed more fully in Chapter V. Other work on the Auger spectra of several elements has been reported by Palmberg and Rhodin[4], Haas et al.[31], Bishop et al.[32] and Coad and Riviere[35]. In general, the spectra of elements in the same period of the Periodic Table are similar, the main difference being the energy at which the Auger peaks appear.

A brief review describing the basic principles of Auger electron emission, the detection techniques used for Auger spectra and a discussion of the information obtained from the Auger spectra etc., has been published by Chang[36].

2.2.2 Electron energy analysers

The electron energy analysers presently used in the Auger electron spectroscopy are basically of two types, viz. the retarding field type and velocity analysers of which two are the 127° sector analyser[2] and the

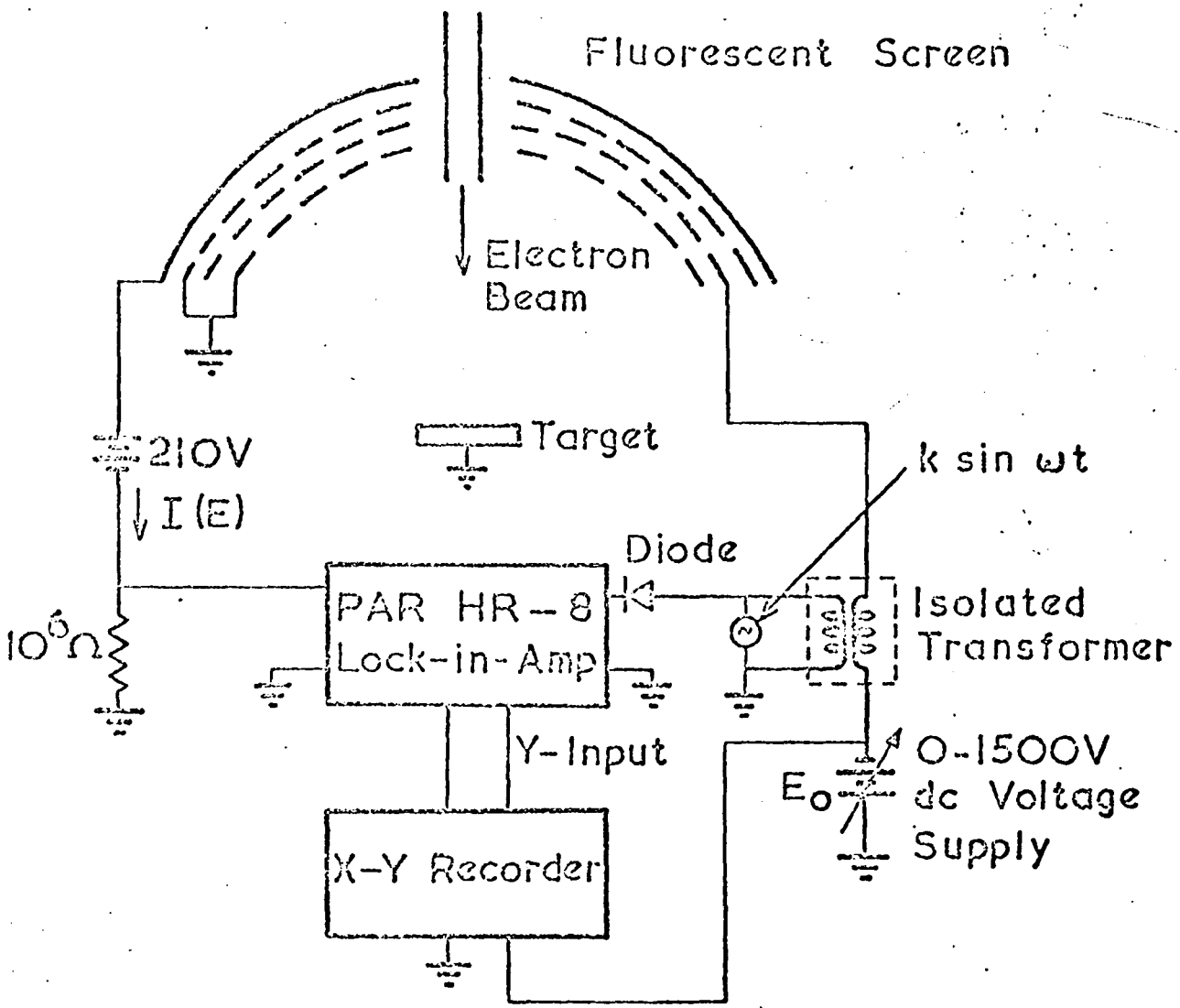

Fig. 2.2 Retarding field analyser used by Palmberg and Rhodin[4].

cylindrical mirror analyser[37]. However the retarding field type is the most commonly used energy analyser (Fig.(2.2)), since with slight modifications it can be adapted from the system used for LEED studies, work function and secondary electron yield measurements. The construction and operation of this type of analyser is also relatively simple. The energy distribution and its derivative are obtained by an electronic differentiation method[38]. For small modulation amplitudes, the first and second harmonic of the collector current are proportional to the energy distribution and its first derivative. This can be shown as follows:

If I(V) be the collected current as a function of the retarding voltage V, and if the applied modulation signal is K sin ωt, then a Tayler's series expansion of I(V + K sin ωt) can be carried out to give

$$I(V + K\sin\omega t) = I(V) + K\sin\omega t\, I'(V) + \frac{K^2\sin^2\omega t}{2!}I''(V) + \frac{K^3\sin^3\omega t}{3!}I'''(V) + \ldots$$

$$= I(V) + K\sin\omega t\, I'(V) + \frac{K^2}{2.2!}(1 - \cos 2\omega t)I''(V) + \frac{K^3}{4.3!}(3\sin\omega t - \sin 3\omega t)I'''(V) + \ldots$$

$$= \left[I(V) + \frac{K^2}{4}I''(V) + \frac{K^4}{64}I^{IV}(V) + \ldots\right] + \left[KI'(V) + \frac{K^3}{8}I'''(V) + \frac{K^5}{192}I^{V}(V) + \ldots\right]\sin\omega t - \left[\frac{K^2}{4}I''(V) + \frac{K^4}{48}I^{IV}(V) + \frac{K^6}{1536}I^{VI}(V) + \ldots\right]\cos 2\omega t - \left[\frac{K^3}{24}I'''(V) + \frac{K^5}{384}I^{V}(V) + \ldots\right]\sin 3\omega t + \ldots\ldots$$

The amplitude of the fundamental frequency is given by

$$A_1 = KI'(V) + \left(\frac{K^3}{8}\right) I'''(V) + \frac{K^5}{192} I^V(V) + ... \qquad (A)$$

and that of the second harmonic is

$$A_2 = \frac{K^2}{4} I''(V) + \frac{K^4}{48} I^{IV}(V) + \frac{K^6}{1536} I^{VI}(V) + ... \qquad (B)$$

In the above equations the higher order terms can be neglected if K is small and then A_1 will be proportional to I'(V) and A_2 to I"(V). If the modulation amplitude K is large enough so that the K^3 term in equation (A) cannot be neglected, then the fundamental frequency will no longer be given by I'(V), but the second harmonic will still be given by I"(V). Thus a relatively larger modulation amplitude may be used when the derivative of the energy distribution is desired. However, with large modulation amplitudes, both the fundamental frequency and the second harmonic become less proportional to I'(V) and I"(V).

The manner in which the maximum second harmonic current varies with the amplitude of modulation, has been reported by Bishop and Riviere[7]. It is found that the current in the second harmonic will increase with the square of the amplitude of the modulation up to an amplitude of about the r.m.s. width of the Auger peak, and after that it will flatten off with increasing modulation to a constant value. However, large modulation amplitudes have an effect on the resolution of the analyser, and are not desirable, particularly when weak fine structure in the Auger spectrum is to be studied.

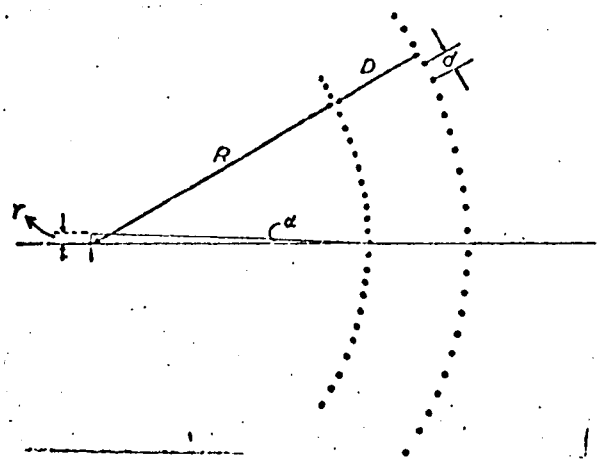

Fig. 2.3 Schematic diagram of a retarding field analyser.

The above mentioned energy resolution is an important parameter of an energy analyser. The resolution R_E is usually defined as the percentage ratio of the energy spread ΔE of the collected electrons to the energy E of these electrons. Thus

$$R_E = \frac{\Delta E}{E} \times 100\ \%$$

The resolution of the retarding field analyser principally depends on the size of the apertures of the retarding grid and its separation from the first grid (Fig.(2.3)). The potential at the centre of a circular aperture of diameter d having a field F on one side differs by $(d/\pi)F$ from the potential at the edge. If this field F arises from a potential difference V between the two grids, separated by a distance D, then this potential difference is $\Delta V = (d/\pi)(V/D)$[39]. The resolution of the analyser is then given by $R_E = \frac{\Delta V}{V} = \frac{d}{\pi D}$. The resolution also depends on the spot size of the incident beam. Ideally it should be a point source of electrons. However in practice it has finite size. In the case of this extended source all the electrons, except those from the centre of the source, will have non-radial paths. If v is the velocity of the electrons from the centre which are just transmitted, then the velocity of the electrons from the edge of the source will be $v/\cos\alpha$. The fractional difference in energy, $(\frac{\Delta V}{V})$, between these electrons is $(1 - \cos^2\alpha) \simeq \alpha^2$. From Fig.(2.3) $\alpha R = r$,

$$\therefore \frac{\Delta V}{V} = \alpha^2 = (\frac{r}{R})^2$$

where R and r are the radii of the first grid and electron source.

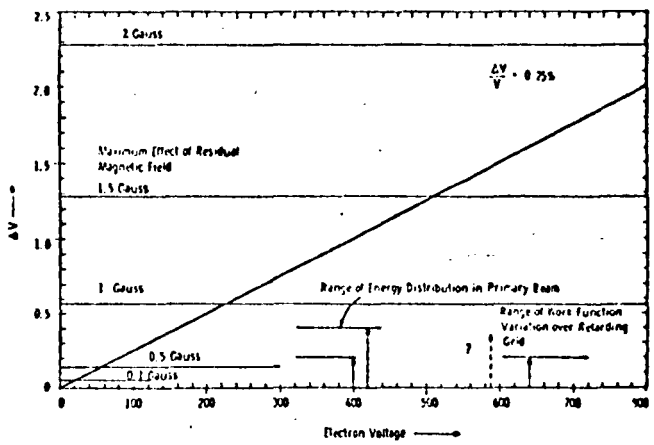

Fig. 2.4 Effect of stray magnetic field on the resolution of a retarding field analyser[40].

The factors which affect the resolution of a retarding field analyser are briefly described below.

a) Field penetration effect: ideally a retarding grid should be an equipotential surface, but in practice the potential variations may occur across each mesh. This results in an energy shift of the Auger peak and also the cut-off may occur at higher energies[16]. To minimise this effect, the grids should be made of smaller mesh size. This is of course limited by constructional difficulties. One very practical solution to this problem, as suggested by Palmberg[16], is to use two retarding grids connected electrically together.

b) The electrons passing through the first grid suffer divergence at each mesh since this grid is usually kept at ground potential. This divergence results in resolution degradation and can be minimised by reducing the diameter of the first grid and making the grid of small mesh size.

c) Deviation of grids from sphericity: these deviations result in a non-radial field between the first grid and the retarding grids. The trajectories of the electrons in such a field will be non-radial which can affect the energy cut-off.

d) Stray magnetic field: stray magnetic fields can have severe effects on the resolution of the energy analysers. This effect is shown graphically in Fig.(2.4)[40]. It follows from Fig.(2.4) that a magnetic field less than 0.5 gauss will have no effect on the resolution for primary energies above 100eV. Since high primary energies (~1 - 3KeV) are used in Auger

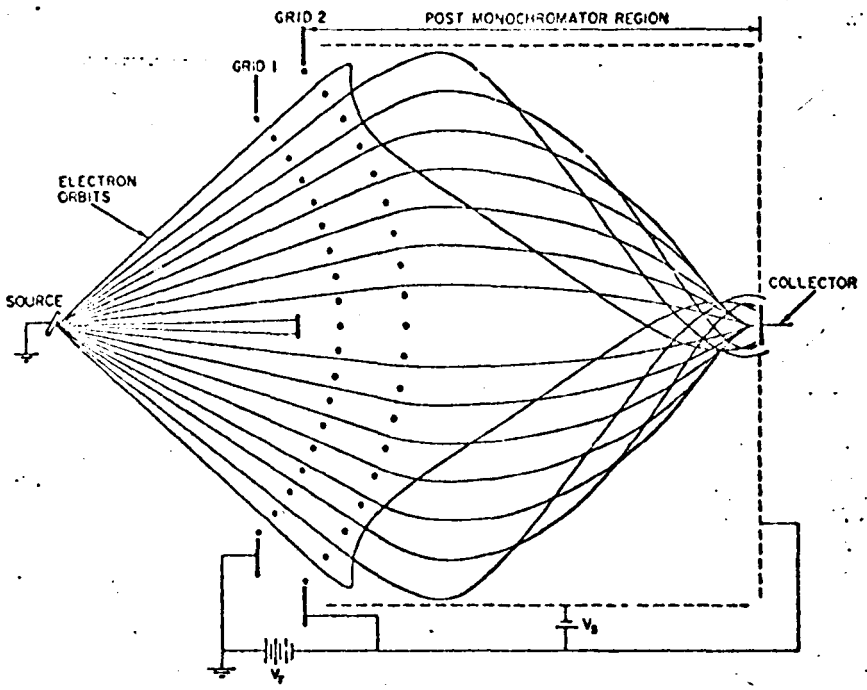

Fig. 2.5 Retarding field analyser with a post monochromator[41].

spectroscopy, a modest magnetic shielding serves to eliminate the effect of stray magnetic fields.

The principle of operation of the retarding field analyser lies in the fact that the electrons with energy less than E (= eV), where V is the voltage applied to the retarding grids, do not reach the collector. This means that the retarding field analyser acts as a high-pass electron energy filter. As the retarding voltage on the grids is decreased, the number of unwanted high energy electrons which can reach the collector increases. These electrons only contribute to the background noise and thus the signal-to-noise ratio of the analyser is considerably and adversely affected. This is the main drawback of retarding field type analysers. One solution to this comparatively poor signal-to-noise ratio has been suggested by Huchital and Rigden[41]. Since for the present purpose (i.e. Auger emission) the only electrons of interest in a retarding field analyser are those which pass the retarding grids with a minimum kinetic energy, Huchital and Rigden[41] suggest the collection of only these slow electrons by focussing them onto a small isolated collector. This is achieved with a post monochromator. Thus all the undesirable fast electrons do not reach the collector. A sketch of the configuration in which this effect is achieved is shown in Fig.(2.5). The authors claimed to have high resolution (0.05%) with this modified retarding field analyser. Jacobi and Hölzl[27] have used a 360^{o} retarding field analyser to study the Auger spectra of thin films. Both reflected and transmitted electrons are collected. The resolution of the instrument is reported to

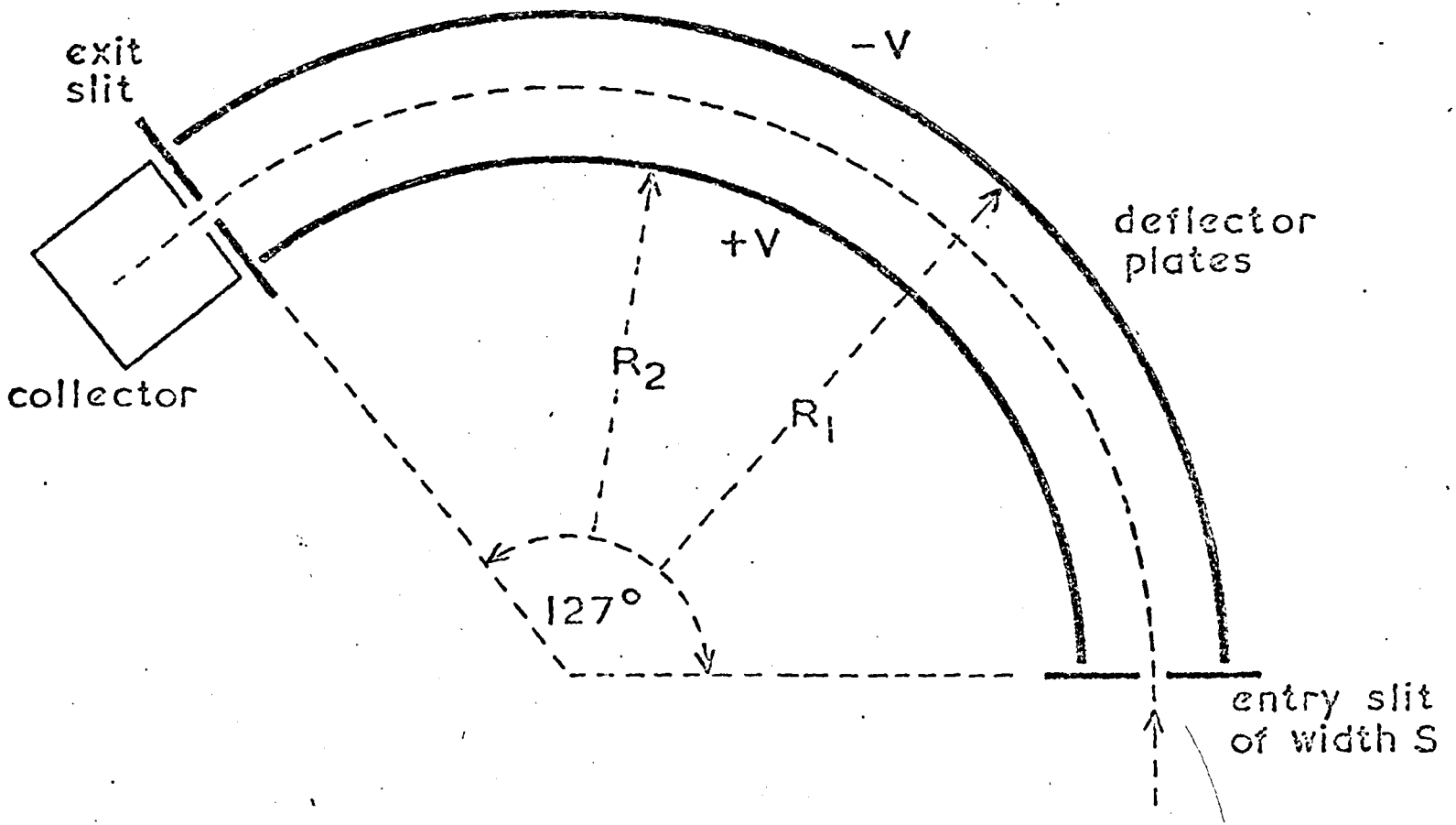

Fig. 2.6 Schematic diagram of a 127^{o} velocity analyser[44].

be 0.7% and 0.6% for reflection and transmission modes respectively.

The sensitivity of the retarding field analyser has been evaluated by Taylor[40] and Chang[42]. The sensitivity limit of detection is determined by the largest attainable signal-to-noise ratio S/N. For some known experimental value of S (which is given by Auger peak height), the limit of sensitivity can be estimated if N is known. In retarding field analysers the largest noise source is shot noise, due to high energy electrons[40]. The shot noise current I_n is given by[43]

$$I_n = (2eIB)^{\frac{1}{2}}$$

where I is the collected current, B is the bandwidth and e is the electronic charge. The maximum experimental value of signal-to-noise ratio, S/N, in the case of clean surface is found to be $>5 \times 10^3$ [42]. The sensitivity of the analyser can be increased by increasing the collected current, I, or decreasing the bandwidth B. In the first case S would increase proportionally to I, but noise would increase only as $(I)^{\frac{1}{2}}$. On the other hand, a decrease in B results in an increase in the data acquisition time. The increase in S can also be attained by using the grazing incidence[16] and also by using the optimum primary energy for maximum ionization of the inner shells[40].

The second type of analysers, presently used in Auger spectroscopy, are the electrostatic focussing analysers. The most commonly used of this type is the 127^0 sector analyser of Hughes and Rojansky[44] and is shown in Fig.(2.6). If V_D is the applied deflecting potential on the plates

of radii R_1 and R_2, then the electrons of energy eV will be refocussed at the exit slit and enter the collector, where

$$V_D = V \ln\left(\frac{R_1}{R_2}\right)$$

It is clear from the above relation that the energy of the electrons passing through the analyser is proportional to the applied deflecting potential on the plates. If R is the mean radius of the deflection plates, and d is the slit width, then the electrons in an energy range ΔV with mean energy V, able to pass through the analyser is given by

$$\Delta V = V\left(\frac{d}{R}\right)$$

$$\therefore \quad \frac{\Delta V}{V} = \frac{d}{R}$$

The collector current, when plotted as a function of deflection voltage, gives the energy distribution of the electrons entering the analyser. The slit width, d, and the mean radius, R, of the deflection plates will remain constant for a particular analyser. The energy spread ΔV is then proportional to V and the sensitivity of the analyser increases with V. The current reaching the collector in this case will be $\frac{dI}{dV}.\Delta V$. Since the collector current in the case of the 127^0 analyser gives the energy distribution, its derivative can be obtained by applying an a.c. modulation voltage to the deflection plates and detecting the first harmonic of the signal at the collector. If K sin ωt is the modulation, then carrying out a Taylor's series expansion of $\frac{dI}{dV}(V + K \sin \omega t)$, the first harmonic

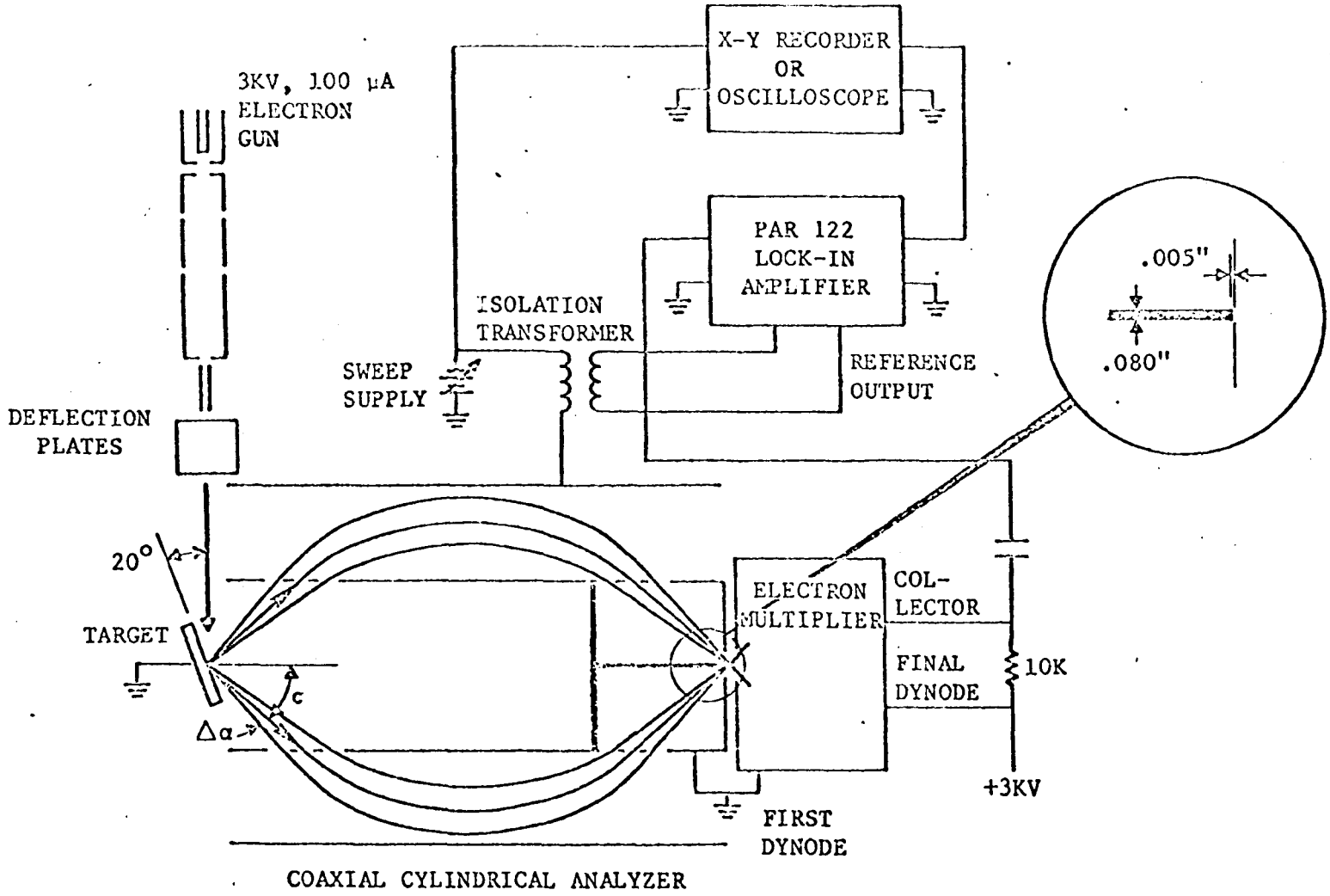

Fig. 2.7 The cylindrical mirror analyser[37].

is given by

$$B_1 = KI''(V) + \frac{K^3}{8} I'^{V}(V) + \ldots.$$

If the modulation is sufficiently small, the higher order terms can be neglected, and in this case B_1 will be proportional to I"(V). Bishop and Riviere[7] report that for lower modulation amplitudes the Auger current increases linearly but decreases as the square root of the amplitude for large modulation values. The Auger current attains its maximum value at some intermediate value of the modulation amplitude.

Recently Palmberg et al.[37] have developed a high sensitivity cylindrical mirror analyser, and this is shown in Fig.(2.7). Like all other electrostatic analysers it acts as a band-pass filter and thus collects less noise. The principle of the analyser is that electrons leaving a source at an angle α form an image of the source at a distance determined by the geometry of the analyser.

If V_a is the voltage applied to the outer cylinder with the inner cylinder grounded, the electrons leaving the target with energy eV will produce a minimum trace width around the axis of the cylinder because of the second order focussing property of the analyser. The value of the ratio $\frac{V}{V_a}$ is determined by the geometry of the analyser and usually lies between 1 and 2. The linearity relationship $\frac{V}{V_a}$ = constant holds well below 100V.

The transmission of the analyser is about 10% which is nearly equal to that of a four grid retarding field analyser and over two orders of

magnitude higher than that of most velocity analysers[37]. The advantage of the cylindrical mirror analyser over the retarding field analyser is thus the reduction in shot noise. Chang[36] estimates that the shot noise in the cylindrical mirror is about 100 times less than the retarding field device. This greatly improved signal-to-noise ratio makes it possible to display the Auger spectra on an oscilloscope. The highest attainable resolution of the analyser for a point source is determined by $\Delta\alpha$ (Fig.(2.7)) and can be varied by changing the entrance or exit slit width. In practice the resolution of the instrument may well be limited by the stray magnetic fields if these are not reduced below about 10mgauss. The measured resolution of the cylindrical mirror analyser of Palmberg et al.[37] was found to be 0.7%.

Pessa et al.[45] have used a cylindrical mirror analyser for the studies of Auger spectra. The focussing or the minimum trace width is obtained at the surface of the inner cylinder instead of axial position. With careful design considerations, they have achieved a resolution of ~0.06%. However, the authors have observed Auger peaks in the energy distribution rather than the differential distribution. Thus the maximum available sensitivity of the instrument has not been fully exploited.

2.2.3 Recent work on characteristic energy losses

Characteristic energy loss spectra of elements and some compounds have been studied by many workers using several methods in both transmission through films and reflection from surfaces. Reviews on the subject have

been published by Klemperer and Shepherd[46] and Raether[47]. Some of the more recent reflection type work is described in this section which is relevant to the work described on Auger spectroscopy. Scheibner and Tharp[24] reported the energy loss spectra of single crystals of tungsten, graphite and copper.

One important feature of their work was an attempt to give a characterisation of the surfaces with LEED studies. The measured losses are attributed to surface plasmons, bulk plasmons and interband transitions. Surface and bulk plasmon losses in tungsten were identified by observing the change in the relative intensities of the peaks with the primary energy. The extreme sensitivity of the surface loss to impurity presence has been demonstrated by Palmberg and others[48,21]. Palmberg showed that when a monolayer of Ba was deposited on the clean Ge surface, the surface loss disappeared and a new loss peak appeared at lower energy. This would be expected according to the theoretical prediction of Stern and Ferrel[10]. However, an additional new loss peak just above the original value of the surface loss was also observed, and has been attributed to a 'shifted surface loss' by the author.

Powell[49] has compared the energy loss spectra from the liquid and solid phases of the same metal in the case of Al, Bi and Au. The angular variations in the relative intensities of surface and bulk losses have been observed particularly in the case of liquid Al. However the results were recorded with a base pressure $\simeq 10^{-6}$ torr and the possibility of surface contaminations may not be discounted. In the case of silver

there are a variety of interpretations of the 4eV loss[50,51]. Seah[52] has recently interpreted this loss as due to bulk plasmons. However, no loss peak has been attributed to that 'corresponding' surface loss. In this connection some preliminary recent experiments by the author on a single crystal of silver indicate that the loss at about 4eV(3.8 ± 0.2eV) in silver may well be a surface plasmon loss and that one at 7.5eV can be interpreted as a bulk loss. Support for this identification came from changing the primary energy from 150eV to 470eV and observing the relative amplitudes of the two peaks. The results indicated that at 150eV the amplitude of ~4eV loss was about three times larger than that of the 7.5eV peak. However at 470eV the amplitude of the 7.5eV peak was roughly twice the amplitude of ~4eV loss. This would be expected due to the greater penetration of the higher energy electrons. Moreover in another recent paper Seah[53] has suggested that 4eV loss in silver is a surface loss. Also more recent work in this laboratory seems to confirm the above identification. In this case the identification is based on the amplitude dependence of these loss peaks on the angle of incidence of the primary beam. Energy loss studies of vanadium and vanadium oxide have been reported by Fiermans and Vennik[54]. In the case of vanadium oxide, the interpretation of the results is based on the assumption that the valence electrons of the material split into two groups, each showing collective oscillations. A number of energy loss peaks have been observed in vanadium and interpreted as due to surface and bulk plasmon losses and their multiples and combinations. It may be pointed out, however, that the Auger spectro-

scopic studies of V and V_2O_5 by the authors[55] revealed that chlorine was present on the V_2O_5 surface and a strong sulphur peak along with a carbon peak confirmed the presence of these elements in the vanadium surface. The effect of these impurities on plasmon losses, particularly on the surface loss, must have been severe. Moss and Blott[56], and Jenkins and Chung[22] have reported the energy losses of copper and these will be discussed more fully in Chapter IV.

2.3 Conclusion

Some of the recent published work on various aspects of Auger spectroscopy have been reviewed and the different parameters involved have been discussed in the light of the experimental results. It may be remembered that the subject is still in its infancy and that most of the work to date is largely of a qualitative nature, since much data regarding the Auger spectra of clean surfaces of several elements is not yet available. Much theoretical work needs to be done. Some work has also been done on the quantitative applications of the technique. Of the various energy analysers, the retarding field type has probably been the most used since it could easily be adapted from LEED systems and these were available in several laboratories when the technique became known. The superior signal-to-noise ratio of the more recently adopted cylindrical mirror analyser, however, makes it ideal for rapid observations. A very brief survey of the recent work on the characteristic energy losses indicates that more work is required - preferably in conjunction with Auger

spectroscopy - to establish the positions of surface and bulk plasmon losses in some elements.

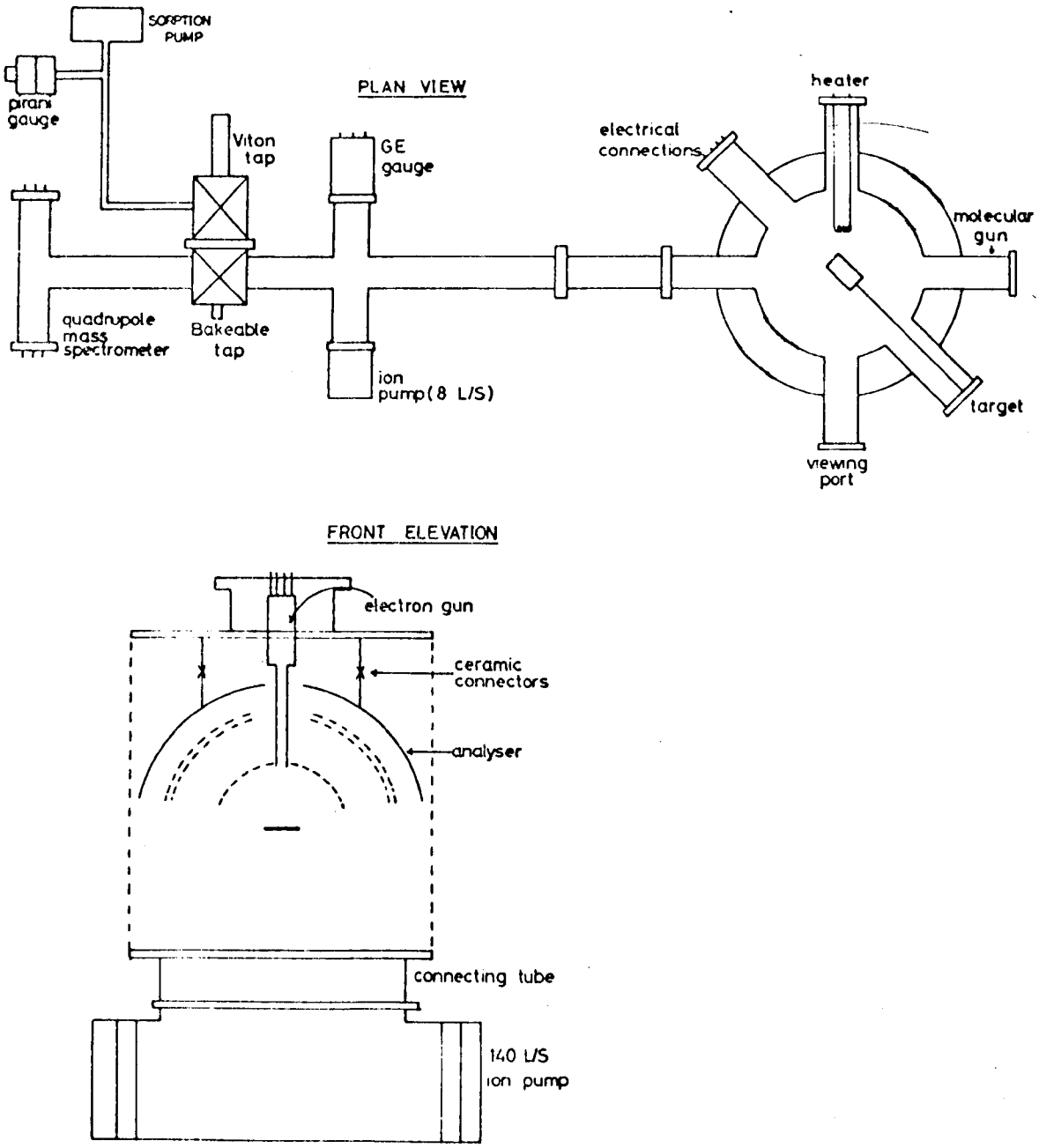

Fig. 3.1 Schematic diagram of the experimental apparatus.

CHAPTER III

EXPERIMENTAL APPARATUS AND METHODS

3.1 Introduction

For any meaningful studies of the secondary electron emission properties of materials, it is necessary that all the experiments should be performed in the contamination free ultra high vacuum environments. This is because the emission properties are extremely sensitive to surface contamination. The details of the ultra high vacuum system employed for the present investigations are described in this chapter.

The technique of the Auger and energy loss spectroscopy is based on the energy analysis of the secondary electrons. For this purpose a three grid retarding field analyser along with an appropriate detection system was constructed. The construction details of the analyser and the circuits of the detection system are included in this chapter.

3.2 Experimental Apparatus

3.2.1 The UHV experimental chamber

The experimental apparatus used for the present investigations is schematically shown in Fig.(3.1). It consists of a cylindrical chamber made of stainless steel type EN58E with low carbon content, and has inner diameter of 6" and height 8". The chamber has got seven appendages which can be used for example for such things as an electron gun, target

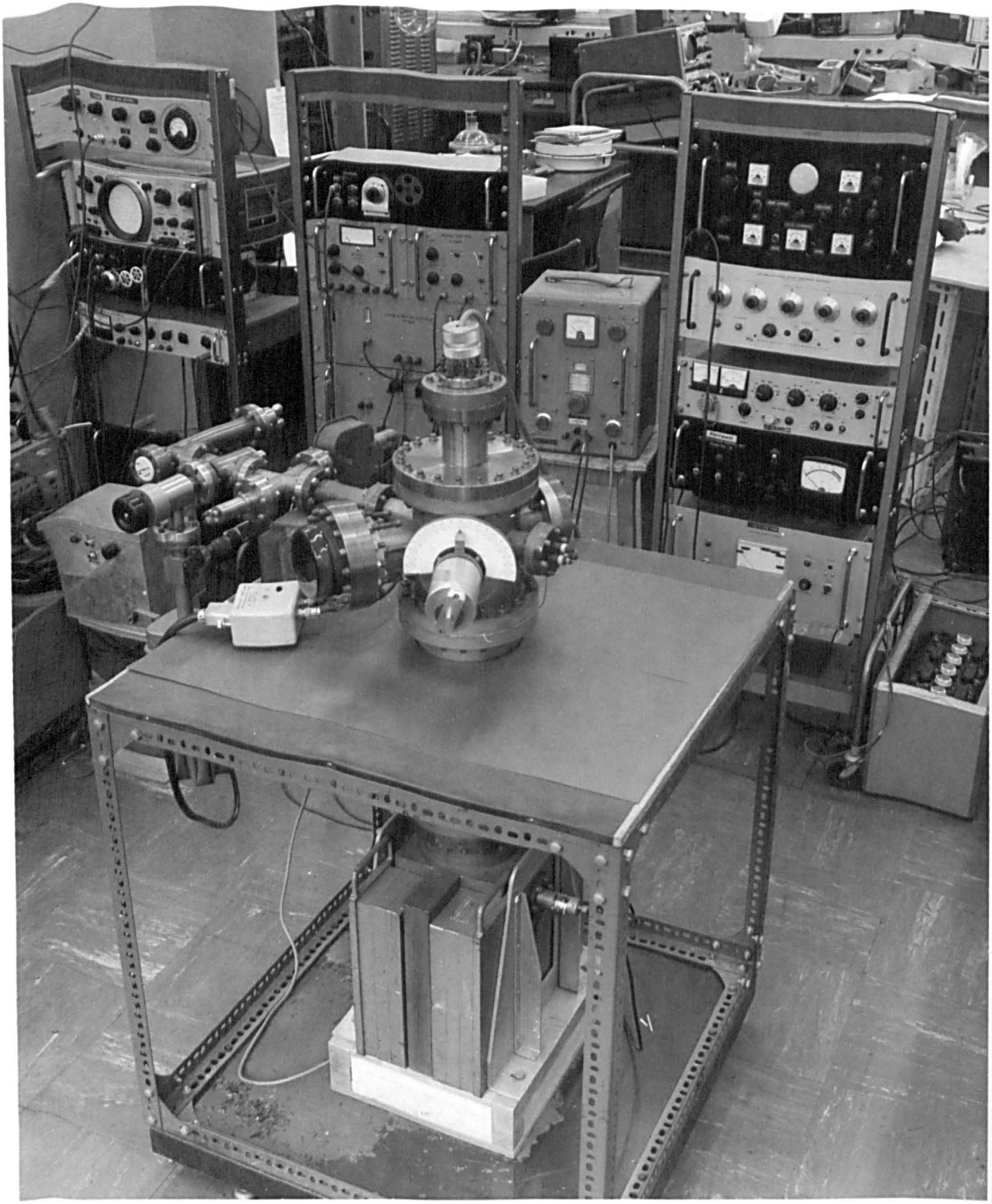

Fig. 3.2

manipulator, molecular gun, sample heater, viewing port and electrical feedthroughs for making electrical connections. Initially the chamber was cleaned chemically, but later on mechanical cleaning by "glass beading" was found quite satisfactory and much easier. In addition it left the surface free from acid and other contaminants. The procedure used for chemical cleaning is briefly as follows:

1) A wash in carbon tetrachloride.
2) After drying, a two minute dip in a hot solution of sodium hydroxide.
3) A rinse in hot water.
4) A dip in 50% concentrated solution of hydrochloric acid.
5) A final rinse in cold water and dry air treatment, followed by air bake at 350^{o}C.

After the cleaning the chamber was leak tested with a mass spectrometer leak detector (20th century). A photographic view of the main chamber is shown in Fig.(3.2).

3.2.2 Pumping scheme

It is well known[57] that vacuum systems pumped by rotary and diffusion pumps are usually contaminated by the back-streaming of the pump oil, which forms a polymerised film on the surface under investigation. It is therefore highly desirable not to use these pumps when the properties characteristic of the clean surface are under investigation. For this reason sputter ion pumps were employed for continuous pumping of the vacuum system. With the use of these pumps, it has proved possible to maintain a solid surface in an environment in which minimum monolayer formation times

are of the order of several hours or even days. A sorption pump and two sputter ion pumps were used to pump the vacuum system. The sorption pump was capable of pumping down the whole system from atmospheric pressure to the 10^{-3} torr necessary to start sputter ion pumps. The sorption pump contains a processed mixture of aluminium and silicon oxides, generally known as molecular sieve. This material has the property of sorbing air molecules when cooled. The sorbed air is released when the material is warmed up to room temperature.

To achieve ultra high vacuum, 8ℓ/sec and 140ℓ/sec sputter ion pumps were used. Unfortunately the 8 ℓ/sec pump was found to be a "very slow starter". This slow starting effect was believed to be due to the accumulation of heavy hydrocarbons, water vapours etc., inside the pump and was cured by chemical cleaning of the pump. The cleaning method used is briefly described below.

1) A wash in carbon tetrachloride.
2) A two minute wash in hot solution of sodium hydroxide followed by a hot water rinse.
3) A dip in 50% strong solution of hydrofluoric acid.
4) A dip in potassium cyanide solution prepared in water with a small amount of potassium hydroxide added to it.
5) A wash in de-ionized water.
6) A rinse in methanol followed by air bake at $350^{o}C$.

After the cleaning the pump was baked under vacuum (at $350^{o}C$) and was leak tested after the bake.

This small 8 ℓ/sec pump was employed to pump the section connecting the quadrupole mass spectrometer to the main chamber. The 140 ℓ/sec pump, connected to the main chamber through a connecting tube of 6" diameter, provided rapid pumping of the main chamber, the large diameter of the connecting tube making it possible to achieve maximum throughput.
In a sputter ion pump the pumping effect is 'realised' by maintaining a cold cathode discharge in a magnetic field and producing a fresh reactive surface of getter metal (generally titanium), by sputtering. The trapping of neutral gas atoms and molecules on the anode surface by the sputtered titanium, is the principal pumping effect. Inert gases like argon and helium are pumped by ion burial in the cathode. Hydrogen is also pumped in this way because it sputters poorly, but penetrates the cathode readily (because of its small ion size). Since the ion current is proportional to the pressure, the pump control unit can be used for measuring the pressure in the vacuum system. However, this can be done reasonably accurately only in the pressure range of 10^{-8} torr. To measure lower pressures a GE type triggered discharge gauge was used. This device is capable of measuring pressures up to 10^{-12} torr. The gauge is basically a very small Penning type gauge, with an additional filament to trigger the discharge off at lower pressures, if necessary. A quadrupole mass spectrometer was also connected to the vacuum system, but it was of no use at pressures below 10^{-8} torr, since it did not have an integral electron multiplier.

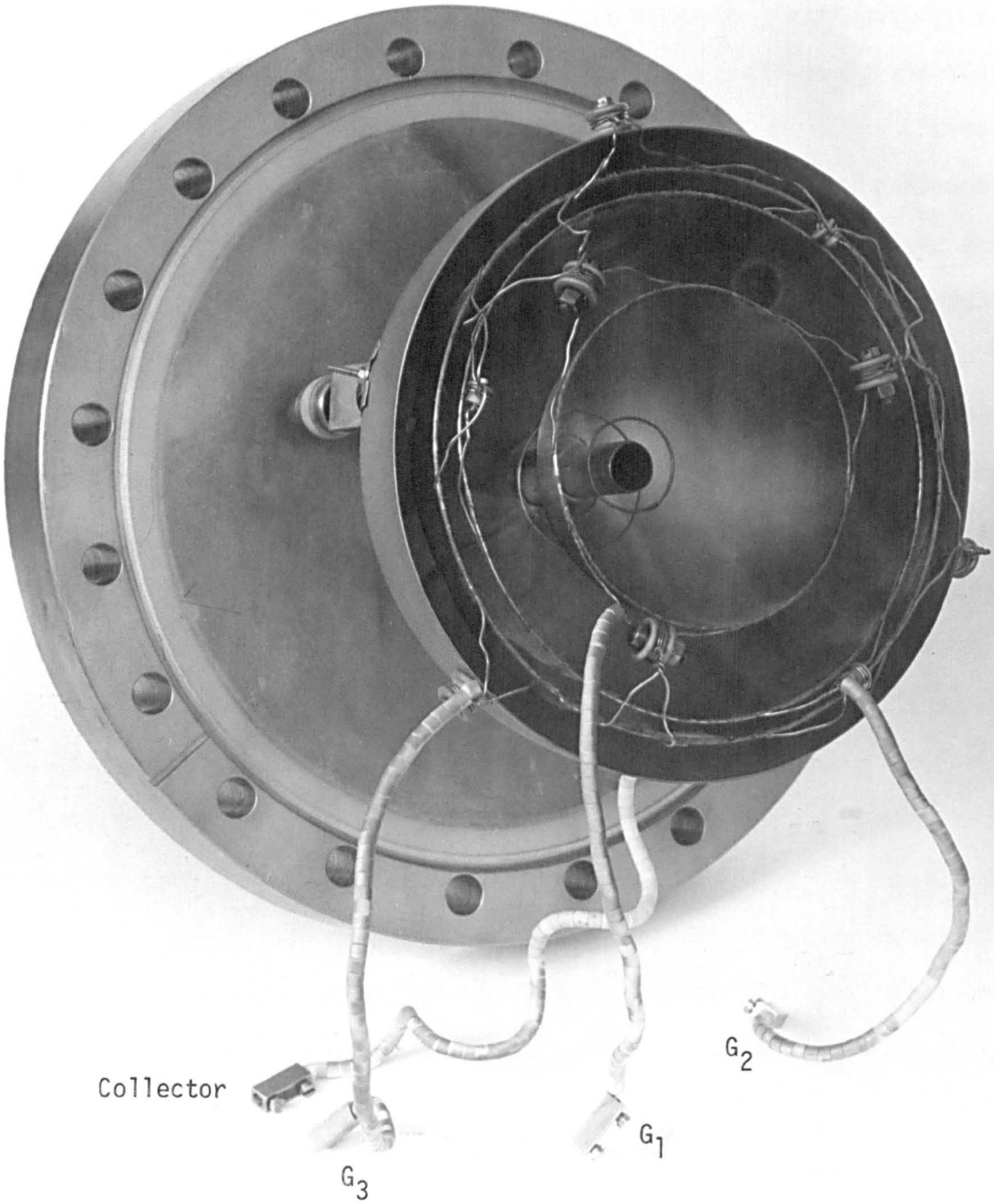

Fig. 3.3

3.2.3 The retarding field analyser

The retarding field analyser used for the energy analysis of the secondary electrons was basically a three grid system and is shown in Fig.(3.3). The hemispherical collector was made of stainless steel and had a diameter of 5". It was connected to the top flange of the main chamber through insulated ceramic connectors. Inside the collector were the three hemispherical tungsten grids, G_1, G_2 and G_3, of diameters 2.5", 4.0" and 4.25" respectively. The grids were held together along with the collector via ceramic connectors. A hole of diameter $\frac{1}{2}$" was made in the centre of the grid assembly to allow the electron beam to strike the sample, positioned at the centre of curvature, at normal incidence. The grids each had a transmission of ~85% and mesh density 64 x 64 meshes/sq.in. The construction method used for these grids was very simple. The tungsten mesh was laid over a round bottom flask of the desired diameter, held inverted in a retort stand. The mesh was then fastened by a ring of nickel wire whose diameter was fractionally bigger than that of the flask. After stretching the mesh inside the ring, they were welded together with a hand-welder. When removed from the flask, the grid was usually stiff enough to retain the hemispherical shape and there was thus no need of any electro-plating, a method which can be used to stiffen grid structures[58].

3.2.4 The electron gun

A Mullard type DG7-32 electron gun was used to provide the beam of primary electrons (Fig.(3.4)). The beam was generally allowed to strike the sample surface at normal incidence although angles of incidence up to 45^{o}

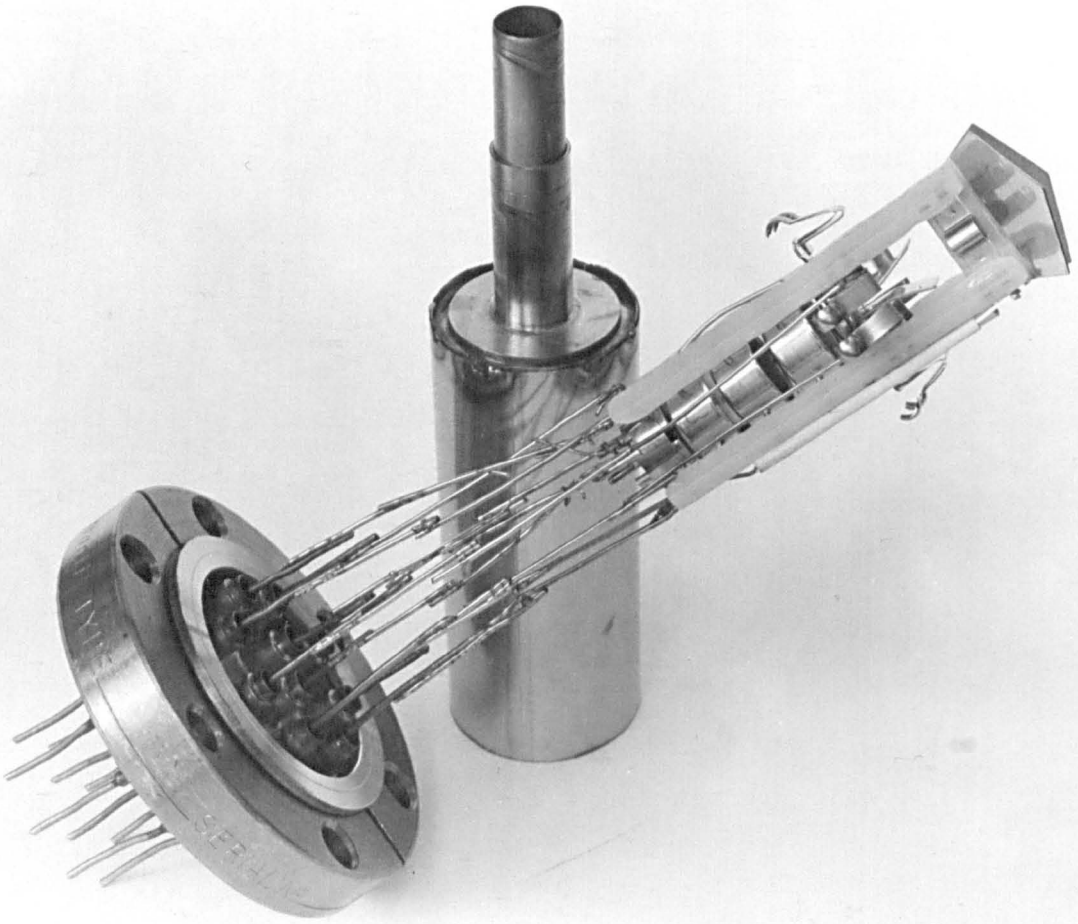

Fig. 3.4

could be used. The gun was focussed electrostatically and had electrostatic X and Y deflection plates. These plates were used to position the electron beam at the centre of the sample, or wherever was necessary for maximum resolution of the analyser. It was found that the gun could be operated satisfactorily in the voltage range of 100 to 2.5KV. It used a replaceable oxide coated cathode. The cathode voltage was supplied by a highly stabilised power supply (Fluke 413c). The filament supply (6.3V, 0.3amps) was derived from a car battery. The above gun could provide beam currents of about 80 microamps at 2KV. This current was dependent on the gun cut-off characteristic which was determined by the position of the cathode assembly with respect to the control grid of the gun. In practice this could be adjusted slightly and with patience a high current (~80μA) could be obtained. The spot size was usually about a millimeter depending on the focussing conditions. The gun was surrounded by a stainless steel shield to stop stray electrons reaching directly to the collector. An identical electron gun, operated by the same control unit, was mounted outside the vacuum system, to check the spot size. Before taking any measurements, the cathode of the electron gun was activated slowly. This activation was essential for proper functioning of the cathode.

Although the energy analyser and the gun assembly was mounted inside the non-magnetic main chamber, still there was a strong stray magnetic field due to the large magnets of the 140 ℓ/sec ion pump. A stray magnetic field can severely affect the resolution of an analyser as pointed out recently by Taylor[40]. In order to eliminate this highly undesirable effect, a pair

of 'netic' and 'co-netic' sheets was used as shielding material. This combination was best suited since the 'netic' has low permeability but high saturation density, while the 'co-netic' has lower saturation density but higher permeability. This arrangement served to reduce the field intensity sufficiently (<<1 gauss) so that there was, in practice, no effect on the resolution for primary energies above 100eV.

3.3 Experimental Methods

3.3.1 The detection method

The technique used for the energy analysis of the secondary electrons was in many ways similar to the one desribed by Palmberg and Rhodin[4] and Heber and Peria[3] and was based on the electronic differentiation method of Leder and Simpson[38]. The retarding field curve obtained by plotting the collector current against the retarding voltage was differentiated electronically. This was done by superimposing a small a.c. voltage (at a frequency of perhaps a few kHz) on the potential applied to the retarding grid. The collector current then contained an a.c. component at the modulation frequency which could be amplified and detected. For small values of the a.c. modulating voltage, the first harmonic of the collector current (a.c. component) was then proportional to the first derivative of the retarding field plot, i.e. it was proportional to the energy distribution function. The second harmonic of this signal (a.c. component of the collector current) was proportional to the second derivative of the retarding field plot, that is the first derivative of the

energy distribution, sometimes referred to as the differential distribution. Although the method of electronic differentiation appears to be simple in principle, in practice the extraction of the first and second harmonic signals can become somewhat complicated.

In a conventional three grid system, usually the first and the third grids are kept at ground potential, and the modulating a.c. voltage along with the retarding voltage are applied to the middle grid. This arrangement is useful in order to eliminate the inevitable capacitative coupling between the retarding grid and the collector, but has a comparatively poor resolution and causes an energy shift particularly at higher primary energies[16]. This is because the retarding grid is not an equipotential surface as pointed out earlier (section 2.2.2), as there are potential variations across the space between the wires forming a particular mesh. The effect can of course be minimised by reducing the mesh size. However, owing to the limitations of the mesh size and transmission considerations, the reduction of the mesh size is not possible practically. The improvement in resolution and energy shift can be achieved if the retarding voltage is applied to the two grids connected electrically together as suggested by Palmberg[16]. This means that altogether four grids are used, such that the first and fourth grids are earthed and the second and third together as retarding grids. A disadvantage of this combination is that with the increased number of grids, the transmission of the analyser is effectively lowered.

FIG 3.5
A.C. BRIDGE CIRCUIT

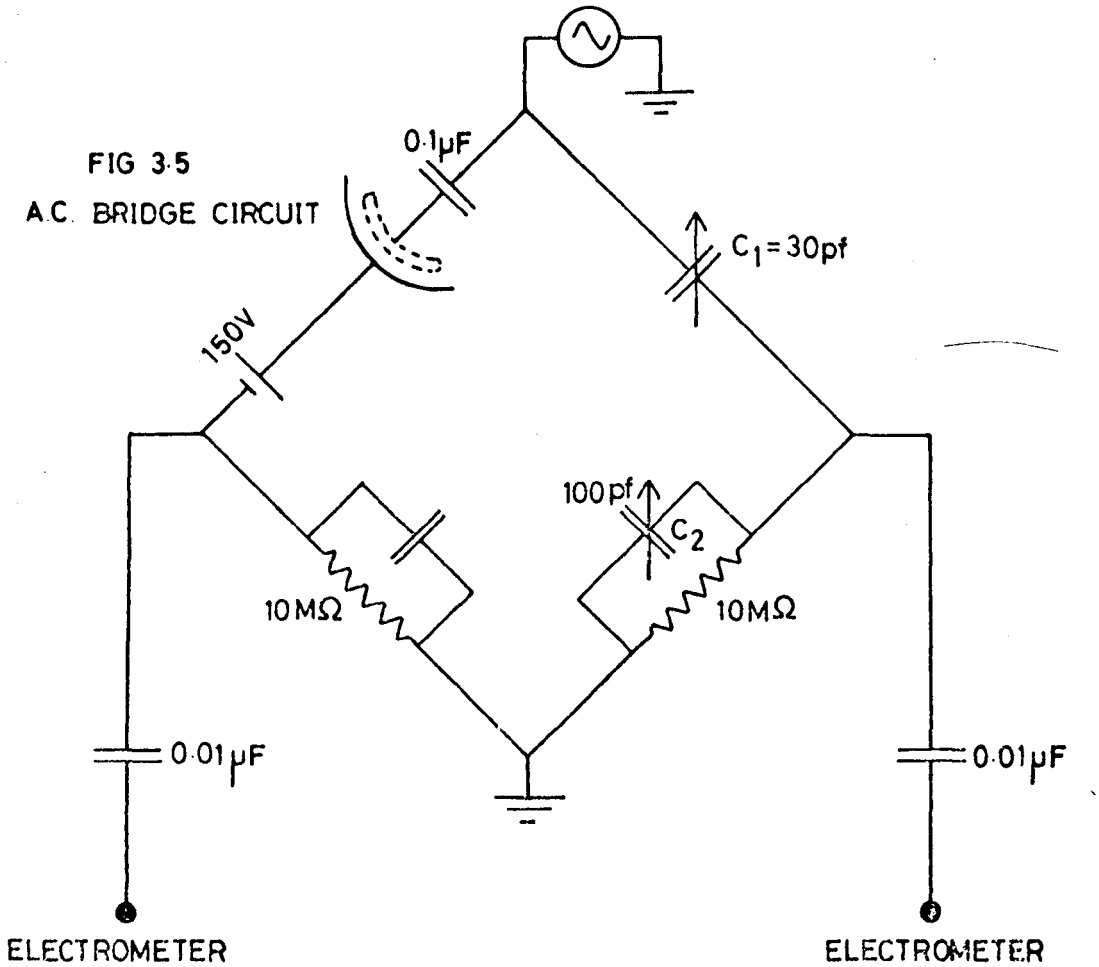

FIG 3.6
TUNED LOAD

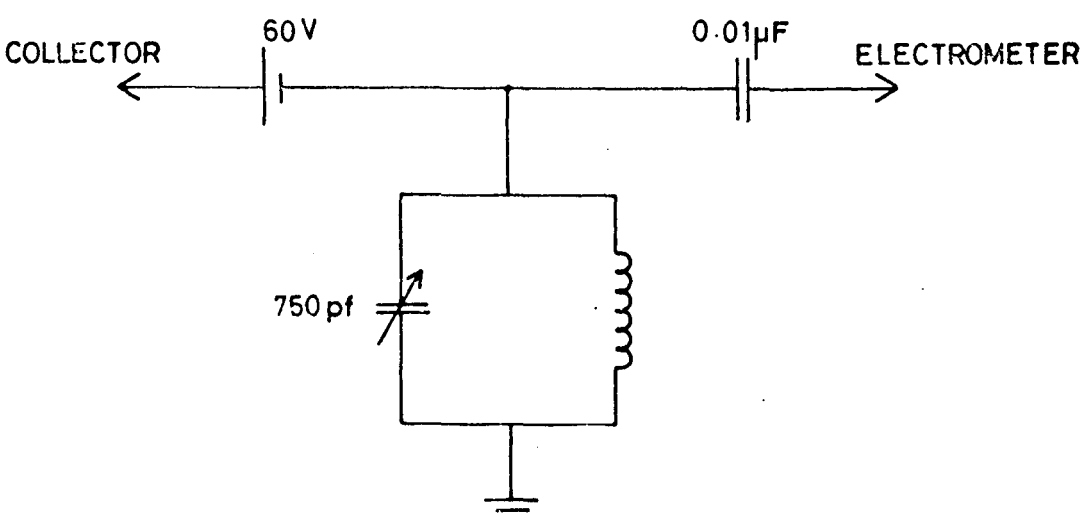

3.3.2 A.C. bridge circuit

For better transmission it is desirable to use three grids in all. The first one is earthed and the second and the third together are used as retarding grids. This combination produces a rather large capacitative pick-up signal (at the modulating frequency) at the collector due to the increased capacity between the retarding grids and the collector. For the extraction of the first and second harmonic signal, this spurious signal must be eliminated otherwise the amplifier of the detection system will be swamped by this unwanted signal. In order to extract the first harmonic, that is to observe the energy distribution, an a.c. bridge circuit (Fig.(3.5)), was designed to neutralise the capacitatively coupled signal. One arm of the bridge was formed by the collector and the retarding grids. The pick-up signal was tuned out by balancing the bridge.

3.3.3 Tuned load

To observe the differential distribution which is the second derivative of the retarding field plot, the detection of the second harmonic is required. Usually the a.c. component of the collector current is passed through a resistive load of the order of 1MΩ and the voltage developed across it, is then amplified. A large voltage can only be achieved if the load resistance is large. However, very large values cannot be used because of the stray capacitance and increased Johnson noise. In addition, the collector current has a large signal at the modulating frequency and a smaller one at the second harmonic. This means that the voltage developed across the load resistor will be larger at the modulating frequency.

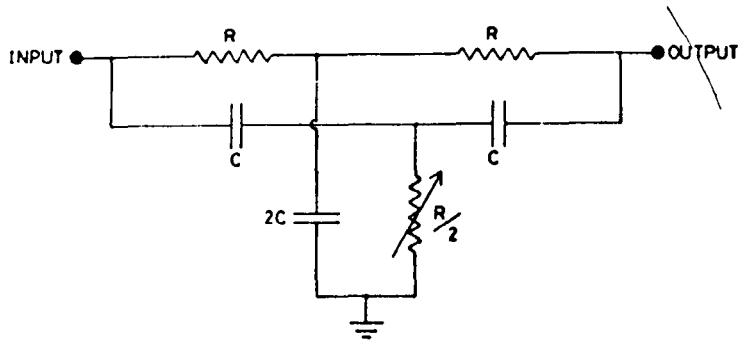
INPUT
R
R
OUTPUT
C
C
2C
R/2
R = 1·5kΩ
C = 0·1μF

Fig. 3.7

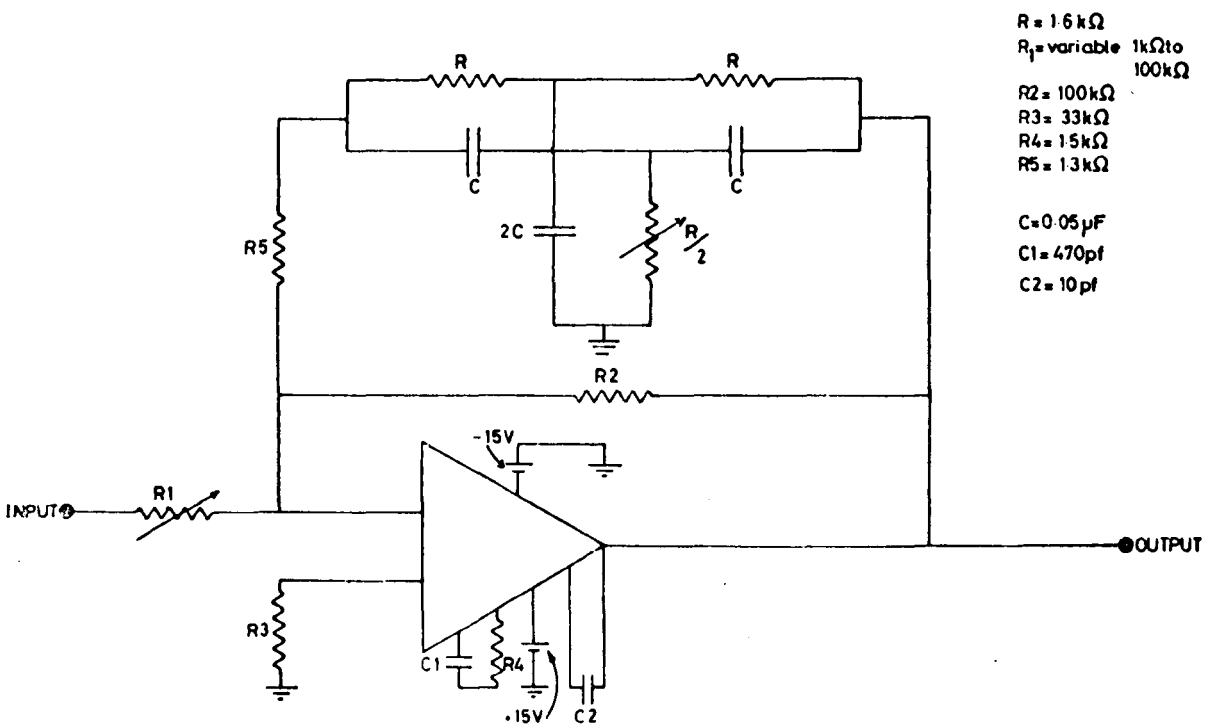
R = 1·6kΩ
R1 = variable 1kΩ to 100kΩ
R2 = 100kΩ
R3 = 33kΩ
R4 = 1·5kΩ
R5 = 1·3kΩ
C = 0·05μF
C1 = 470pf
C2 = 10pf
R
R
C
C
2C
R/2
R5
R2
-15V
INPUT
R1
OUTPUT
R3
C1
R4
+15V
C2

Fig. 3.8

This could overload the electrometer of the detection system and extraction of the desired second harmonic would become difficult. One simple way to overcome the difficulties mentioned above is to use a tuned load. The tuned load used in the present work was simply a parallel resonant circuit and is shown in Fig.(3.6). It was tuned to a frequency twice the modulation frequency. The resonance impedance of this load was about $10^{11}\Omega$ but the impedance at the modulation frequency was quite low. This gave a good rejection of the unwanted signals at the fundamental frequency. A higher resonance impedance ($10^{8}\Omega$) and rejection ratio could be achieved by using special ferrite pot core inductors.

3.3.4 Filter circuits

Although the level of the unwanted signal was sufficiently lowered by the tuned load, it was virtually eliminated by means of a two stage filter. The first stage consisted of a passive filter which rejected the fundamental frequency. It employed a usual twin tee circuit, and is shown in Fig.(3.7). The second stage consisted of an active filter circuit as shown in Fig.(3.8). This used a high gain operational amplifier (709). The circuit was designed to accept and amplify the second harmonic component only.

For a measurement of the derivative of the energy distribution (differential distribution) it is essential that the voltage applied to the reference channel of the phase sensitive detector should be at a frequency twice that applied to the retarding grids. This was derived from a rectifier bridge circuit coupled with a filter circuit as shown in

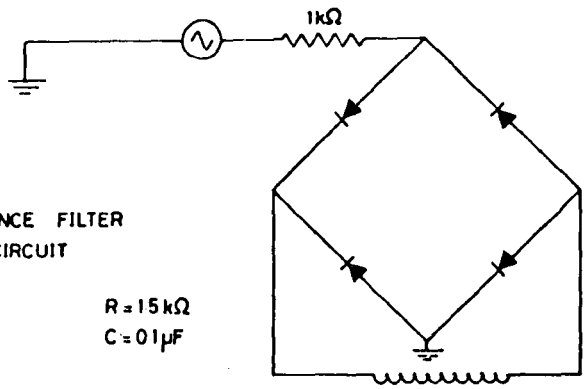

FIG 3.9
REFERENCE FILTER
CIRCUIT

R = 15 kΩ
C = 0.1 μF

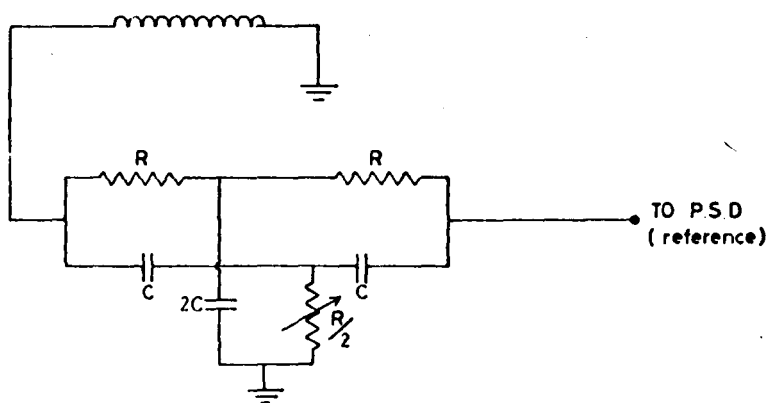

FIG 3.10
FILTER CIRCUIT
(FOR MODULATION)

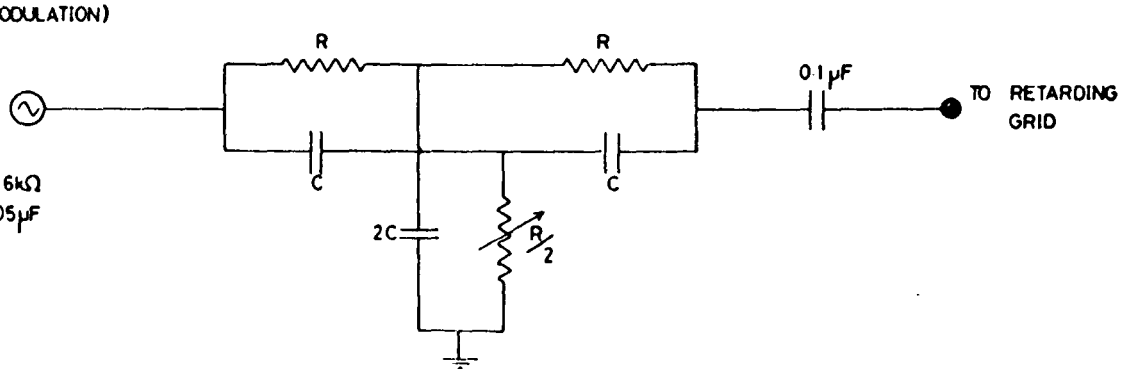

R = 16 kΩ
C = 0.05 μF

Fig.(3.9). Since only a fraction of the modulation voltage was required for the reference, a step-down (2:1) transformer was used to limit the amplitude of the reference signal.

In view of the fact that the second harmonic of the collector current is extracted for the differential distribution, it is very important not to have a second harmonic distortion on the modulation voltage. The a.c. modulation voltage for the present work was derived from a signal generator (Advance) which did have some second harmonic distortion This was reduced to a negligible level by placing a filter circuit - though a tuned transformer (step-up) may have been better - between the signal generator and the retarding grids. The filter circuit is shown in Fig.(3.10) and was tuned to reject twice the modulation frequency.

3.3.5 Pumping procedure

The pumping procedure can be described briefly as follows. The vacuum system was sealed after checking all the electrical connections inside the system. Also special care was always taken to align the target with the analyser at an optimum position for higher resolution of the analyser. Both the bakeable and viton taps were then closed. The sorption pump was cooled by liquid nitrogen contained in a dewar. After a few minutes both the taps were opened slowly. At this stage the sorption pump pumped the whole system and the pressure was measured by a Pirani gauge connected in the roughing line. When the pressure in the system was about 10^{-3}torr, which could be usually achieved in about 15 minutes, the sputter ion pumps were then switched on. Once the pumps started, the pressure in the system

fell rapidly. At this stage both the taps were closed and the pressure was measured by a triggered discharge gauge. The pump control units could also be used to measure the pressure. When the pressure reached the 10^{-7}torr range (usually it took an hour or so) the system was then leak checked by spraying hydrogen around the joints and observing the change in pressure on a chart recorder or meter of the control unit of the triggered discharge gauge. After about 24 hours the pressure in the system was usually about 10^{-8}torr. The quadrupole mass spectrometer was used for a final leak check. After the bake out of the vacuum system, a pressure in the range of 10^{-10} torr was achieved.

3.3.6 Sample preparation

Initially solid samples were used for the optimization of the analyser. During the Auger measurements the sample surfaces were found to be contaminated in almost all cases. Usually observed contaminants were carbon, sulphur and oxygen. Although oxygen could be removed by sample heating, it was found almost impossible to remove carbon permanently, presumably because of segregation of this element on to the sample surface. One effective way of removing such contaminants is to use an argon ion bombardment technique[59]. This method could not be used since the diode sputter ion pumps are known to have poor pumping speed for argon. Under these circumstances, the most suitable method to obtain clean surfaces was to evaporate the materials in ultra high vacuum environments. Thus all the samples were evaporated in the form of thick films, usually on glass substrates. However, in some cases the stainless steel substrates were

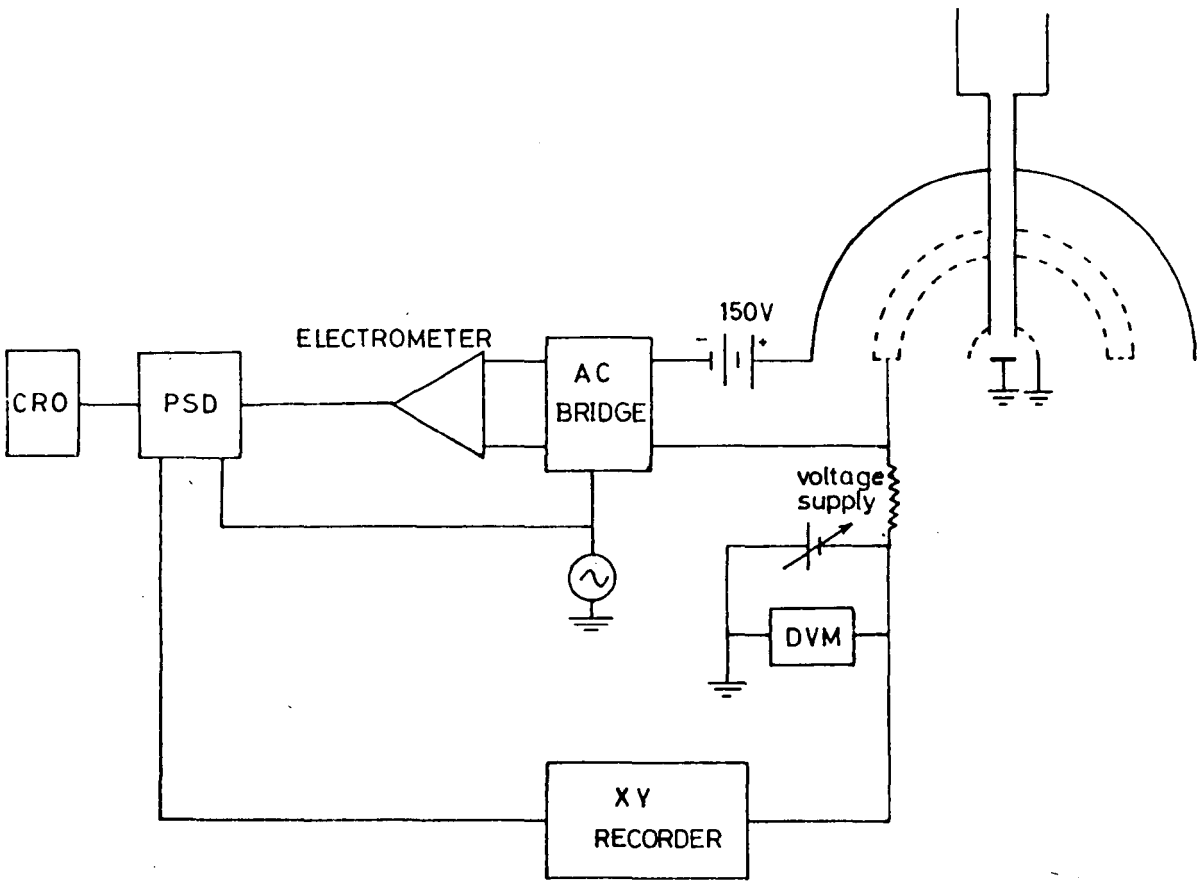

Fig. 3.11 Schematic diagram of the apparatus used for obtaining the characteristic energy loss spectra.

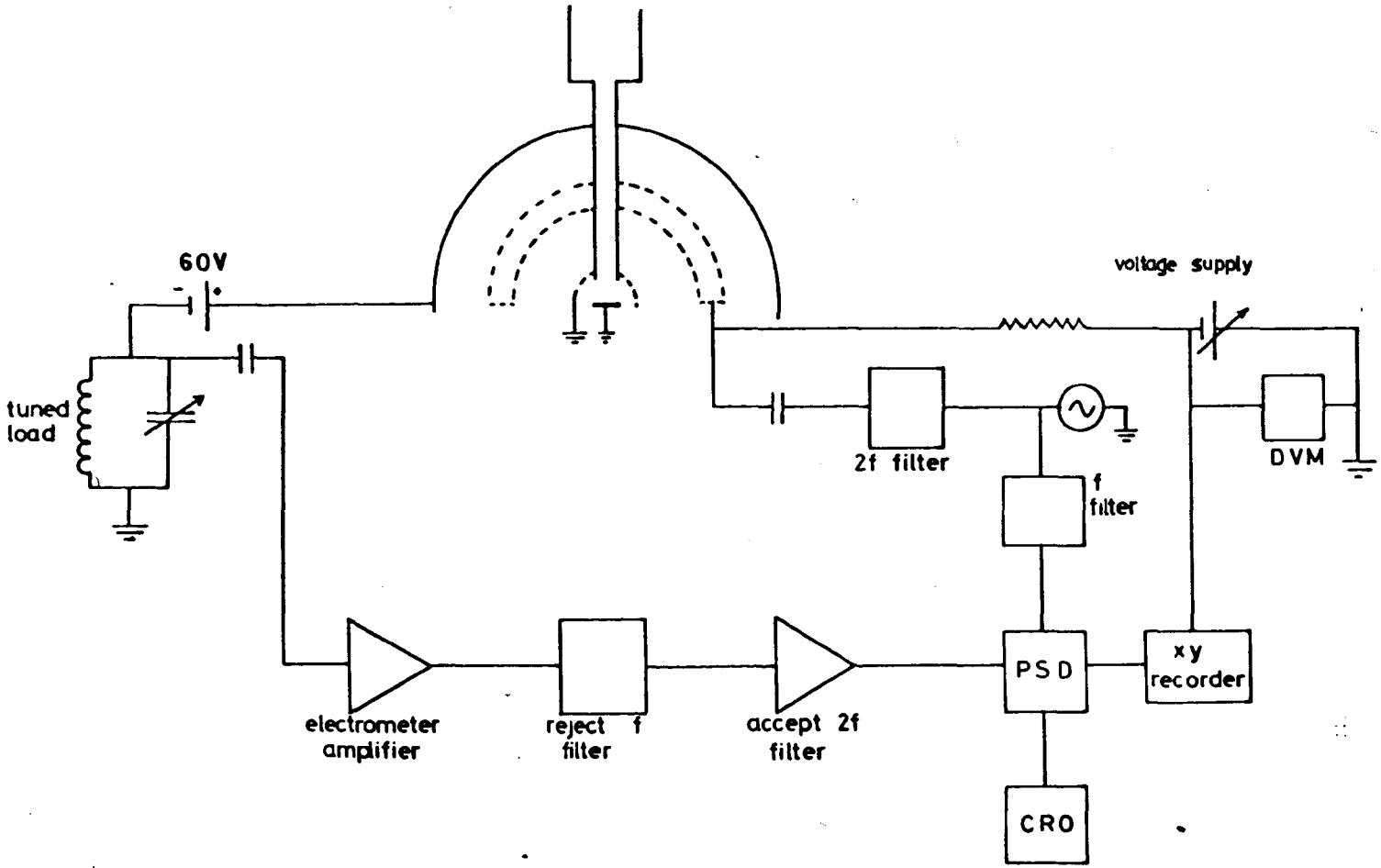

Fig. 3.12 Schematic diagram of the apparatus used for obtaining the Auger spectra.

also used.

3.3.7 CEL measurements

The experimental scheme used to observe the characteristic energy losses is shown in Fig.(3.11). First of all the modulation voltage was applied to the grids G_2 and G_3 and the pick-up signal was tuned out by adjusting the C_1 and C_2 capacitors in the bridge circuit. The electrometer amplifier was used in the differential mode. The retarding voltage was applied to G_2 and G_3. A blocking capacitor was placed between the retarding grids and the signal generator. In order to suppress the tertiary emission from the collector, it was kept at +150V. The retarding voltage was scanned by using a fifteen turn helipot driven by a variable speed motor. The output of the electrometer amplifier was fed into a phase sensitive detector. The phase of the reference signal was checked on the oscilloscope. A fraction of the sweep voltage and the output of the phase sensitive detector were fed to the X and Y channels of the XY recorder. The energy loss voltages were measured accurately with a digital voltmeter. Usually the energy losses were observed on an expanded scale by scanning the high energy end of the distribution curve only. Throughout the measurements, the target and the first grid were kept at ground potential.

3.3.8 Auger spectra measurements

A schematic diagram for observing the Auger spectra is shown in Fig.(3.12). The collector current was fed to a tuned load - tuned to a frequency twice that of the modulation signal. The voltage signal developed

across the tuned load was applied to the electrometer amplifier via a capacitor to block the d.c. bias on the collector - this bias of about +60V was sufficient to suppress the majority of tertiary electrons from the collector. The amplified signal was then fed into a two stage filter and then this filter output was fed to the phase sensitive detector. The spectra could be displayed on an XY recorder by applying the sweep voltage and the PSD output to the X and Y channels of the recorder. Usually it took about 20-25 minutes to plot the entire energy spectra from 0-1000eV.

3.4 Conclusion

The details of the experimental apparatus and technique have been described and discussed. In particular, the main features of the circuitry designed to obtain the derivative of the energy distribution are described. A design of the three grid system for better resolution and pick-up neutralising circuit have also been discussed. The performance of the analyser can be easily assessed from the results described in the next chapter.

CHAPTER IV

RESULTS AND DISCUSSION

4.1 Introduction

Experimental results obtained with the retarding field analyser described in the previous chapter are presented in this chapter.

Preliminary measurements were made to assess the performance of the analyser in terms of resolution and sensitivity. For this purpose Auger electron and energy loss spectra of ZrC and TiC were studied. These results are presented in section 4.2.

In section 4.3, Auger electron and energy loss spectra of clean copper and gold surfaces are described. A comparison of these results is made in section 4.4, with those obtained from copper black and gold black.

4.2 Preliminary Results

Auger electron spectra and characteristic energy losses of ZrC and TiC samples were investigated to assess the operating characteristics such as resolution and sensitivity of the analyser. To observe the Auger spectra, the first derivative of the energy distribution curve was plotted. The Auger peak energies were measured from zero energy to the maximum negative slope of the peak. This position, of course, would not correspond to the actual position of the peak maximum in the energy distribution, but it is the most readily identifiable feature in the differential distribution.

However, the characteristic energy losses were observed in the energy distribution curve and the loss peaks were measured with respect to the primary peak. Lower modulation amplitudes of the sinusoidal a.c. voltage were used where the primary interest was to observe the fine structure under optimum resolution conditions, and relatively larger modulations were applied where the aim was to achieve maximum sensitivity. The frequency of the modulating voltage was kept at 1050 Hz and usually a 1 second time constant was used on the P.S.D. (phase sensitive detector). Primary beam angles of incidence up to 45^{0} could be used but generally normal incidence was used. The primary energy, the primary beam current and modulation voltages used are given with each spectrum. In addition where a primary beam incidence other than normal is used, the angle of incidence is also given. In Auger spectra measurements, sometimes it was found necessary to reduce the gain of the electrometer amplifier to observe the low energy Auger peaks. In such cases this reduction factor is given for a particular spectrum.

The samples could be heated if necessary by a 1000 Watt projection lamp filament. The filament was held just below the sample and could be used in addition for internal baking of the vacuum system. When the samples were cleaned by the electron bombardment method, this filament also served as a source of electrons. In this case the sample was kept at a high positive potential. All the measurements were made at a base pressure in the low 10^{-10}torr range.

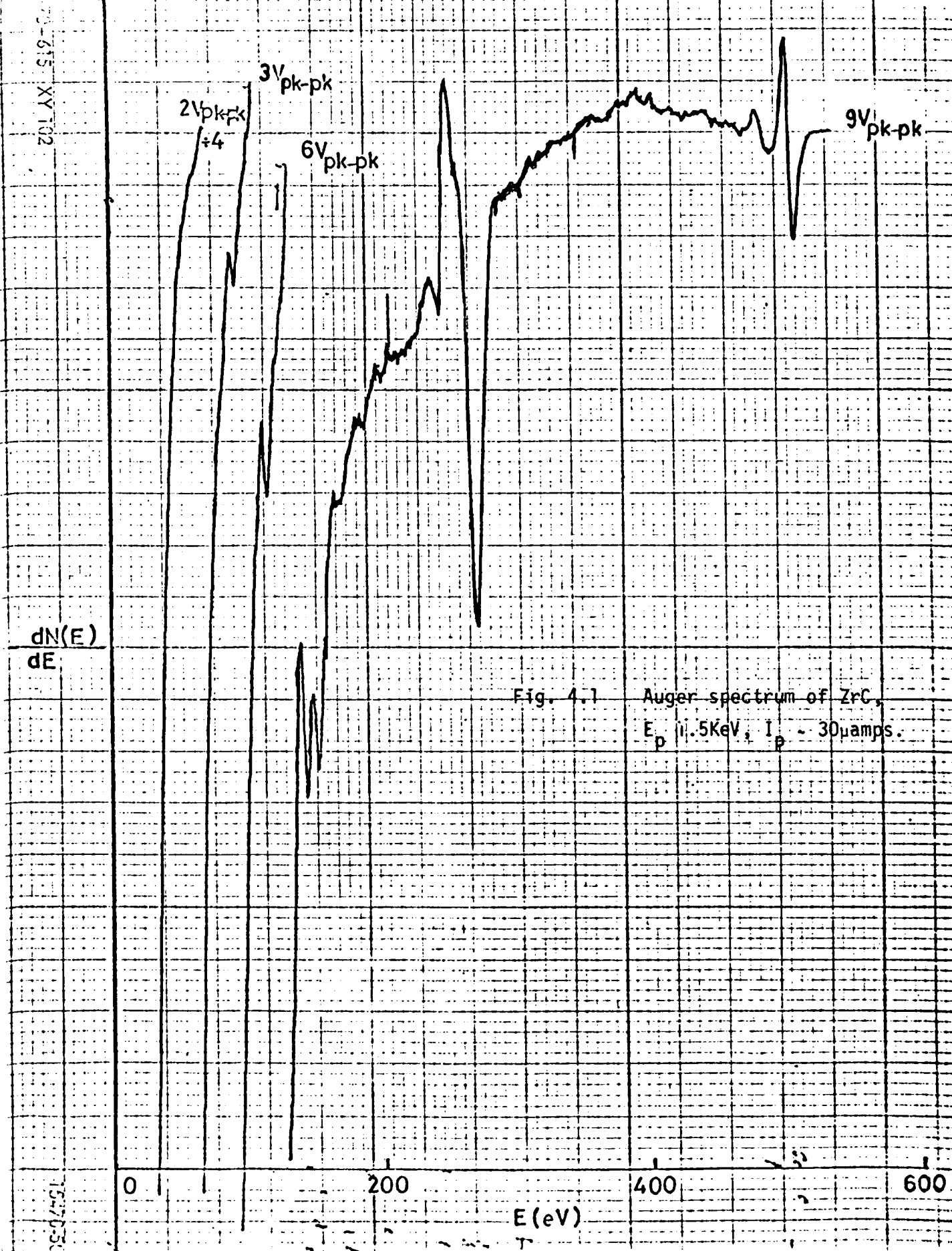

Fig. 4.1 Auger spectrum of ZrC, E_p 1.5KeV, I_p ~ 30μamps.

One of the main purposes of these preliminary investigations was to observe the operating characteristics of the analyser (such as resolution and sensitivity). The resolution of the instrument is demonstrated in Figs. (4.9) and (4.3b). The measured 'half width' (ΔE) of the elastic peak for a primary energy (E) of 1000eV is about 2eV. This gives an instrumental resolution ($\Delta E/E$) of 0.2%. Although this resolution could perhaps be improved, it is still excellent for Auger spectroscopic studies since the Auger peaks are usually 2-10eV wide. The shape of the slow peak is shown in Fig. (4.3b). The primary energy in this case was 1.5KeV. The peak is quite symmetrical and narrow (peak-to-peak half width only ~3eV) indicating the high resolution of the analyser. The high transmission (~61%) and greater collection efficiency (larger angle of collection 180^{o}) of the present analyser have greatly enhanced its sensitivity. This is evident from Figs. (4.3a) and (4.6). Fig. (4.6) also shows the increased sensitivity when the differential distribution is plotted instead of the energy distribution.

4.2.1 Auger spectra of ZrC and TiC

ZrC

The sample investigated was a mechanically polished ZrC circular disc of diameter 1". Fig. (4.1) shows an Auger electron spectrum of this sample in the energy range 0-550eV, for a primary energy of 1.5KeV. In addition to the peaks which could be attributed to Zr and carbon, a relatively large peak just above 500eV is also seen in the spectrum. This peak is identified as due to oxygen. In an attempt to remove oxygen

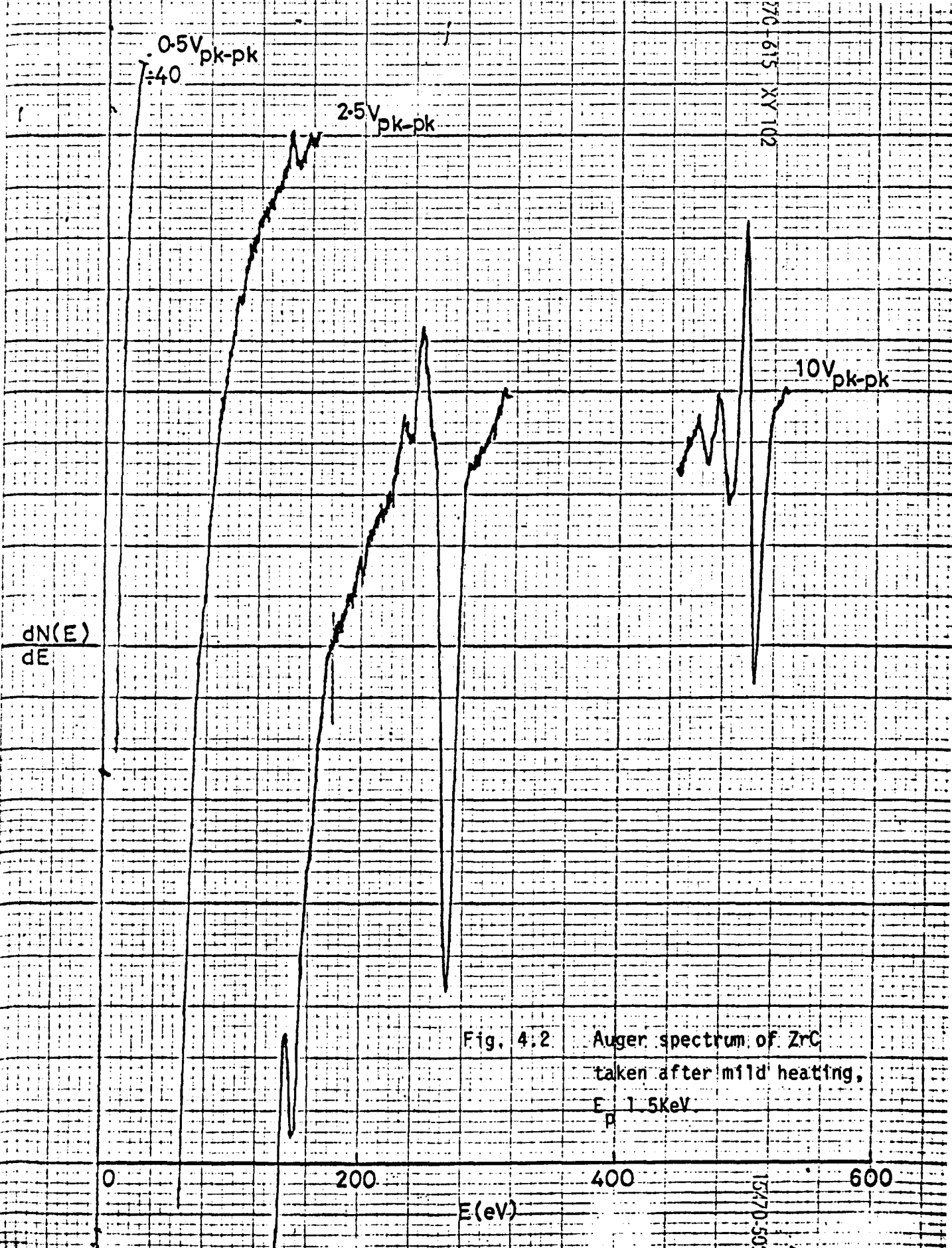

Fig. 4.2 Auger spectrum of ZrC taken after mild heating, E_p 1.5KeV.

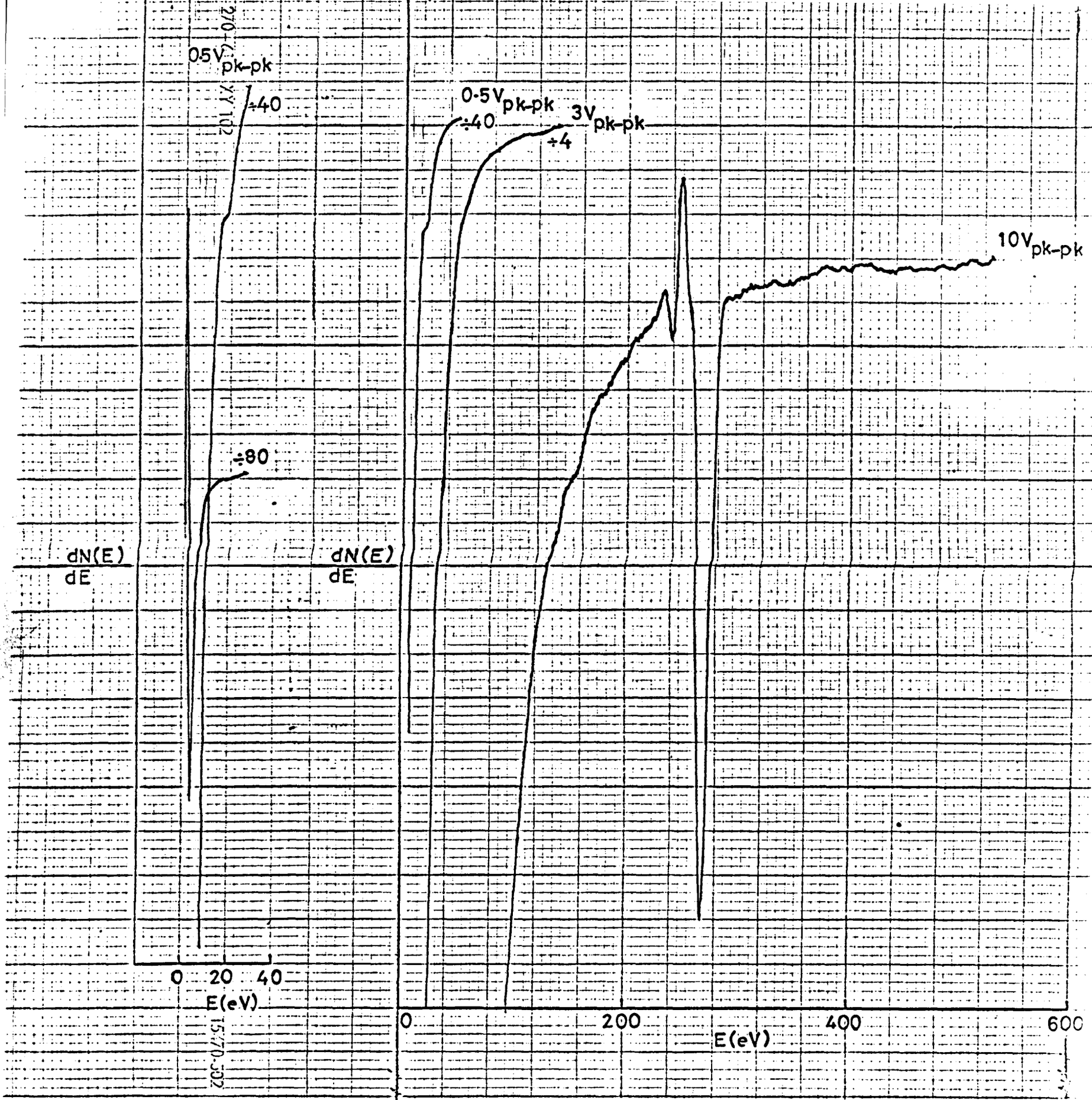

Fig. 4.3b The slow peak due to true secondaries, E_p 1.5KeV.

Fig. 4.3a Auger spectrum of ZrC taken after flashing by electron bombardment, E_p 1.5KeV.

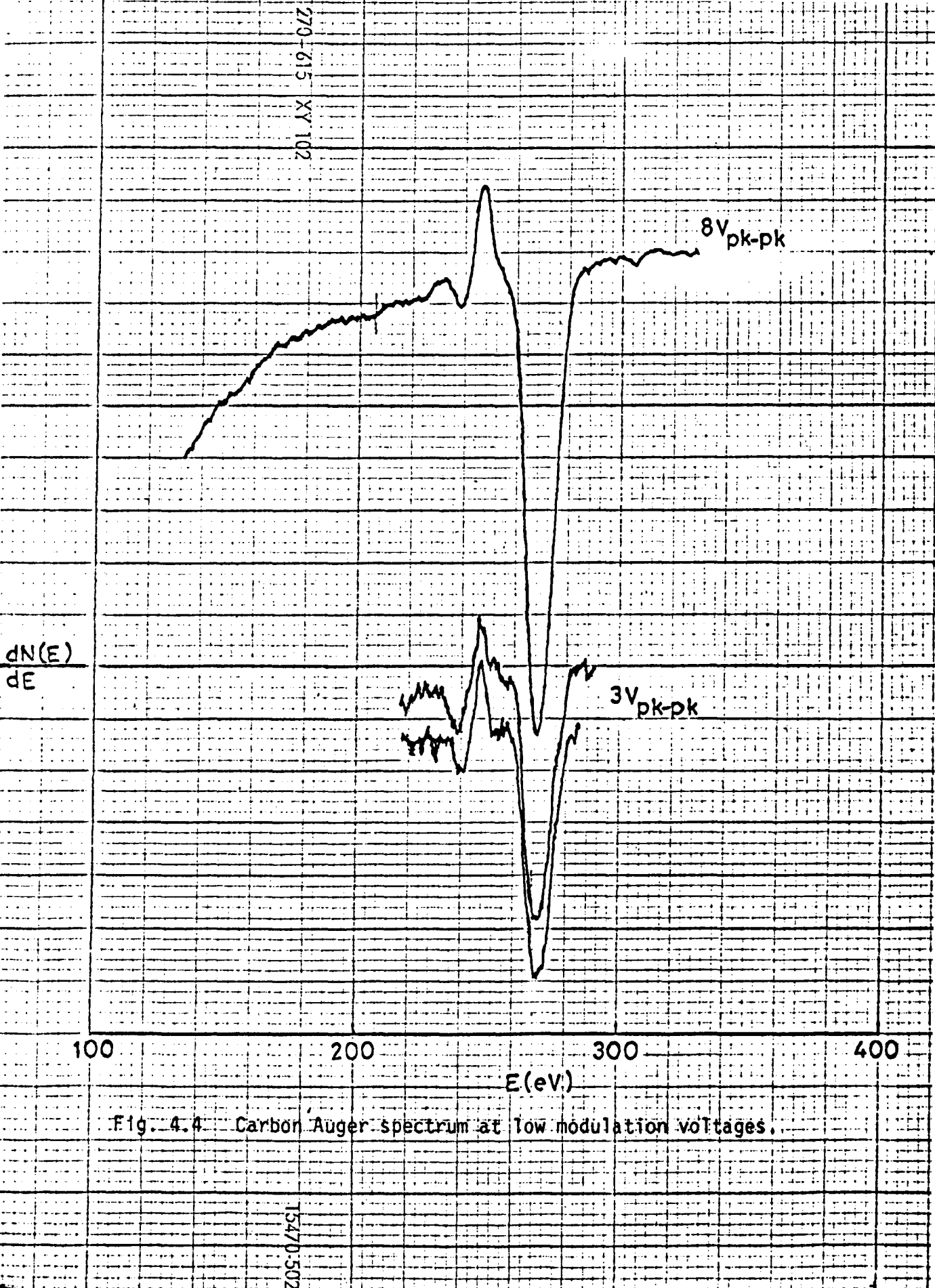

Fig. 4.4 Carbon Auger spectrum at low modulation voltages.

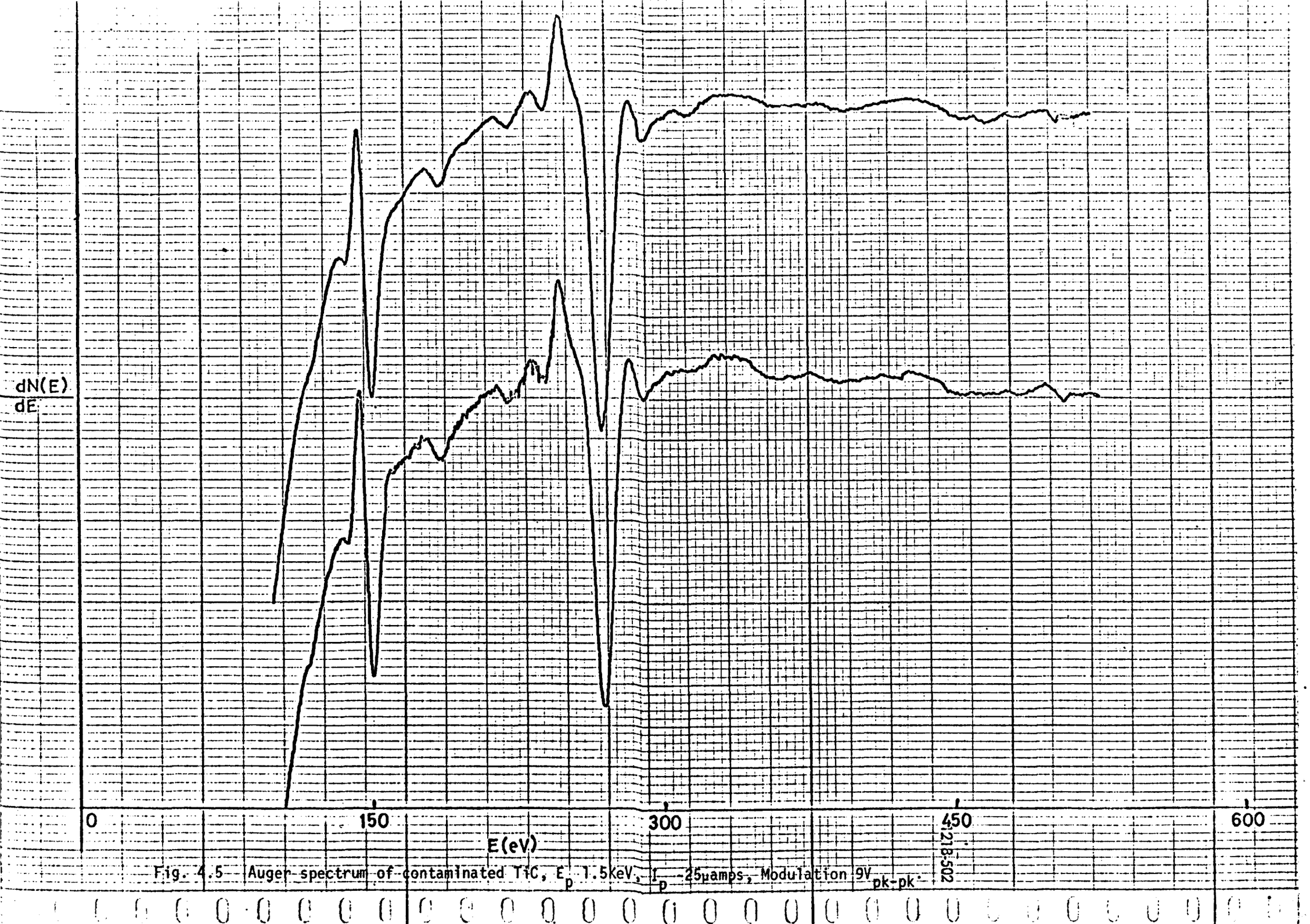

Fig. 4.5 Auger spectrum of contaminated TiC, E_p 1.5keV, I_p ~25μamps, Modulation 9V$_{pk-pk}$

Fig. 4.6 A comparison of the Auger peaks of TiC as observed in the energy distribution and differential distribution.

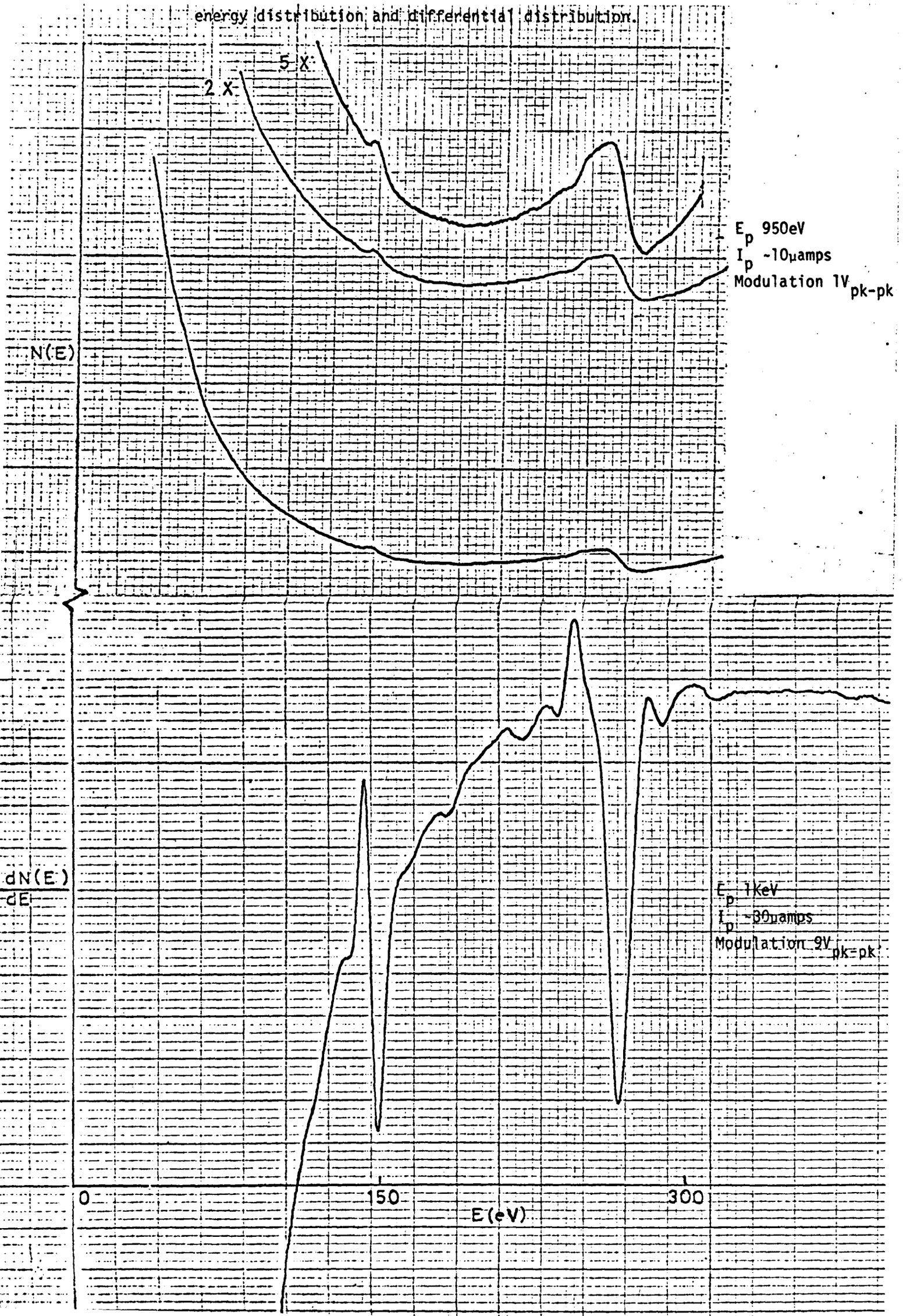

from the surface, the sample was heated up to ~250^{o}C. The Auger spectrum taken immediately after the heat treatment is shown in Fig. (4.2). Only three main peaks are observed in the spectrum. The third and new one appeared at 148eV. No peaks could be detected below 148eV. The sample was then flashed to ~800^{o}C by electron bombardment. The spectrum recorded immediately afterwards is shown in Fig.(4.3a). A large peak at 270eV and a small one at 239eV are the main features of the spectrum. A new peak at 18eV is also just resolved. No other peaks which could be attributed either to Zr or oxygen as seen in the previous spectra, were detected. Fig.(4.3b) shows the slow peak, due to true secondary electrons created by 1.5KeV primary electrons. The measured half-width (peak-to-peak) of this peak is only ~3eV. When small modulation voltage was used, there was some evidence for the existence of a peak at about 253eV as shown in Fig.(4.4).

TiC

An Auger spectrum of a heavily contaminated TiC sample is shown in Fig.(4.5). This spectrum was taken after heating the sample up to ~400^{o}C. The two main peaks seen in the spectrum occur at about 270 and 150eV and are believed to be due to carbon and sulphur respectively. The smaller peaks occur at 137, 186, 223, 241 and 291eV. Further heating of the sample did not produce any change in the spectrum. A comparison of the Auger peaks observed in the energy distribution and differential distribution is shown in Fig.(4.6).

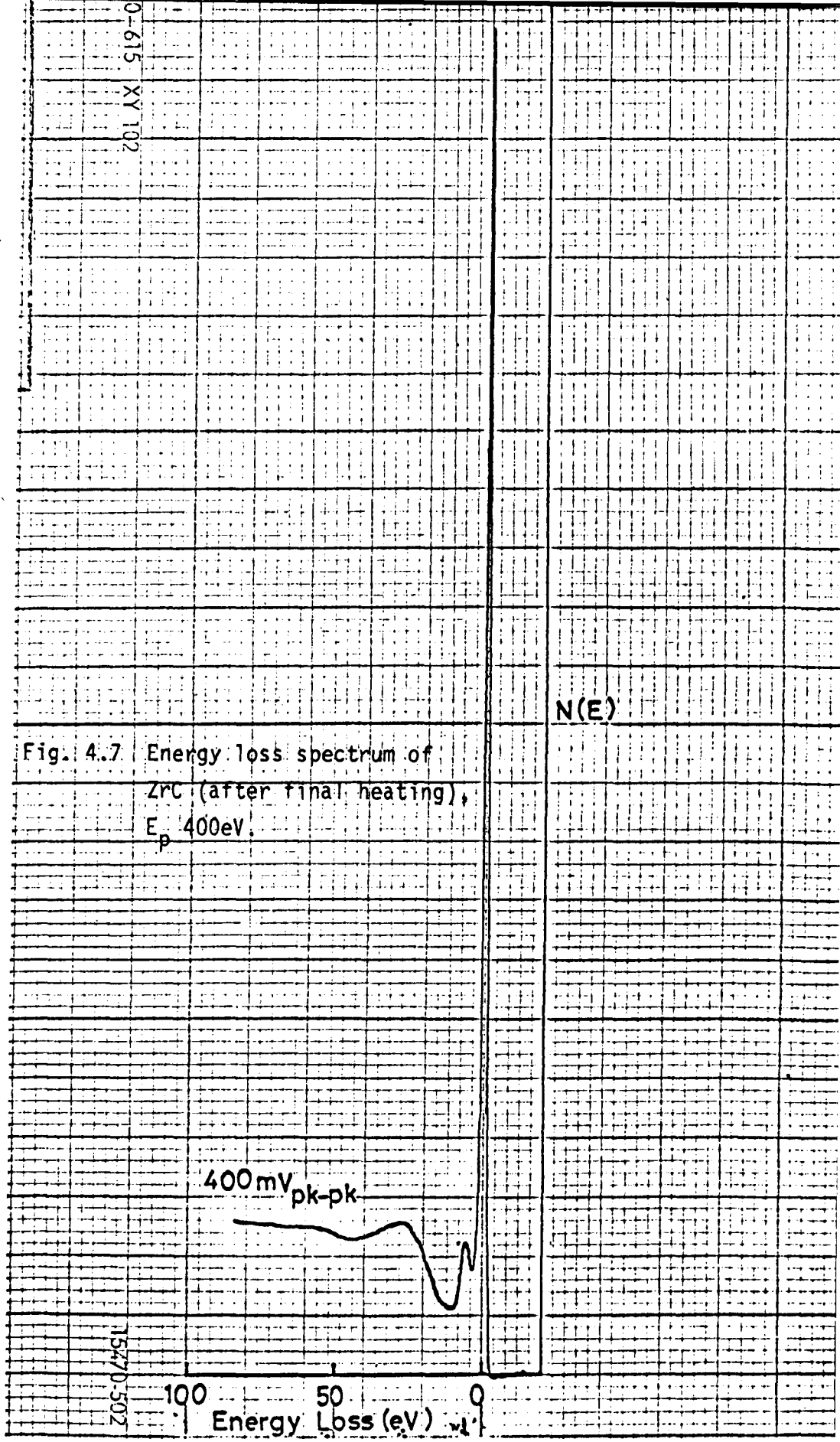

Fig. 4.7 Energy loss spectrum of ZrC (after final heating), E_p 400eV.

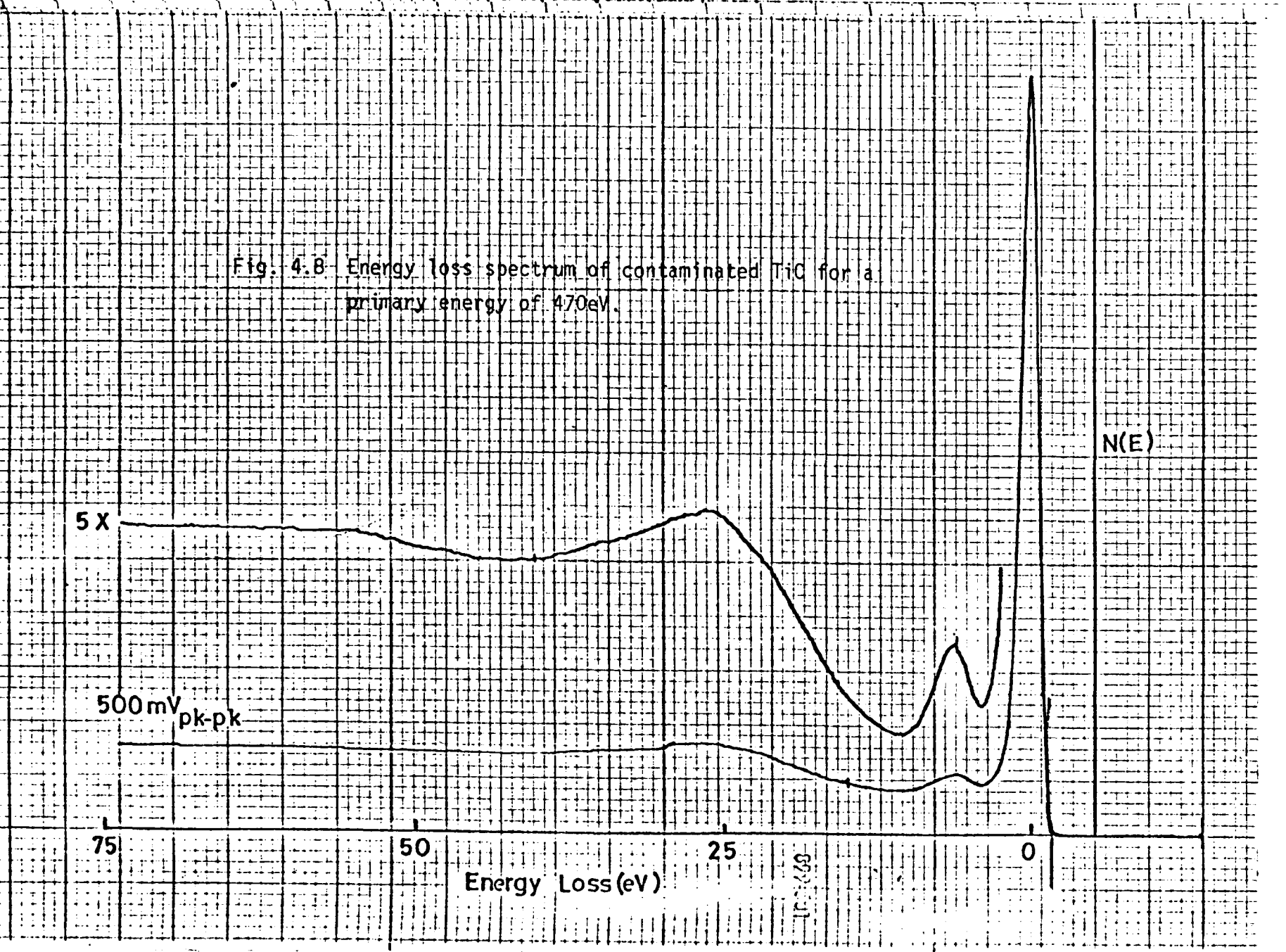

Fig. 4.8 Energy loss spectrum of contaminated TiC for a primary energy of 470eV.

Fig. 4.9 Energy loss spectrum of contaminated TiC for a primary energy of 1KeV.

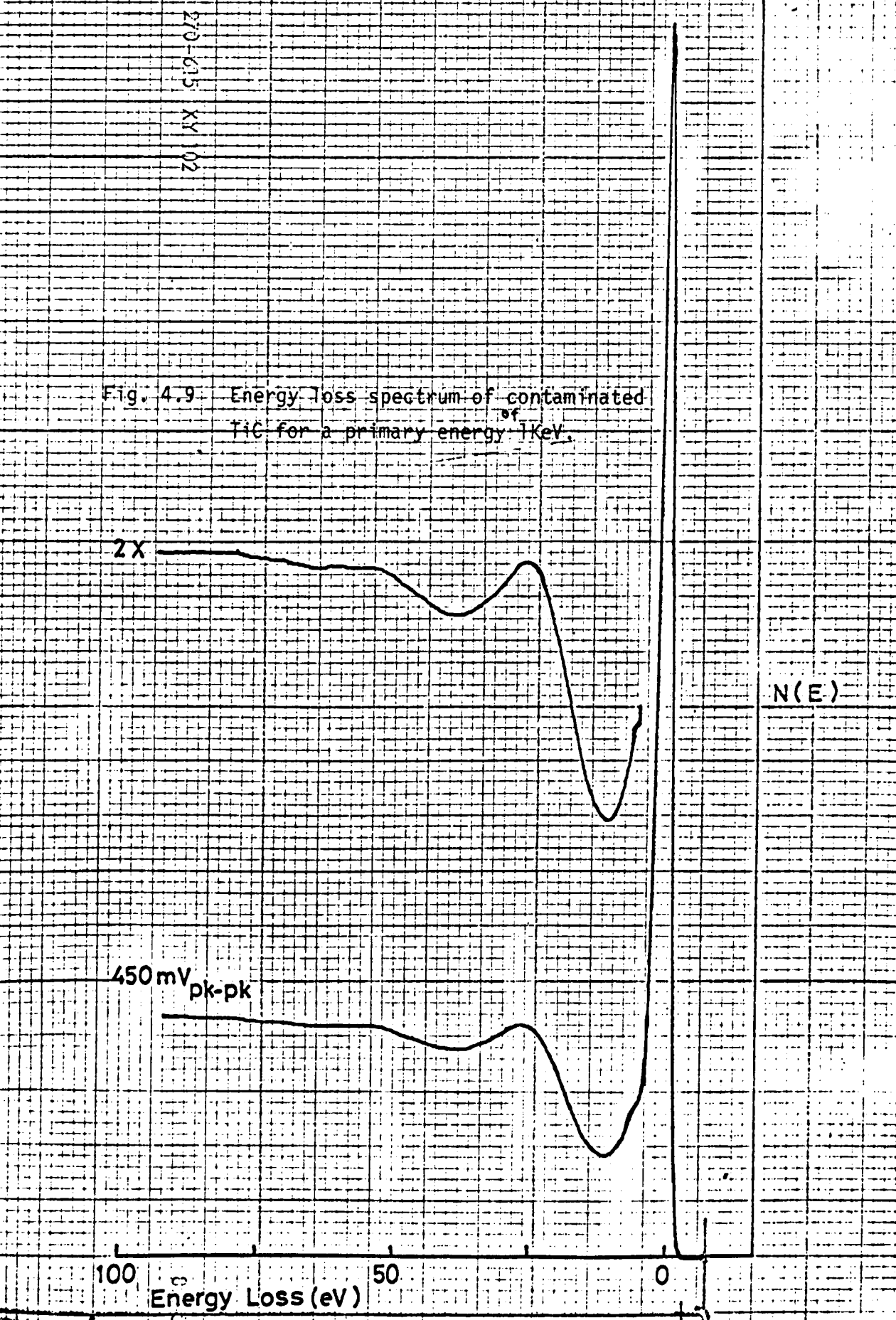

4.2.2 Characteristic Energy Loss Spectra of ZrC and TiC

ZrC

The energy loss spectrum of ZrC was taken after the final heating of the sample and is shown in Fig.(4.7). A primary energy of 400eV was used in this case. The energy loss peaks occur at 6, 26 and 52eV.

TiC

The characteristic energy loss spectra of a contaminated TiC sample are shown in Figs.(4.8) and (4.9) for primary energies of 470 and 1000eV. The observed loss peaks occur at 6, 26 and 52eV.

4.2.3 Discussion

The Auger peaks arising from Zr, C and from other elements present as contaminants are listed and identified in Table 4.1. The calculated energy and the transition involved are also given. For calculations of the Auger transition energies, the formula of Burhop[15] was used. (see Chapter I, section 1.3.1). The formula can be written in the general form as follows

$$E_Z = E_f(Z) - E_B(Z) - E_C(Z+1)$$

The energy values of atomic energy levels for these calculations were taken from the X-ray energy level data reported by Bearden and Burr[60].

Table 4.1

Auger peak energies of Zr, C and other elements present as contaminants on ZrC surface

Element	Transition	Calculated energy (eV)	Observed energy (eV)
Zr	$M_5N_1N_{2,3}$	95	91
	$M_4N_1N_{2,3}$	97	
	$M_5N_{2,3}N_{2,3}$	117	114
	$M_4N_{2,3}N_{2,3}$	119	
	M_5N_1V	126	Not resolved
	M_4N_1V	128	
	$M_5N_{2,3}V$	148	143
	$M_4N_{2,3}V$	150	152 ?
	$M_5V\ V$	174	169
	$M_4V\ V$	176	
C	$K\ L_{2,3}L_{2,3}$	267	270
	$K\ L_1L_{2,3}$	258	253
	$K\ L_1L_1$	243	239
O	$K\ V\ V$	516	507
	$K\ L_1V$	500	487
	$K\ L_1L_1$	477	470
S	$L_{2,3}V\ V$	149	148
Ar	$L_3M_{2,3}M_{2,3}$	215	212
	$L_3M_1M_{2,3}$	203	201
	$L_3M_1M_1$	186	187

The agreement between the calculated and the observed Auger energies is generally good. However the calculated values are usually a few volts higher than the observed values since the work function of the suppressor grid is not taken into account and consequently all measurements are relative to the Fermi level.

The identification of the observed Auger peaks is straightforward in most cases, the exception being among some of the minor peaks. In the Auger spectrum of ZrC, the Auger peaks arising from Zr were observed only before heating the sample (Fig(4.1)). The Auger peaks at 91, 114, 143 and 169eV are identified as due to Zr. These energy values are in agreement with those reported by Haas et al.[31] except for a small difference in energy values presumably due to the difference in the binding energies of the energy levels in the Zr element as opposed to those of Zr in ZrC.

It may be remarked that instead of one peak near 150eV as reported by Haas et al.[31], two peaks at 143 and 152eV were resolved (i.e. a separation of 9eV). Although one is tempted to allocate both these peaks to Zr as arising from the ionization of the M_4 and M_5 shells, respectively, this seems to be doubtful since the energy separation of the M_4 and M_5 energy levels in Zr is known to be only 2.4eV[60]. Alternatively, the peak at 152eV may be due to sulphur, although this identification cannot be made with certainty since a peak believed to be due to sulphur appeared at 148eV after heating the sample up to ~250^{o}C (Fig.(4.2)). Apart from the carbon and oxygen Auger peaks, there are three barely resolved peaks at 187, 201 and 212eV. These may be due to Argon, the energies of the possible

transitions involved are 186 ($L_3M_1M_1$), 203 ($L_3M_1M_{2,3}$)and 215 ($L_3M_{2,3}M_{2,3}$).

Mild heating of the sample did not affect the oxygen and carbon Auger peaks but all the Auger peaks identified as due to Zr disappeared. In addition a medium size sulphur peak emerged at 148eV. Both carbon and sulphur[2] are known to segregate on to the surface due to heating. It is also known that the escape depth of the Auger electrons is extremely shallow[43,27]. If one assumes that the surface coverage of carbon and sulphur due to segregation was thick enough as compared to the escape depth of the Zr Auger electrons of energy <175eV, then one would not observe any Auger peaks due to Zr.

It may also be pointed out that as a result of heating both carbon and oxygen peaks appeared to be shifted to slightly lower energies (~2-3eV), possibly due to some chemical reaction on the surface. Further heating (~800^{o}C) of the sample though removed the oxygen and sulphur, but no Zr Auger peak was detected (Fig.(4.3)). However, a new, barely resolved peak appeared at about 18eV. Coad and Riviere[61] have recently reported the Auger spectrum of graphite. They report Auger peaks at 16, 237, 253 and 269eV. These are in close agreement with the observed values of 18, 239, 253 and 270eV (Fig.(4.3)). It may be therefore concluded that the ZrC surface at this stage was completely covered with carbon due to segregation after heating, and further this coverage was sufficient to prevent the escape of any of the Zr Auger electrons.

The Auger spectrum of TiC (Fig.(4.5)) did not show any titanium peaks after heat treatment although large titanium peaks have been reported[32] around 400eV. The reasons for the absence of titanium peaks are again very much the same as in the case of ZrC viz. surface contaminants. Sulphur and chlorine have been reported[32] as the main contaminants in a titanium surface and both were observed in the present spectrum (4.5) and could not be removed by simple heating. The small peak at 138eV is probably also due to sulphur ($L_{2,3}M_1M_{2,3}$ - 138eV). In addition to the chlorine Auger peak at 186eV ($L_{2,3}VV$ - 187eV), there were two more small peaks at 223 and 291eV. These peaks seem to appear along with the carbon peak. However, these peaks cannot be explained from the known energy levels of carbon. Alternatively these peaks may be due to some unknown impurities on the surface. (For example Ca is known[62] to have a peak at about 290eV, $L_{2,3}M_{2,3}M_{2,3}$ - 291.) In such a case these peaks would have little effect on the spectrum since they are very small.

Since the ZrC sample showed an Auger spectrum similar to that of graphite (Fig.(4.3)), one would expect the energy loss spectrum of the surface to be similar to graphite. This has actually been observed in the present case (Fig.(4.7)). Although TiC did not show the graphite Auger spectrum (4.5), its energy loss spectrum was found, surprisingly similar to that of graphite (Figs.(4.8) and (4.9)). Similar results of energy loss spectrum of carbon on nickel surface have been reported by Coad and Riviere[61]. The measured energy loss values (for ZrC and TiC) are 6, 26, and 52eV. These values are in agreement with those reported by Coad and

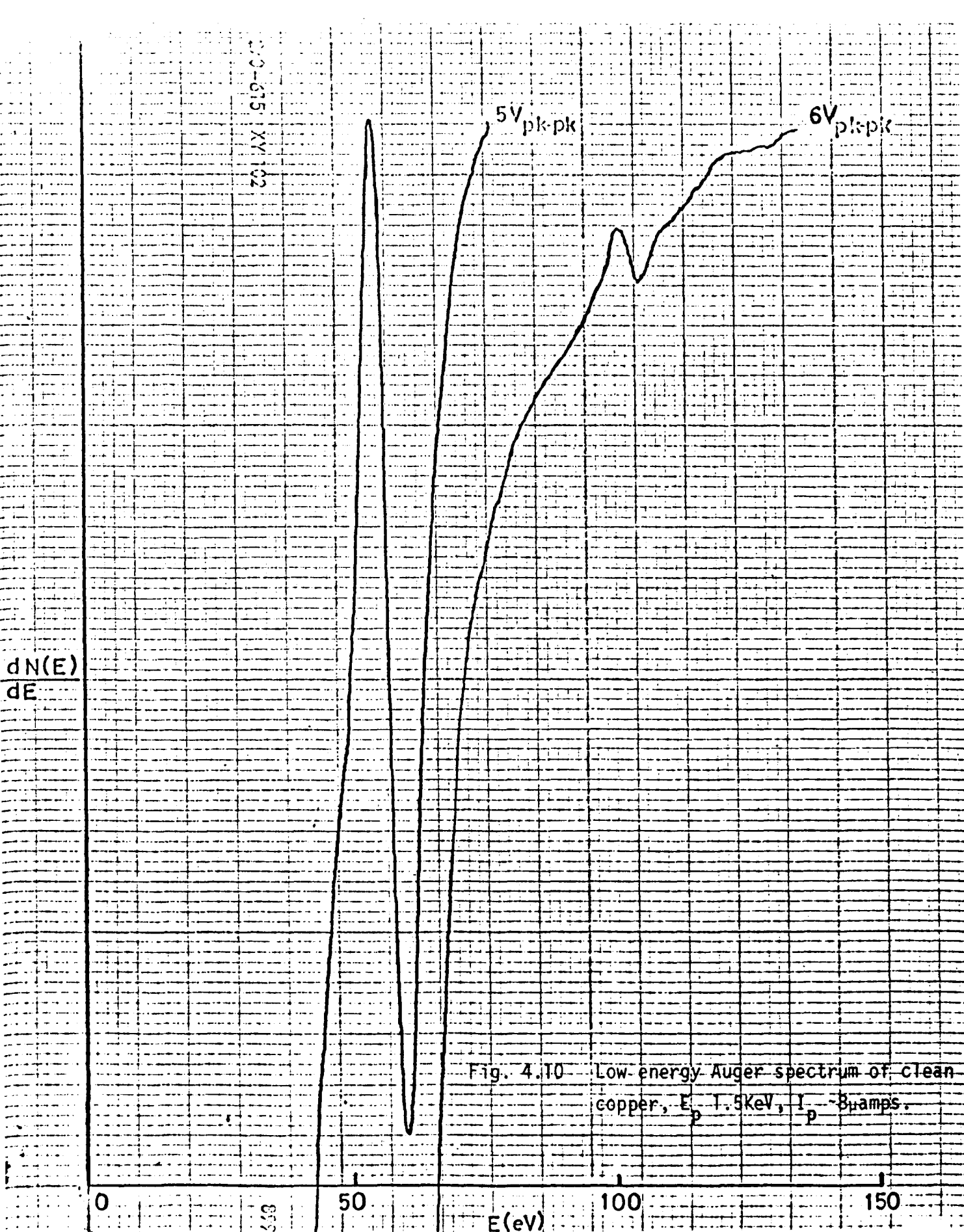

Fig. 4.10 Low-energy Auger spectrum of clean copper, E_p 1.5KeV, I_p ~8μamps.

Riviere[61] and Scheibner and Tharp[24], except for the small difference in energy values. This difference is attributed to the different density of carbon in different forms[63]. Assuming four valence electrons free per atom in carbon for a density of 2.25 gm/cm^3, the value of the bulk plasmons ($\hbar\omega_p$) is ~25eV. This in in close agreement with the observed value of 26eV. The loss peak at 52eV is then a multiple of the bulk plasma loss. The loss peak at 6eV is presumably due to an interband transition[24].

4.3 The Auger Electron and Characteristic Energy Loss Spectroscopy of Clean Copper and Gold Surfaces

In order to obtain clean surfaces both copper and gold samples were prepared by evaporation in ultra high vacuum conditions. In both cases thick films of spectroscopically pure copper and gold were evaporated onto glass substrates. Several evaporations were performed for both copper and gold and the Auger spectrum was taken immediately after each evaporation. Tungsten baskets were used for the evaporation of both copper and gold.

4.3.1 Auger spectra of copper and gold

Cu

A low energy Auger electron spectrum of a clean copper surface for a primary energy of 1.5KeV is shown in Fig.(4.10). Only two peaks were observed in the low energy region (0 - 150eV), a large peak at 61eV and a small one at 107eV. The LMM (high energy region) Auger spectrum of copper was plotted for a primary energy of 2KeV and beam current of ~10μ amps

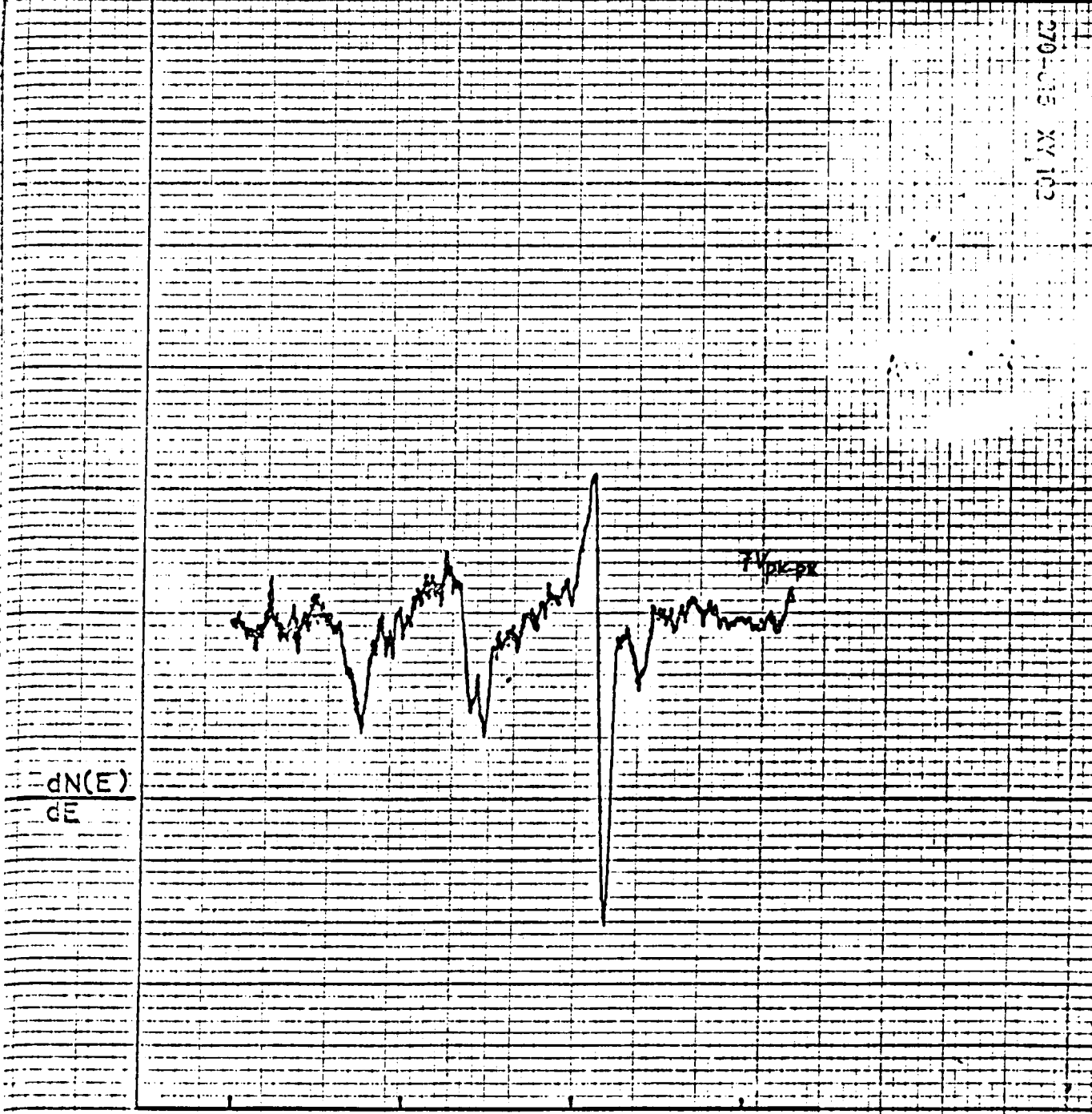

Fig. 4.11 High energy Auger spectrum of clean copper.
E_p 2KeV, I_p ~10μamps.

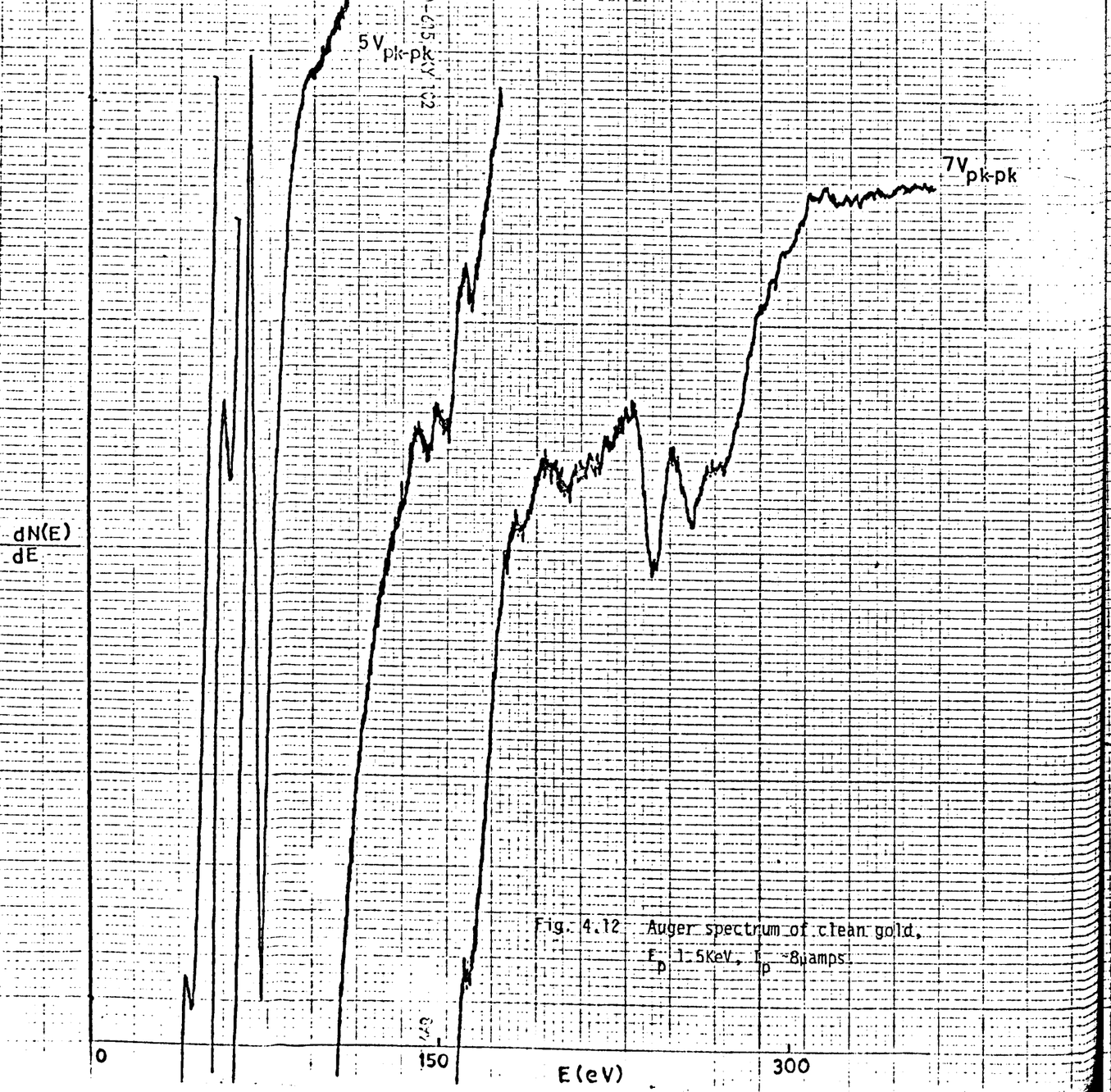

Fig. 4.12 Auger spectrum of clean gold.
E_p 1.5KeV, I_p ~8μamps.

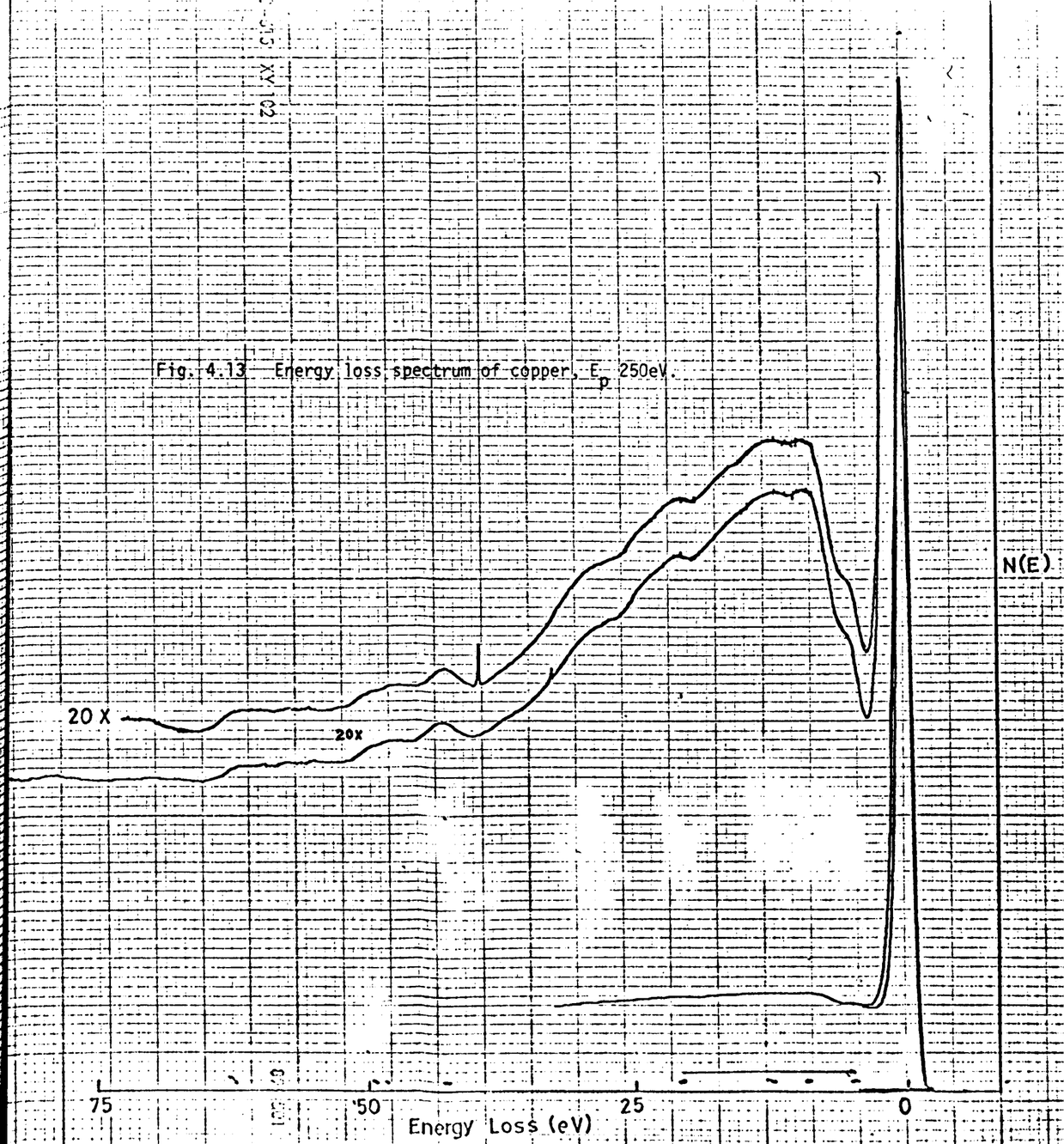

Fig. 4.13 Energy loss spectrum of copper, E_p 250eV.

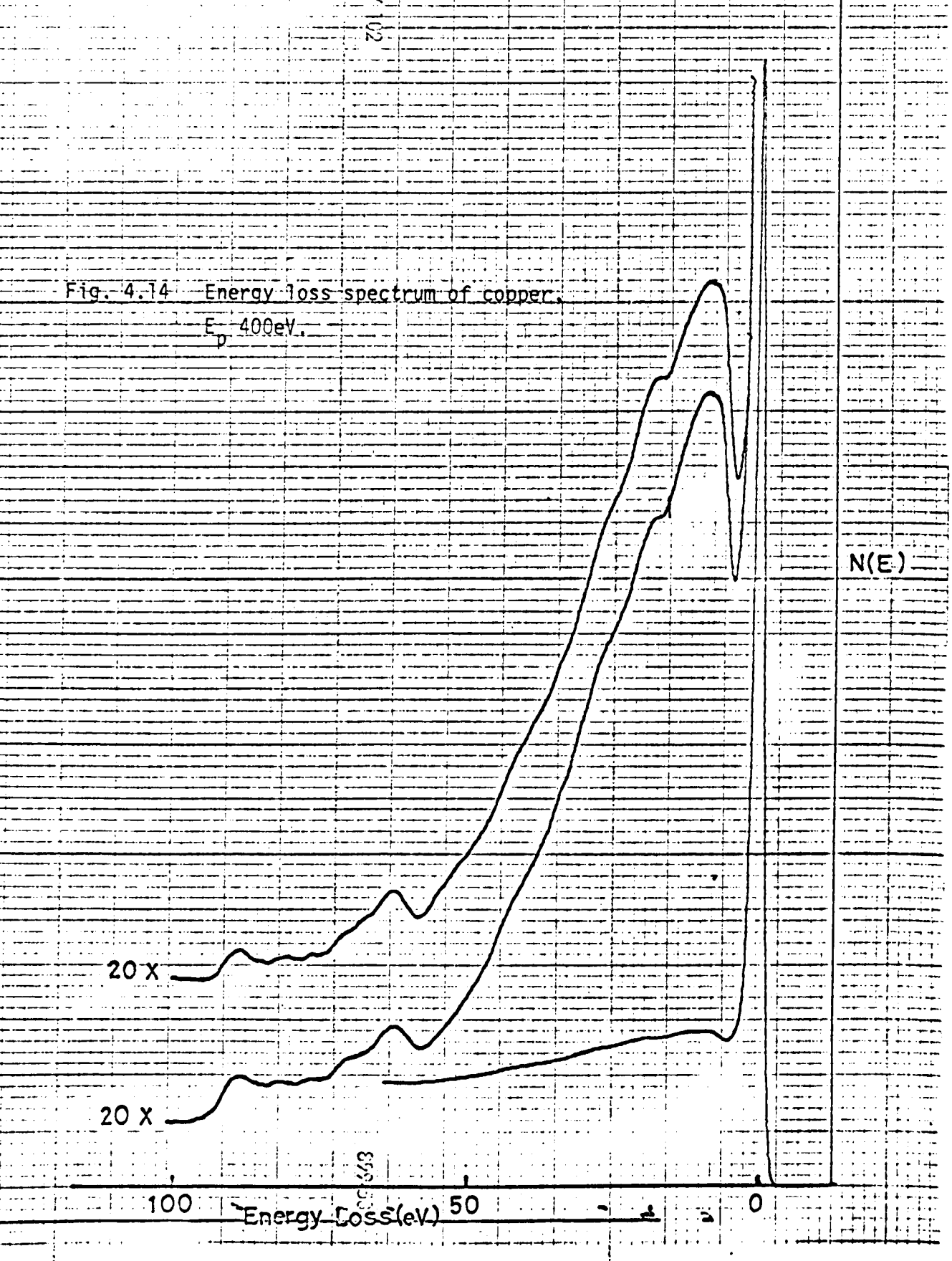

Fig. 4.14 Energy loss spectrum of copper. E_p 400eV.

and is shown in Fig.(4.11). Since no Auger peak was observed between 156 - 700eV energy, only the 700 - 1000eV energy region is shown. The small peaks recently reported in the LMM spectrum of copper by Jenkins and Chung[64], could not be observed due to primary energy and beam current limitations. However, two peaks at 838 and 846eV were found instead of one reported by the above authors. Similar 'doublets' have been reported by Aksela et al[65] using a cylindrical mirror analyser. The other peaks in the LMM spectrum occur at 773, 918 and 938eV.

Gold

The Auger electron spectrum of gold was explored in the energy range of 0 - 1000eV. No Auger peaks could be detected above 260eV. In the low energy region no peak was found below 44eV, as reported by Haas et al.[31] and Palmberg and Rhodin[4]. The Auger spectrum, believed to be that of a clean gold surface, is shown in Fig.(4.12). A primary energy of 1.5KeV was used in this case. The main peaks seen in the spectrum are found at energies of 260, 243, 74, 60 and 44eV. A number of smaller peaks have also been resolved between the energies of 74 and 243eV.

4.3.2 Characteristic energy loss spectra of copper and gold

Cu

The energy loss spectrum of a clean copper surface for primary energies of 250 and 400eV is shown in Figs.(4.13) and (4.14) respectively. A broad loss peak at 9.5eV seen in the spectrum of Fig.(4.14) was resolved into two peaks at 8.6 and 11.8eV as shown in Fig.(4.13). In addition a

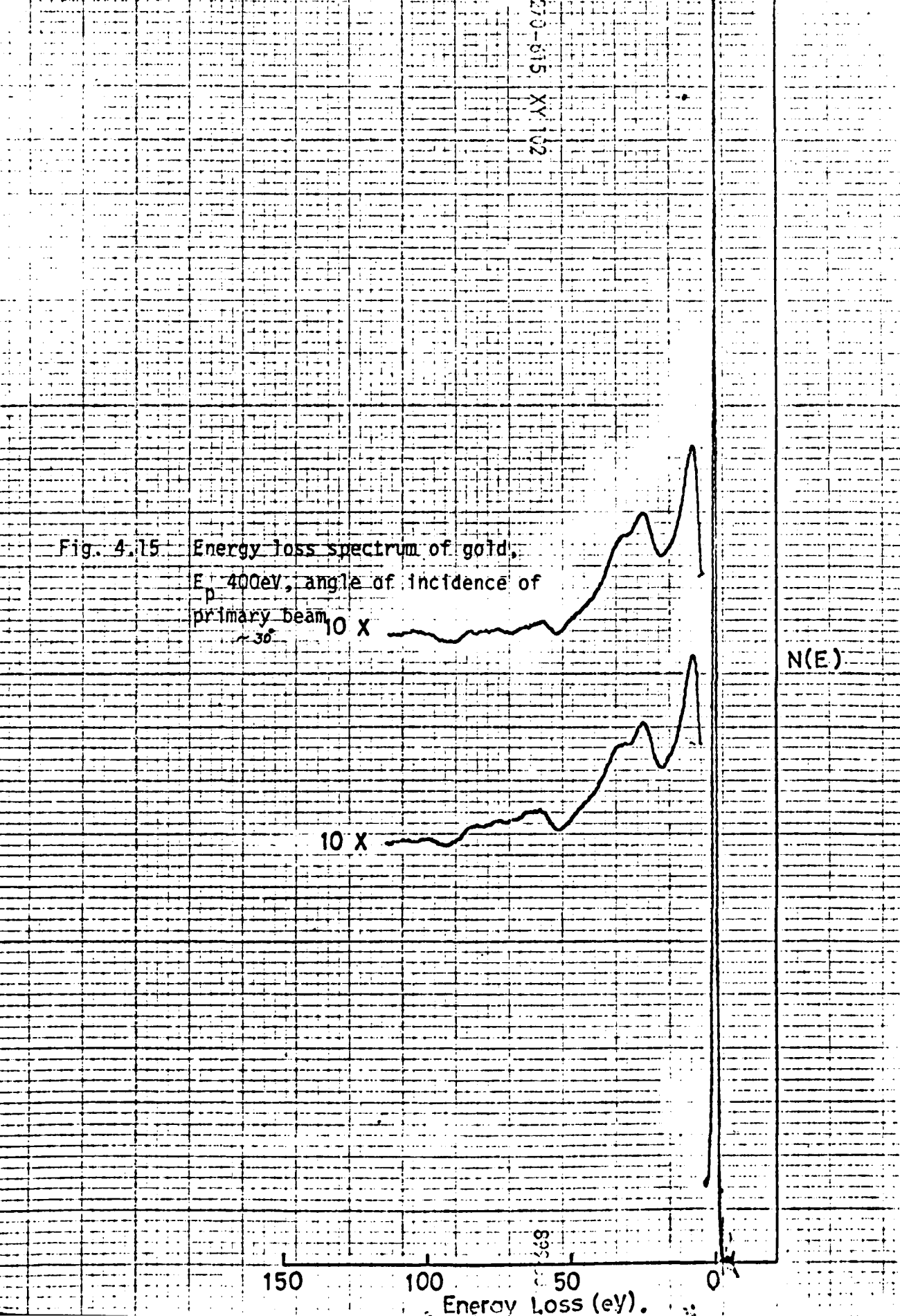

Fig. 4.15 Energy loss spectrum of gold, E_p 400eV, angle of incidence of primary beam ~30°

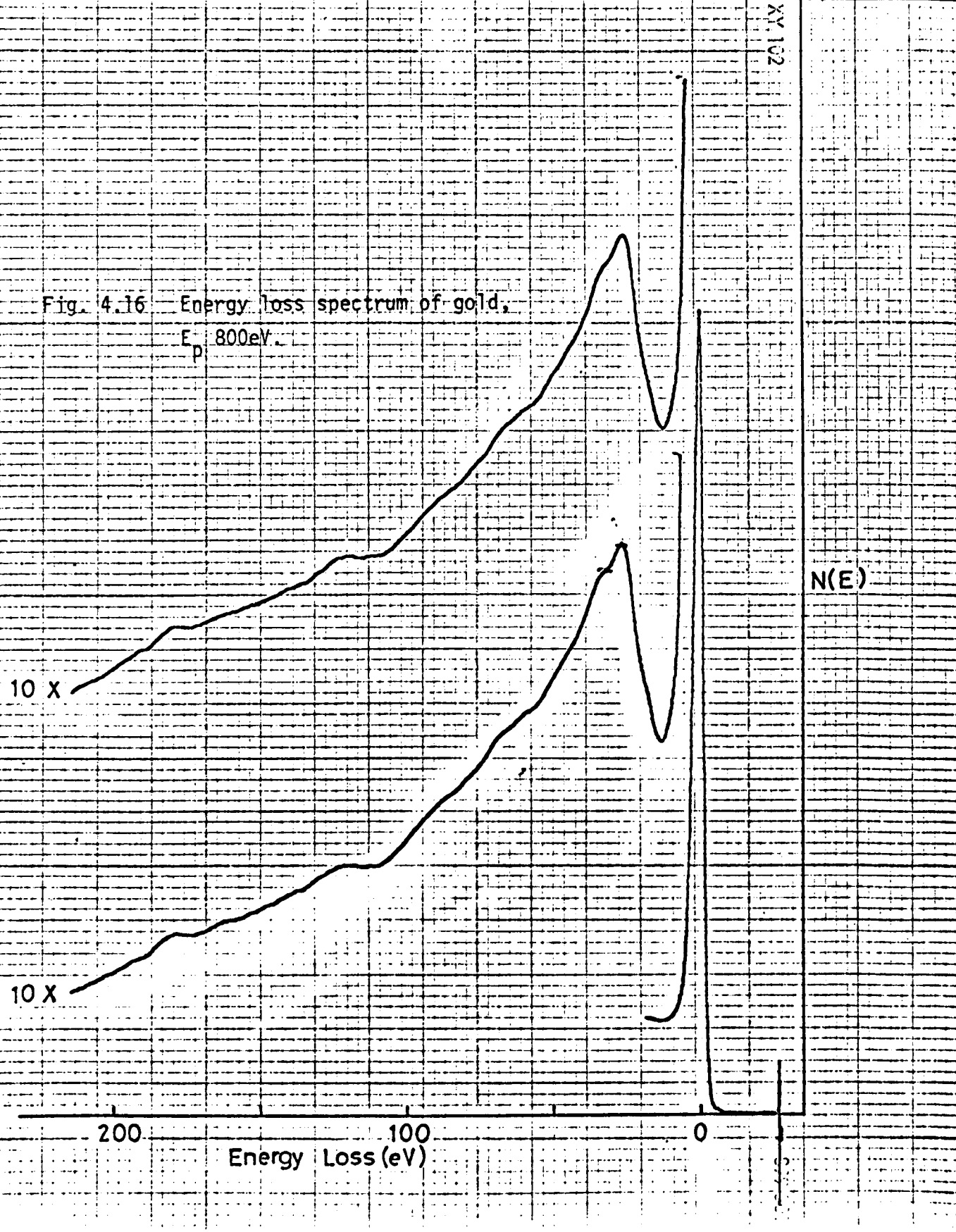

Fig. 4.16 Energy loss spectrum of gold, E_p 800eV.

small and poorly resolved loss peak at about 5eV was also resolved. Other significant loss peaks occur at 42.3eV (Fig.(4,13)), 62.5 and 88eV (Fig. (4.14)). No increase in intensity of loss peak at 20.4eV was noticed with increased primary energies.

Gold

The energy loss spectrum of a clean gold surface is shown in Figs.(4.15) and (4.16). The primary energies used for these spectra were 400 and 800eV respectively. The main feature of the spectrum as shown in Fig.(4.15) is a large loss peak at 7.3eV and a relatively small one at about 25.6eV with a shoulder at 33.4eV. The intensity of the 25.6eV loss peak was found to increase with increased primary energies while that of the 7.3eV peak decreased. The increase in the intensity of 25.6eV loss peak is evident from the spectrum of Fig.(4.16). This spectrum was obtained for a primary energy of 800eV. The other resolved loss peaks occur at 62 (Fig.(4.15)),120 and 179eV (Fig.(4.16)).

4.3.3 Discussion

The Auger peaks observed in the Auger spectrum of a clean copper surface are listed in Table 4.2. The approximately calculated energy values and probable transitions are also given.

Table 4.2

Comparison of Auger peak energies of clean copper surface observed in the present work with those of other authors.

Transition	Calculated energy (eV)	Observed energy (eV)	Palmberg and Rhodin (4)	Aksela et al. (65)	Jenkins and Chung (64)
$M_{2,3}V\ V$	63	61	62	-	62 59
$M_1\ V\ V$	110	107	109	-	109
$L_3M_{2,3}M_{2,3}$	771	773	795	777.5	772
L_3M_2V	846	838	-	839.2	843
L_3M_3V	849	846	875	846.4	
$L_3V\ V$	921	918		918.9	919
$L_2V\ V$	941	938	950		939

A comparison with the Auger energy values of copper reported by Palmberg and Rhodin[4] Aksela et al.[65] and Jenkins and Chung[64] is also presented in the table. The low energy Auger peak (MMM spectrum) agree well with those reported by the other workers. However the separation between the Auger peaks arising from $M_3V\ V$ and $M_2V\ V$ transitions reported by Jenkins and Chung[64] could not be observed since relatively large modulation (~5 V_{pk-pk}) was used at this stage to maximise the sensitivity. The associated fine structure reported by the authors was not resolved for the same reason. In the L M M spectrum, the Auger peak energies reported by

Palmberg and Rhodin[4] are much higher than those found in the present work. However, the energy values reported by Aksela et al.[65] and Jenkins and Chung[64] are in good agreement. The minor Auger peaks reported by the latter authors were not seen due to limited beam current (~10μamps) and primary energy (~2KeV).

All the Auger peaks in the LMM spectrum were thought to originate from the ionization of L_3 shell, except the peak at 938eV. This was allocated to the L_2VV transition. The largest peak in the LMM spectrum occurred at 918eV and is attributed to the L_3VV transition. That this allocation of the two peaks is correct is perhaps confirmed by the fact that the separation between L_2 and L_3 energy levels of copper is the same as observed for the L_2VV (938eV) and L_3VV (918eV) Auger transitions[60]. Aksela et al.[65] have reported two Auger peaks at 839 and 846eV observed in the energy distribution curve, but have not allocated the second peak to any transition. In the present work two peaks are observed at 838 and 846eV. The origin of these peaks may lie in the L_3M_2V and L_3M_3V transitions respectively. This allocation, however, is questionable, since the energy separation of the M_2 and M_3 energy levels is only 2.7eV as compared to the 8eV separation of the Auger peaks due to L_3M_2V and L_3M_3V transitions. The third peak in the LMM spectrum allocated to $L_3M_{2,3}M_{2,3}$ is found at 773eV and is wider than the L_3VV peak. This seems to suggest that the Auger peaks due to the M_2 and M_3 shells may be responsible for the broadening of the Auger peak in the $L_3M_{2,3}M_{2,3}$ transition. All the Auger peaks found in the Auger spectrum of clean gold have been identified as due

to gold. The measured energy values along with the calculated energies and transitions involved are tabulated in Table 4.3.

Table 4.3

Auger peak energies of clean gold surface found in the present work and by other workers

Transition	Calculated energy (eV)	Observed energy (eV)	Palmberg and Rhodin (4)	Haas et al. (31)
O_3VV	45	44	43	44
O_2VV	63	60	58	
N_6VV	77	74	72	
O_1VV	99	100	100	
$N_5N_6N_6$	145	145	150	144
$N_5N_7N_7$	157	154		156
$N_5N_6O_2$	167	164	167	164
$N_5N_6O_3$	190	185		
$N_5O_2O_3$	205	205		
N_5N_7V	245	243	246	
N_4N_7V	263	260	263	

Auger spectra of gold have previously been reported by Palmberg and Rhodin[4] and Haas et al.[31]. However, the latter authors have not tabulated all the observed Auger peak energies. Therefore only a few tabulated values

of these authors are included in Table 4.3 along with the energy values found by the former authors. In general there is good agreement with the values reported by these authors. However, instead of the 150eV peak found by Palmberg and Rhodin[4], two peaks were resolved at 145 and 154eV possibly originating from the $N_5N_6N_6$ and $N_5N_7N_7$ transitions respectively. Twomore peaks not seen by Palmberg and Rhodin[4] were found at 185 and about 205eV, and may have their origin in the transitions $N_5N_6O_3$and $N_5O_2O_3$ respectively. The peak at 205eV appears to be wide, presumably due to an unresolved nearby peak possibly due to the $N_5O_3O_3$ transition. The Auger peaks at 243 and 260eV are considered to be due to N_5N_7V and N_4N_7V transitions respectively. The measured separation of these two peaks (17eV) is in close agreement with the reported separation (18eV) of the N_5 and N_4 energy levels of gold[50]. Similarly the separation between the O_3VV and O_2VV Auger transitions is about the same as the separation between the O_3 and O_2 energy levels of gold. It may be pointed out, however, that the small separation (3.6eV) between the N_6VV and N_7VV transitions was not seen in this spectrum due to the large modulation amplitude used. This separation was observed in the gold black spectrum (Section 4.2) with small modulation voltage.

Characteristic energy losses from copper have been investigated by many authors, and some of the recent results are compared with the present ones in Table 4.4.

Table 4.4

Characteristic energy losses in copper as found in the present work and by other workers (eV)

Present work	5.1	8.6	11.8	20.4	28.7	42.3	62.5	88.2
Powell[67]	4.4	7.2		19.9	27.1			
Scheibner and Tharp[24]	4	9.2		20.5	28			
Moss and Blott[56]	4.4	7.6		19.5	28.5	40	50	69

There is general agreement on the interpretation of the low lying loss at about 5eV as being due to an interband transition. However, there are a variety of interpretations of surface and bulk plasmon losses. Some of the workers[66,67,56,68] identify a bulk plasmon with the loss at about 20eV and a surface plasmon with the loss at 7.5eV, while others[50,47,24] consider the 7.5eV loss as being a bulk plasmon, but do not mention any surface loss. Assuming one free electron per atom in copper, the calculated values of the bulk ($\hbar\omega_p$) and surface plasmon ($\hbar\omega_p/\sqrt{2}$) losses are 10.8 and 7.6eV respectively. In the present work two loss peaks were resolved at about 8.6 and 11.8eV. Most of the workers have not reported the loss at 11.8eV, but agree that the loss at 7.5eV (in the present work at 8.6eV) is a surface plasmon loss. If the 8.6eV peak is a surface loss, then the 11.8eV loss is probably a bulk plasmon loss. No intensity changes were

noticed for the 20eV loss peak with a change in primary energy, a feature usually associated with the bulk loss. The loss peaks at 20.4 and 28.7eV are thought to be the multiple and combination losses of the 8.6 and 11.8eV losses. The loss peaks at 42.3 (Fig.(4.13)), 62.5 and 88.2eV (Fig.(4.14)) are too strong in intensity to be considered as multiples of the bulk plasmon loss. The origin of these losses is not known. More recently a number of energy loss peaks have been reported by Jenkins and Chung[22]. However, the authors do not attempt an explanation of the origin of their various peaks.

The energy loss values of gold are presented in Table 4.5 along with the reported values of Robins[51] and Powell[49].

Table 4.5

Characteristic energy losses in gold as found in the present work and by other workers (eV)

Present work	7.3	25.6	33.4	62	120	179.4
Robins[51]	6.3	16	25.8	32.6		
Powell[49]	6.2	10.8	16.3	24.8	33.2	

Robins[51] considers a loss at 6.3eV as a surface plasmon loss and bulk loss at 25.8eV. For solid gold, Powell[49] identifies ~6.4eV surface loss and a bulk loss of ~34eV. For evaporated gold the author identifies 10.8 and 16.3eV losses as surface and bulk losses. The calculated values

of surface and bulk plasmons for one free electron per atom, are 9eV and 6.3eV. The dependence of the peak intensity on the primary energy, as observed in the present work, suggests that the loss peaks at 7.3eV and 25.6eV are surface and bulk plasmon losses respectively. The loss peak at 33.4eV is then probably a combined loss of bulk and surface losses. The loss peaks at 62, 120 and 179eV cannot be associated with the multiple losses due to bulk loss or ionization losses and therefore no interpretation is proposed at present for these loss peaks.

4.4 Auger Electron and Characteristic Energy Loss Spectroscopy of Copper Black and Gold Black

Owing to numerous technical applications (for example electron collectors, microwave windows, cylindrical energy analysers and other places where secondary electron emission is an undesirable factor), the study and preparation of low yield surfaces is of considerable practical importance. Recently Thomas and Pattinson[69] have reported the preparation of low yield surfaces such as copper black and gold black. However, the yield measurements do not provide detailed information about the surface composition, which may be highly important for any understanding of the low yield phenomena exhibited by these surfaces. Thus the surface composition of some samples of Au and Cu black has been determined by the technique of Auger spectroscopy. The samples were prepared in the manner described by Thomas and Pattinson[69], in a commercial coating unit at a residual pressure of ~0.5 torr of Argon. They were subsequently transferred to the UHV chamber for study.

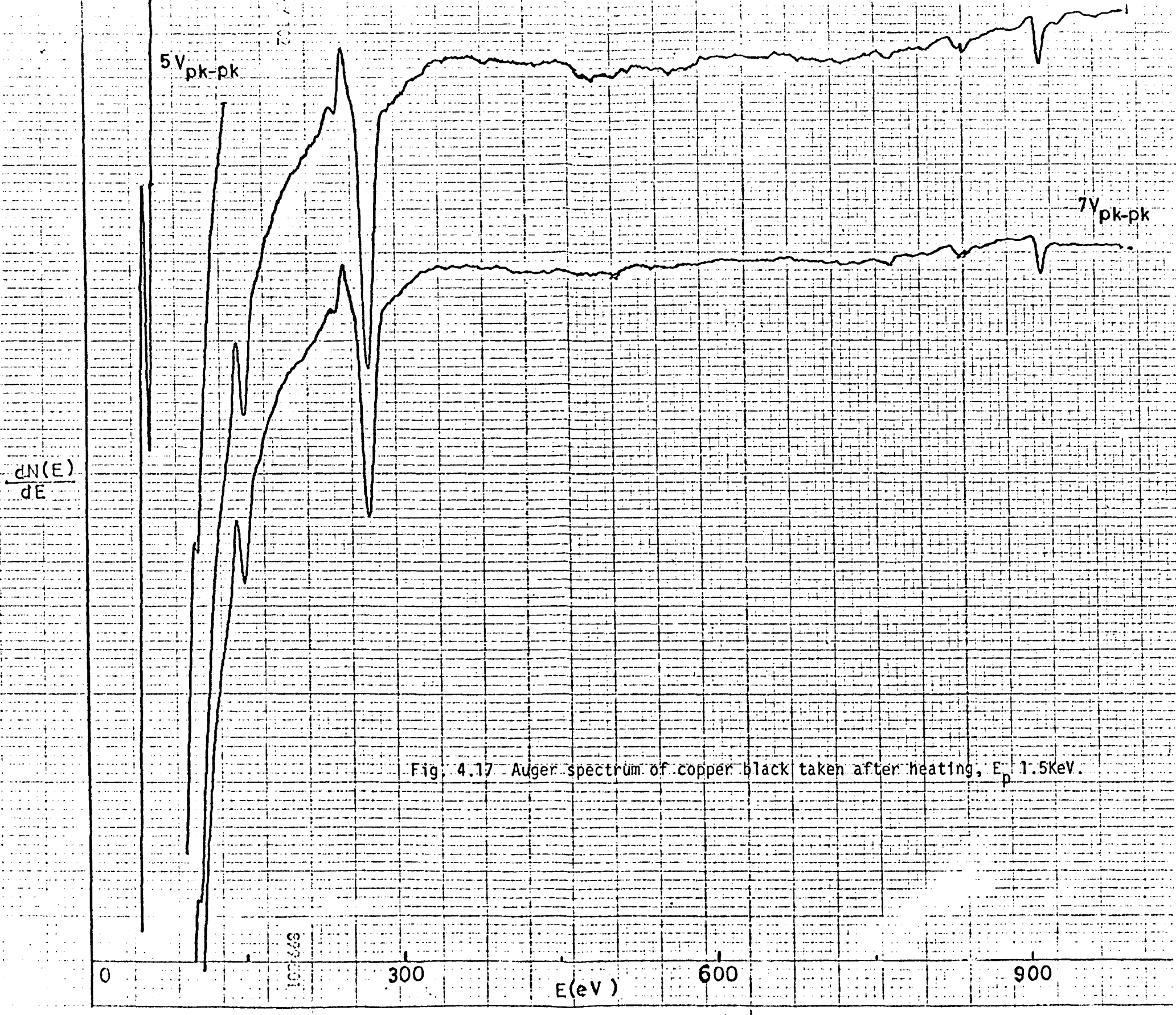

Fig. 4.17 Auger spectrum of copper black taken after heating, E_p 1.5KeV.

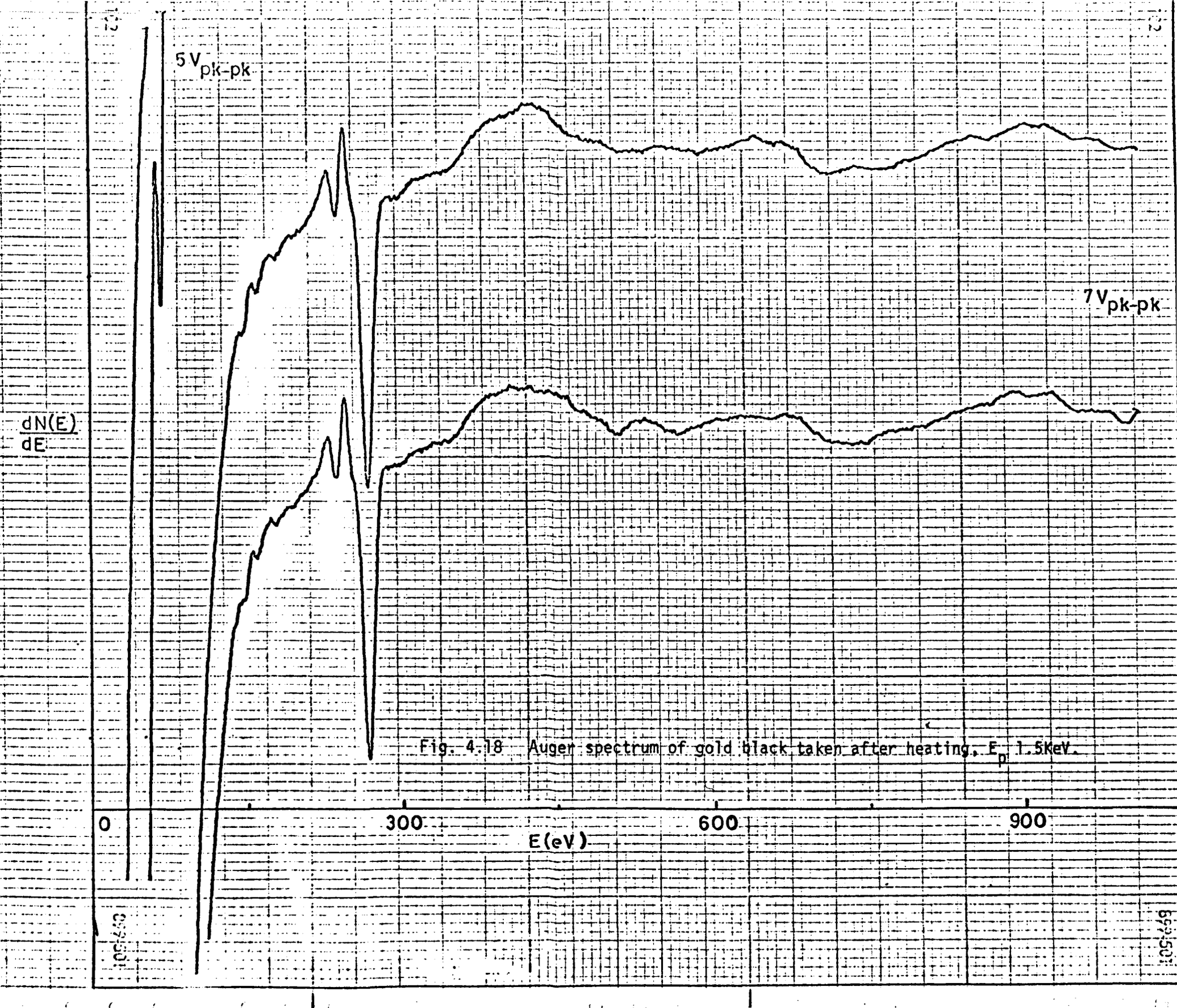

Fig. 4.18 Auger spectrum of gold black taken after heating, E_p 1.5KeV.

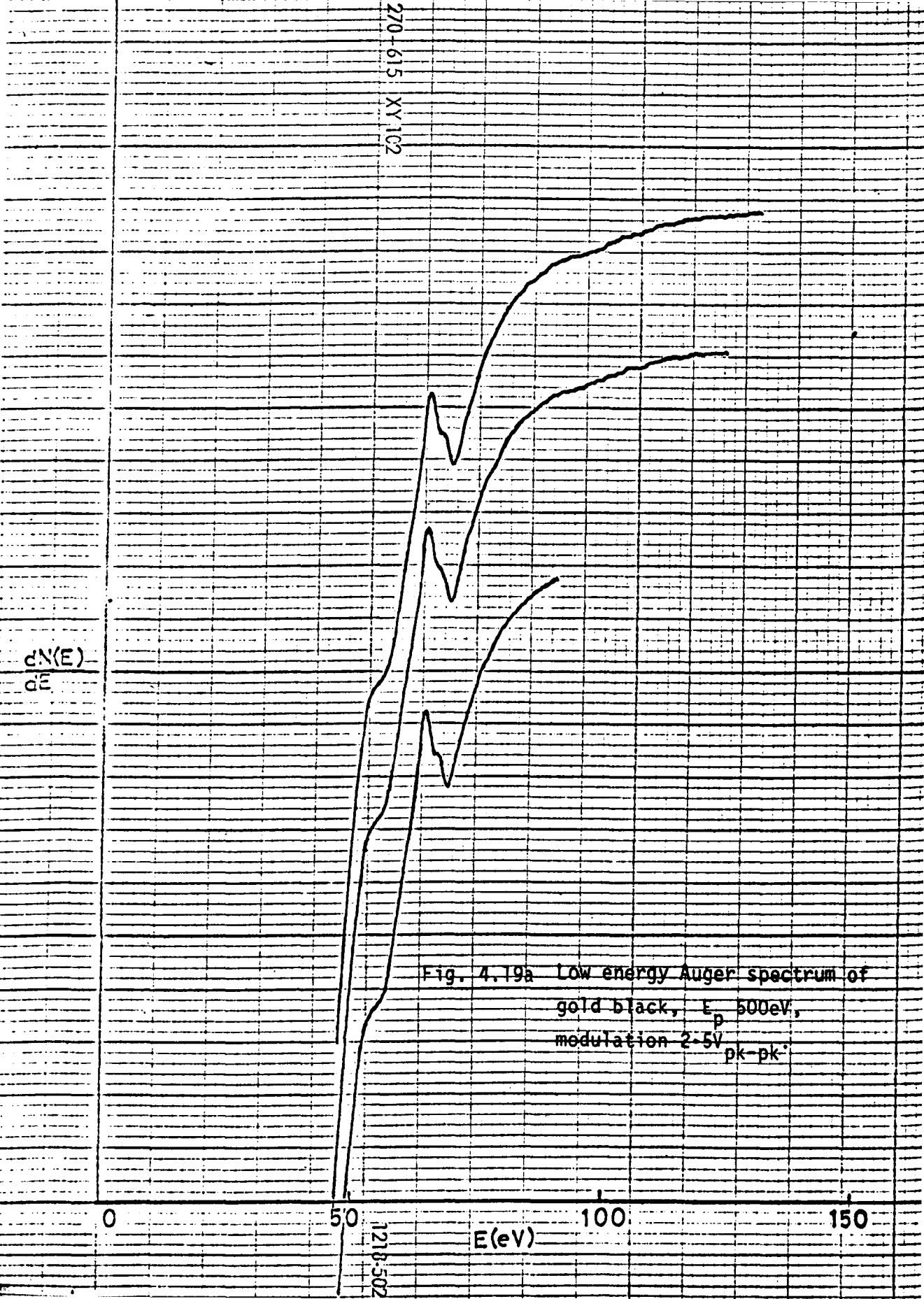

Fig. 4.19a Low energy Auger spectrum of gold black, E_p 500eV, modulation 2-5V_{pk-pk}.

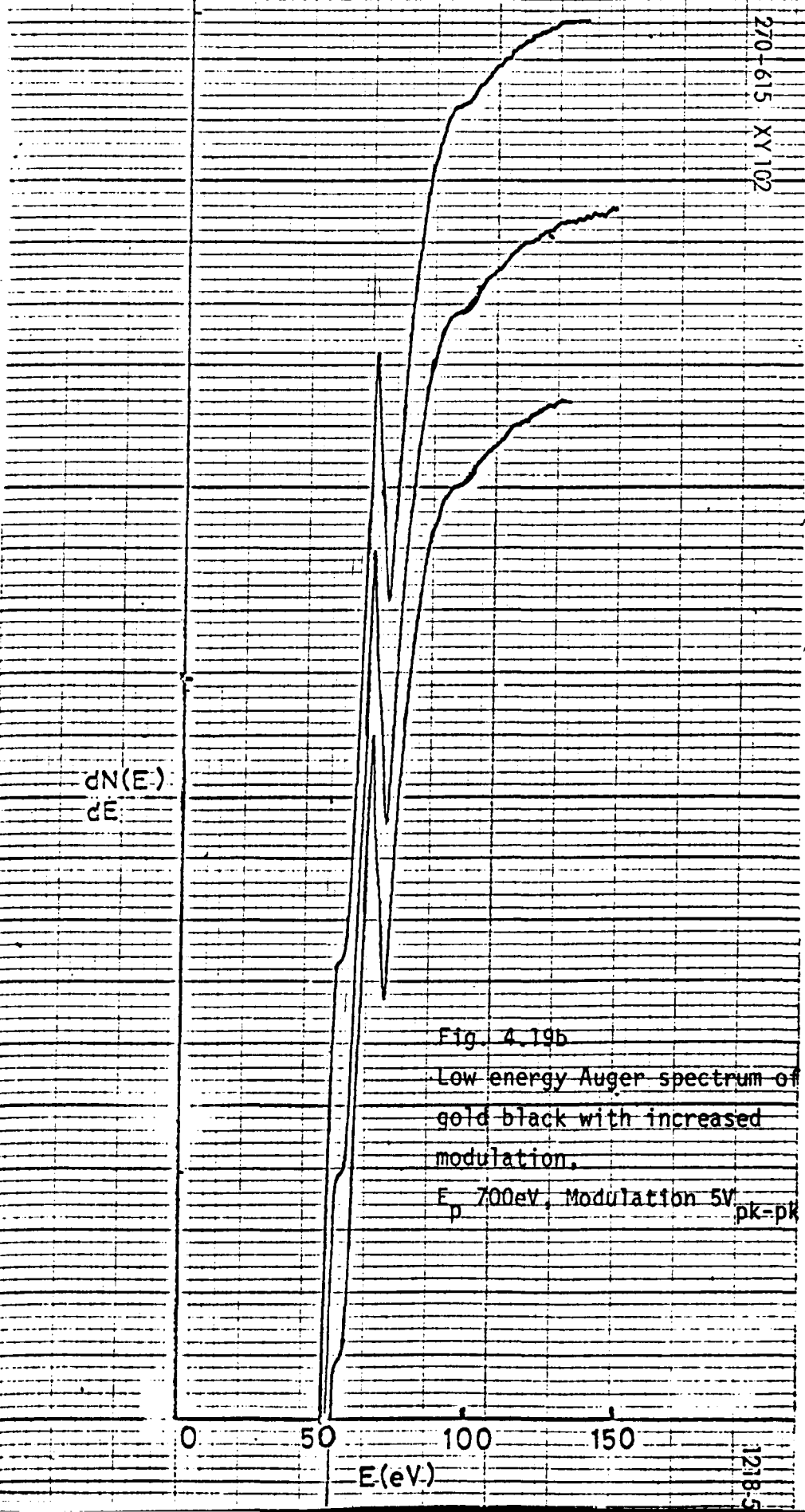

Fig. 4.19b

Low energy Auger spectrum of gold black with increased modulation.

E_p 700eV, Modulation 5V$_{pk-pk}$

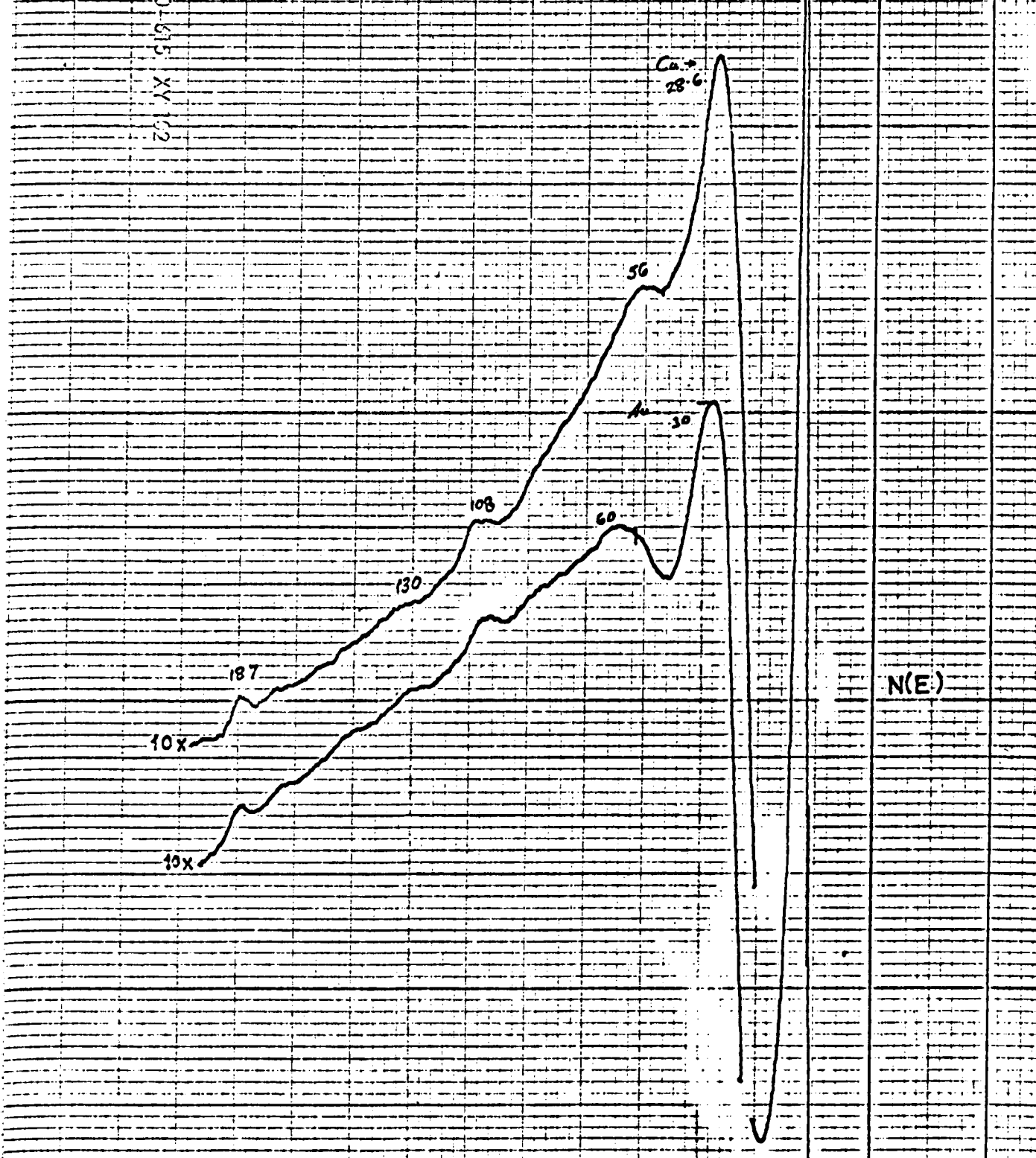

Fig. 4.20 Energy loss spectra of copper black and gold black, E_p 800eV.

4.4.1 Auger spectra of copper black and gold black

Copper Black

The Auger spectrum of copper black for a primary energy of 1.5KeV taken after heating (~250^{o}C) is shown in Fig.(4.17). Prior to the heating a medium size oxygen peak at 512eV (and a small oxygen peak at 491eV) and a small peak at 382eV, presumably due to nitrogen, were also detected, but no Auger peak at 150eV, which would be due to sulphur, was observed. Further heating (~400^{o}C) did not produce any significant change in the Auger spectrum which is shown in Fig.(4.17).

Gold Black

The Auger electron spectrum of a gold black sample for a primary energy of 1.5KeV is shown in Fig.(4.18). This spectrum was taken after mild heat treatment of the sample. Figs.(4.19a) and (4.19b) show the low energy spectrum (<150eV) for primary energies of 500 and 700eV respectively taken before heating. A small peak at 100eV is clearly resolved in Fig. (4.19b) and it could not be resolved after heating the sample. With a lower modulation amplitude (~2.5V_{pk-pk}), a small peak at about 68.2eV was resolved at shown in Fig.(4.19a). This peak, however, could not be resolved when relatively larger modulation amplitudes (>4V_{pk-pk}) were applied as may be seen from Fig.(4.19b).

4.4.2 Characteristic energy loss spectra of copper black and gold black

Characteristic energy losses of copper black and gold black surfaces are shown in Fig.(4.20). The similarity of the loss spectra of

both the samples is quite surprising. The energy loss values are given on the graph for quick comparison. With the exception of the first two peaks which show a small difference in energy, all the other loss peaks have approximately the same energy values.

4.4.3 Discussion

The Auger peaks found in the spectra of copper black and gold black are compared with those observed in the spectra of clean copper and gold surfaces, in Tables 4.6 and 4.7.

Table 4.6

Comparison of Auger peak energies of clean copper with copper black

Transition	Clean Copper	Copper Black
$M_{2,3}VV$	61	62
M_1VV	107	107
$L_3M_{2,3}M_{2,3}$	773	772
L_3M_2V	838	838
L_3M_3V	846	846
L_3VV	918	917
L_2VV	938	940

Table 4.7

Comparison of Auger peak energies of clean gold with gold black

Transition	Clean Gold	Gold Black
O_3VV	44	Not resolved
O_2VV	60	60
N_6VV	74	71
O_1VV	100	100
$N_5N_6N_6$	145	142
$N_5N_7N_7$	154	150
$N_5N_6O_2$	164	163
$N_5N_6O_3$	185	183
$N_5O_2O_3$	205	Not resolved
N_5N_7V	243	242
N_4N_7V	260	Not resolved

It is evident from the tables that almost all the Auger peaks observed in the spectra of clean copper and gold samples, were also found in the Auger spectra of copper black and gold black. The other peaks observed in the Auger spectra of copper black and gold black occur at 150 (copper blackonly), 242 and 272eV (in both spectra). The first one (at 150eV) appeared after heating the sample and is identified as due to sulphur. The other two peaks are due to carbon, which presumably arises from oil

vapour contamination in the evaporation chamber (which was oil pumped). Since the samples were prepared in a residual pressure of Argon, occlusion of Argon in the sample films was not discounted. Contrary to expectations, no Auger peaks corresponding to Argon were observed. The likely Auger transitions, $L_3M_{2,3}M_{2,3}$, $L_3M_1M_{2,3}$ and $L_3M_1M_1$ of Argon should theoretically give peaks at 215, 203 nnd 186eV.

Two small peaks observed in gold black as shown in Fig.(4.19a) are due to the N_7VV and N_6VV transitions. The separation of these two peaks is about 3.2eV. This is in close agreement with the known separation of 3.6eV between the N_6 and N_7 energy levels[60].

Although the Auger spectra of copper black and gold black surfaces were very similar to those of clean copper and gold surfaces, the energy loss spectra were found to be quite different from those of the pure metals. For carbon on nickel, Coad and Riviere[61] have reported that although the nickel Auger peaks could be observed in the Auger spectrum of a carbon covered nickel surface, the energy loss spectra were very similar to that of graphite energy loss spectra. In the present work carbon was detected in both the copper black and gold black surfaces. If one assumes that the loss peaks at 28.6eV in copper black and 30eV in gold black are bulk plasmon losses of carbon, then the loss peaks at 56 and 60eV could be multiple losses. However the other loss peaks at 108, 130 and 187 cannot be explained in this way. No interpretation of these loss peaks can be offered at present.

4.5 Conclusion

The excellent performance of the analyser has been demonstrated by the preliminary results from ZrC and TiC samples. The measured resolution of the analyser is about 0.2%. This figure may be compared with one of about 1-2% obtainable with most commercially available models.

Auger spectroscopic analysis of ZrC and TiC samples show that the carbon segregation after heating the samples makes it impossible to detect the Auger peaks of Zr and Ti. Auger electron spectra and characteristic energy losses of clean copper and gold surfaces have been investigated. A comparison of the Auger spectra of copper black and gold black with that of clean copper and gold surfaces, reveals that the surfaces of copper black and gold black were composed of copper and gold respectively. Carbon was the only significant impurity found on these surfaces. The energy loss spectra of copper black and gold black are very similar, but different from that of clean copper and gold surfaces.

CHAPTER V

RESULTS AND DISCUSSION

5.1 Introduction

The Auger electron spectrum of an element may reflect chemical effects such as chemical shifts in the Auger spectrum, due to different chemical environments. Small changes in the spectrum may take place due tothe shifts in the inner energy levels because of redistribution of valence electrons on forming a chemical bond. Larger changes may occur if the Auger electrons originate from transitions involving the valence band. Changes of this type would reflect the changed valence band after chemical bonding. In order to observe these changes in the Auger spectrum, it is essential that the spectrum of an element in the clean form should be known with certainty. In addition the changes in the spectrum should be slow enough to permit experimental observations. Auger spectra believed to be characteristic of clean Be, Al and Fe have been obtained. The changes in the spectra of these elements due to oxidation were also observed. In addition and as far as possible concurrently the characteristic energy loss spectra of these elements for the clean and oxidised surfaces were observed. The details of all these observations and discussion on them are presented in this chapter.

5.2 Auger Spectra of Be, Al and Fe

In order to obtain clean surfaces, thick films of all the three metals were evaporated onto glass and stainless steel substrates in ultra high vacuum. The metals used were of high purity, i.e. Be 3N, Al 5N and Fe 5N. The pressure in the system at evaporation was usually 10^{-9}torr or lower, and in particular there was no significant increase in pressure after the first few evaporations. In each case a number of evaporations were performed without breaking the ultra high vacuum to repeat the experimental observations. The Auger spectra were taken immediately after each evaporation. The changes in the spectra due to chemisorption of the residual oxygen in the UHV system, were noted along with the development of the oxygen Auger peak until the samples were oxidised and there were no further changes in the spectra. By reducing the oxygen Auger peak below the detection level with the subsequent evaporations, the whole experiment could be repeated. Although the oxidation rate (as indicated by the build-up of the oxygen Auger peak) was somewhat faster after first evaporation, particularly for aluminium, it was sufficiently slow for careful measurements to be taken in the subsequent evaporations because after each oxidation of the film, the level of the residual oxygen was lowered. This allowed the sample surface to be maintained free of oxygen for several hours. Throughout the experiment occasional checks on the common contaminants such as carbon, sulphur, chlorine etc., were made by plotting the Auger spectrum from 0-550eV, since these contaminants are known to have Auger peaks in this energy range.

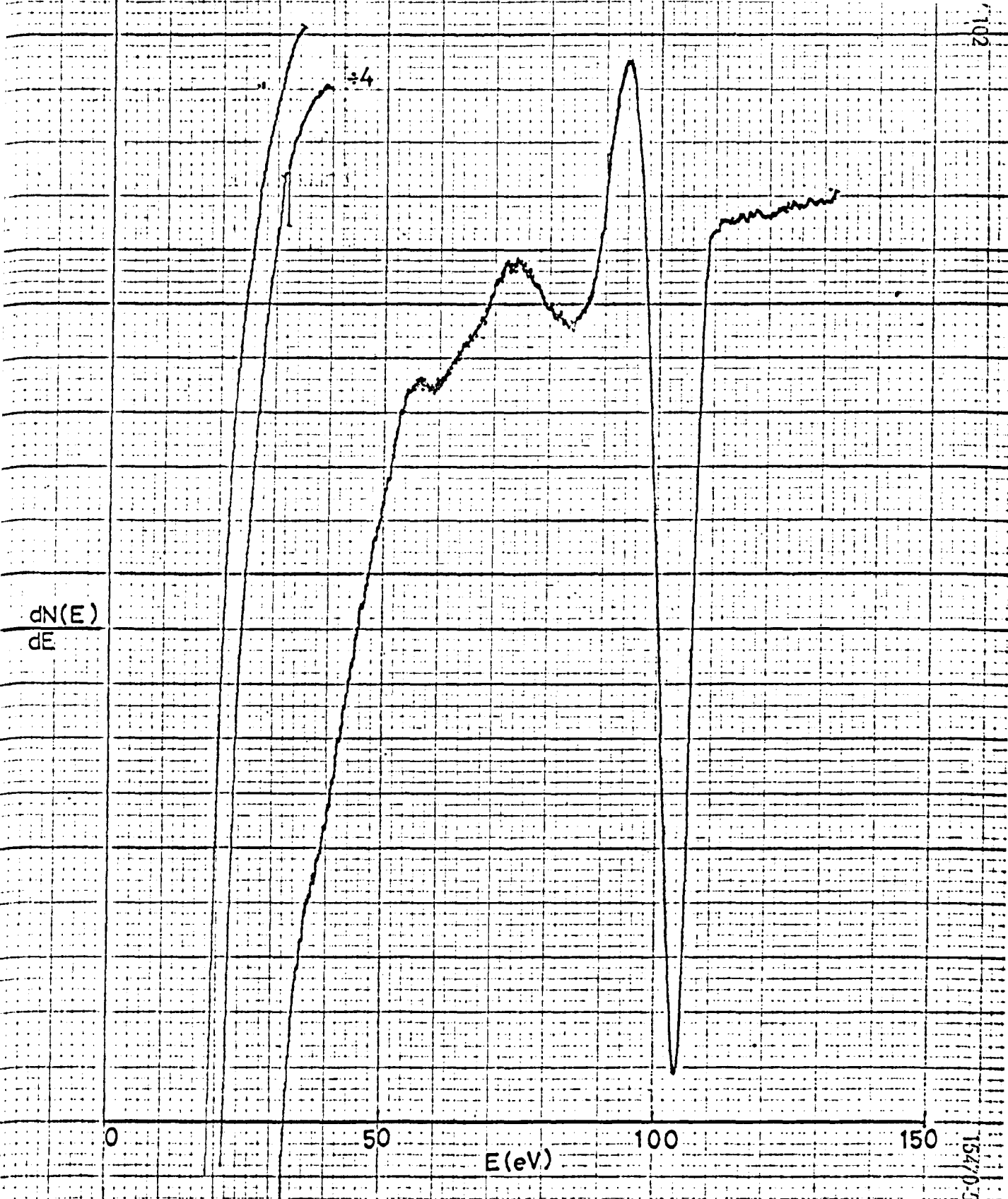

Fig. 5.1 Auger spectrum of clean Be surface, E_p 1.5KeV, I_p ~25μamps Modulation $4V_{pk-pk}$.

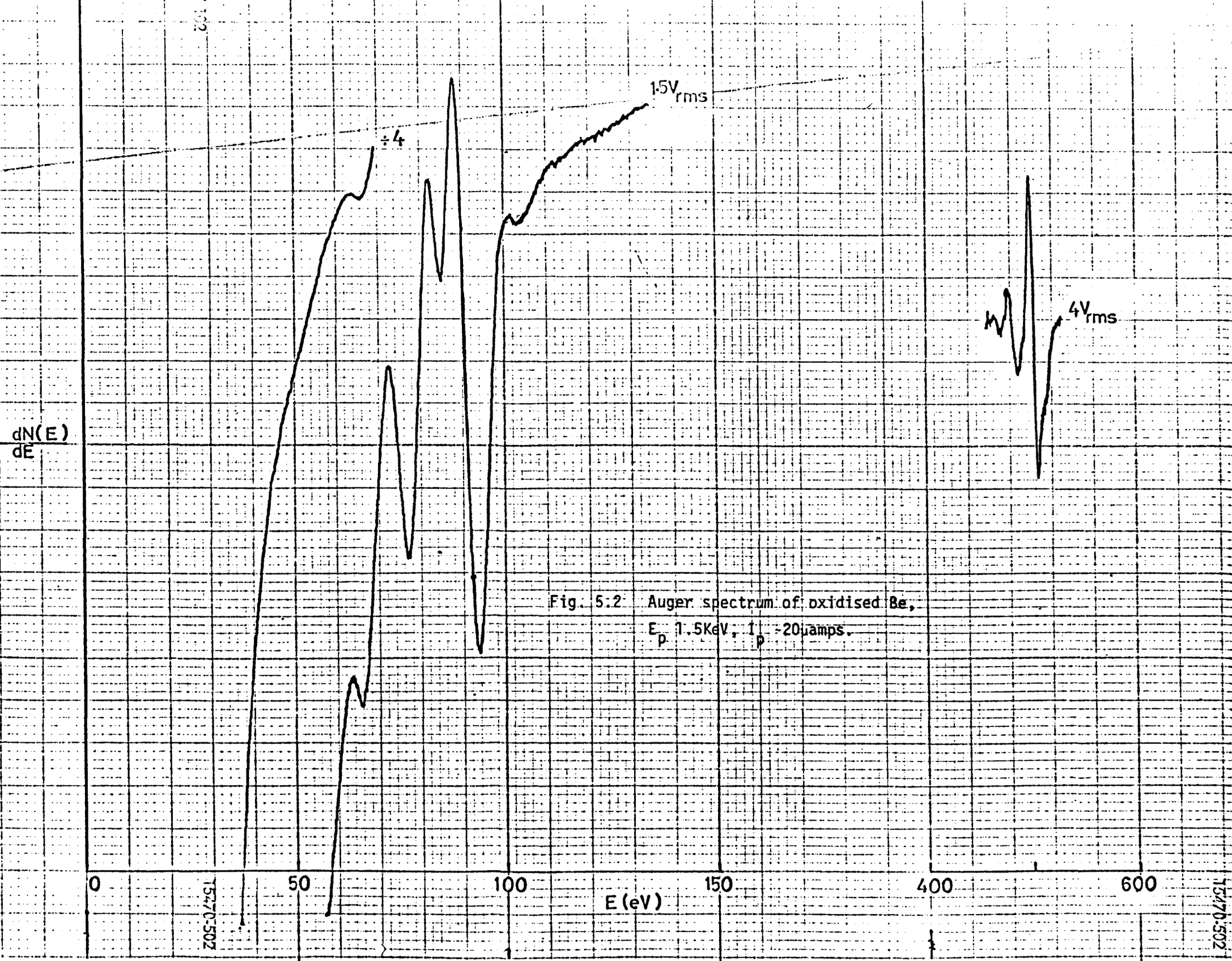

Fig. 5.2 Auger spectrum of oxidised Be, E_p 1.5KeV, I_p ~20μamps.

Primary beam currents of 20-25μamps were used for Be and Al Auger spectra, and for Fe only 15-20μamps were used. For all the Auger spectra a primary energy of 1.5KeV was used, except for the high energy (400-750eV) Auger spectrum of Fe where a primary energy of 2KeV was used. Generally the applied modulation voltages were up to $4V_{pk-pk}$ for low energy (<120eV) Auger spectra and $11V_{pk-pk}$ for high energy (>120eV) Auger spectra of the three elements.

5.2.1 Be

The Auger spectrum of a clean Be surface is shown in Fig.(5.1). The main feature of the spectrum is a large peak at 104eV and two small ones at 84 and 60eV. There is also some indication of a very weak peak near 40eV, but it could not be resolved. The Auger spectrum of a fully oxidised Be surface, along with the oxygen Auger peak, is shown in Fig.(5.2). A whole sequence of changes in the Auger spectrum of Be from the clean state until it is oxidised is shown in Appendix Ia. The amplitude of the oxygen Auger peak, at various stages of oxidation, is also given along with the Auger spectra of Be.

The effect of the oxidation is evident from the sequence of Appendix Ia. As the oxygen is just detected from its Auger peak on the surface, the 60eV peak has already disappeared. New peaks at 79, 95 and 67eV appear as the oxidation proceeds further. The peak at 84eV becomes narrow and shifts to 86eV. All these peaks (95, 86, 79 and 67eV) shift to slightly lower energies as the surface is oxidised. The amplitude of the 94eV peak increases with increase in the oxygen Auger peaks and at the same time the

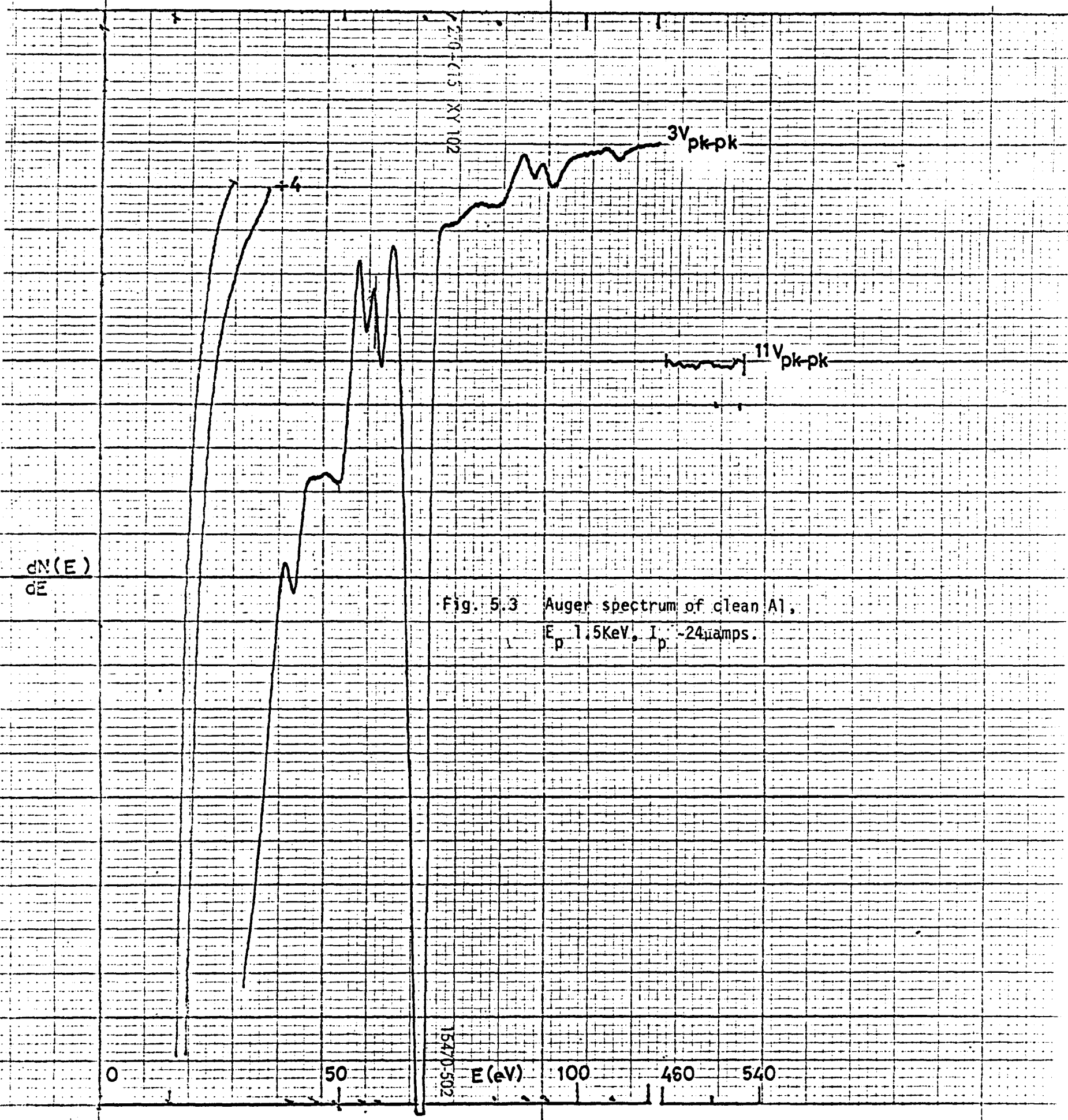

Fig. 5.3 Auger spectrum of clean Al, E_p 1.5KeV, I_p ~24μamps.

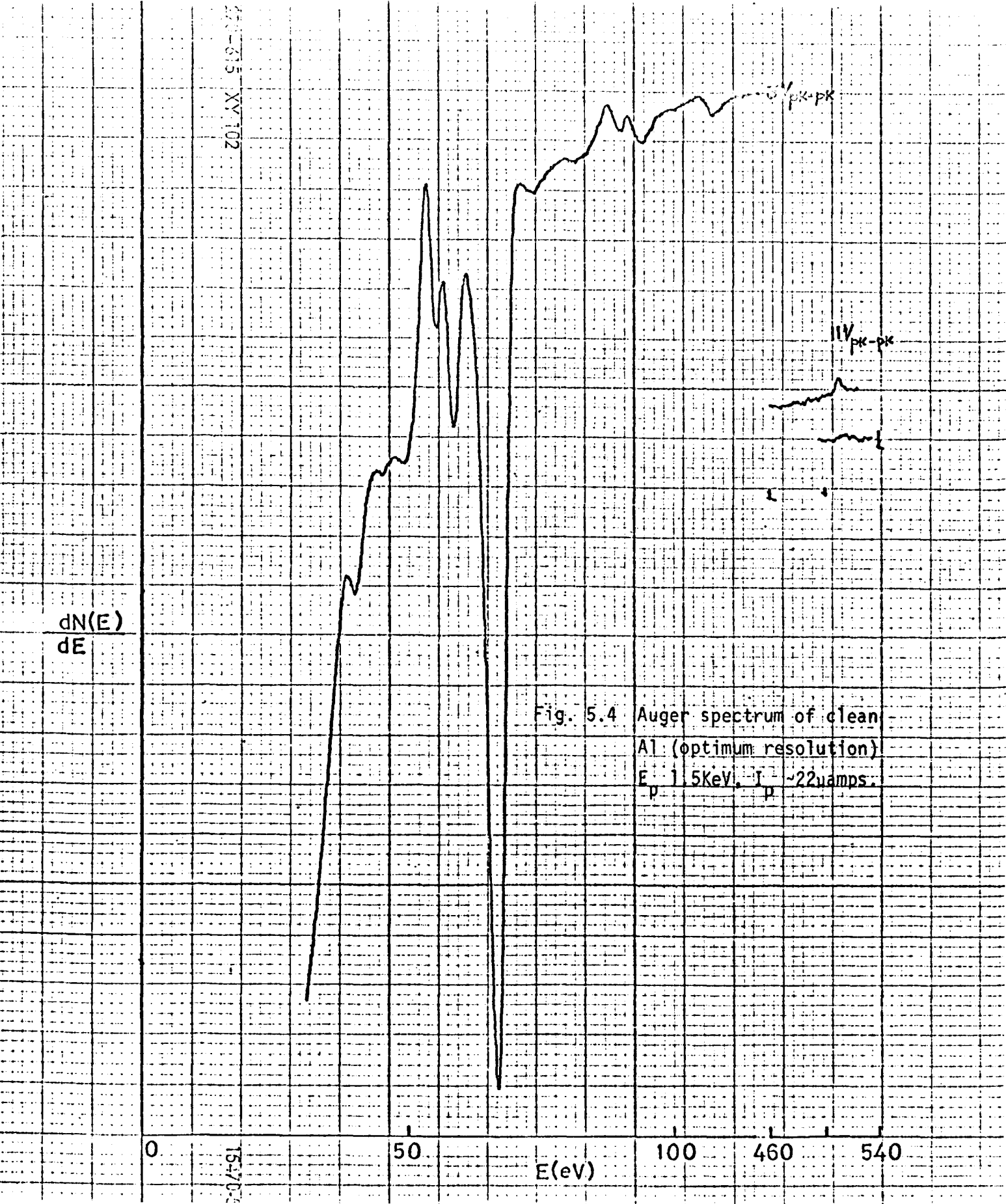

Fig. 5.4 Auger spectrum of clean Al (optimum resolution) E_p 1.5KeV. I_p ~22μamps.

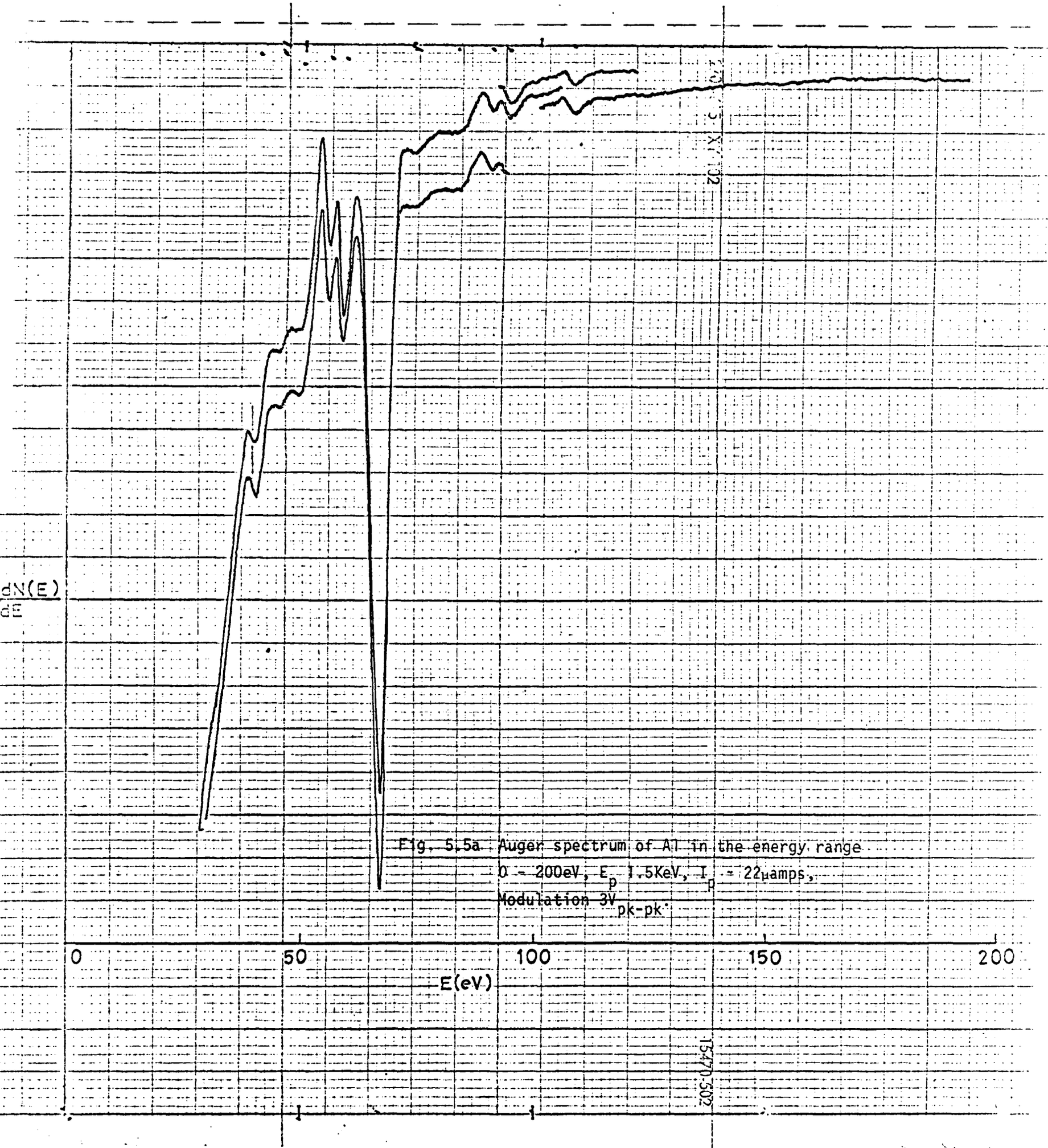

Fig. 5.5a Augen spectrum of Al in the energy range 0 - 200eV, E_p 1.5KeV, I_p = 22μamps, Modulation $3V_{pk-pk}$.

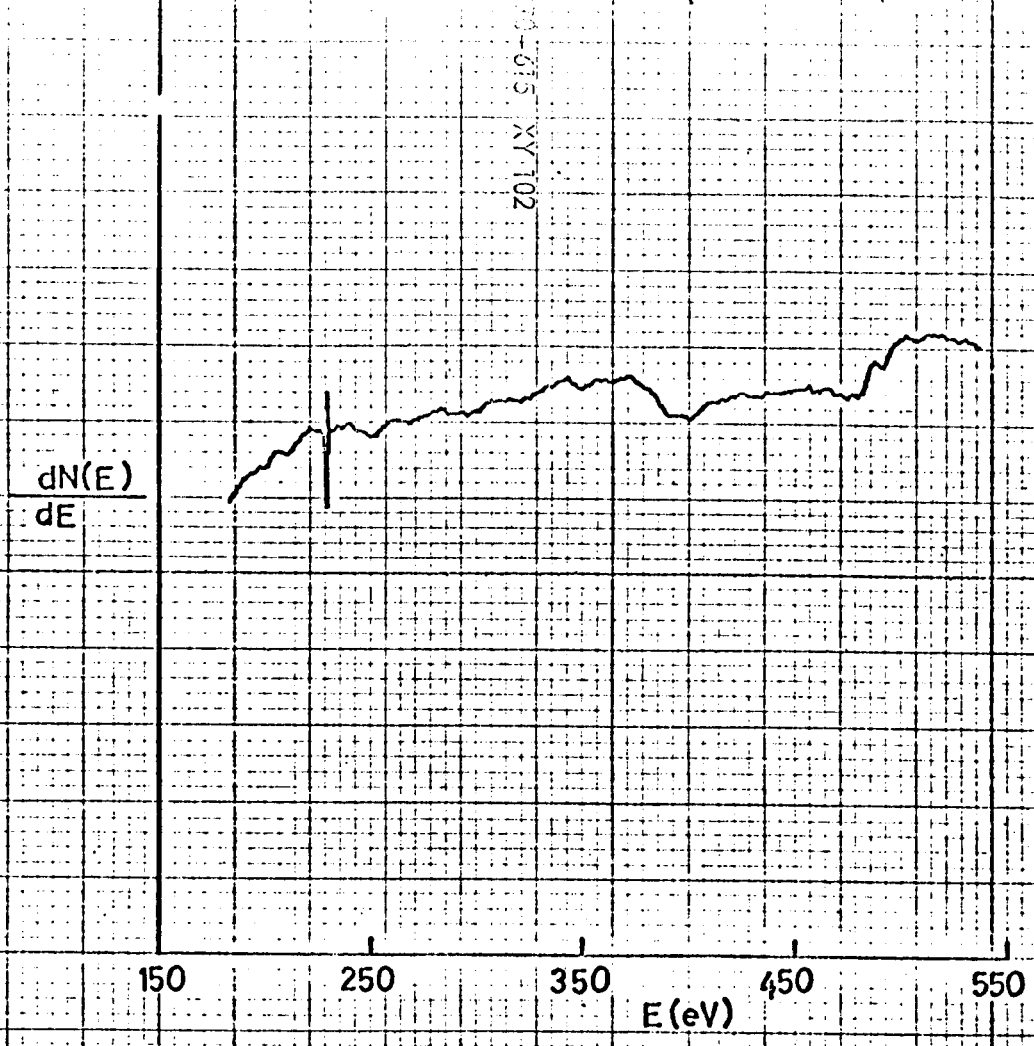

Fig. 5.5b Auger spectrum of Al in the energy range 200-550eV showing no impurity peaks such as O, C, N or Cl. E_p 1.5KeV, I_p ~22μamps, Modulation $11V_{pk-pk}$.

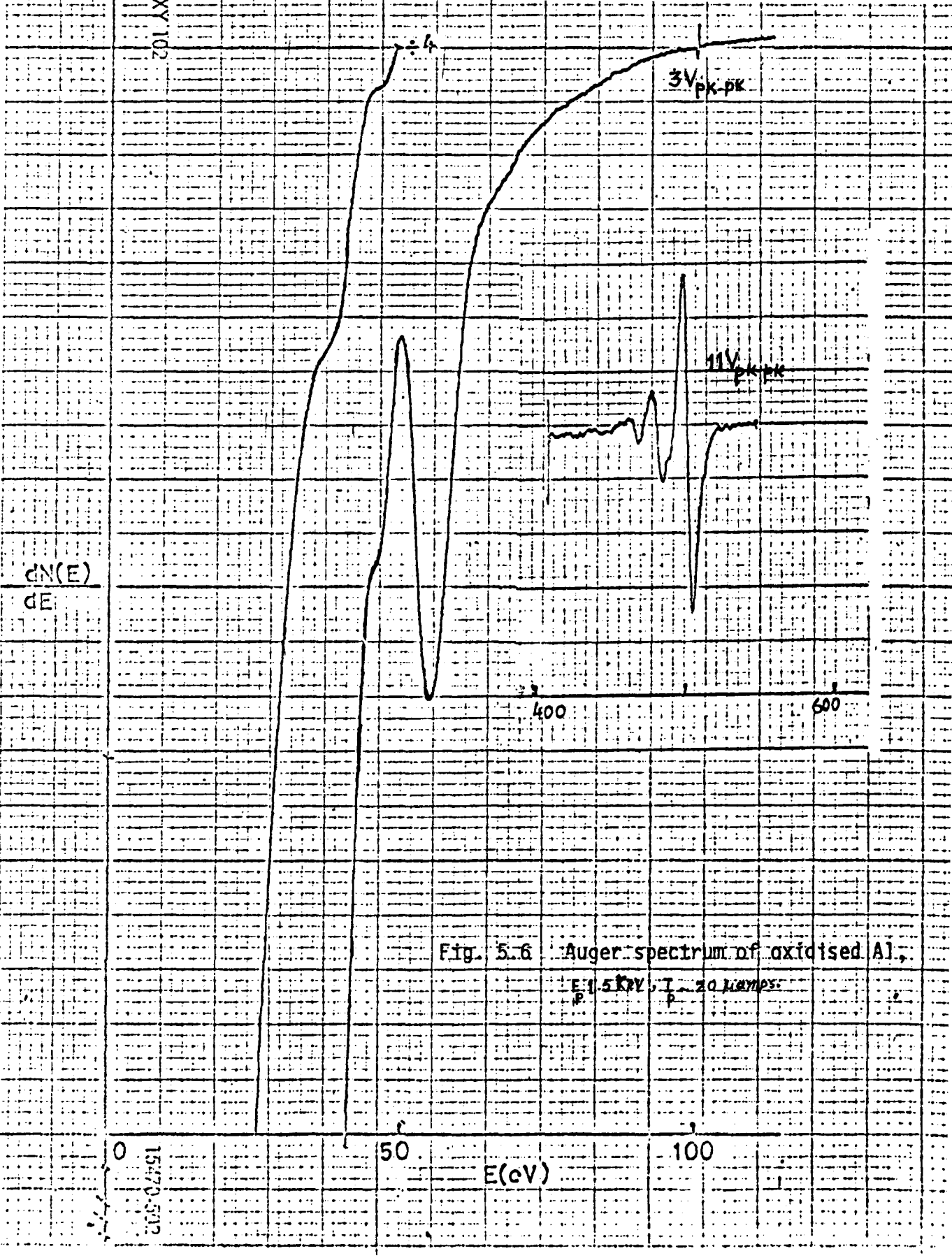

Fig. 5.6 Auger spectrum of oxidised Al,
E_p 1.5 KeV, I_p ~ 20 microamps.

amplitude of the 104eV peak decreases. At an intermediate stage of oxidation oxidation, the amplitudes of both the peaks become almost equal. Finally when the surface is fully oxidised the peak at 104eV is barely resolved, and the one at 94eV becomes the largest peak in the spectrum. The other peaks are found at 85, 77 and 66eV. The large oxygen triplet found on the oxidised surface is also shown in the sequence. The peak values occur at 506, 488 and ~470eV.

A full spectrum for the oxidised surface was plotted and it showed no other peaks except oxygen and the oxidised Be peaks. The Auger spectrum of the clean Be surface was reproduced by reducing the oxygen below detection level as shown in Appendix Ia.

5.2.2 Al

The main peaks in the low energy Auger spectrum of Al have been reported already (Suleman and Pattinson[21]). However, further examination of this surface under high resolution and sensitivity has revealed a great deal of fine structure which could not be resolved earlier. Figures (5.3) and (5.4) show the Auger spectra of a clean Al surface. A number of small peaks are clearly seen in the spectrum along with the main Auger peaks at 67.1eV. The oxygen peak could not be detected as may be seen in the figures. In order to make certain that no impurity was present on the clean Al surface, an Auger spectrum from 0-550eV was plotted. As shown in Figs.(5.5a) and (5.5b) no peaks between 107-550eV were detected. A fully oxidised spectrum is shown in Fig.(5.6). The main peak in this spectrum occurs at 54.5eV. There are two small peaks also

found in the spectrum which occur at 45.7eV and 36.8eV. All these peaks (54, 45, 36eV) were found to shift to a slightly lower (~1eV) energy after exposure to air. The oxygen triplet is shown in Fig.(5.6). The peaks occur at 505, 484 and 469eV.

A sequence of changes in the Auger spectrum of clean Li until it is oxidised is shown in Appendix Ib. These changes are similar to those found in the Auger spectrum of clean Be, i.e. the Auger peaks due to a clean surface disappear and 'new peaks' appear and develop until the oxidation reaches completion. As may be seen from the sequence, the two small peaks at about 45.4 and 49.7eV could not be resolved due to a new peak which emerges at about 46.3eV, even though no oxygen peak was detectable (a peak comparable to noise level was found at 514eV). When a small oxygen peak was detected, the peak originally at 40.3eV had already disappeared and the amplitude of the 67eV peak had decreased considerably.

At a still further stage of oxidation two additional new peaks appeared at 55.3 and 37eV and at the same time, the 67eV peak became very much more attenuated The peaks at 73 and 82.4eV, which occur on the clean surface, at this stage could no longer be detected. The amplitude of the 55.3eV peak increased further with the increase in the oxygen Auger peak. The peaks originally at 67. 89.8, 93.5 and 107eV could barely be resolved. When the surface was oxidised, these peaks (viz. those at 67, 89.8, 93.5 and 107eV) could no longer be detected and the large peak at 55.3eV shifted to 54.5eV. The only other small peaks which could be

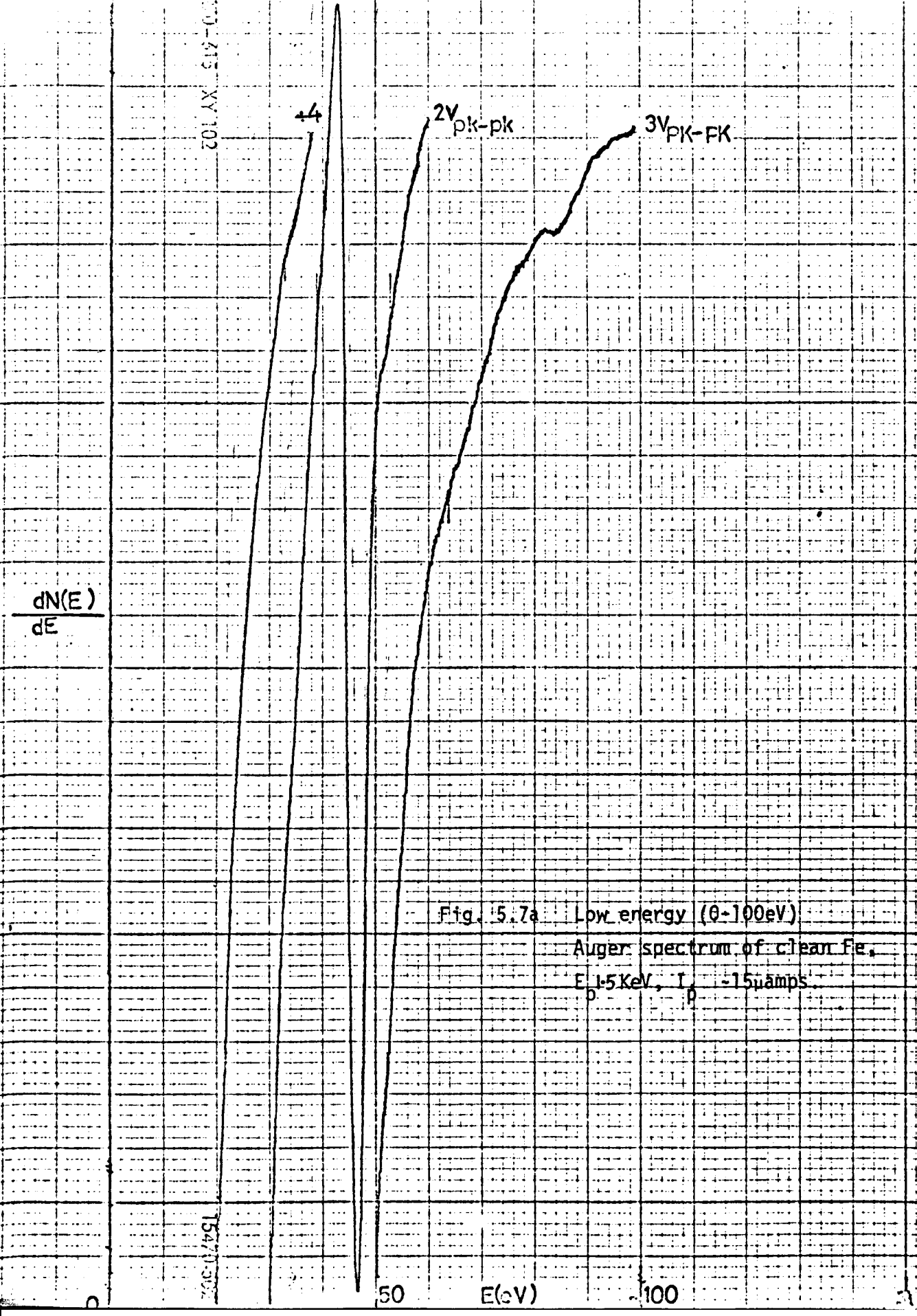

Fig. 5.7a Low energy (0-100eV) Auger spectrum of clean Fe, E_p 1.5KeV, I_p ~15μamps.

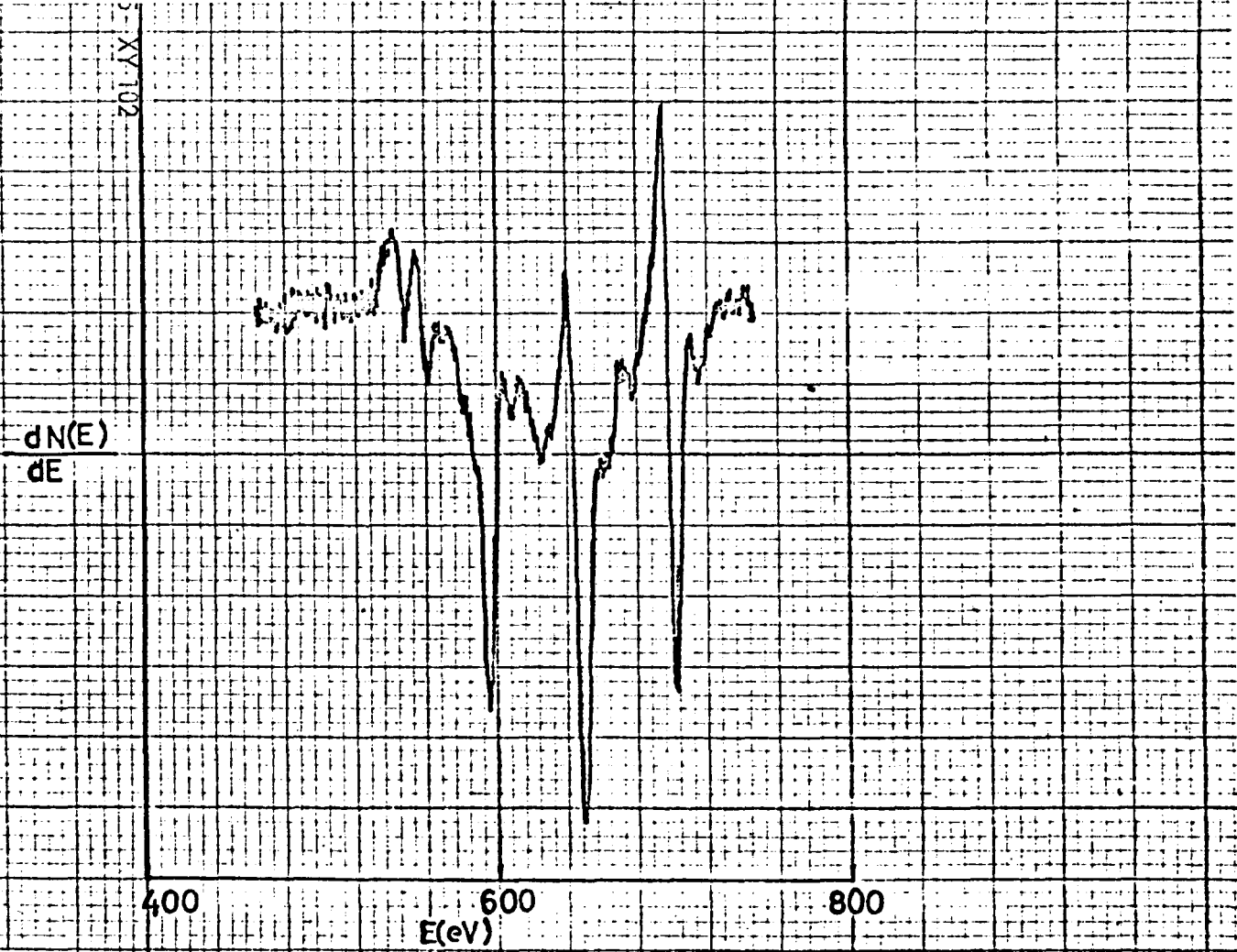

Fig. 5.7b High energy (450-750eV) Auger spectrum of clean Fe, E_p 2KeV, I_p ~ 18.6uamps, Modulation 11V_{pk-pk}.

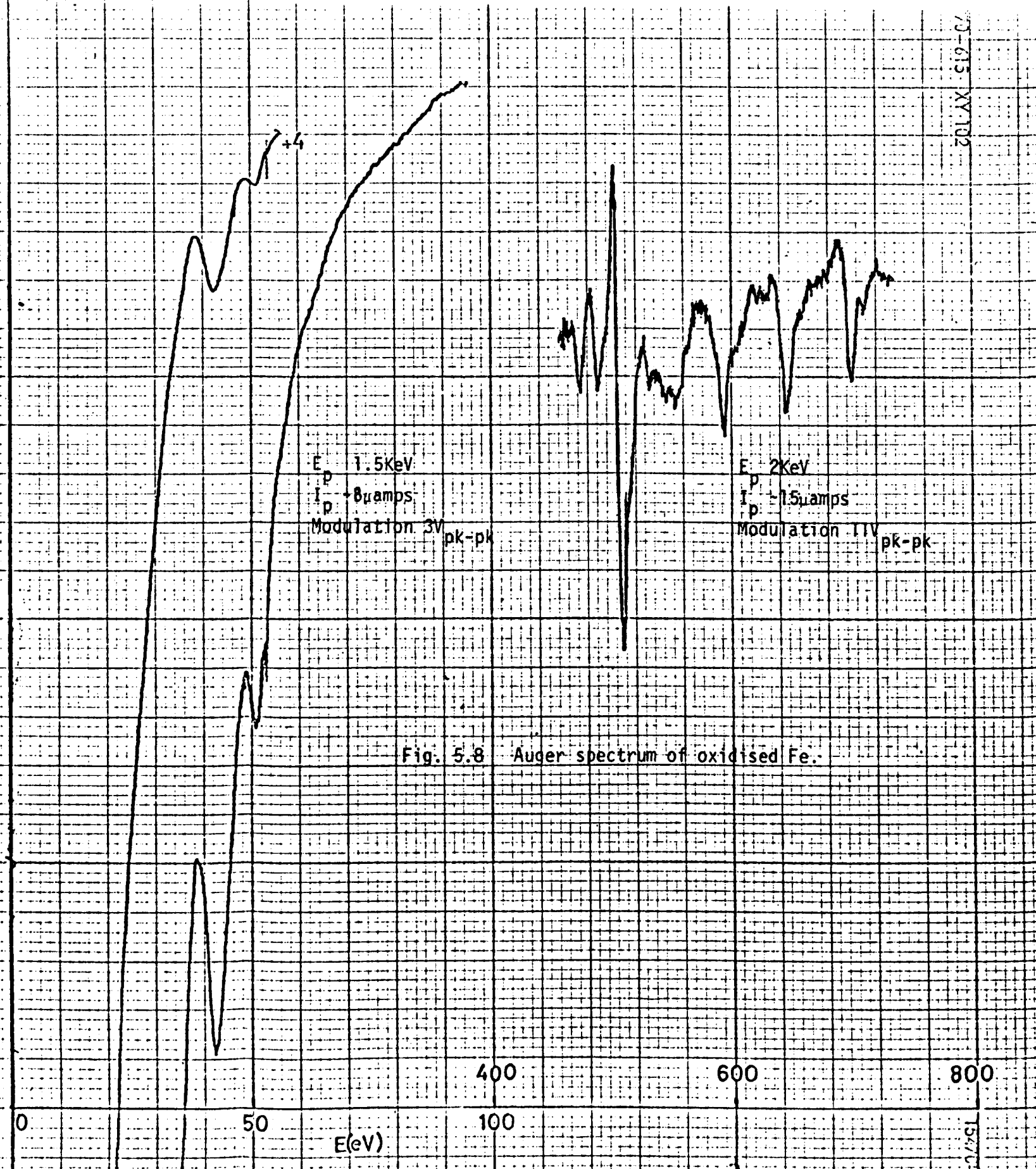

Fig. 5.8 Auger spectrum of oxidised Fe.

observed,on this oxidised surface, were found at 45.7 and 36.8eV. No other peaks were found in the energy region 0-550eV except the oxygen triplet at 505, 484 and 469eV.

5.2.3 Fe

The Auger spectrum of clean Fe is shown in Figs.(5.7a) and (5.7b). In the low energy region (~100eV) a large peak is found at 46.5eV and a small one at 84eV. There was also some evidence for the existence of a peak at ~35eV, but it could not be fully resolved. Three large peaks at 702, 649 and 595eV are the main feature of the high energy (450-750eV) Auger spectrum of Fe (Fig.(5.7b)). A number of small peaks may also be seen in the same spectrum. The effects of oxidation was noted only for the low energy Auger spectrum of Fe. The Auger spectrum of an oxidised Fe surface is shown in Fig.(5.8). Instead of a peak at 46eV for the clean surface, two peaks at 42.5 and 51eV were found in the oxidised spectrum. The largest peak seen in the higher energy Auger spectrum of the oxidised surface is attributed to oxygen and occurs at 510eV with two small peaks at 490 and 472eV. Although the high energy Auger peaks of Fe at 702, 649 and 595eV appeared to be shifted (~2eV) towards lower energy on oxidation, accurate measurement of these shifts could not be made because of the contracted energy scale. A sequence of the changes in the low energy Auger spectrum of Fe due to oxidation is shown in Appendix Ic. At the initial stages of oxidation the peak at 84eV had disappeared. At an intermediate stage when the surface of Fe was partially oxidised, three peaks were

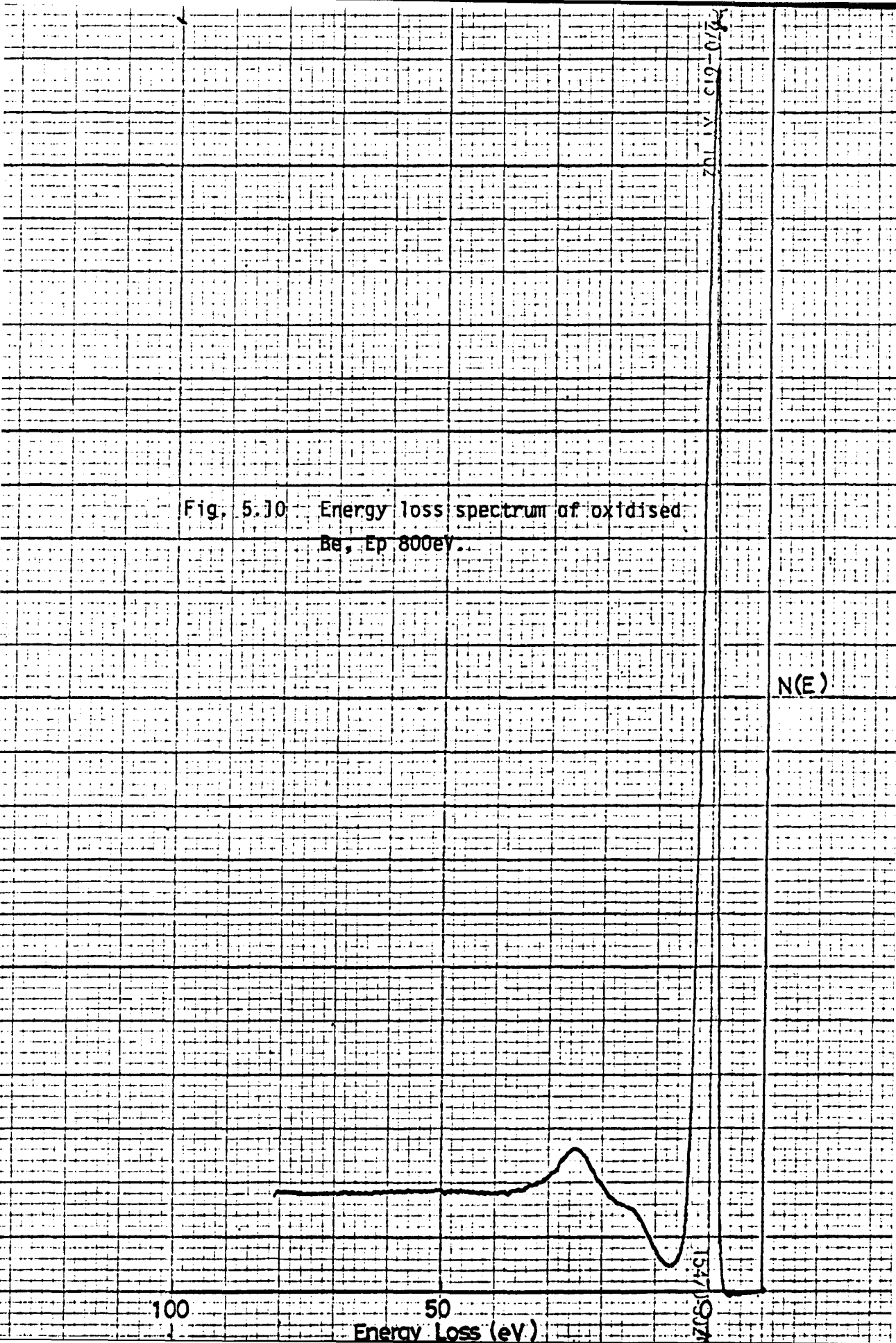

Fig. 5.10 Energy loss spectrum of oxidised Be, Ep 800eV.

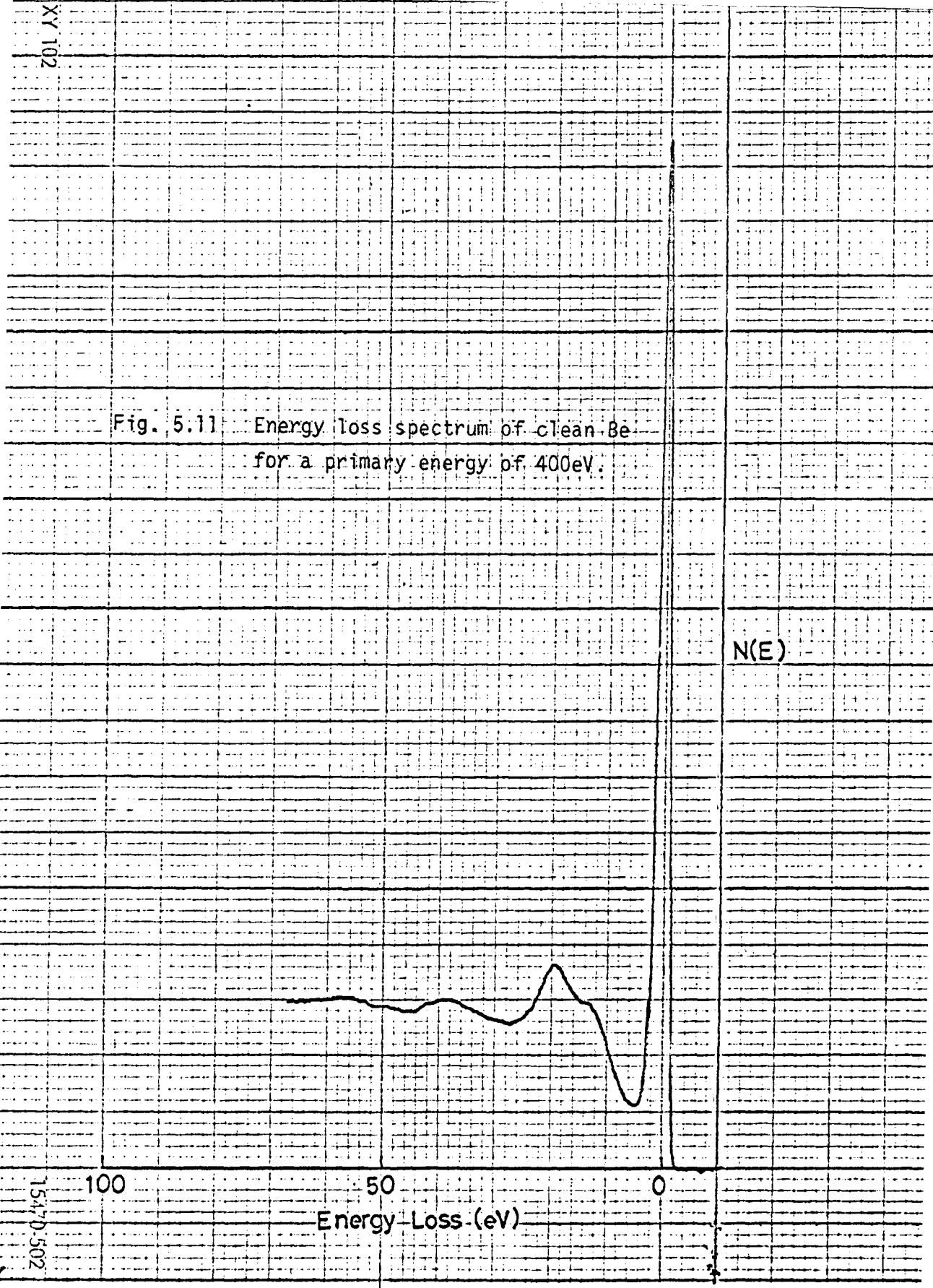

Fig. 5.11 Energy loss spectrum of clean Be for a primary energy of 400eV.

found: one at 46eV due to the clean surface and the other two due to the oxidised surface at 42eV and 50eV. Finally, as the surface was completely oxidised, the peak at 46eV disappeared and one at 50eV shifted to 51eV. The other peak found in the oxidised surface spectrum was observed at 42.5eV.

5.3 Characteristic Energy Loss Spectra of Be, Al and Fe

5.3.1 Be

The energy loss spectra of clean - as determined by the Auger spectrum - and oxidised Be surfaces for a primary energy of 800eV are shown in Figs.(5.9) and (5.10). Only two loss peaks at 14 and 25eV are found in the loss spectrum of oxidised Be. In the clean Be energy loss spectrum, loss peaks occurred at 13, 19, 38 and 57eV. Two additional loss peaks were observed at ~77eV and ~112eV in the differential distribution curve. The intensity of the loss peak at 19eV was found to decrease for low primary energies. This is shown in Fig.(5.11). The energy loss spectrum in this case (Fig.(5.11)) was plotted for a primary energy of 400eV. The effect of oxidation on the energy loss spectrum was also observed and this is shown in Appendix 2a. As may be seen, the intensity of the loss peak at 13eV decreases and it also shifts gradually to lower energy values, until it has completed disappeared. A new loss peak emerges at 12eV and then shifts to 14eV, at the same time the 19eV peak shifts to 25eV. No further change in the loss spectrum was noticed.

Fig. 5.13 Energy loss spectrum of oxidised Al.
E_p 800eV.

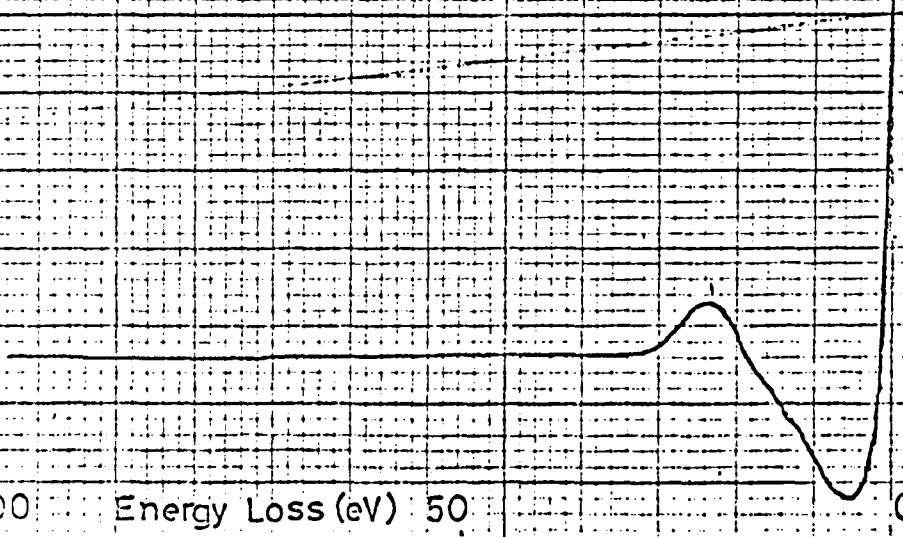

Fig. 5.15 Energy loss spectrum of clean Fe for a primary energy of 800eV.

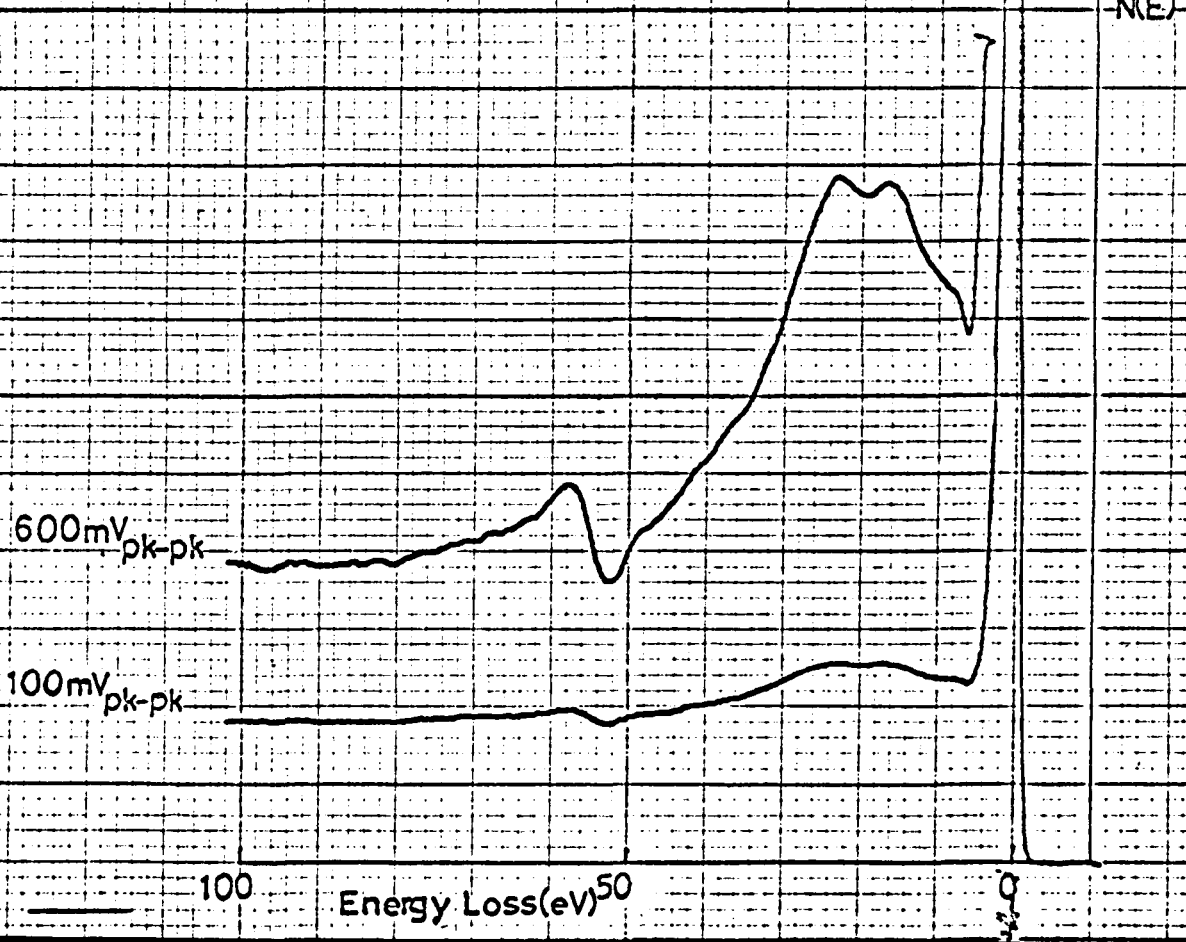

Fig. 5.16 Energy loss spectrum of clean Fe for a primary energy of 500eV.

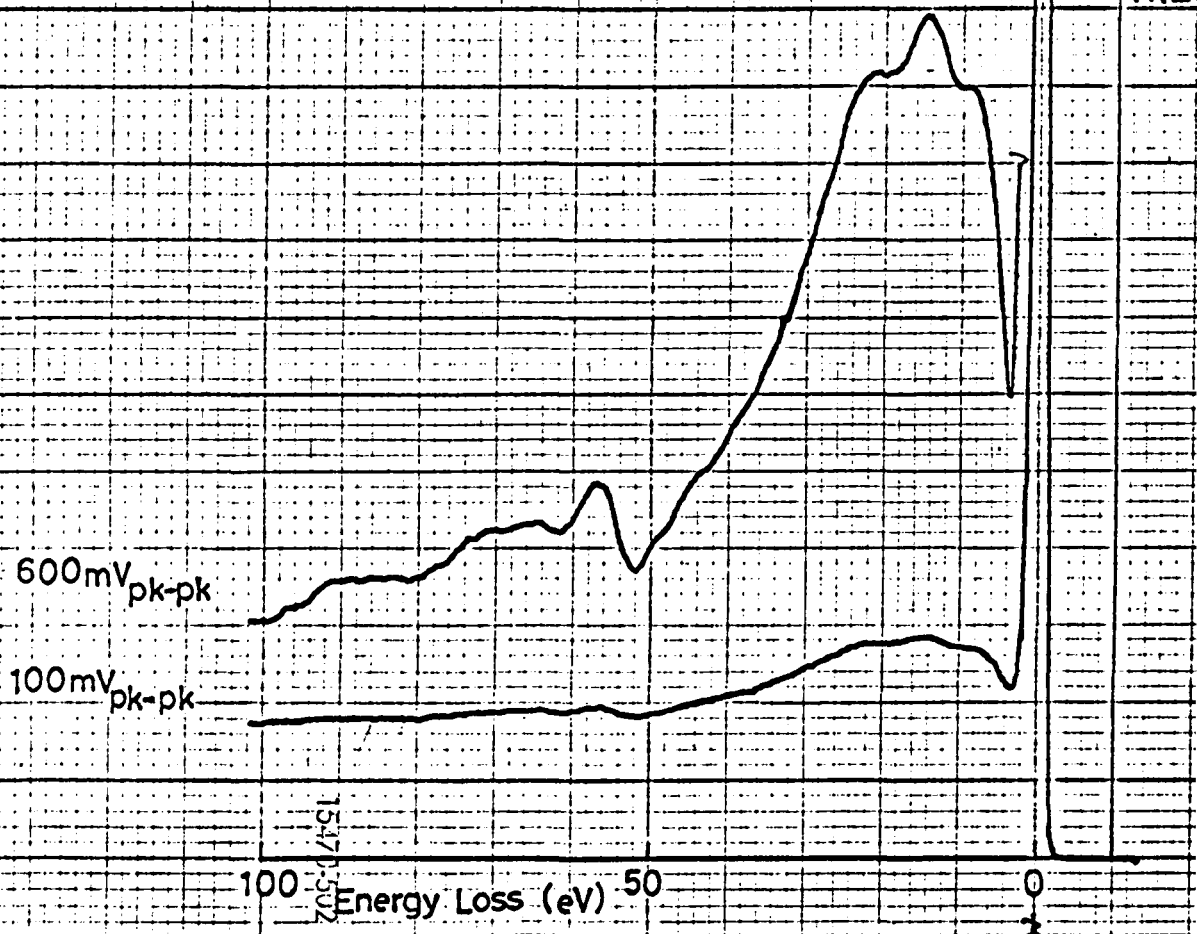

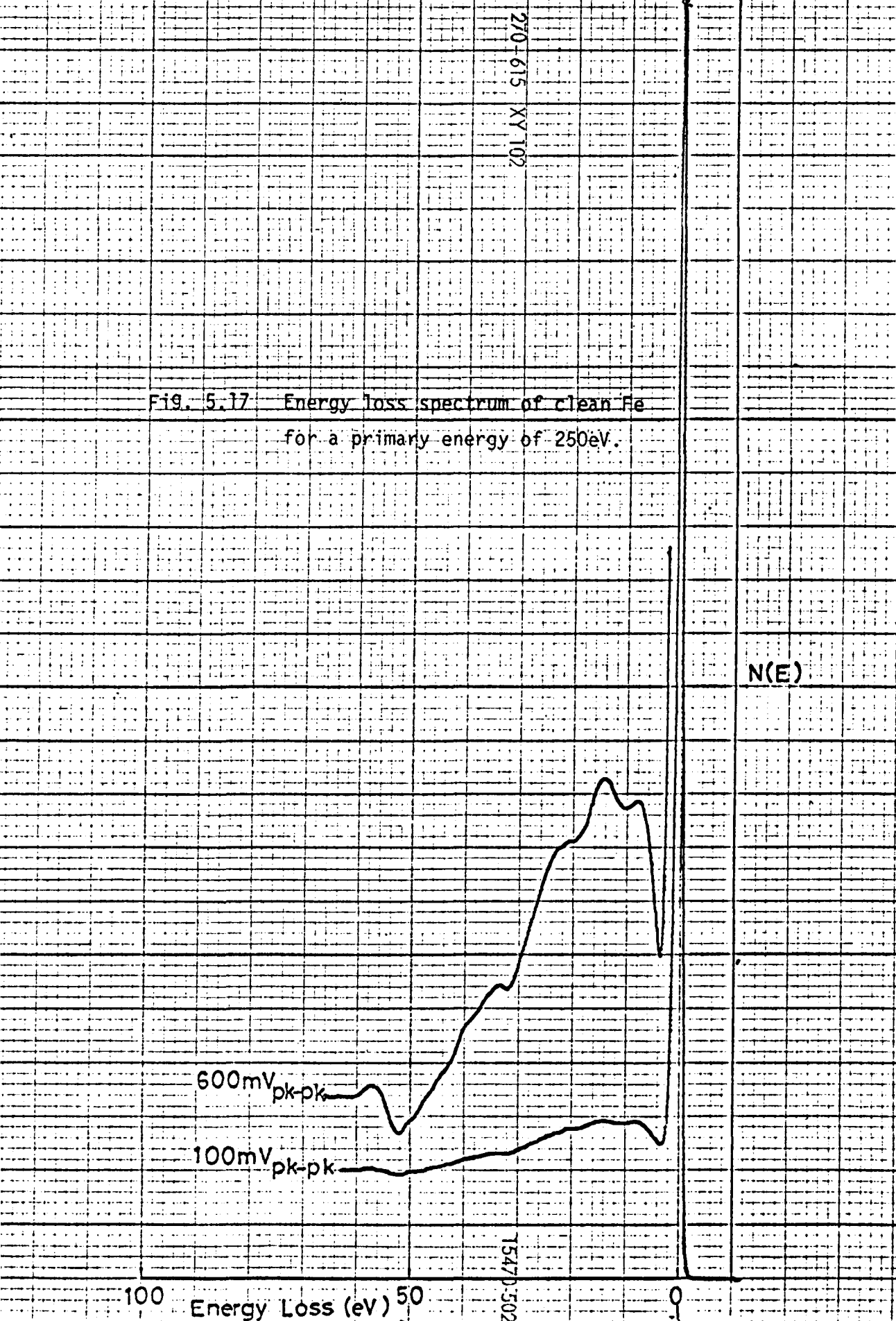

Fig. 5.17 Energy loss spectrum of clean Fe for a primary energy of 250eV.

5.3.2 Al

Fig.(5.12) shows the energy loss spectrum of clean Al for a primary energy of 800eV. The loss peaks seen in the spectrum occur at 11, 15.6, 26.4, 31.4, 46.5, 62.3 and 77.9eV. The energy loss spectrum of the oxidised surface showed only one loss peak at 22.1eV (Fig.5.13). The changes due to oxidation in the loss spectrum of clean Al were similar to those observed for Be and are shown in Appendix 2b. In this case the loss peak at 11eV shifts to lower energies before disappearing. Also the intensity of all other peaks decreases as the surface is oxidised and a new loss peak at 21.5eV emerges and finally shifts to 22.1eV at which time the surface is fully oxidised.

5.3.3 Fe

The energy loss spectrum of a clean Fe surface for a primary energy of 1000eV is shown in Fig.(5.14). The main loss peaks occur at 16, 23, 57 and 92eV. A very weak peak may also be seen at about 39eV. Figs.(5.15), (5.16) and (5.17) show the energy loss spectra for primary energies of 800, 500 and 250eV respectively. The loss peaks seen in these spectra occur at 8, 16, 23 and 57eV (Fig.(5.15)), 8, 14, 22 and 57eV (Fig.(5.16)) and 8, 14, 22, 33.5 and 57eV (Fig.(5.17)). The loss peak at 8eV was also resolved for a 1KeV primary energy, only however under optimum resolution. The 92eV peak could not be observed at primary energies less than 1KeV. A sequence of changes due to oxidation in the energy loss spectrum of Fe for a primary energy of 1KeV is shown in Appendix 2c. The intensity of the loss peak at 16eV decreases slowly with oxidation and the peaks at 8eV and

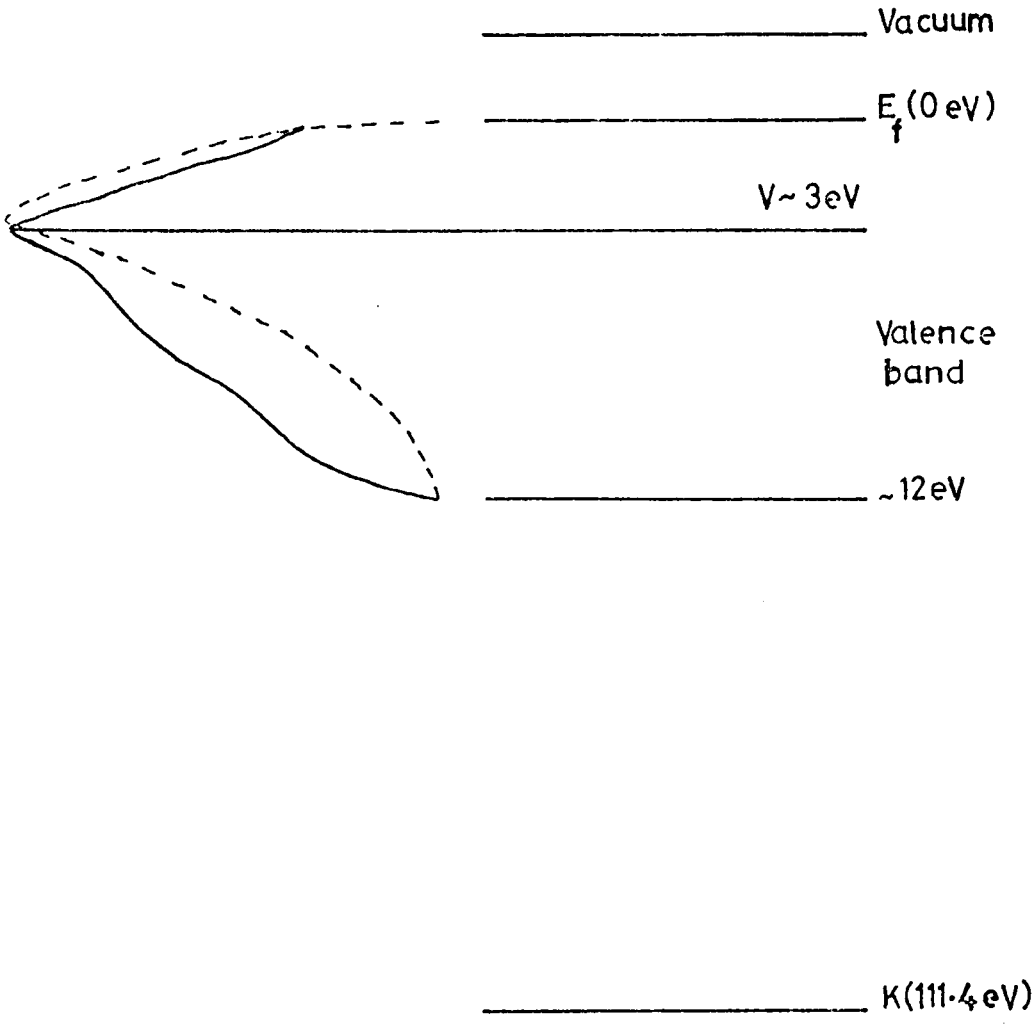

Fig. 5.18a Energy band diagram of Be with experimental (dotted line) and theoretical (solid line) density of states.

and 92eV became such that they could no longer be resolved. The 16eV peak gradually disappeared and a new peak at 9eV appeared. Finally the 9eV peak could not be seen and the loss peaks initially at 23 and 57 shifted to 24 and ~58.5eV.

5.4 Discussion

5.4.1 Be

The results for Be will first be discussed. The Auger spectrum of a clean Be surface shows a large peak at 104eV and two small ones at 84 and 60eV. The binding energy of the Be K-shell is known[60,70] to be ~111eV and the width of its valence band is ~12eV[71]. From this data one may expect an Auger peak around 100eV due to K-shell ionization. However, in order to calculate the energy of Auger electrons arising from K-shell ionization, one must consider the energy distribution of electrons within the ~12eV wide valence band of Be. The energy band diagram for Be is shown in Fig.(5.18a). The electron density of states (both experimental[72] and theoretical[71]) for Be is also shown in the figure, and this shows a maximum at ~3eV. Assuming that the electrons in the maximum take part in the Auger process, then for V ≈ 3eV, the calculated value of the KVV transition is 105eV. This is in good agreement with the measured value of 104.5eV. There are two more peaks in the Auger spectrum of Be and their origins cannot be traced easily since the energy values of these peaks are too low to be considered as a possible transition due to K-shell ionization. One possible explanation is that these peaks may be plasma losses from the

main Auger peak[18,20]. In this case the Auger electrons originating from the KVV transition may have suffered energy losses in the excitation of plasmons. The measured value of a strong bulk plasmon loss in the energy distribution curve, for a clean Be surface was found to be 19eV. The observed Auger peak at 84eV is about 20.5eV below the main Auger peak, indicating that the peak (84eV) may well be a plasma loss from the main peak. The Auger peak ~60eV then may be considered a second order plasma loss from the main peak, since a strong second order plasma loss was also found in the energy loss spectrum. Table 5.1 gives the Auger and associated peaks observed in the Auger spectrum of clean Be

Table 5.1

Energy values of Auger and associated peaks observed in the Auger spectrum of clean Be

Transition		Calculated energy (eV)	Observed energy (eV)
KVV		105	104.5
	First order plasma loss	84	
	Second order plasma loss	~60	

Musket and Fortner[73] have recently reported the Auger spectrum of a solid Be sample. They found two large peaks at 104 and 92eV and four small peaks

below 92eV. The authors attribute the 92eV peak to a $1s2s2s$ transition. However, in the present investigations, no peak was found at 92eV for a clean Be surface, but for a partially oxidised surface two large peaks were observed at 104 and 94eV (Appendix Ia). This spectrum was found to be very similar to that reported by Musket and Fortner[73], except for the amplitudes of the peaks below 94eV. This is not surprising in view of the fact that these authors did detect a small oxygen Auger peak even on their so-called "clean" Be surface. It therefore appears to be almost certain that the 92eV peak (and the small peaks below the 92eV peak) found by Musket and Fortner were due to a partially oxidised Be surface and not due to the $1s2s2s$ transition as they suggested.

In the Auger spectrum of oxidised Be, Auger peaks were found at 104, 94, 85, 77 and 66eV. In order to interpret the Auger spectrum of BeO, one should take into account the energy shift in the Be K-shell and changes in the valence band due to the formation of BeO. The possibility of cross-transitions (involving the Be K and oxygen L-shells) should also be considered, since such transitions are thought most likely to be responsible for some Auger peaks in the Auger spectrum of compounds[74]. The energy shift in the Be K-shell on forming BeO, has been reported by Lukirskii and Brytov[75] (3.2eV), Swanson and Codling[76] (6.3eV) and Hayasi et al.[77] (3.8eV). All these authors used soft X-ray spectroscopy for their results. Hamrin et al.[70] have recently reported the energy shift in the K-shell of Be and the valence band of BeO. They used ESCA for their investigations and their results will be used here for help in

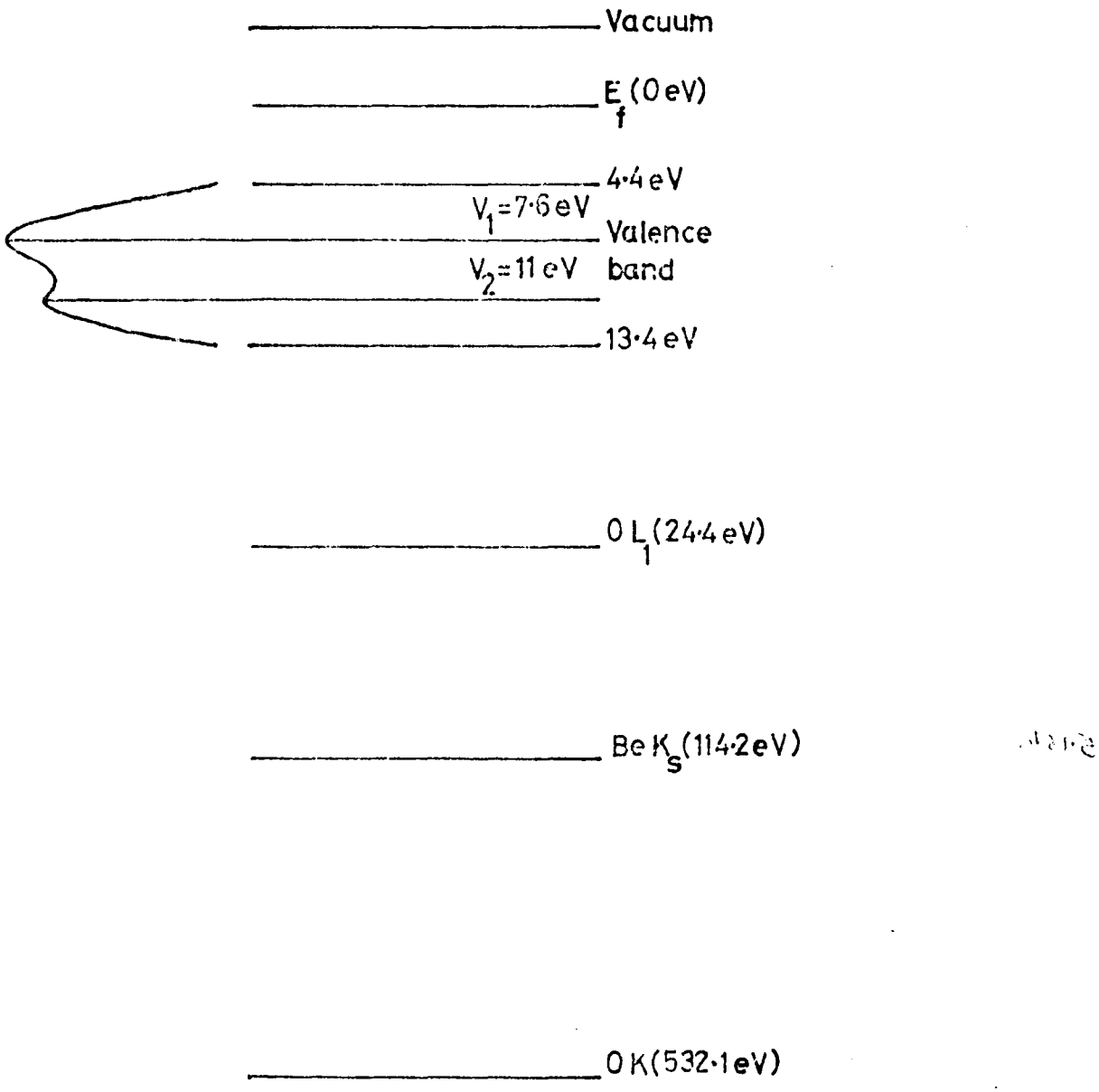

Fig. 5.18b Energy band diagram of BeO[70].

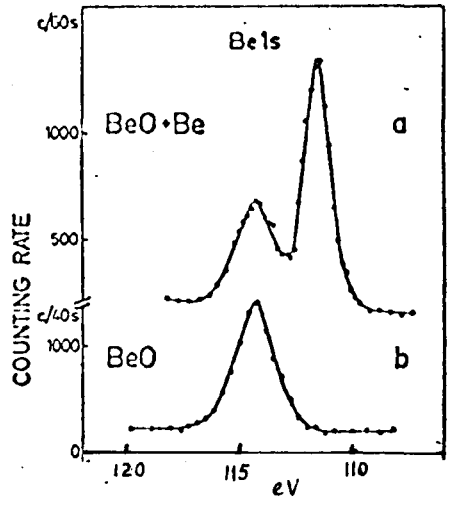

Fig. 5.19 ESCA spectra showing K shell binding energies of partially (a) and fully oxidised (b) Be sample.

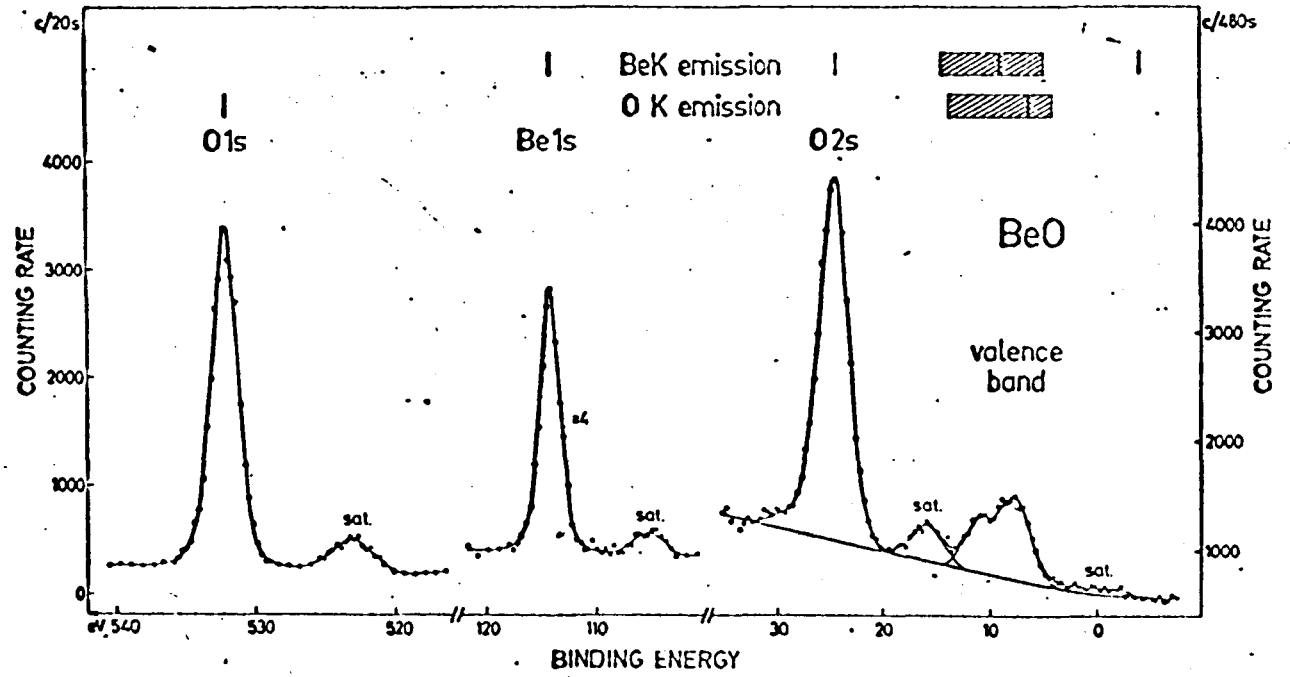

Fig. 5.20. Electron spectrum from BeO excited with MgKα radiation. The energy position of the valence band as derived from Be*K* and O*K* emission spectra are shown at the top of the figure.

the present interpretation of the Auger spectrum of BeO. More recently Fomichev [78] has studied the energy levels and valence band of BeO by X-ray emission and absorption method. His results are in close agreement with those of Hamrin et al.[70]. The energy band diagram for BeO constructed from ESCA results is shown in Fig.(5.18b). The ESCA spectra giving the binding energies of the Be K-shell in a partially and fully oxidised sample are shown in Fig.(5.19). Fig.(5.20) shows the valence band and Be and Oxygen K-shell binding energies in BeO. It is evident from this ESCA data that the Be K-shell shifts by 2.8eV to a higher binding energy in BeO, and in the partial oxidation of Be, two binding energies of K-shell are found - one due to clean Be at 111.4eV and the other due to oxidised Be at 114.2eV. Now there are two maxima in the valence band occurring at 7.6 and 11eV. The oxygen L_1 energy level has a binding energy of 24.4eV (Fig.(5.20)). From the energy diagram of Fig.(5.18b), if V_1 and V_2 are the two maxima in the valence band at 7.6 and 11eV and K_s the shifted Be K-shell with a binding energy of 114.2eV, then the various possible transitions giving rise to the Auger peaks in the BeO Auger spectrum may be listed in Table 5.2 along with the observed energy values of the peaks.

Table 5.2

Auger peak energies of BeO

Transition		Calculated energy (eV)	Observed energy (eV)
K V V	(clean Be)	105	104
$K_s V_1 V_1$	(oxidised Be)	99	94
$K_s V_2 V_1$	(" ")	96	
$K_s V_2 V_2$	(" ")	92	85
$K_s L_1(0) V_1$	(" ")	82.2	77
$K_s L_1(0) V_2$	(" ")	78.8	
$K_s L_1(0) L_1(0)$	(" ")	65.4	66

The agreement between the energies of the observed Auger peaks and those energies calculated on the above basis is surprisingly good. At the intermediate stage of oxidation of a Be surface two large Auger peaks were observed at 104 and 94eV. These peaks are believed to be due to clean Be and oxidised Be surfaces respectively. This interpretation is confirmed perhaps by the ESCA spectrum of the K-shell binding energies of a partially oxidised Be sample which shows two peaks, one at 111.4eV due to clean Be and the other at 114.2eV due to oxidised Be.

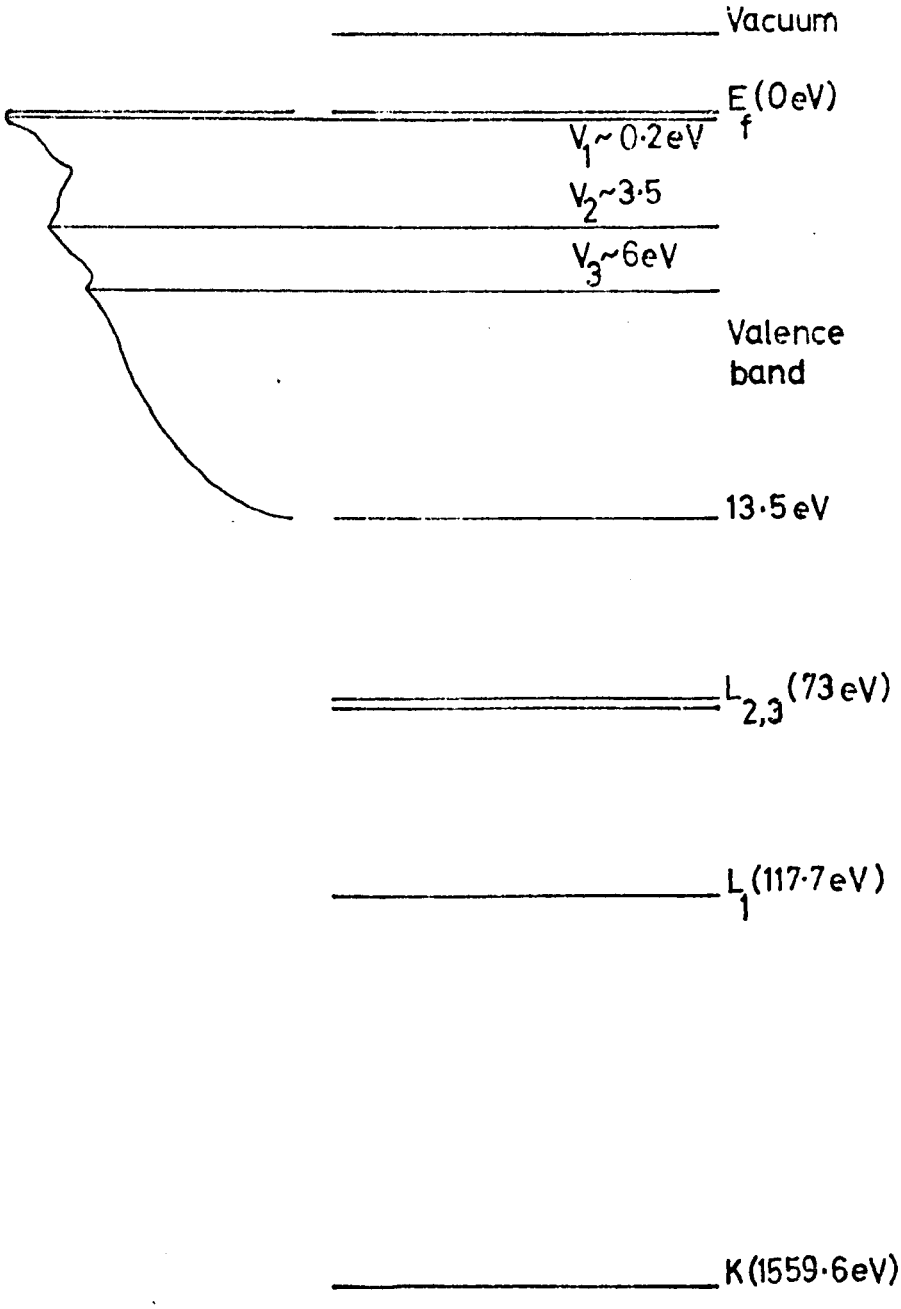

Fig. 5.21 Energy band diagram of Al.

5.4.2 Al

A considerable number of Auger peaks were found in the Auger spectrum of clean Al. All these peaks had energies less than 110eV, and most of these were thought to originate from the Al L-shell ionization with the participation of valence electrons in the subsequent Auger process. To account for the various transitions involving the valence band, it is relevant to give consideration to the density of states of the valence band for Al[79]. This is shown in the energy diagram of Fig.(5.21). The density of states of valence band for Al has three maxima at about 0.2, 3.5 and ~6eV. If the hypothesis is made that Auger peaks in the Al Auger spectrum can result from these maxima (represented here for convenience by the symbols $V_1 \simeq 0.2$eV, $V_2 \simeq 3.5$eV and $V_3 \simeq 6$eV) then the various possible transitions which may take place due to these "energy levels" within the valence band after initial ionization of the L_1 and $L_{2,3}$ energy shells of Al, are listed in Table 5.3 along with the observed energies of the peaks in the Auger spectrum of a clean Al surface. It may be seen, there is substantial agreement between the measured Auger peak energies and the calculated values from the theoretical density of states of the Al valence band. It may be pointed out that for the calculated energies no correction has been made for the work function of the analyser and the changed energy levels after the initial ionization (Chapter I, section 1.3.1).

Table 5.3

Energy values of Auger and associated peaks observed in the Auger spectrum of clean Al

Transition	Calculated energy (eV)	Observed energy (eV)	Peak width (eV)
$L_1V_1V_1$	117.3		
$L_1V_2V_2$	110.7	107	~2.77
$L_1V_3V_1$	111.5		
$L_1V_2V_1$	114.0		
$L_1V_3V_2$	108.2	(93.5) ??	~1.85
$L_1V_3V_3$	105.7	(89.8) ??	~1.85
Plasmon gain from 67eV peak ~82.4			
$L_{2,3}V_1V_1$	72.6	~73	
$L_{2,3}V_2V_2$	66		
$L_{2,3}V_3V_1$	66.8	67.1	~6.5
$L_{2,3}V_2V_1$	69.3		
$L_{2,3}V_3V_2$	63.5	58.3	~1.85
$L_{2,3}V_3V_3$	61	55	~1.85
Plasmon loss from 67eV peak ~49.7			
$L_1L_2V_1$	44.5	~45.4	
$L_1L_2V_2$	41.2	40.3	~1.85
$L_1L_2V_3$	38.7		

Therefore one would expect the calculated energies to be somewhat higher than the measured values. However, the energies of the Auger peaks at 93.5 and 89.8eV are much lower than the expected values. Both these peaks have approximately the same energy separation and peak widths (peak-to-peak) as those observed at 55 and 58.3eV. Since the 55 and 58.3eV peaks which are allocated to $L_{2,3}V_3V_2$ amd $L_{2,3}V_3V_3$ respectively, show relatively good agreement with the calculated energies, one may consider the origin of the 93.5 and 89.8eV peaks as being in the 'corresponding' transitions due to an L_1 ionization. However, due to the relatively large difference from the calculated energies, the interpretation of these two peaks (93.5 and 89.8eV) is much more tentative and other interpretations must not be ruled out. It has been shown earlier in the Auger spectrum of Be, that Auger electrons may suffer energy loss in the excitation of plasmons and they appear on the low energy side of the main Auger peak. For such a peak, the energy differences between the main Auger peak and the one on the low energy side should approximately be equal to the energy loss value of the bulk plasmons. In the Auger spectrum Al, the peak at 49.7eV is believed to be due to a plasmon loss from the main Auger peak at 67eV. This belief was further strengthened since a strong bulk loss for clean Al was found at 15.6eV in the energy distribution curve.

The peak at 82.4eV also appeared to be associated with the main 67eV Auger peak. Its energy difference from the 67eV peak is approximately equal to the excitation energy of the bulk plasmons. The indications are that this may be a plasmon gain peak analogous to the plasmon loss peak

observed in the low energy side of the Auger peaks. For a typical 'electron gas' metal like Al, the mean free path of exciting plasmons is <50Å for electrons of energies $\lesssim$1KeV[47]. Such an energetic primary electron then may be assumed to be capable of exciting large numbers of plasmons, as well as knocking out inner shell electrons along its path in the solid. The inner shell vacancies which initiate the Auger process are thus within the spatial range of the plasma waves. In addition, the plasmon life time (10^{-15} - 10^{-14}sec)[47,80] is similar to that of the inner shell vacancy life time (10^{-17} - 10^{-14}sec)[17]. It is not unlikelytherefore that some Auger electrons could gain plasmon energy and appear on the high energy side of the Auger peak. Interpretation of peaks as due to a plasmon gain mechanism in the Auger spectra of other elements, have been recently reported by Coad and Riviere[34] and Jenkins and Chung[22]. An alternative explanation of the plasmon gain process in terms of dynamical screening by the conduction electrons, has been given by Watts[81]. The calculated amplitude ratio of the plasmon gain peak and the main Auger peak is found to be 1:24 which is in close agreement with the observed ratio[21]. Auger spectra of the elements in the same period of the Periodic Table, are known to be very similar[4,31]. The Auger spectrum of clean Al observed in the present investigations confirms this trend, since it is similar to that reported for Si[82,83]. As the Al surface is oxidised, only three Auger peaks are observed at 36.8, 45.7 and 54.5eV.

The chemical shift in the binding energy of $L_{2,3}$ shell of Al in Al_2O_3 has been reported by several workers. Swanson and Powell[84],

Codling and Madden[85] report a shift of ~3 - 4eV. Fomichev[86] found a shift of 2.7eV in the $L_{2,3}$ shell of Al in Al_2O_3 and a similar shift (~2-3eV) has been found in ESCA results[87]. This shift is very similar to the one found in the Be K-shell in BeO. Assuming that the valence band of Al_2O_3 has a similar structure as in the BeO, then the observed Auger peaks in Al_2O_3 spectrum may be attributed to the transitions as follows.

Transition	calculated energy	Observed energy
$L_{2,3}V_1V_1$	(60.5)	54eV
$L_{2,3}V_2V_1$	(57.1)	
$L_{2,3}V_2V_2$	(53.7)	45.7eV
$L_{2,3}L_1(0)V_1$	(43.7)	36.8eV
$L_{2,3}L_1(0)V_2$	(40.3)	

5.4.3 Fe

The Auger spectrum of Fe has been reported by Aksela[65] et al. and Coad and Riviere[35]. The results of these authors are compared in Table 5.4 with those found in the present work.

Table 5.4

Comparison of energy values of Auger and associated peaks observed in the Auger spectrum of clean Fe in the present work with the other workers

Transition	Calculated energy(eV)	Observed energy(eV)	Coad and Riviere (35)	Aksela et al. (65)
L_2VV	715	715	712	
L_3VV	702	702	700	701.2
Plasma loss from 702eV peak		678		
$L_2M_{2,3}V$	664	662		650.3
$L_3M_{2,3}V$	651	649	647	646.5
L_2M_1V	625	625		
L_3M_1V	612	608	606	
$L_2M_{2,3}M_{2,3}$	608			
$L_3M_{2,3}M_{2,3}$	595	595	594	596.5
$L_2M_1M_{2,3}$	569	561	559	
$L_3M_1M_{2,3}$	556	548	546 513	
M_1VV	86	84	82	
$M_{2,3}VV$	47	46.5	46	

From Table 5.4 it is evident that there is good agreement on the energy values and the allocation of various transitions with the results reported by Coad and Riviere[35] and Aksela et al.[65]. However, the energy values of the Auger peaks reported by Haas et al.[31] are higher than those observed in the present work and there is also disagreement on the allocation of the three main Auger peaks which these authors have allocated to L_2 instead of L_3 ionization. In the present work the allocation of these peaks was checked by measuring the energy separation of the Auger peaks attributed to L_2 and L_3 ionization, and comparing this separation with the energy separation of L_2 and L_3 energy levels with X-ray data of Bearden and Burr[60]. The Auger peaksat 715 and 702eV are allocated the L_2VV and L_3VV transitions respectively. The measured energy separation of these two peaks is 13eV which is equal to the energy separation of the binding energies of the L_2 and L_3 energy levels of Fe. Similar 'energy separation agreement' between the Auger peaks and L_2 and L_3 energy levels was found for Cu (Chapter IV). The amplitude of the L_3VV Auger peak is greater than that of the L_2VV Auger peak for both Cu and Fe. This is in agreement with the relative ionization probabilities of the L_3 and L_2 shells ($L_3 > L_2$) as stated by Burhop[15]. Therefore it seems most likely that the allocation of Haas et al.[31] is incorrect and the main tripletsin the LMM spectra of Cu and Fe are due to ionization of the L_3 shell. In the Auger spectrum of oxidised iron two peaks at 42.5 and 51eV were found. As pointed out earlier in the case of Be and Al, the changes in the Auger spectrum due to oxidation result from the chemical shift of the energy levels and changes in the valence band.

A shift of ~1.5eV was found in the $M_{2,3}$ ionization loss on forming iron oxide. The shift in the valence band will be somewhat higher than that of the $M_{2,3}$ shell as generally found in ESCA results[87]. If such a shift was ~5eV, then the 42.5eV peak could be due to a $M'_{2,3}V'V'$ transition where $M'_{2,3}$ and V' are the shifted $M_{2,3}$ energy level and valence band. The peak at 51eV could also be due to the ionization of the shifted $M_{2,3}$ and electrons near the Fermi level with binding energies of ~1.5eV. Similar changes in the Auger spectrum of vanadium have recently been reported by Coad and Riviere[34] on forming vanadium oxide.

5.4.4 CEL spectra of Be, Al and Fe

The characteristic energy losses of Be and Al have been reported by several workers[67,88,47,89,90]. The energy loss values of clean Be and Al found in the present work are compared with the results of Powell[67] and Powell and Swan[88] in Tables 5.5 and 5.6.

Table 5.5

Characteristic energy losses in clean Be as found in the present work and by Powell[67] (eV)

Present work	13	19	38	57	77	112
Powell[67]	11.9	19.9	39.4	58.4		

Table 5.6

Characteristic energy losses in clean Al as found in the present work and by Powell and Swan[88] (eV)

Present work	11	15.6	26.4	31.4	46.5	62.3	77.9			
Powell and Swan[88]	10.3	15.3	20.5	25.6	30.5	41.1	46.1	56	61.4	77
							91.8	108.6		

Assuming two free electrons per atom for Be, the calculated value of the bulk plasmons using the formula $\hbar\omega_p = 28.8(\frac{n_v d}{A})^{\frac{1}{2}}$ eV (where d is the density of Be, A its atomic weight and n_v is the number of free electrons), is 18.4eV. The surface loss is then given by $\hbar\omega_p/\sqrt{2}$ and is thus 13eV. These values of surface and bulk plasmons agree well with the measured values of 13 and 19eV respectively. The other peaks in the energy loss spectrum of Be are probably multiples of the bulk plasmon loss. A loss peak at 112eV is thought to be due to Be K-shell ionization.

For Al, the calculated values of the surface and bulk plasmons, for three free electrons per atom, are 11.2eV and 15.8eV respectively. In the energy loss spectrum of Al, two strong peaks found at 11 and 15.6eV show excellent agreement with the calculated values for surface and bulk plasmons, and therefore these peaks (at 11 and 15.6eV) are attributed to surface and bulk plasmon losses respectively. The loss peak at 26.4eV is attributed to a combination of surface and bulk plasmon losses. All the other peaks in

the loss spectrum can also be attributed to multiples of the bulk plasmon loss.

The energy losses of clean Fe found in the present work are given in Table 5.7. A comparison with some of the published work[66,89,90] is also made in the table.

Table 5.7

Characteristic energy losses in clean Fe as found in the present work and by other workers (eV)

Present work	8	14	16	22	23	33.5	39	57	92
Robins and Swan[66]	5.3	8	15.8		23			56.6	
Martin and Leder[89]			15.8	19.4				56.1	
Kleinn[90]	7			21.5		36.5		56.9	

The loss peaks at 23 and 16eV are somewhat lower than the calculated values of 26.4 and 18.7eV for the bulk and surface plasmons respectively, assuming 6 free electrons per atom in Fe. The plasmon losses may be shifted to lower energy values due to nearby interband transitions and this may explain the lower energy values observed in the present work. The loss peak at 57 and

the one at 92eV are most probably the ionization losses due to ionization of the $M_{2,3}$ and M_1 energy levels. This is confirmed by the 'corresponding' Auger peaks being found in the Auger spectrum of iron. At lower primary energies (≤500eV) the loss peak at 16eV was found to shift to 14eV. The loss peak at 8eV and the one at 14eV showed the characteristics of surface and bulk plasmons for lower primary energies (≤500eV) indicating that perhaps at these energies all 6 electrons do not participate in plasmon oscillations. Two small loss peaks observed at 22 and 33.5eV for a primary energy of 250eV are identified as due to the combination and multiples of the 14 and 8eV peaks. A weak peak at 39eV was found for a primary energy of 1KeV and is identified as due to the combination of surface and bulk plasmon peaks at 16 and 23eV respectively. The extreme sensitivity of the surface plasmon loss to the oxidation of Be, Al and Fe is evident from the spectra of Appendix 2a,b,c. The surface loss is found to shift to lower energy values gradually before disappearing. In the energy loss spectra of oxidised Be, Al and Fe a broad peak is found at ~25eV (for Al at 22.1 eV) For Be a small peak at 14eV is also found. This peak is possibly due to an interband transition between the oxygen 2s energy level and the valence band of BeO. The loss peak ~25eV is thought to be due to the ionization of the oxygen 2s energy level in the oxidised surfaces of Be, Al and Fe.

5.5 Conclusion

The Auger electron spectra of Be, Al and Fe have been investigated. The results indicate that the Auger spectra of these metals may be

tentatively interpreted in terms of transitions involving the structure within the valence band. This structure in the valence band is identified with the peaks in the theoretical density of states. Considerable changes in the Auger spectra of these elements are found as a result of oxidation. By taking into account the chemical shifts of the inner energy levels and the changes in the valence band, the Auger spectra of the oxidised surfaces can be explained. Plasmon losses observed in the energy loss spectra of clean metal surfaces show good agreement with the theoretically calculated energy values. The Auger spectra (and surface loss in the energy loss spectra) of these metals are extremely sensitive to the surface oxidation and can only be investigated under extremely good ultra high vacuum conditions.

CHAPTER VI

CONCLUSIONS AND SUGGESTIONS FOR FUTURE WORK

The three grid retarding field analyser constructed for the present investigations has proved to be an excellent tool for energy analysis over the whole range of the secondary electrons spectrum. Analysers of this type are now available commercially. However, even disregarding their high price, these analysers have too limited an energy resolution for detailed examination of Auger phenomena. For example a conventional three grid system has a resolution of about 1-2%. Although some improvements have been reported, e.g. Palmberg[16] who describes the inclusion of a fourth grid, this results in the reduction of the sensitivity of the instrument since the transmission is inevitably lowered due to the fourth grid. In contrast only three grids were used in the present instrument. The measured resolution of the device is ~0.2%. A high sensitivity for the analyser has been achieved by using three high transmission (~85%) grids, and also because of a greater collection efficiency due to a collection angle of 180^{o}. A fourth grid, therefore, was found undesirable. The excellent performance of the analyser is evident from the results described in Chapters IV and V.

A comparison of the Auger spectra of Cu black and Au black surfaces with those of clean Cu and Au surfaces has revealed that these low secondary electron yield surfaces were mainly composed of Cu and Au. No evidence was found for argon occlusion in these surfaces since no Argon Auger peaks

could be detected in the Auger spectra of Cu black and Au black. However the characteristic energy loss spectra of these surfaces (Cu black and Au black) were found to be very similar to each other, but completely different from those of clean Cu and Au.

The Auger electron spectra of clean Be, Al and Fe have been investigated. These results suggest that the peaks in the Auger spectra can be related to the peaks in the theoretical density of states of the valence bands of these elements. In addition some peaks in the Auger spectra are believed to originate from plasmon energy loss and gain mechanisms. Peaks of this type are found to be usually associated with a large Auger peak. The effect of oxidation on the Auger spectra of clean surfaces has also been observed. The changes (in the Auger spectra) which take place as a result of oxidation can be explained in terms of chemical shifts in the inner energy levels and the changes in the valence band. Some Auger peaks in the Auger spectra of oxidised surfaces are also believed to be due to cross-transitions between the energy levels of the oxygen and metal atoms.

With respect to the experimental apparatus, some modifications have been made in order to improve its overall performance. For example, only one metal could be evaporated previously without breaking the ultra high vacuum. However, in some experiments (such as escape depth measurements) it may be necessary to evaporate two materials one onto another without opening the vacuum system to air. For this purpose a special evaporation section and a sample manipulator have been constructed and

will be connected to the main chamber. The main feature of this manipulator is that a relatively large translational motion can be obtained in addition to the rotary motion. This will make it possible to take the sample into the evaporation section for evaporation purposes and then bring it back into the main chamber to align the evaporated sample with the analyser. In addition to the facility of evaporation of two metals in UHV, this arrangement will eliminate any possibility of contamination of the analyser assembly due to evaporation.

In order to achieve a further increase in sensitivity, arrangements have been made to incorporate an electron gun at grazing incidence to the sample. This gun (GEC 3HP7) can be operated up to about 3KeV and can provide beam currents of ~100 μamps. A new tuned load has also been constructed. The resonance impedance of this load at a frequency twice the modulation frequency is ~50MΩ, and ~50KΩ at the modulation frequency. It is expected that the grazing incidence gun and the improved tuned load will improve the sensitivity of the analyser considerably. Although a relatively favourable signal-to-noise ratio can be obtained with a retarding field analyser, its sensitivity is ultimately limited due to shot noise[40]. In addition, the time required for data acquisition is usually of the order of minutes and this may be undesirably large if changes in the Auger spectrum are taking place within this time. In such experiments any such changes in the Auger spectrum would not be detected and a fast scanning device would need to be used. For this purpose a cylindrical mirror analyser is being constructed. Instead of a conventional one stage

device[37], a two stage analyser is being built. It is expected that the resolution of this two stage analyser would be better by an order of magnitude than that of the one stage analyser[91]. Because of its superior signal-to-noise ratio, the Auger spectrum of a sample obtained with a cylindrical mirror analyser can be displayed on an oscilloscope or may be recorded on an X-Y recorder in a few seconds to observe any rapid changes which may take place in the Auger spectrum.

The technique of Auger spectrosoppy is only a few years old and a considerable amount of work has yet to be done. This is evident from the fact that the Auger spectra of all elements in the 'clean form' have not yet been investigated. The data regarding the various parameters (such as ionization, cross-section, escape depth etc.) involved in Auger emission is not yet available. The position on the theoretical side of the technique is even worse. For example, the transition probabilities for various transitions are not known.

Since the technique of Auger spectroscopy at present is in its initial stages of development, its potential for various technical applications is not yet fully known. However, already it has been applied to monitor the impurity segregation on various surfaces[2] and the fractionally thick coverage of impurities such as carbon on photocathodes[29]. The present results strongly suggest the desirability of complementary studies of the characteristic energy losses and Auger spectra, since the surface composition can be determined with the help of the Auger spectrum.

It is evident that in the near future it will become established as one of the most versatile methods for surface analysis.

Appendices 1a, 1b and 1c

Sequences of changes in the Auger spectra of Be, Al and Fe due to oxidation are shown in Appendices 1a, 1b and 1c respectively. Primary beam currents of 20-25μamps were used for Be and Al Auger spectra and for Fe only 15-20μamps were used. For all the Auger spectra a primary energy of 1.5KeV was used, except for the high energy (400-750eV) Auger spectrum of Fe where a primary energy of 2KeV was used. Modulation voltages up to $4V_{pk-pk}$ for low energy Auger spectra (<200eV) and $11V_{pk-pk}$ for high energy spectra (>200eV) were used for the three elements. The amplitude of the oxygen Auger peak at various stages of oxidation is also shown along with the spectra of Be, Al and Fe.

Appendix 1a

Graphs 1-7 show successive oxidation of Be with increasing oxygen level (1 → 7)

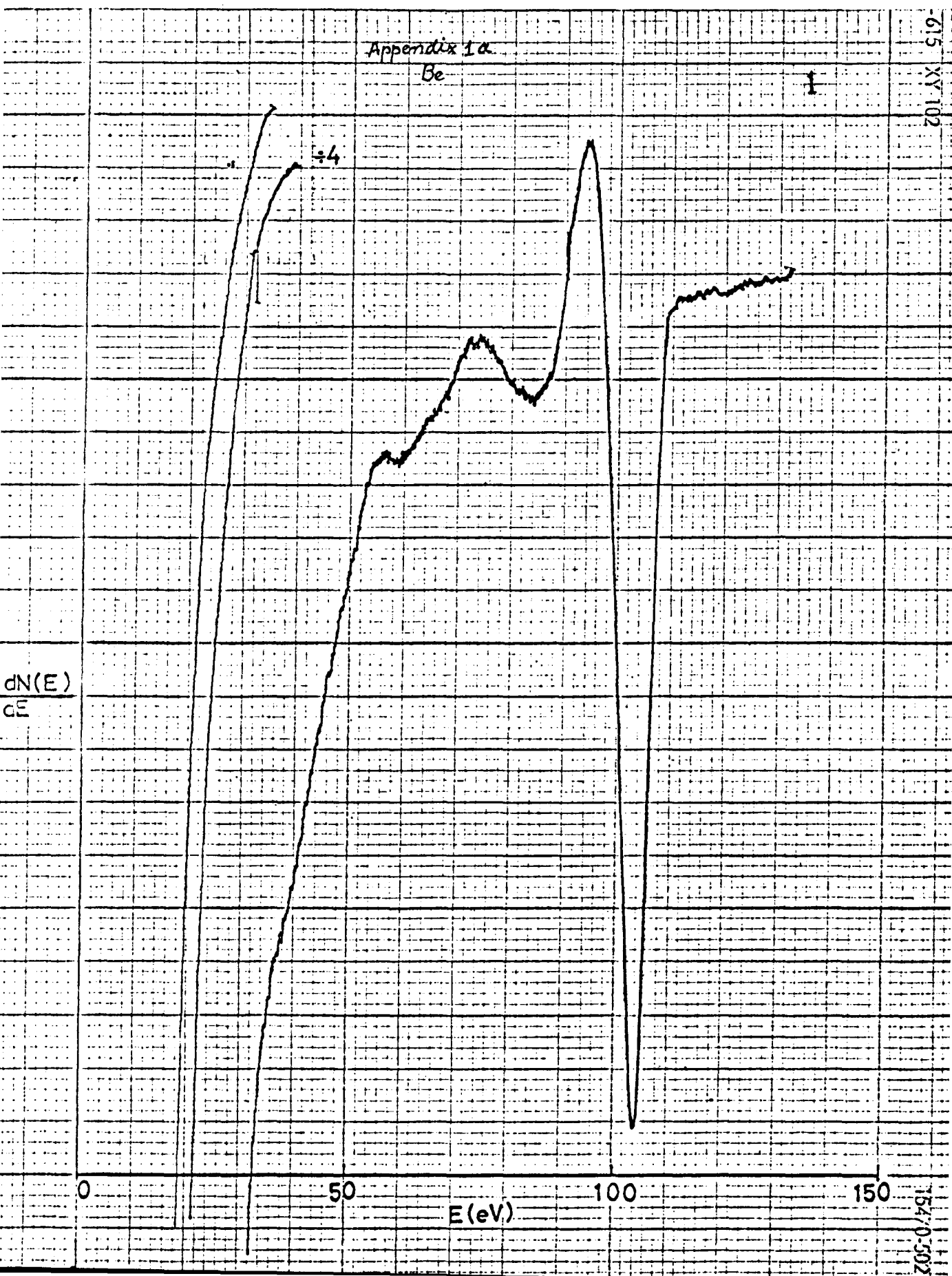
Appendix 1a
Be
÷4
dN(E)
dE
0
50
100
150
E(eV)
615 XY 102
1540-502

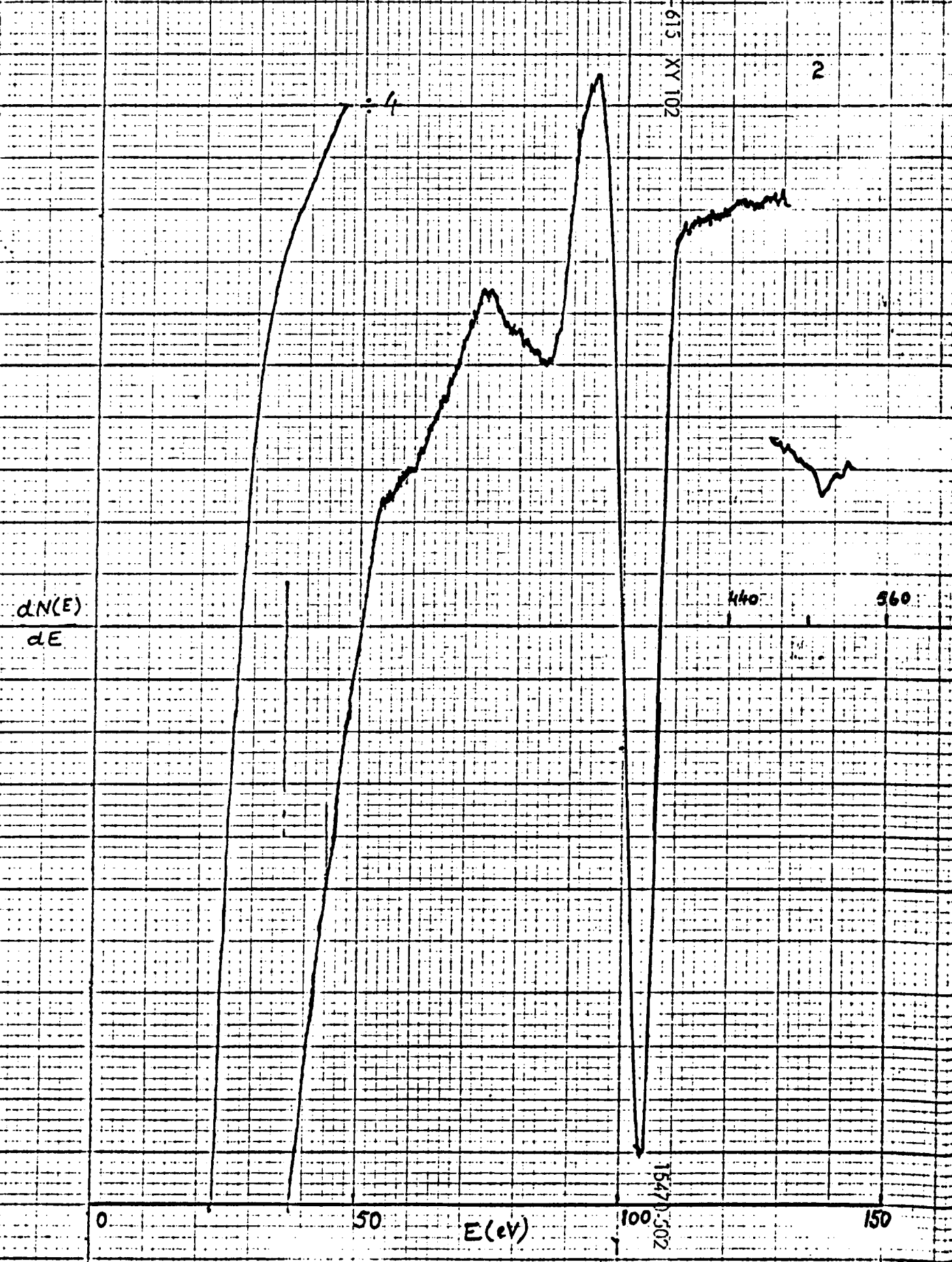
615 XY 102
2
dN(E)
dE
440
560
0
50
E(eV)
100
150
1547-502

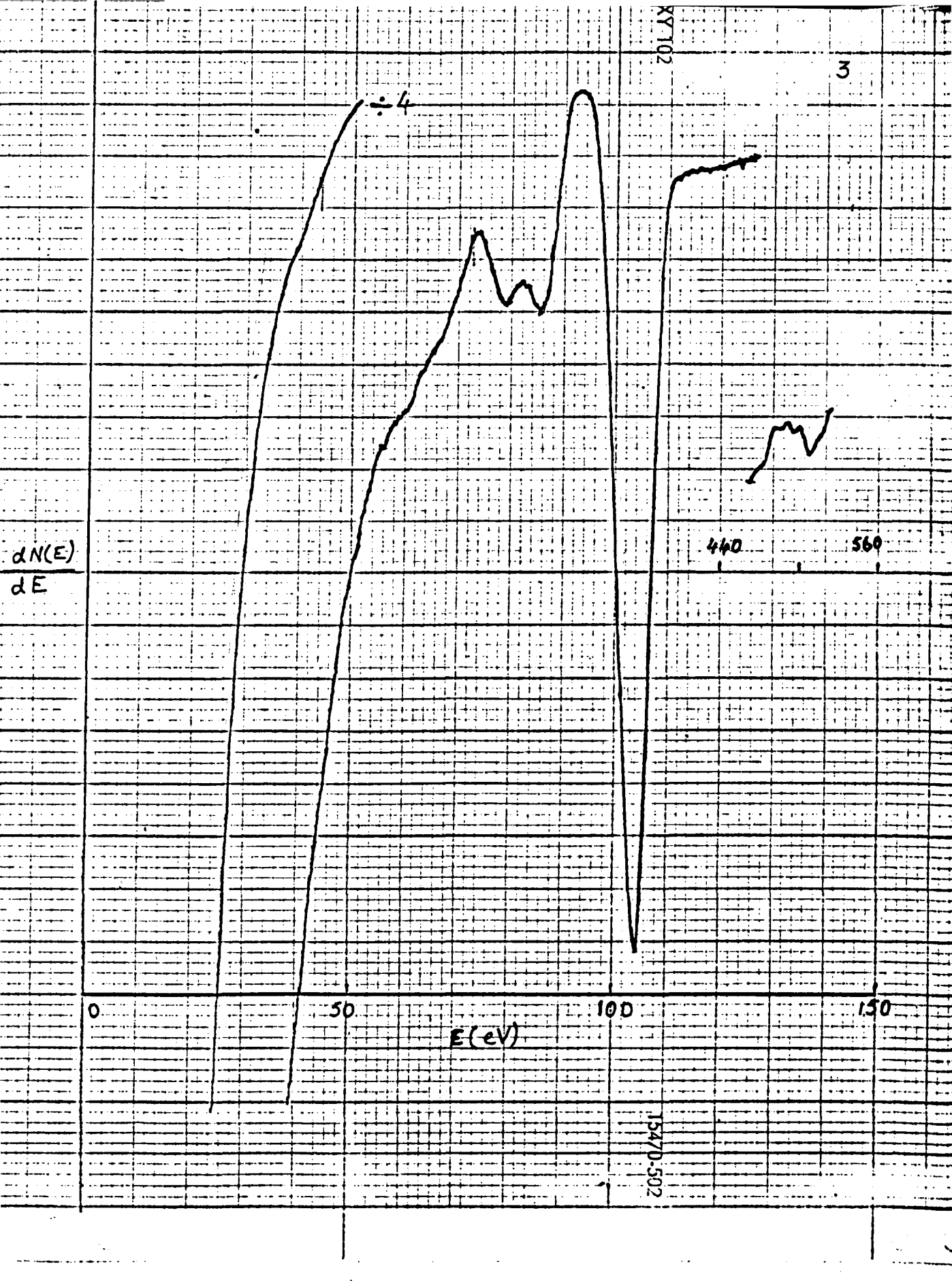
XY102
3
÷4
440
560
dN(E)
dE
0
50
100
150
E(eV)
1547D-502

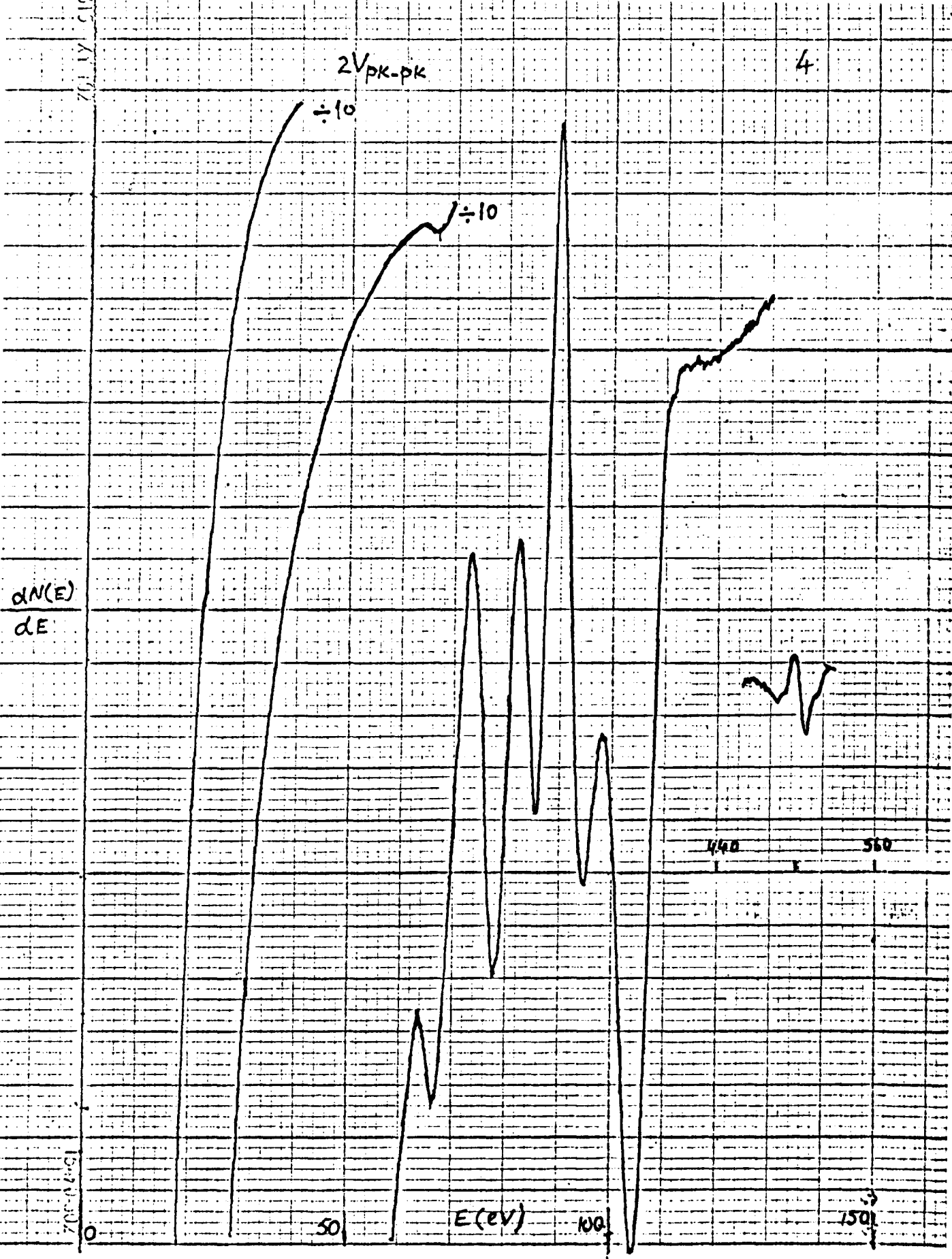
2V pk-pk
÷10
÷10
dN(E)
dE
440
560
0
50
E (eV)
100
150

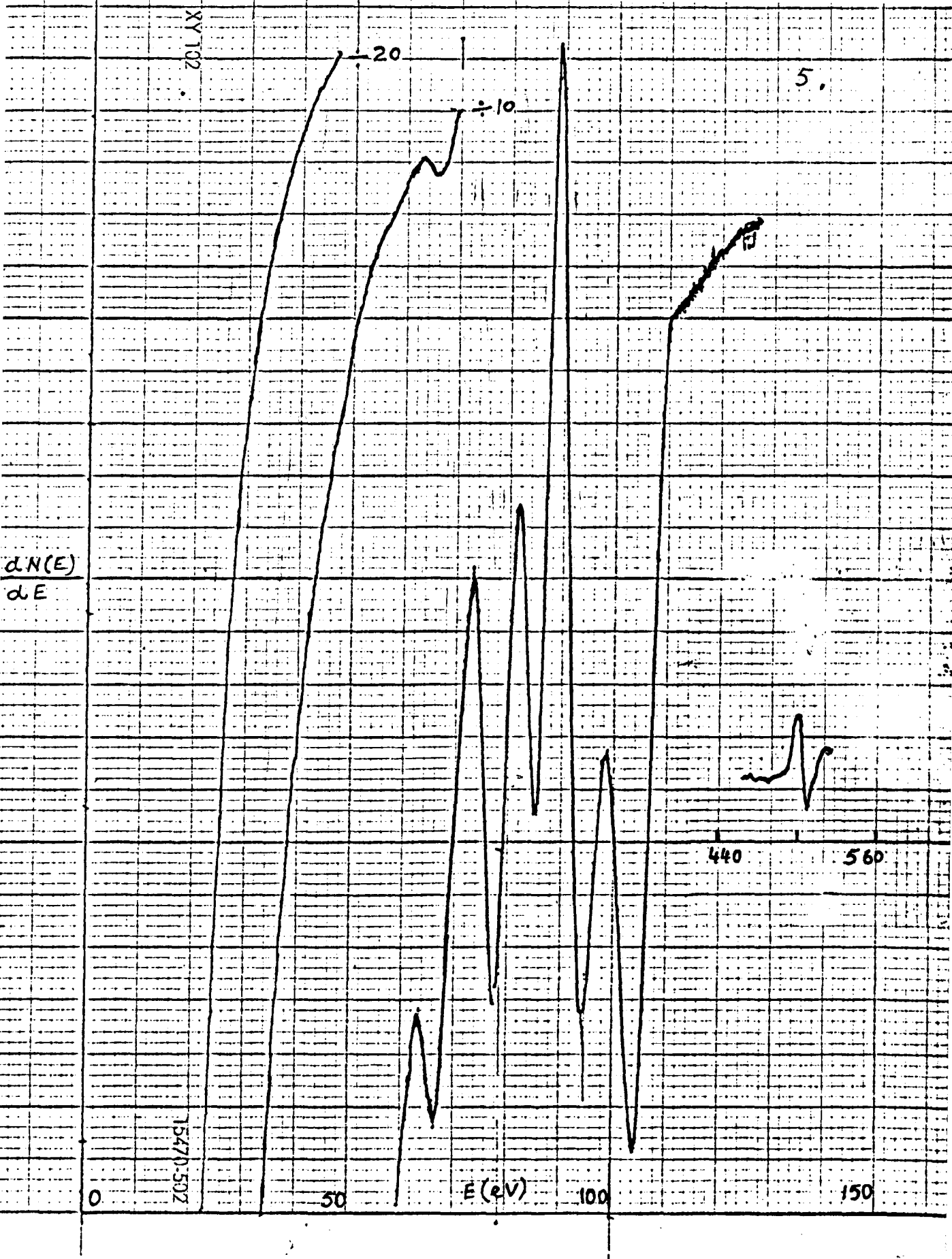
XY 102
÷20
÷10
5.
dN(E)
dE
440
560
0
50
E (eV)
100
150
15470-502

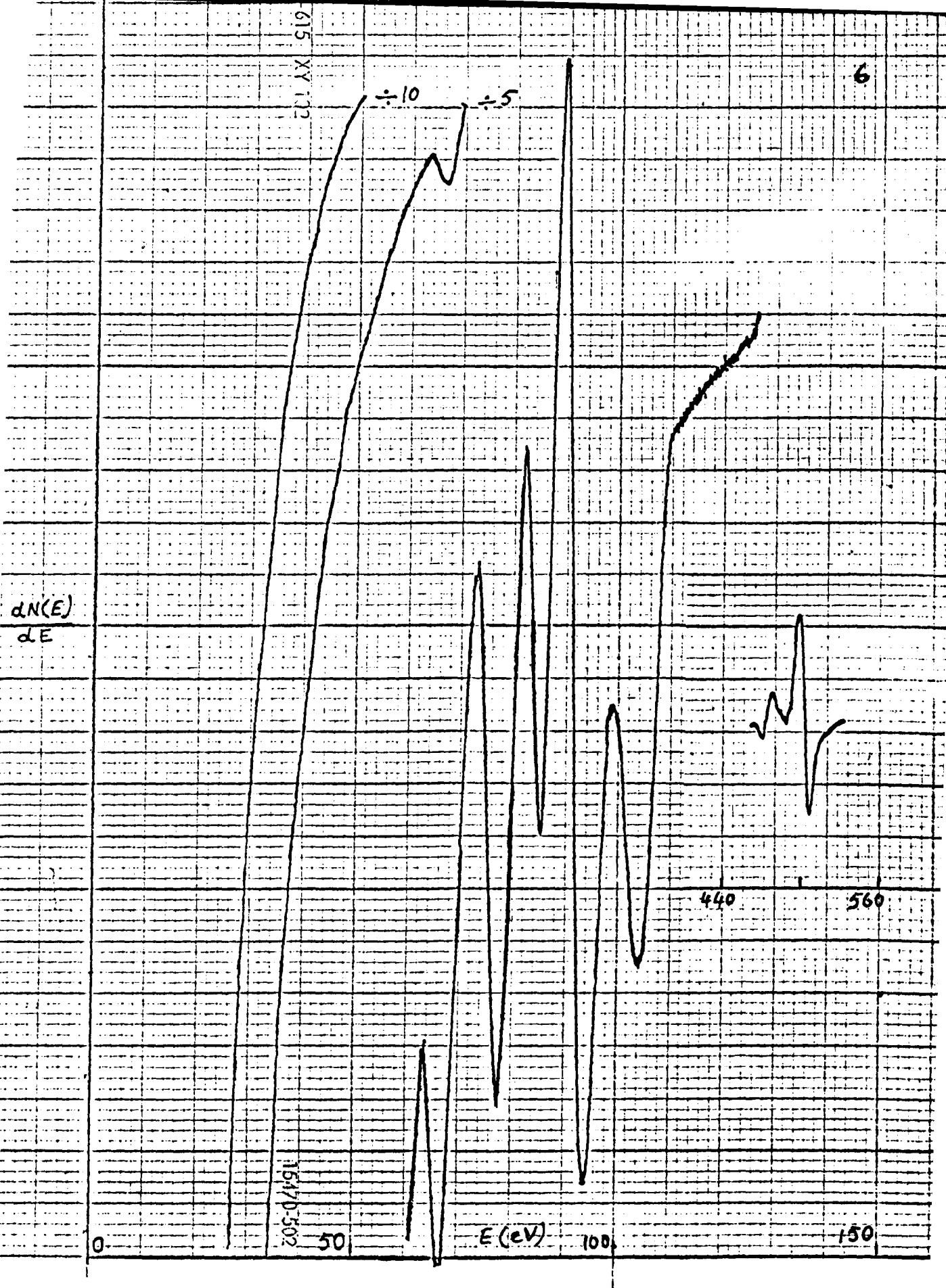
6
÷10
÷5
dN(E)
dE
440
560
0
50
E (eV)
100
150

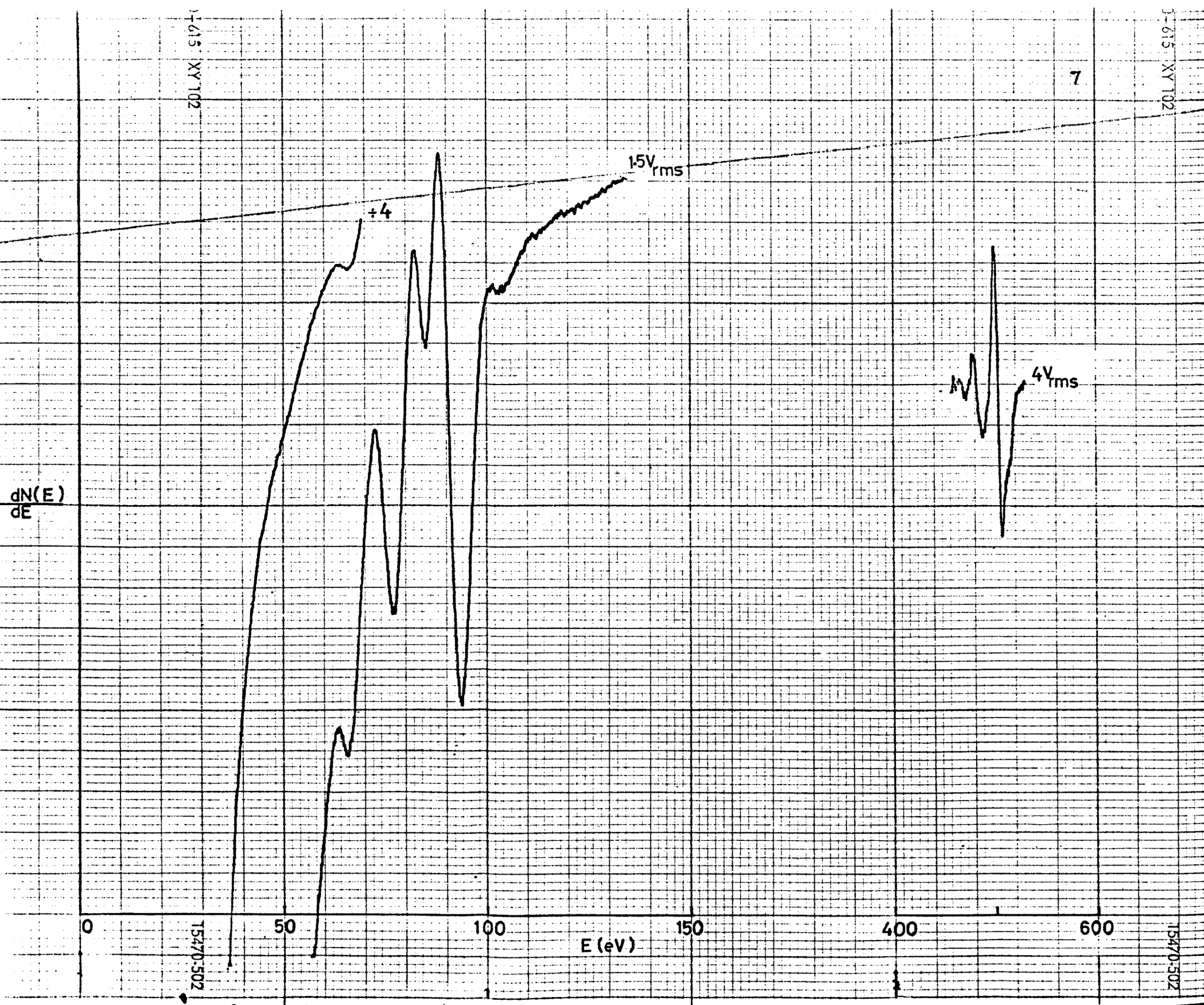
7
1.5V rms
÷4
4V rms
dN(E)
dE
0
50
100
150
400
600
E (eV)
1547D-502
1547D-502

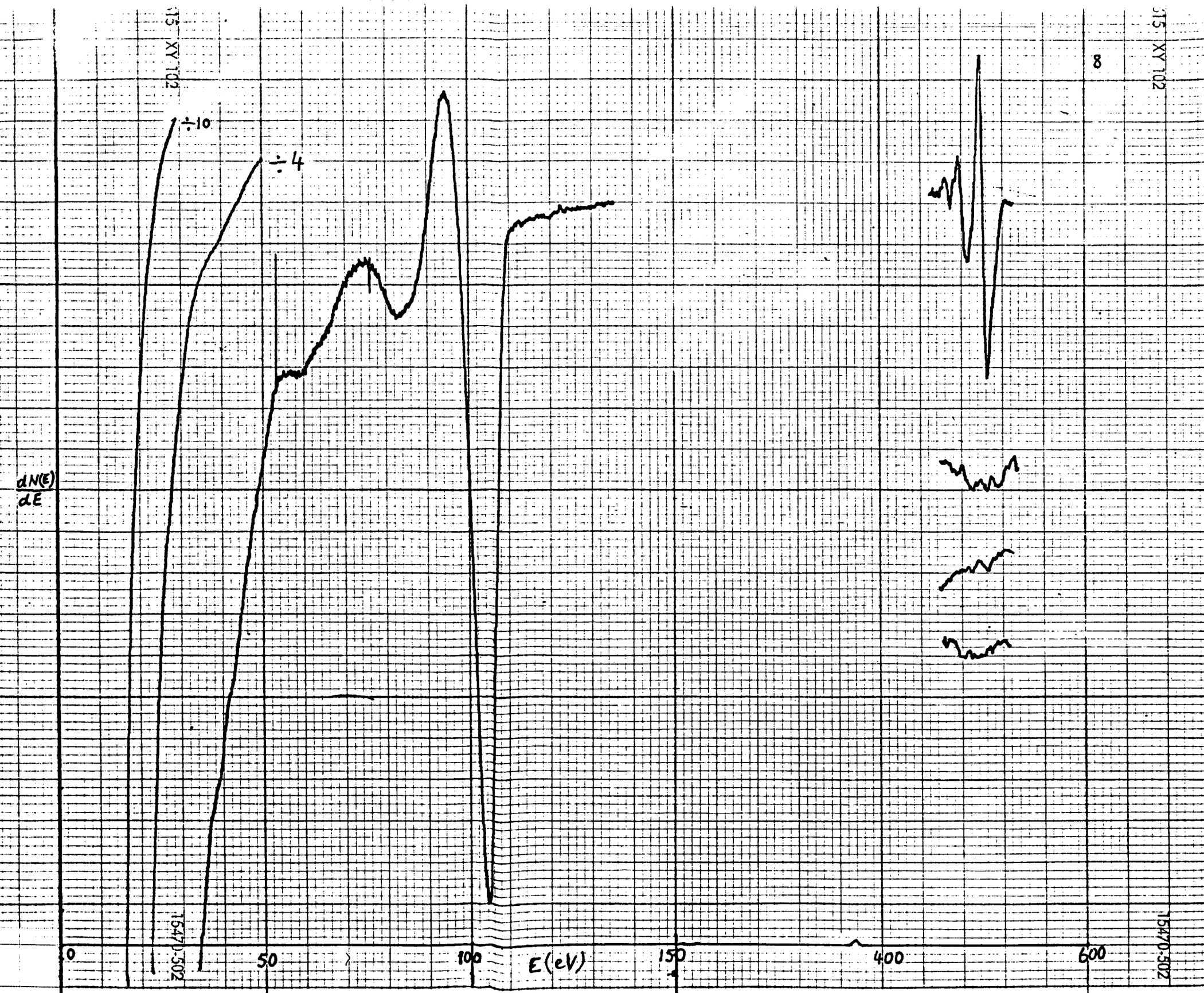
8
÷10
÷4
dN(E)/dE
0
50
100
E(eV)
150
400
600
15470-502


X 10²
÷4
÷2
dN(E)/dE
0
200
400
600
E(eV)
1534-0-302

Appendix 1b

Graphs 1-7 show successive oxidation of Al with increasing oxygen level (1 → 7).

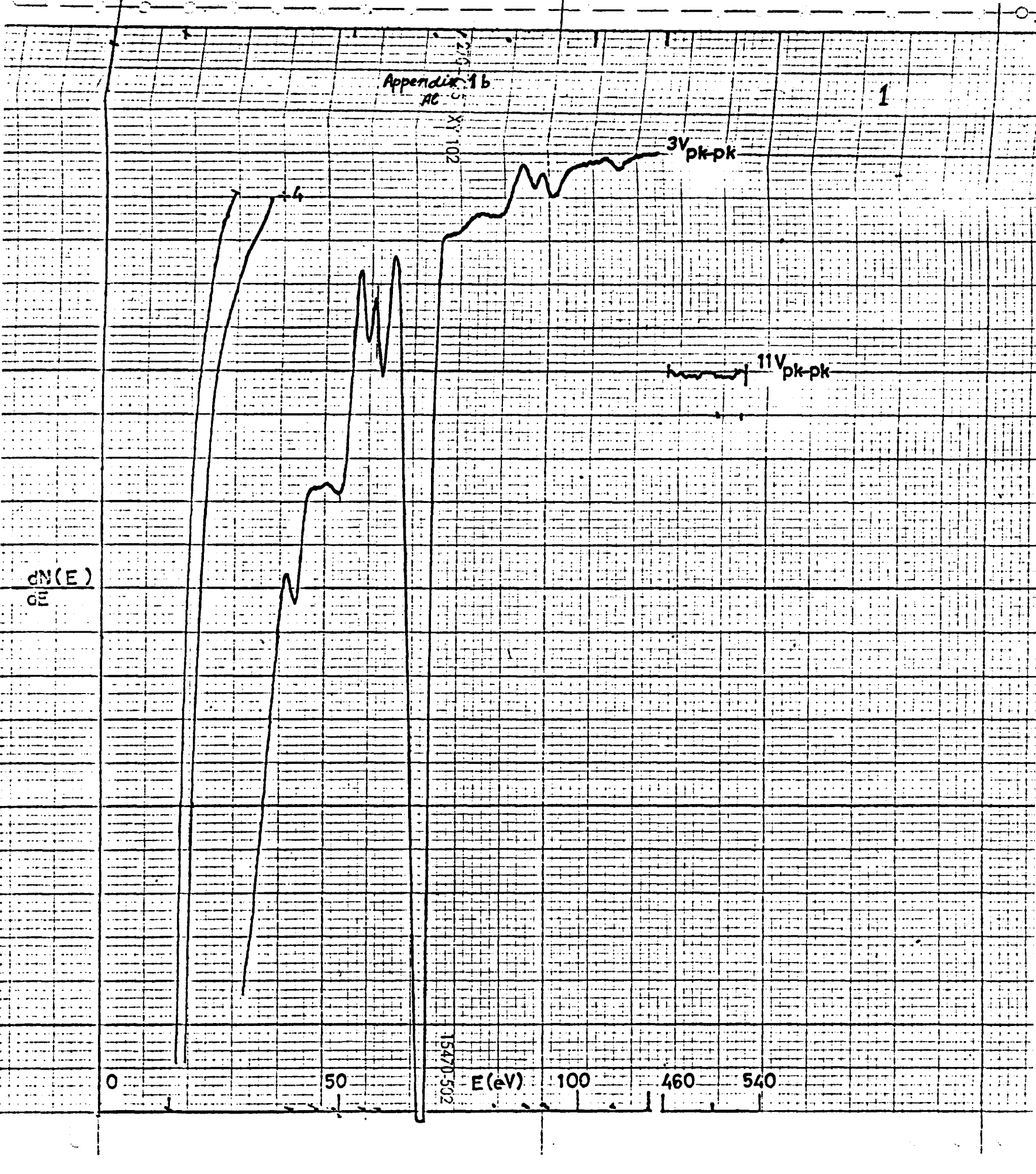
Appendix 1b
AC
XY 102
1
3V pk-pk
11V pk-pk
dN(E)/dE
0
50
E(eV)
100
460
540
15470-502

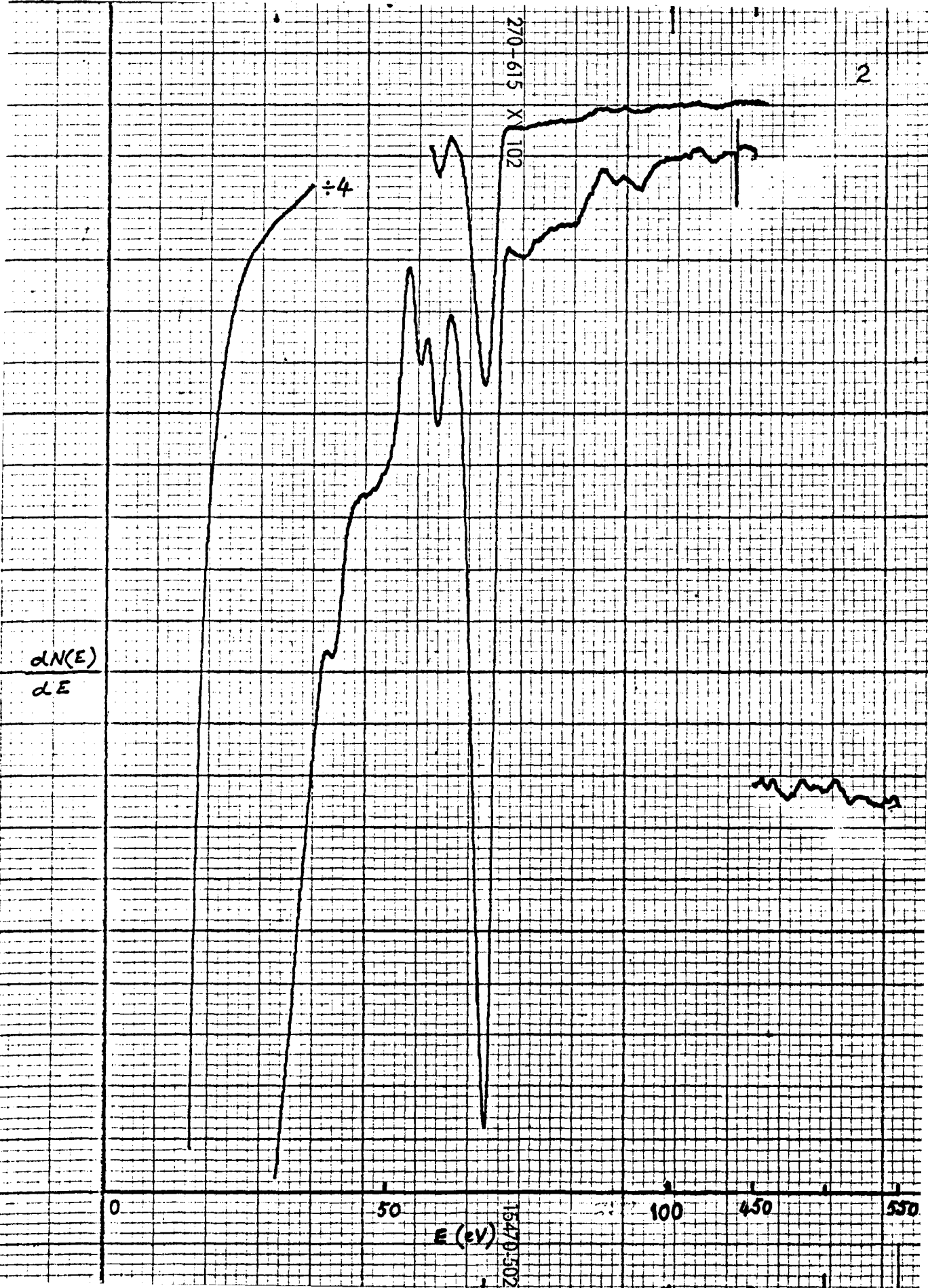
270-615 X 102
2
÷4
dN(E)
dE
0
50
100
450
550
E (eV)
1547-502

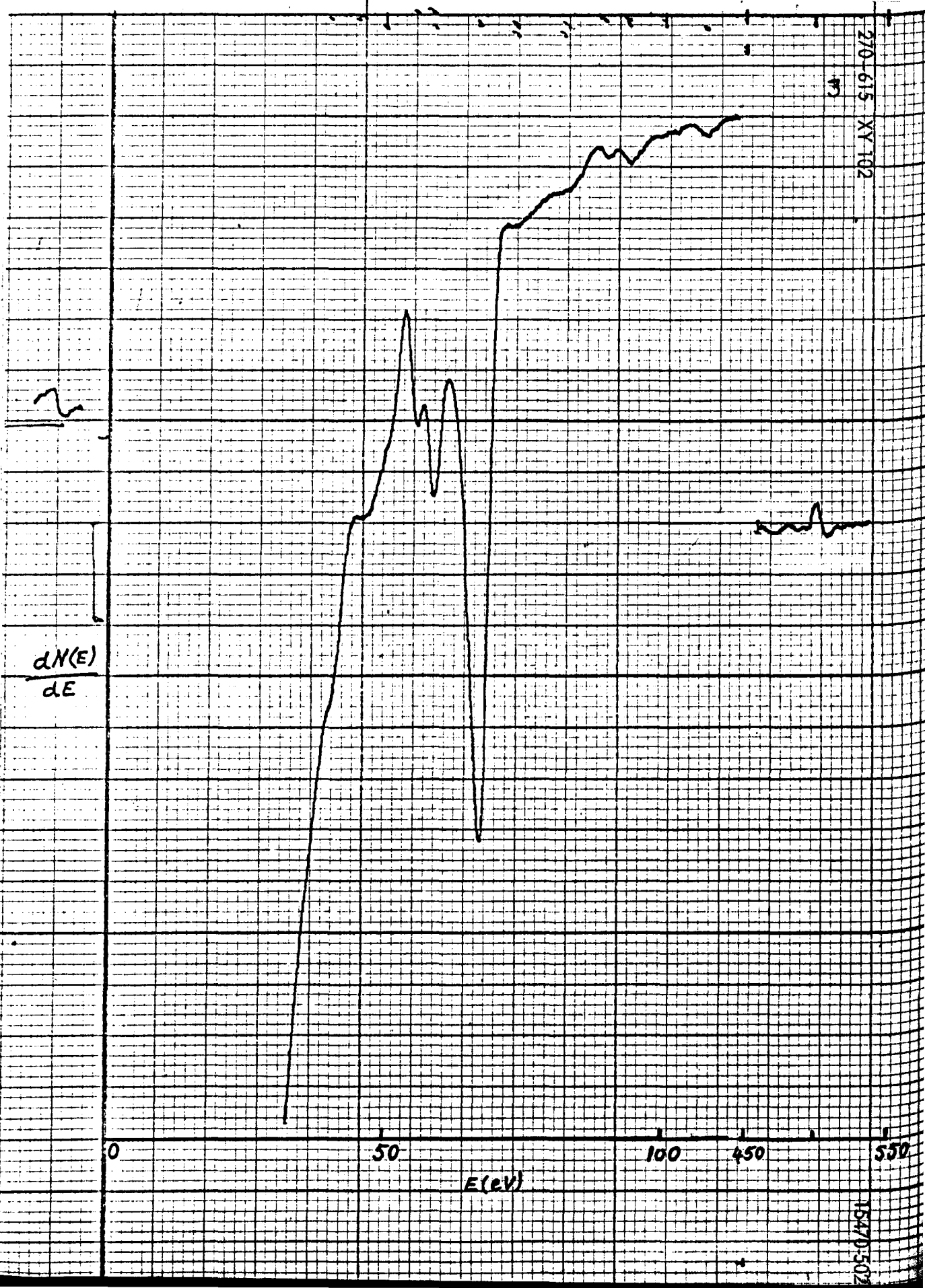
270-615 XY 102
dN(E)/dE
0
50
100
450
550
E(eV)
1540-502

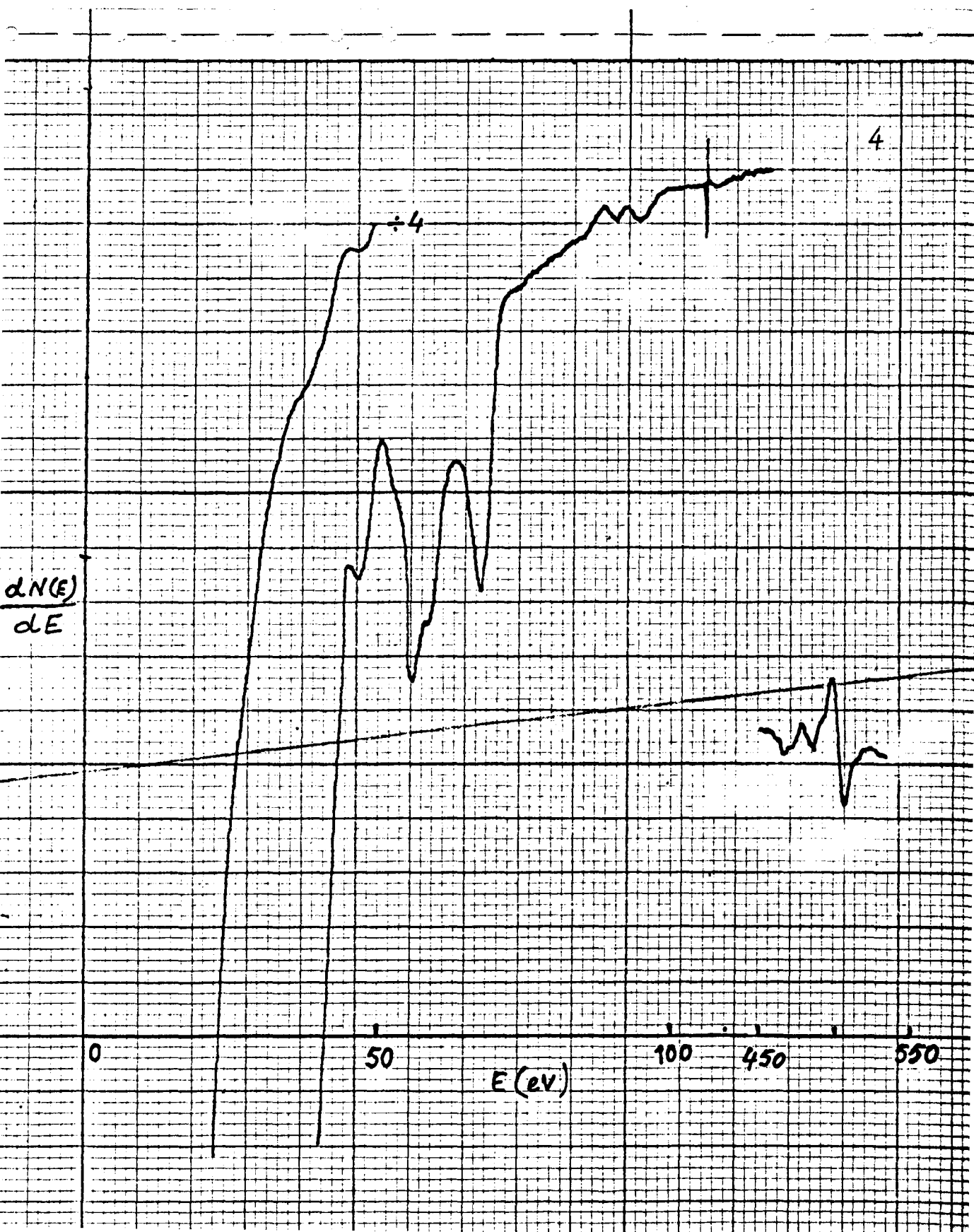
4
÷4
dN(E)/dE
0
50
100
450
550
E (eV)

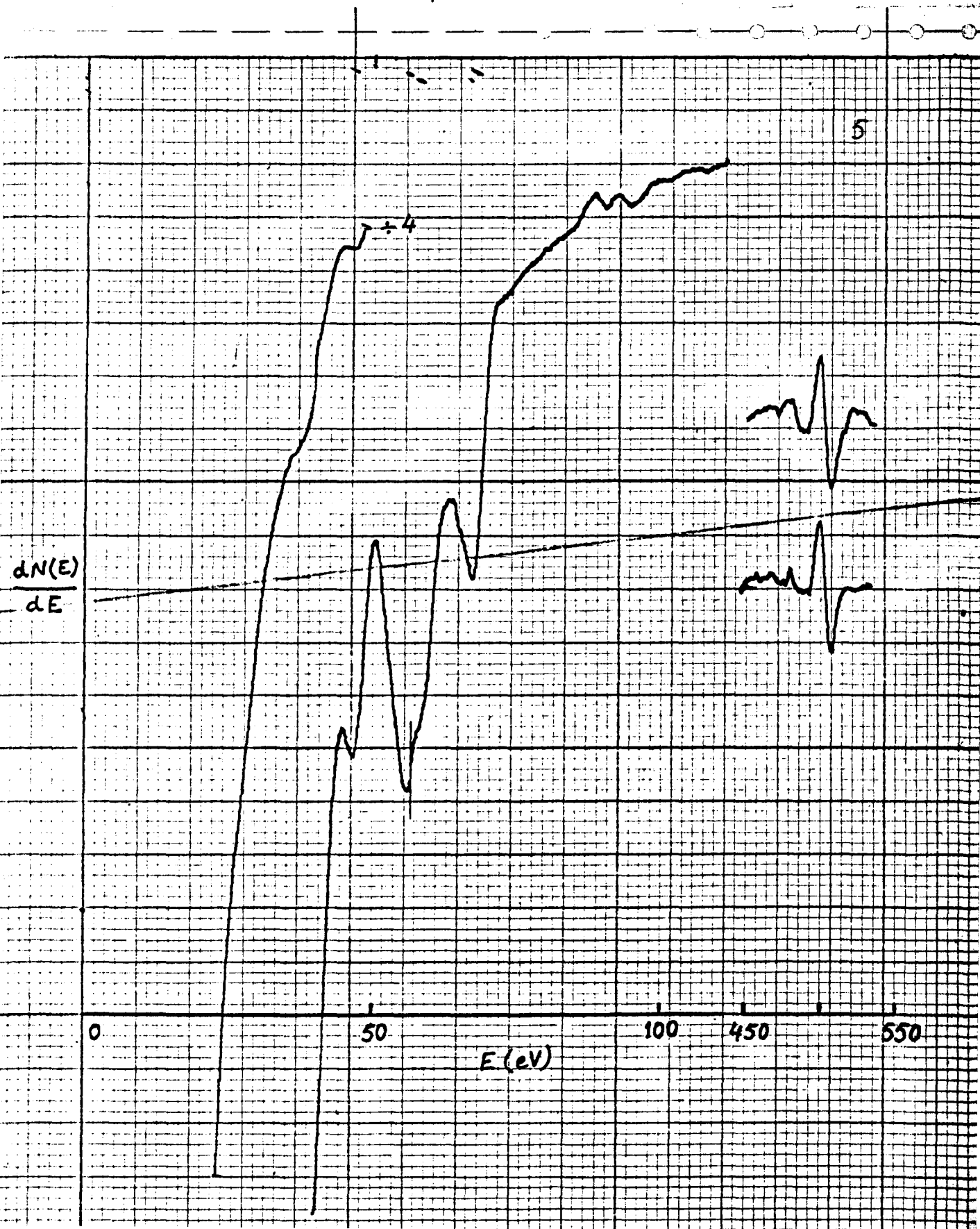
5
÷4
dN(E)
dE
0
50
100
450
550
E (eV)

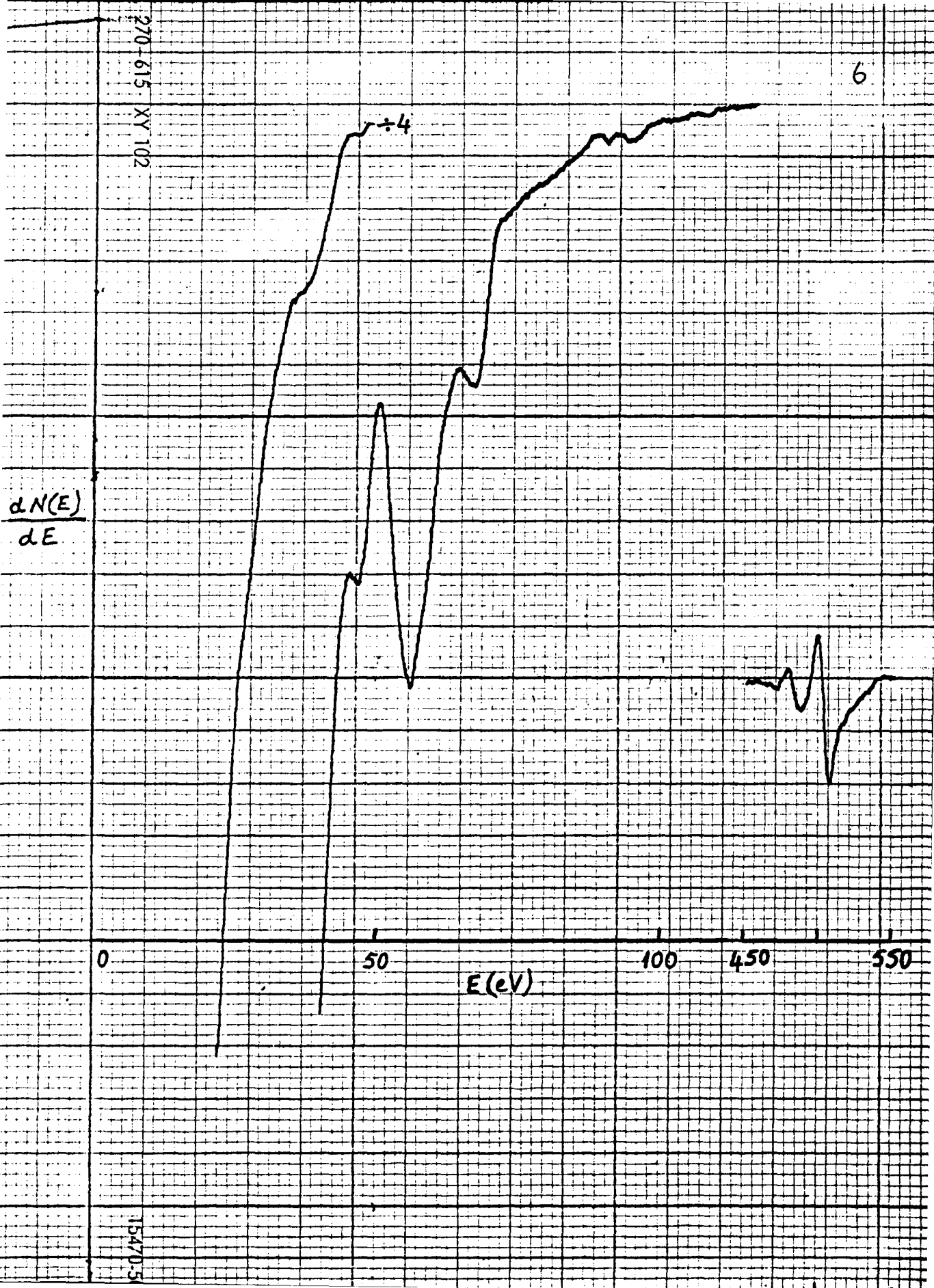
6
270-615 XY 102
÷4
dN(E)
dE
0
50
100
450
550
E(eV)
15470-5

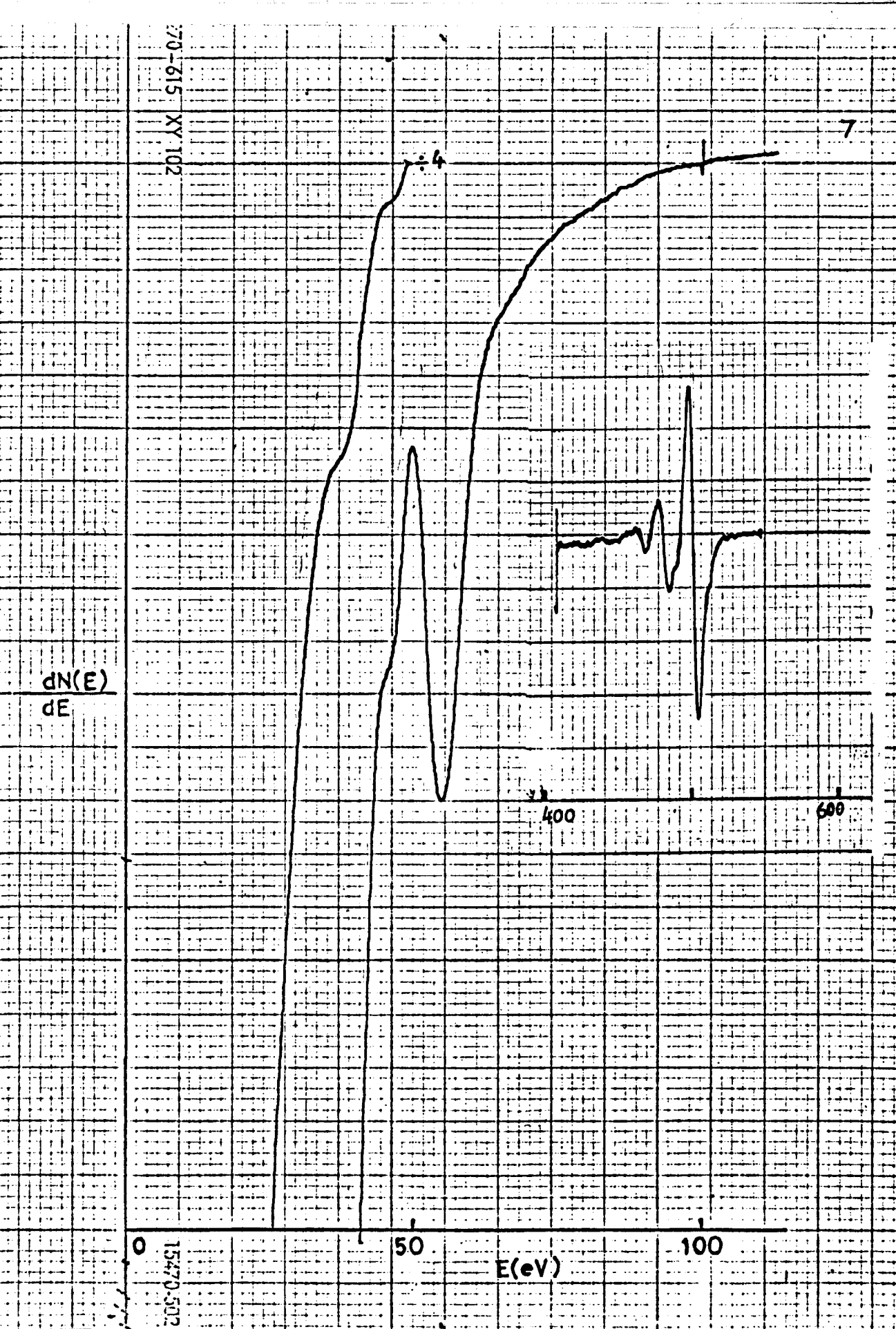
7
÷4
dN(E)
dE
400
600
0
50
100
E(eV)

Appendix 1c

Graphs 1-5 show successive oxidation of Fe with increasing oxygen level (1 → 5).

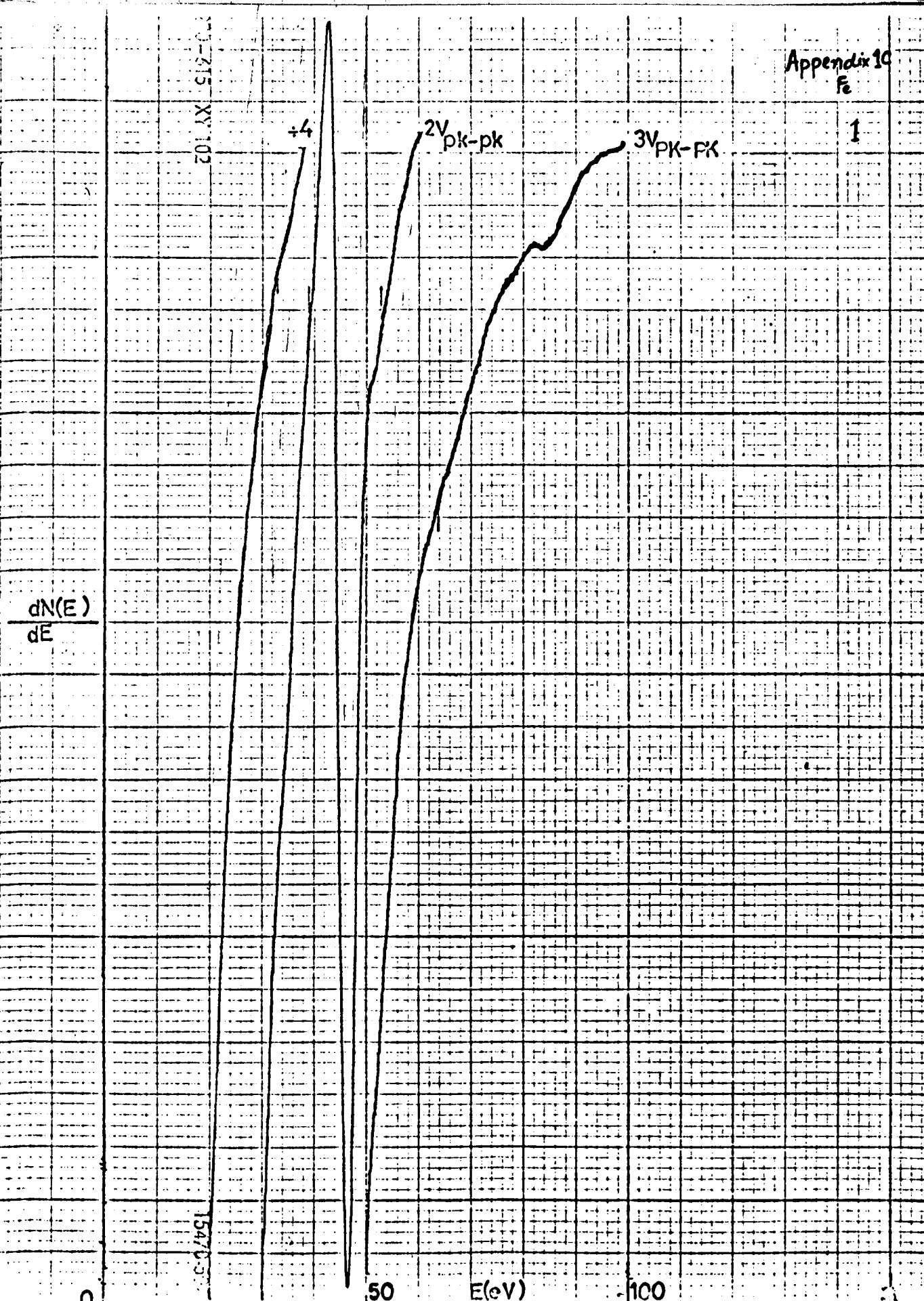
Appendix 10
Fe
1
÷4
2V pk-pk
3V PK-PK
dN(E)
dE
E(eV)
50
100
0

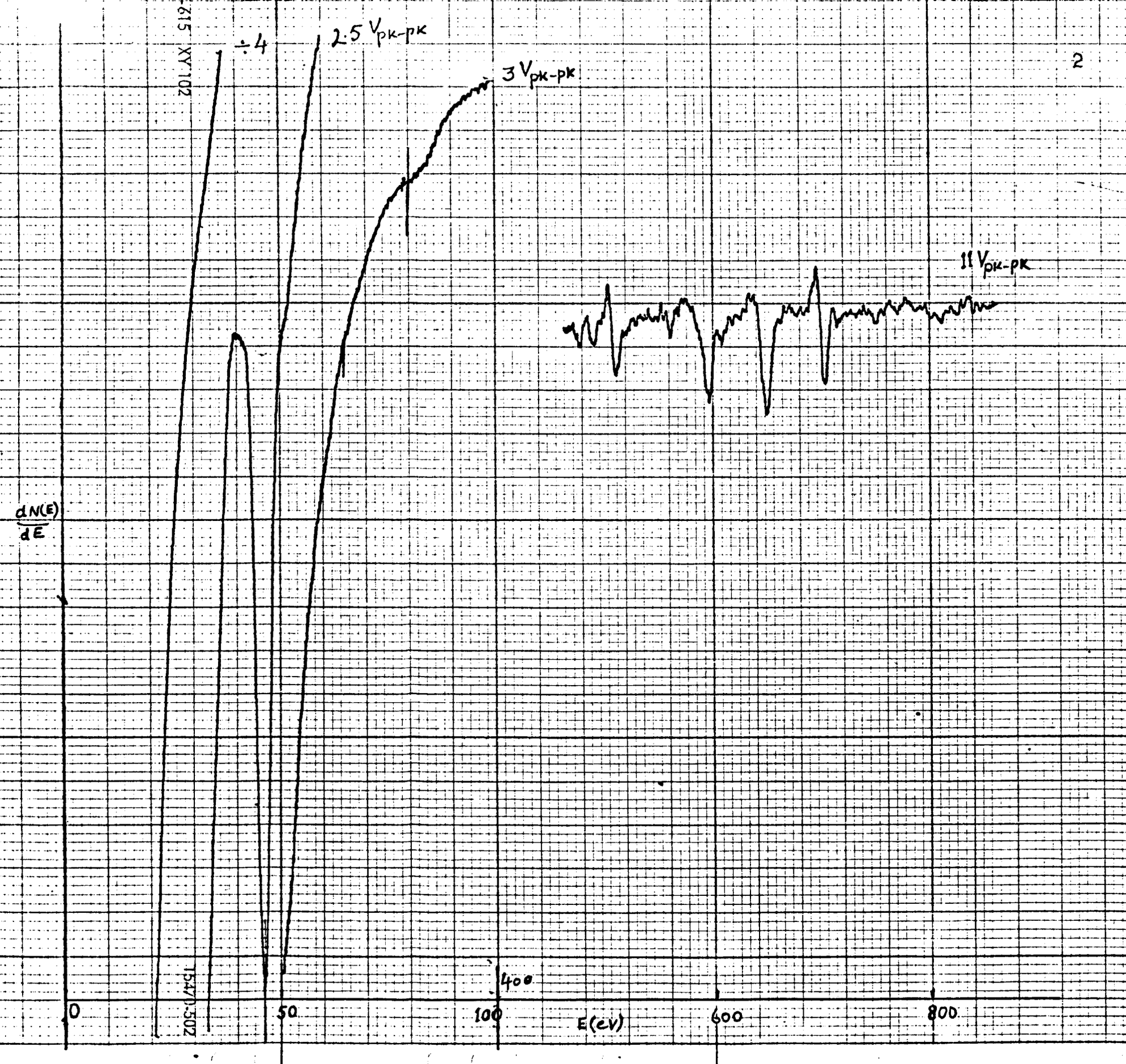
÷4
2.5 V_{pk-pk}
3 V_{pk-pk}
11 V_{pk-pk}
$\frac{dN(E)}{dE}$
0
50
100
400
600
800
E(eV)

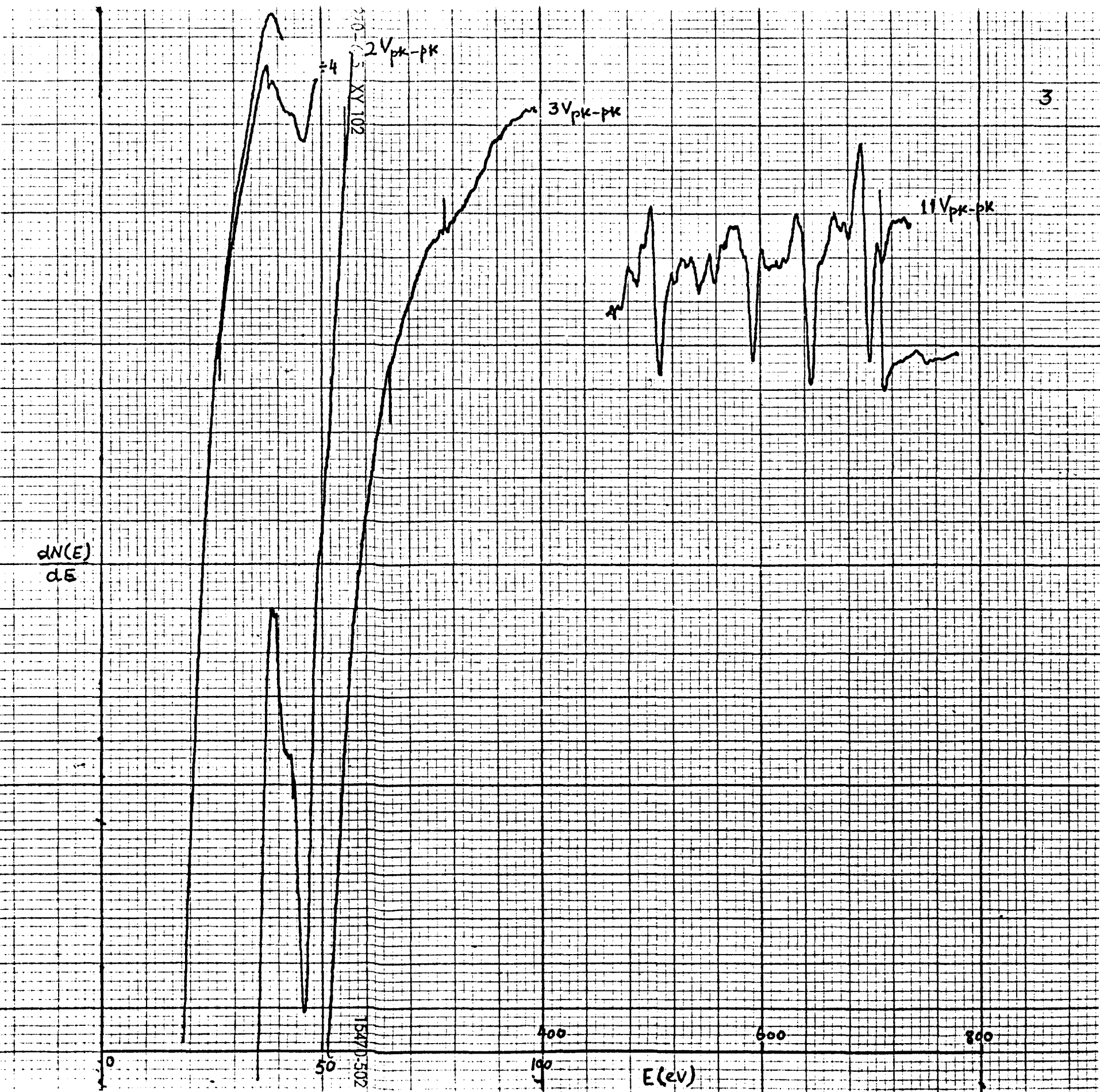
3
2 Vpk-pk
÷4
3 Vpk-pk
11 Vpk-pk
dN(E)
dE
0
50
100
400
600
800
E(eV)

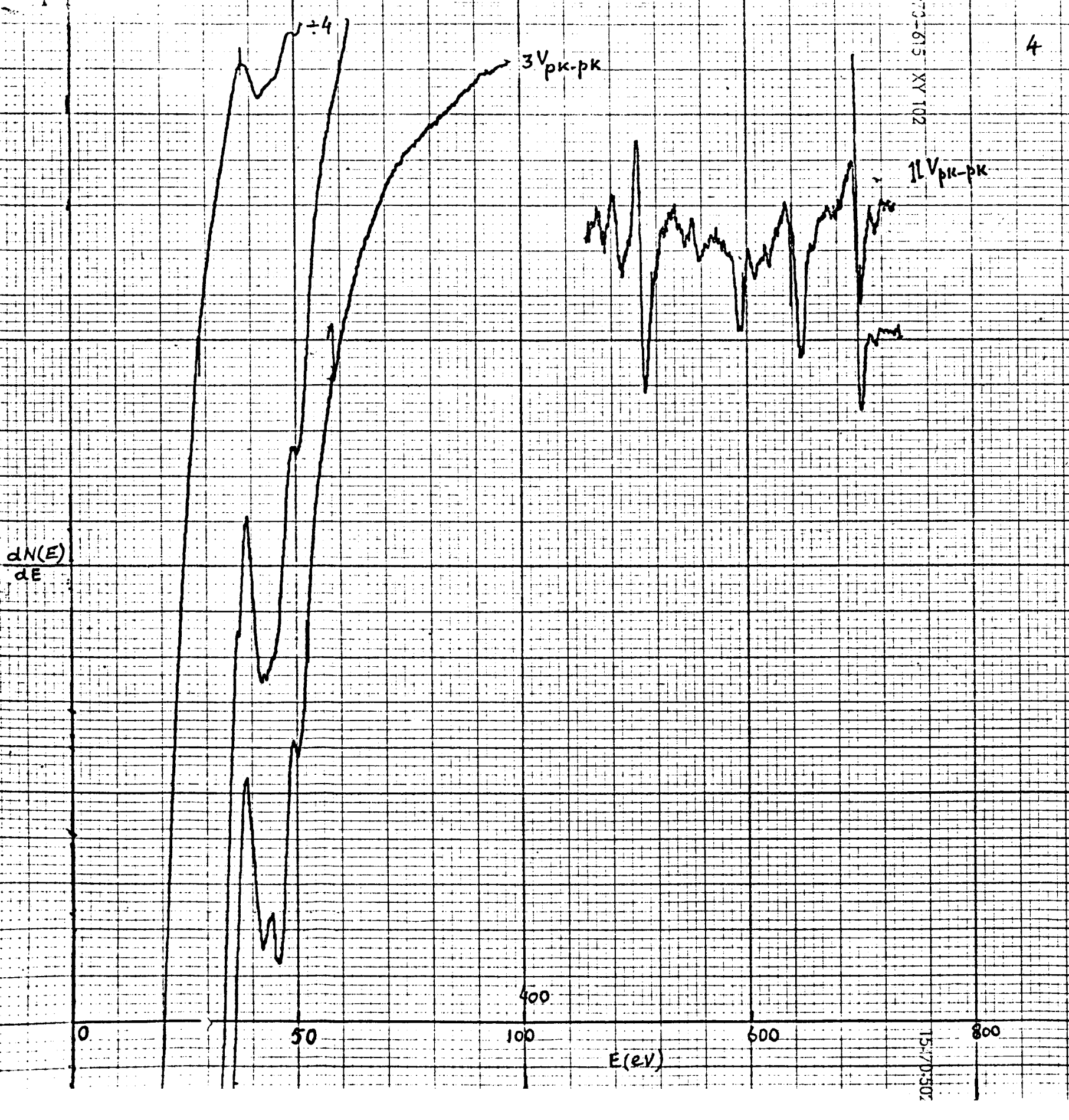
÷4
3 V pk-pk
1 V pk-pk
dN(E)
dE
0
50
100
400
600
800
E(eV)

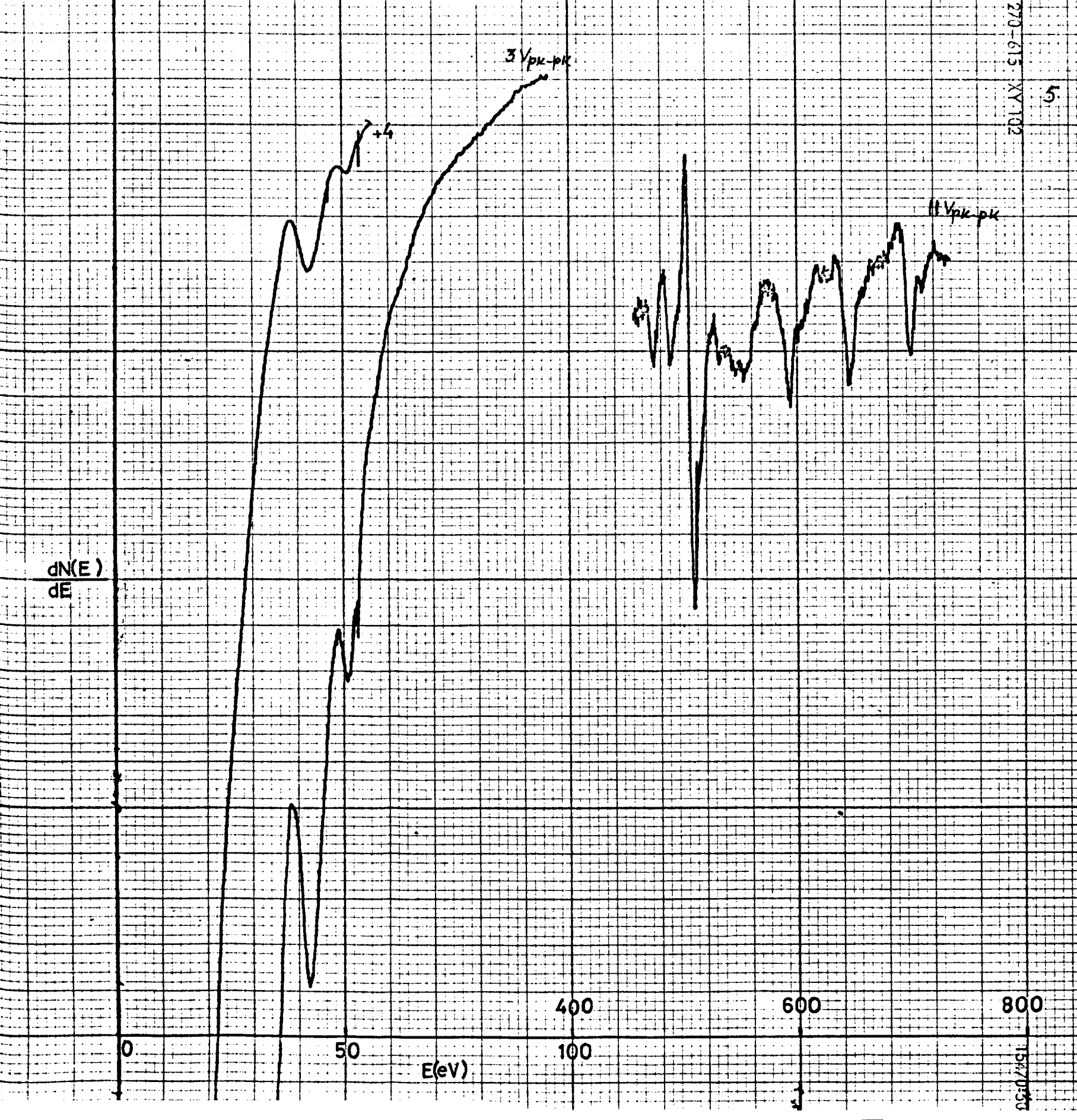
3 Vpk-pk
+4
11 Vpk-pk
dN(E)
dE
0
50
100
400
600
800
E(eV)

Appendices 2a, 2b and 2c

Sequences of changes in the energy loss spectra of Be, Al and Fe due to oxidation, are shown in Appendices 2a, 2b and 2c respectively. For Be and Al a primary energy of 800eV and for Fe 1KeV was used. Modulation voltages up to 600mV and primary beam currents up to 15μamps were usually used.

Appendix 2a

Appendix 2a
Be

N(E)

100 50 0

Energy Loss (eV)

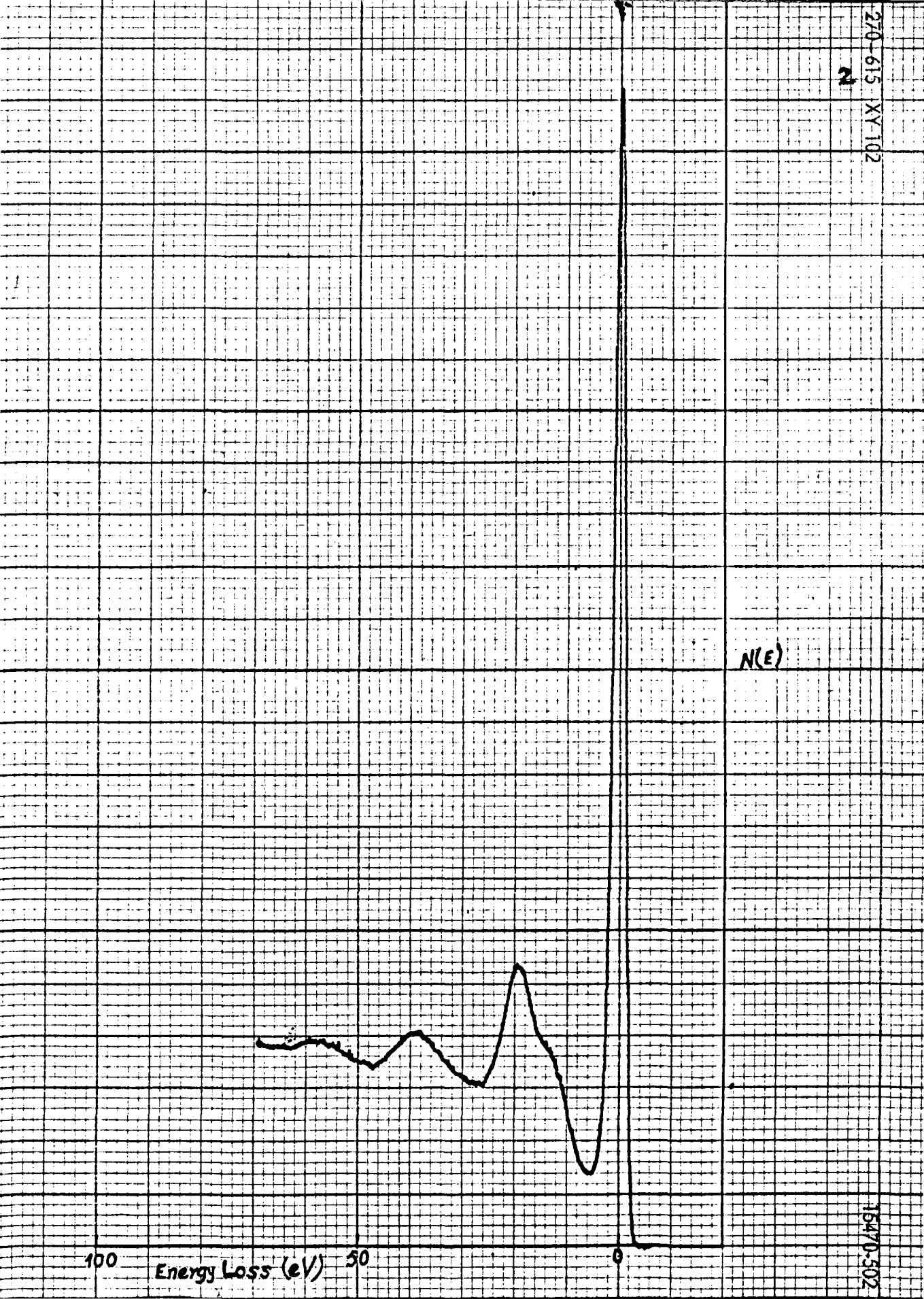

3
N(E)
100
Energy Loss (eV)
50
0

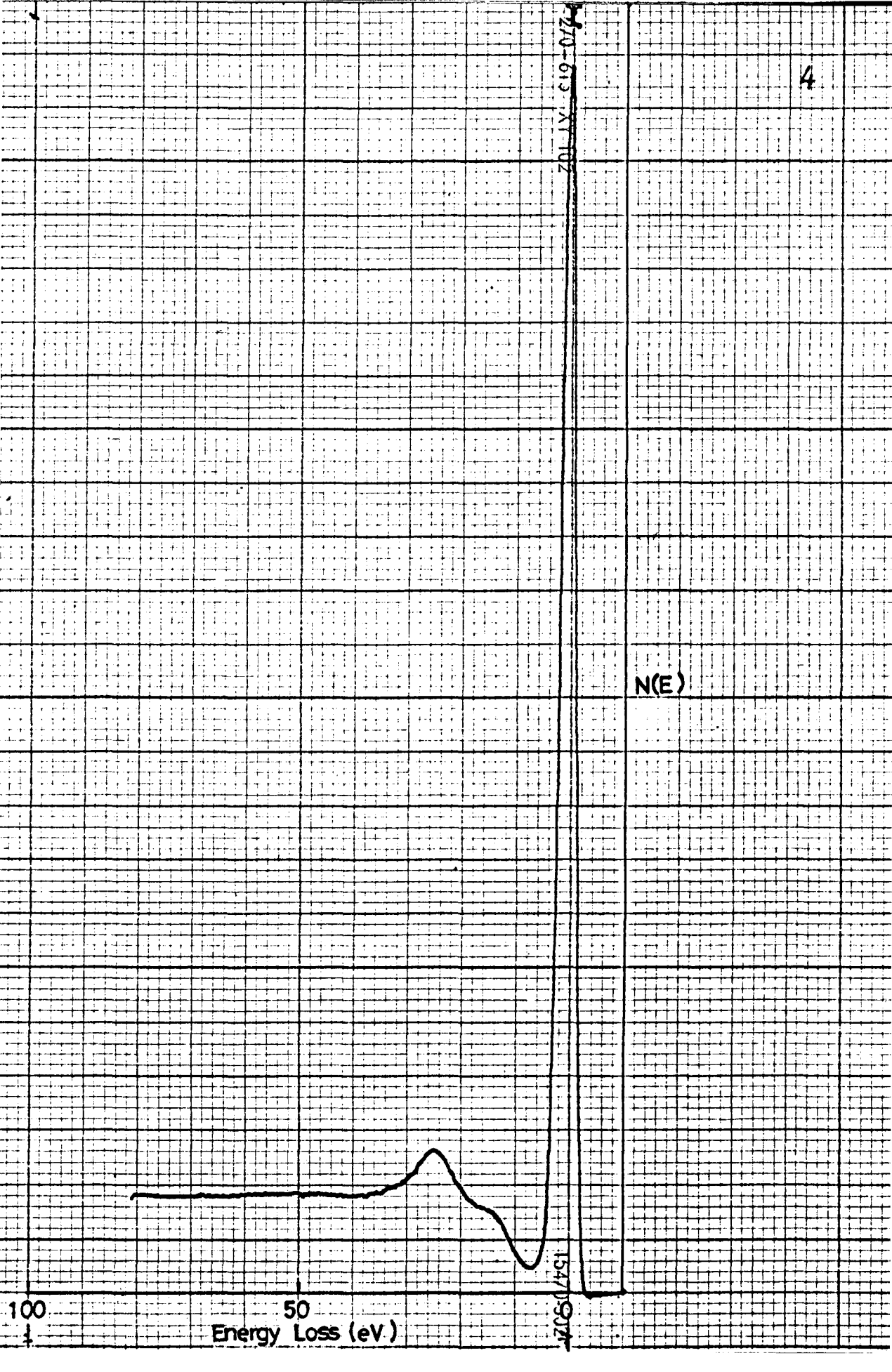
4
N(E)
100
50
0
Energy Loss (eV.)

Appendix 2b

Appendix 2b

Al

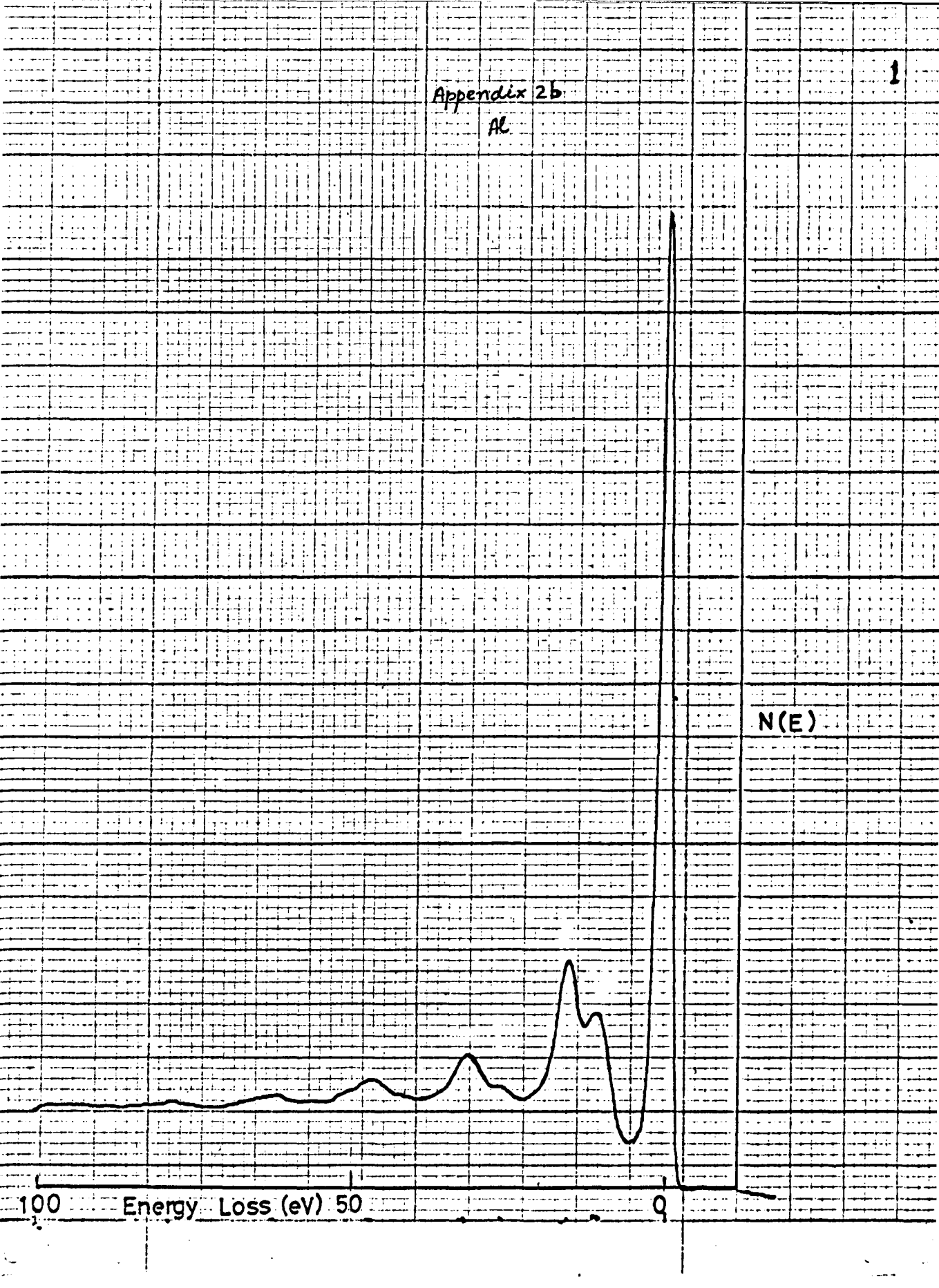

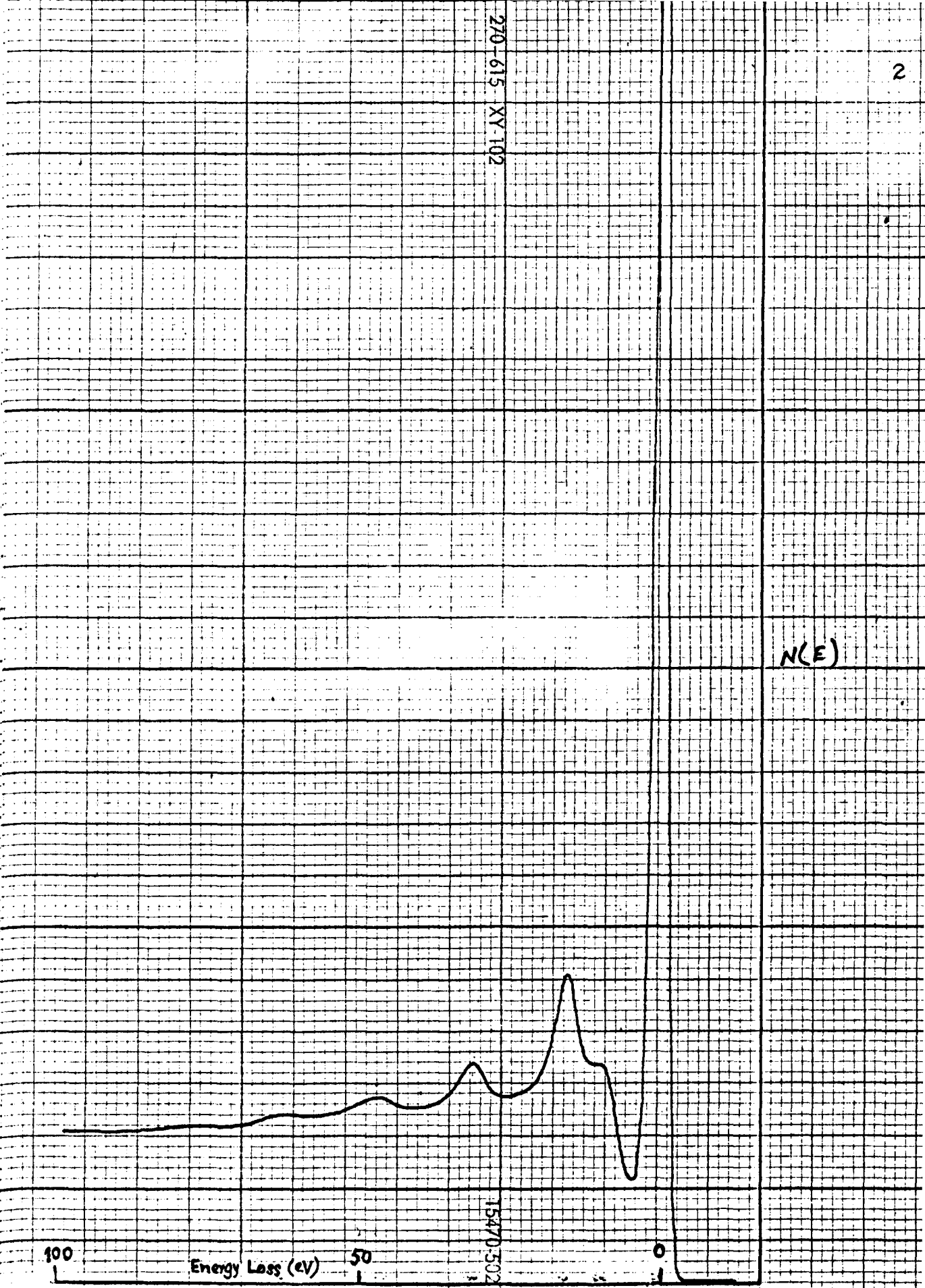
270-615-XY102
N(E)
100
Energy Loss (eV)
50
0
15470-502

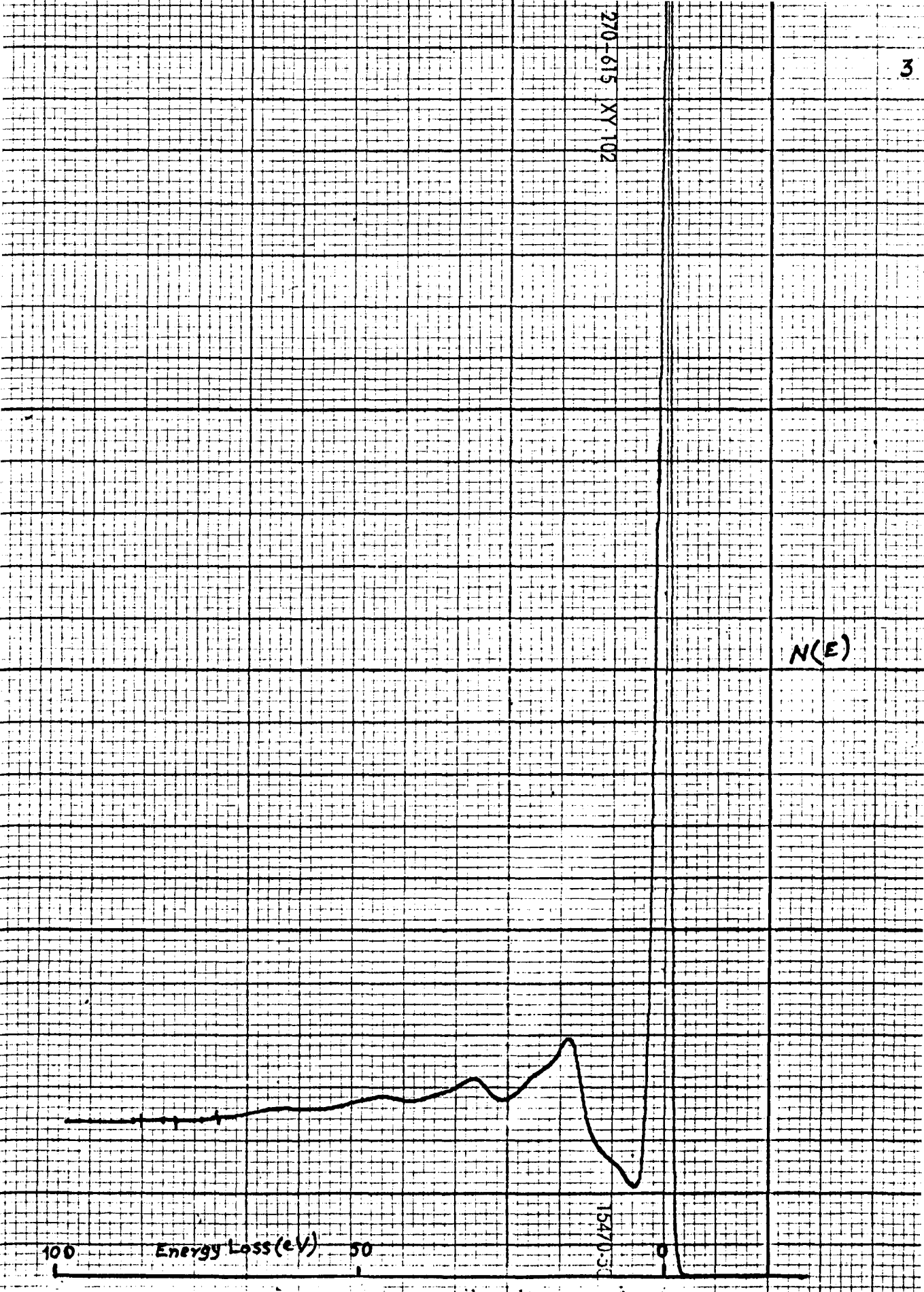
270-615 XY 102
N(E)
100
Energy Loss (eV)
50
0

N(E)
Energy Loss (eV)
100
50
0

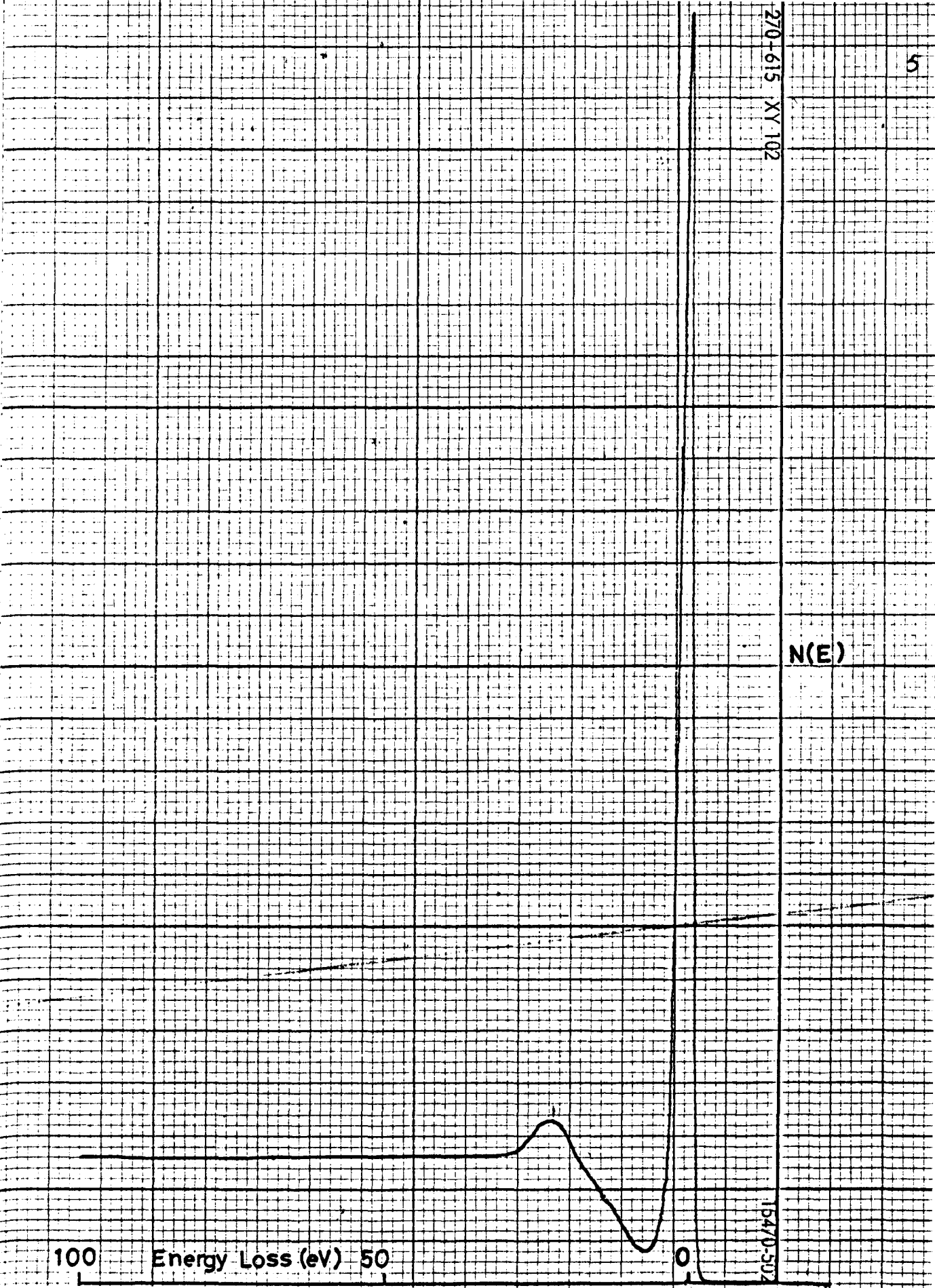
270-615 XY 102
5
N(E)
100
Energy Loss (eV)
50
0
15470-502

Appendix 2C

Fe.

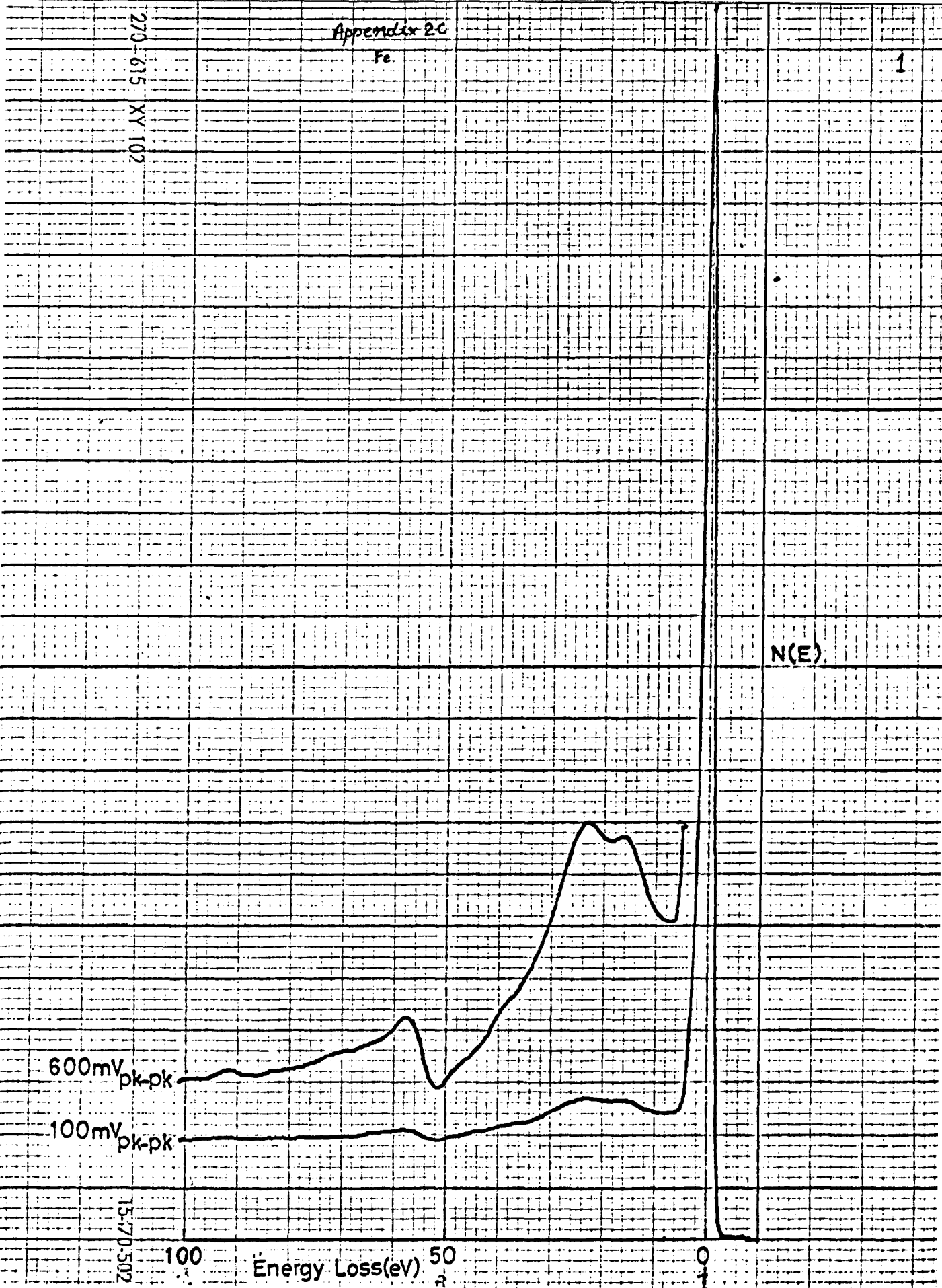

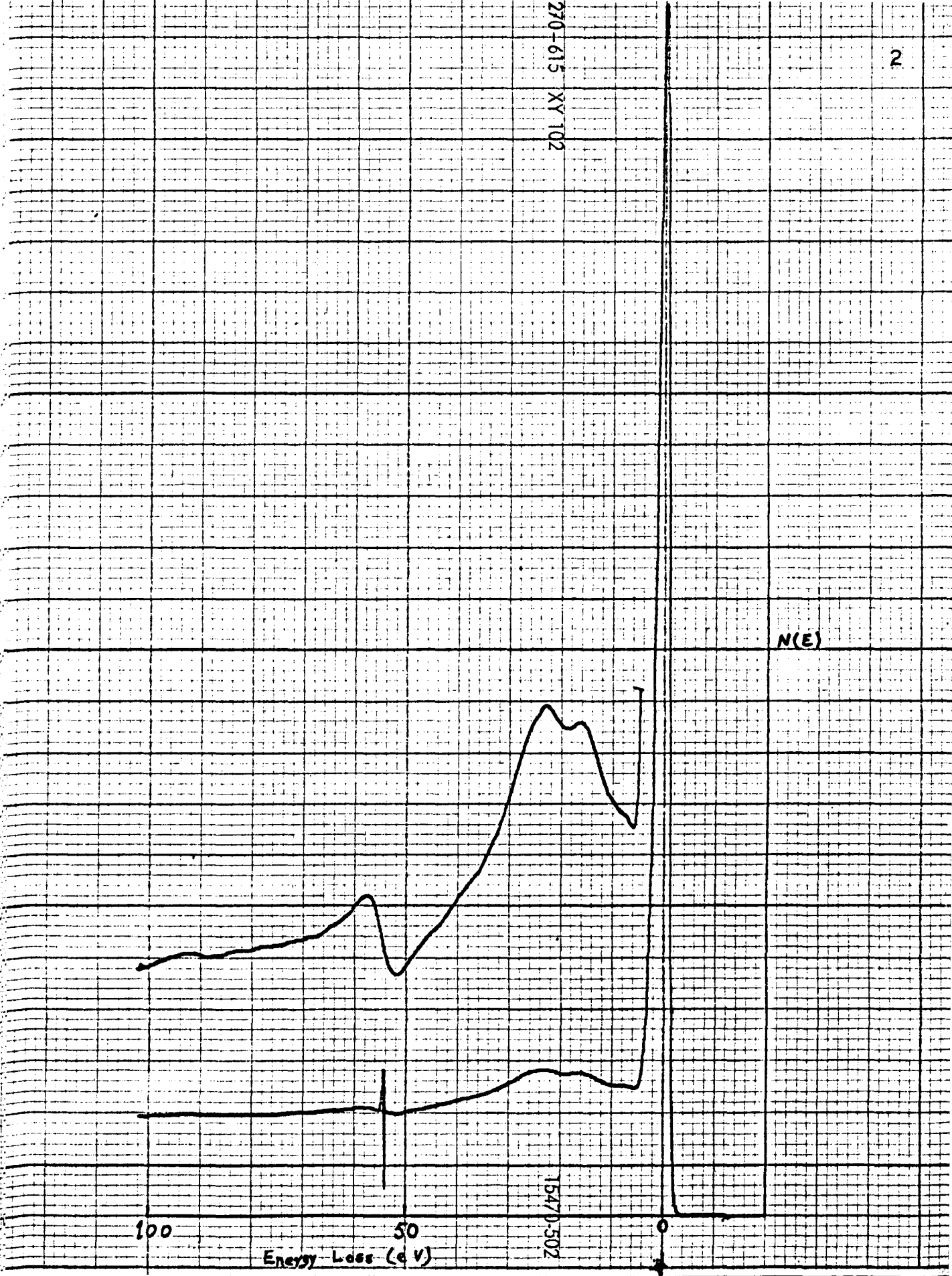
270-615 XY 102
N(E)
100
50
0
Energy Loss (eV)
1547-502

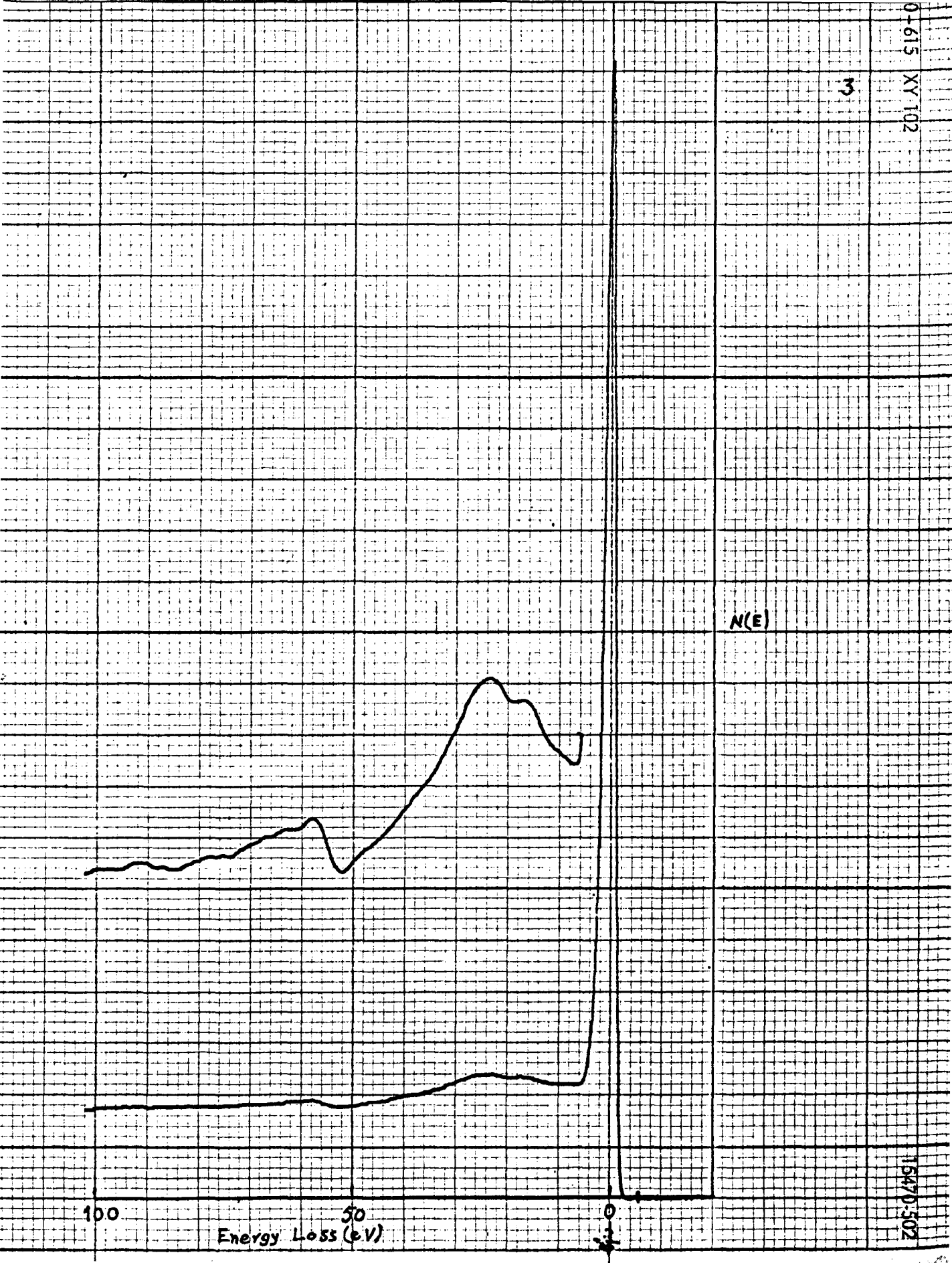
N(E)
100
50
0
Energy Loss (eV)

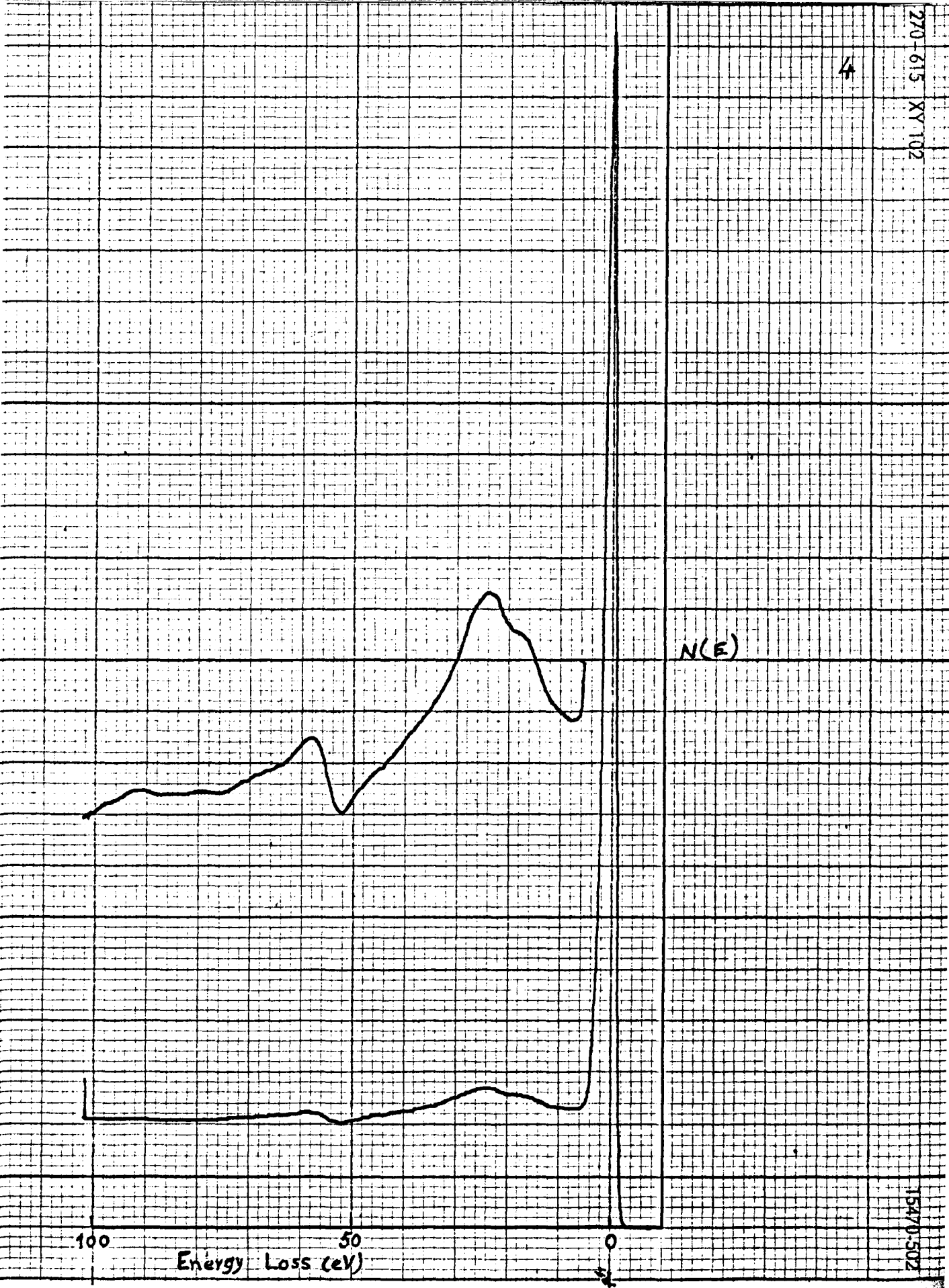

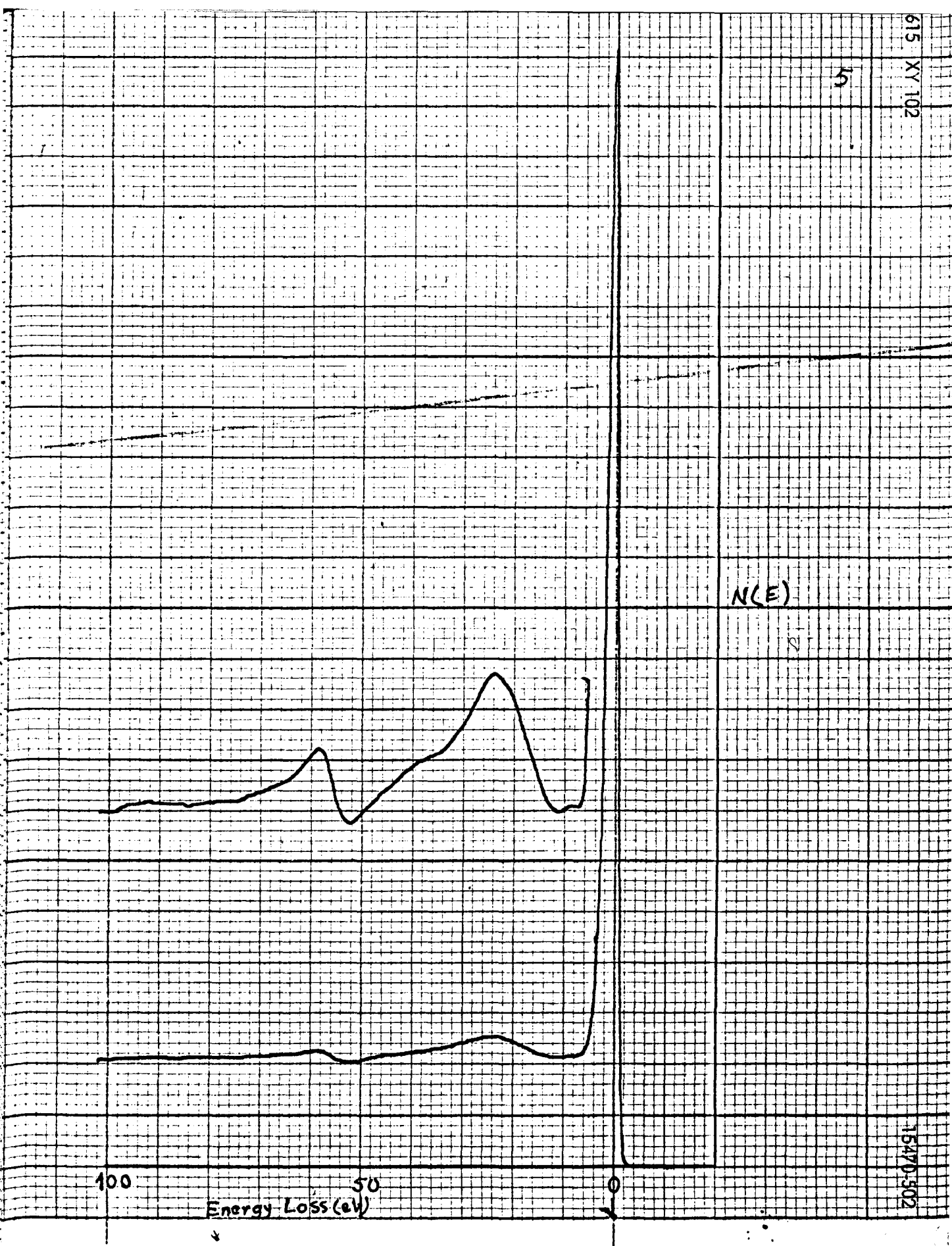
615 XY 102
N(E)
100
50
0
Energy Loss (eV)
15470-502

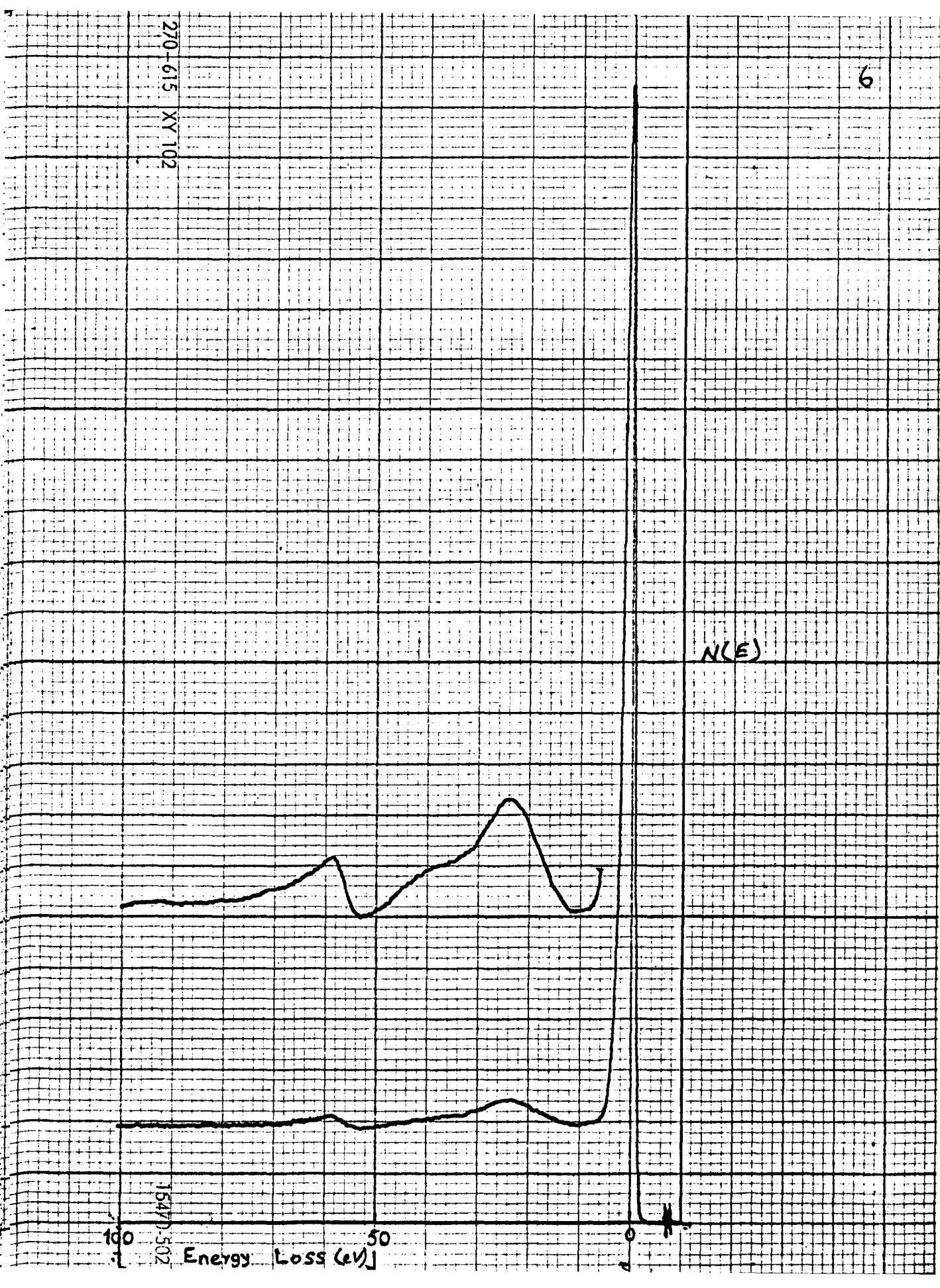
270-615 XY 102
N(E)
100
50
0
Energy Loss (eV)
1547) 502

REFERENCES

1. Lander, J.J., Phys. Rev. 91, 1382, 1953.
2. Harris, L.A., J. Appl. Phys. 39, 1419, 1968.
3. Weber, R.E. and Peria, W.T., J. Appl. Phys. 38, 4355, 1967.
4. Palmberg, P.W. and Rhodin, T.N., J. Appl. Phys. 39, 2425, 1968.
5. Bruining, H., Physics and Applications of Secondary Electron Emission, (Pergamon Press) 1954.
6. Gerlach, R.L., J. Vac. Sci. and Tech. 8, 599, 1971.
7. Bishop, H.E. and Riviere, J.C., J. Appl. Phys. 40, 1740, 1969.
8. Bohm, D. and Pines, D., Phys. Rev. 82, 625, 1951.
   85, 338, 1952.
   92, 609, 1953.
9. Ritchie, R.H., Phys. Rev. 106, 874, 1957.
10. Stern, E.A. and Ferrell, R.A., Phys. Rev. 120, 130, 1960.
11. Auger, P., J. Phys. Radium 6, 205, 1925.
12. Bergstrom, I. and Nordling, C. in Alpha, Beta and Gamma Ray Spectroscopy, Vol.II, Ed. K. Siegbahn (North Holland, Amsterdam) 1965.
13. Worthington, C.R. and Tomlin, S.G., Proc. Phys. Soc. A69, 401, 1956.
14. Houston, J.E. and Park, R.L., Appl. Phys. Letts. 14, 358, 1969.
15. Burhop, E.H.S., The Auger Effect and other Radiationless Transitions, (University Press, Cambridge) 1952.
16. Palmberg, P.W., Appl. Phys. Letts. 13, 183, 1968.
17. Listengarten, M.A., Bull. Acad. Sci., USSR Phys. Ser. 26, 182, 1962.

18. Mularie, W.M. and Pusch, T.W., Surface Sci. 19, 469, 1970.

19. Suleman, M. and Pattinson, E.B., J. Phys. F. (Metal Phys.) 1, L24, 1971.

20. Taylor, N.J., Surface Sci. 15, 169, 1969.

21. Suleman, M. and Pattinson, E.B., J. Phys. F. (Metal Phys.) 1, L21, 1971.

22. Jenkins, L.H. and Chung, M.F., Surface Sci. 26, 151, 1971.

23. Harrower, G.A., Phys. Rev. 102, 340, 1956.

24. Scheibner, E.J. and Tharp, L.N., Surface Sci. 8, 247, 1967.

25. Palmberg, P.W., Proc. of Conference on "La Structure et les Proprietes des Surfaces Solides, July 1969.

26. Charig, J.M. and Skinner, D.K., Surface Sci. 19, 283, 1970.

27 Jacobi, K. and Hölzl, J., Surface Sci. 26, 54, 1971.

28. Weber, R.E. and Johnson, A.L., J. Appl. Phys. 40, 314, 1969.

29. Uebbing, J.J., J. Appl. Phys. 41, 802, 1970.

30. Vrakking, J.J. and Meyer, F., Appl. Phys. Letts. 18, 226, 1971.

31. Haas, T.W. et al., Phys. Rev. B1, 1449, 1970.

32. Bishop, H.E. et al., Surface Sci. 24, 1, 1971.

33. Haas, T.W. and Grant, J.T., Phys. Letts. 30A, 272, 1969.

34. Coad, J.P. and Riviere, J.C., Phys. Letts. 35A, 185, 1971.

35. Coad, J.P. and Riviere, J.C., Z. Physik 244, 19, 1971.

36. Chang, C.C., Surface Sci. 25, 53, 1971.

37. Palmberg, P.W. et al., Appl. Phys. Letts. 15, 254, 1969.

38. Leder, L.B. and Simpson, J.A., Rev. Sci. Instr. 29, 571, 1958.

39. Heddle, D.W.O., J. Phys. E. (Sci. Instr.) 4, 589, 1971.

40. Taylor, N.J., Rev. Sci. Instr. 40, 792, 1969.

41. Huchital, D.A. and Rigden, J.D., Appl. Phys. Letts. 16, 348, 1970.

42. Chang, C.C., Surface Sci., 23, 283, 1970.

43. Spangenberg, K.K., Vacuum Tubes (McGraw Hill, New York) 1948.

44. Hughes, A.L. and Rojansky, V., Phys. Rev. 34, 284, 1929.

45. Pessa, M. et al., Acta Polytech. Scand. Ph 65, 1969.

46. Klemperer, O. and Shepherd, J.P.G., Adv. Phys. 12, 355, 1963.

47. Raether, H., Springer Tracts in Modern Physics Vol. 38 (Springer-Verlag, Berlin) 1965.

48. Palmberg, P.W., J. Appl. Phys. 38, 2137, 1967.

49. Powell, C.J., Phys. Rev. 175, 972, 1968.

50. Ehrenreich, H. and Philipp, H.R., Phys. Rev. 128, 1622, 1962.

51. Robins, J.L., Proc. Phys. Soc. 78, 1177, 1961.

52. Seah, M.P., Surface Sci. 17, 161, 1969.

53. Seah, M.P., Surface Sci. 24, 357, 1971.

54. Fiermans, L. and Vennik, J., Phys. Stat. Sol. 41, 621, 1970.

55. Fiermans, L. and Vennik, J., Surface Sci. 24, 541, 1971.

56. Moss, A.R.L. and Blott, B.H., Surface Sci., 17, 240, 1969.

57. Kulov, S.J. and Sherstnev, L.G., Instr. and Exptl. Techniques, July-Aug., 917, 1967

58. Palmberg, P.W. et al., Rev. Sci. Instr. 35, 244, 1964.

59. Roberts, R.W., Brit. J. Appl. Phys. 14, 537, 1963.

60. Rearden, J.A. and Burr, A.F., Rev. Mod. Phys. 39, 125, 1967.

61. Coad, J.P. and Riviere, J.C., Surface Sci. 25, 609, 1971.

62. Dooley, G.J. and Haas, T.W., J. Vac. Sci. and Tech. 7, S90, 1970.

63. Leder, L.B. and Suddeth, J.A., J. Appl. Phys. 31, 1422, 1960.

64. Jenkins, L.H. and Chung, M.F., Surface Sci. 24, 125, 1971.

65. Aksela, S. et al., Z. Physik,237, 381, 1970.

66. Robins, J.L. and Swan, J.B., Proc. Phys. Soc. 76, 857, 1960.

67. Powell, C.J., Proc. Phys. Soc. 76, 593, 1960.

68. Jordan, L.K. and Scheibner, E.J., Surface Sci. 10, 373, 1968.

69. Thomas, S. and Pattinson, E.B., J. Phys. D. (Appl. Phys.) 3, 1469, 1970.

70. Hamrin, K. et al., Physica Scripta 1, 277, 1970.

71. Loucks, T.L. and Cutler, P.H., Phys. Rev.A133, 819, 1964.

72. Sagawa, T., Soft X-ray Band Spectra and the Electronic Structure of Metals & Materials,Ed. D.J. Fabian (Academic Press, London) p.29, 1968.

73. Musket, R.G. and Fortner, R.J., Phys. Rev. Letts. 26, 80, 1971.

74. Gallon, T.E. and Matthew, J.A.D., Phys. Stat. Sol. 41, 343, 1970.

75. Lukirskii, A.P. and Brytov, I.A., Soviet Phys. Solid State 6, 33, 1964.

76. Swanson, N. and Codling, K.J., Opt. Soc. Am. 58, 1192, 1968.

77. Hayasi, T. et al., Sci. Rep. Tohoku Univ. Ser. 1, 52, 1, 1969.

78. Fomichev, V.A., Soviet Phys. Solid State 13, 754, 1971.

79. Ashcroft, N.W., Optical Properties and Electronic Structure of Metals and Alloys, Ed. F. Abeles (North-Holland, Amsterdam) p.336. 1966.

80. Braundmeir Jr. A.J.et al., Phys. Letts. 32A, 241, 1970.

81. Watts, C.M.K., Private communication, 1971.

82. Maguire, H.G. and Augustus, P.D., J. Phys. C (Solid State) 4, L174, 1971.

83. Grant, J.T. and Haas, T.W., Surface Sci. 23, 347, 1970.

84. Swanson, N. and Powell, C.J., Phys. Rev. 167, 592, 1968.

85. Codling, K. and Madden, R.P., Phys. Rev. 167, 587, 1968.

86. Fomichev, V.A., Soviet Phys. Solid State 8, 2312, 1967.

87. Siegbahn, K. et al., Atomic, Molecular and Solid State Structure by means of ESCA, (Almqvist and Wiksell Boktryckeri AB, Upsala, Sweden) 1967.

88. Powell, C.J. and Swan, J.B., Phys. Rev. 115, 869, 1959.

89. Marton, L. and Leder, L.B., Phys. Rev. 94, 203, 1954.

90. Kleinn, W., Optik 11, 226, 1954.

91. Zashkvara, V.V. et al., Soviet Phys. Tech. Phys. 11, 96, 1966.